University of Exeter

College of Engineering, Mathematics and Physical Science

Multi-objective Optimisation in Additive Manufacturing

Giovanni Strano

May, 2012

Submitted by Giovanni Strano, to the University of Exeter as a thesis for the degree of Doctor of Philosophy in Engineering, in May 2012.

Abstract

Additive Manufacturing (AM) has demonstrated great potential to advance product design and manufacturing, and has showed higher flexibility than conventional manufacturing techniques for the production of small volume, complex and customised components. In an economy focused on the need to develop customised and hi-tech products, there is increasing interest in establishing AM technologies as a more efficient production approach for high value products such as aerospace and biomedical products.

Nevertheless, the use of AM processes, for even small to medium volume production faces a number of issues in the current state of the technology. AM production is normally used for making parts with complex geometry which implicates the assessment of numerous processing options or choices; the wrong choice of process parameters can result in poor surface quality, onerous manufacturing time and energy waste, and thus increased production costs and resources. A few commonly used AM processes require the presence of cellular support structures for the production of overhanging parts. Depending on the object complexity their removal can be impossible or very time (and resources) consuming.

Currently, there is a lack of tools to advise the AM operator on the optimal choice of process parameters. This prevents the diffusion of AM as an efficient production process for enterprises, and as affordable access to democratic product development for individual users.

Research in literature has focused mainly on the optimisation of single criteria for AM production. An integrated predictive modelling and optimisation technique has not yet been well established for identifying an efficient process set up for complicated

products which often involve critical building requirements. For instance, there are no robust methods for the optimal design of complex cellular support structures, and most of the software commercially available today does not provide adequate guidance on how to optimally orientate the part into the machine bed, or which particular combination of cellular structures need to be used as support. The choice of wrong support and orientation can degenerate into structure collapse during an AM process such as Selective Laser Melting (SLM), due to the high thermal stress in the junctions between fillets of different cells.

Another issue of AM production is the limited parts' surface quality typically generated by the discrete deposition and fusion of material. This research has focused on the formation of surface morphology of AM parts. Analysis of SLM parts showed that roughness measured was different from that predicted through a classic model based on pure geometrical consideration on the stair step profile. Experiments also revealed the presence of partially bonded particles on the surface; an explanation of this phenomenon has been proposed. Results have been integrated into a novel mathematical model for the prediction of surface roughness of SLM parts. The model formulated correctly describes the observed trend of the experimental data, and thus provides an accurate prediction of surface roughness.

This thesis aims to deliver an effective computational methodology for the multi-objective optimisation of the main building conditions that affect process efficiency of AM production. For this purpose, mathematical models have been formulated for the determination of parts' surface quality, manufacturing time and energy consumption, and for the design of optimal cellular support structures.

All the predictive models have been used to evaluate multiple performance and costs objectives; all the objectives are typically contrasting; and all greatly affected by the part's build orientation.

A multi-objective optimisation technique has been developed to visualise and identify optimal trade-offs between all the contrastive objectives for the most efficient AM production. Hence, this thesis has delivered a decision support system to assist the operator in the "process planning" stage, in order to achieve optimal efficiency and sustainability in AM production through maximum material, time and energy savings.

Contents

List of Tables....11

List of Figures....13

Author's declaration....19

Nomenclature....25

1. Introduction....29

1.1 Research Background and Rationale....29

1.1.1 Criteria and Complexity in Additive Manufacturing....29

1.1.2 Multi-objective Optimisation....32

1.2 Research Objectives and Contributions....33

1.2.1 Overall aim and objectives....33

1.2.2 Research Methodology and Development....34

1.2.3 Principal contributions....35

1.3 Thesis overview....36

2. Background....39

2.1 Advanced material structures in aerospace....39

2.1.1 Aerospace materials and lightweight applications....39

2.1.2 Lightweight structure components with complex and optimal geometries....42

2.1.3 Lightweight cellular structures....45

2.1.4 Conventional manufacturing of complex aerospace components....47

2.1.5 Conventional manufacturing of lightweight cellular structures....49

2.2 Additive Manufacturing....57

2.2.1 Introduction to additive manufacturing....57

2.2.2 Technical aspects of additive manufacturing.....58
2.2.3 AM for aerospace and defence applications.....59
2.2.4 State of art of main AM processes for aerospace applications.....63
2.2.5 Limits and challenges of AM for production in aerospace.....70
2.3 Multi-objective Optimisation.....72
2.3.1 Multi-criteria decision analysis for optimisation of industrial processes.....72
2.3.2 Importance of Multi-object optimisation in industrial design.....73
2.3.3 Basic multi-objective optimisation concepts - dominance and Pareto front.....78
2.3.4 Solution methods.....80
2.4 Conclusions.....87

3. Multi-objective Optimisation of Selective Laser Sintering Processes for Surface Quality and Energy Saving.....89
3.1 Introduction.....89
3.1.1 Previous works on multi-object Optimisation in AM.....90
3.1.2 Importance of surface finish in industrial design and applications.....92
3.1.3 Issues in surface finish of AM parts.....94
3.1.4 Model for roughness prediction of AM parts.....96
3.1.4.1 Theoretical models based on geometrical considerations.....96
3.1.4.2 Models based on experimental data interpolation.....96
3.2 Models for multi-object optimisation of Selective Laser Sintering processes.....98
3.2.1 Computational model for surface roughness prediction 98
3.2.2 Effects of sloping angles on the surface roughness of SLS polymer parts…….....100
3.2.3 Mathematical formulation.....103
3.2.4 Model for energy prediction.....104
3.3 Multi-Objective problem definition and algorithm implementation.....106
3.4 Results and discussion.....108

3.5 Conclusions.....115

4. Multi-Objective Optimisation of Selective Laser Melting Processes for Manufacturing Time and Surface Quality.....117

4.1 Introduction.....117

4.1.1 Surface roughness in Selective Laser Melting process…….....118

4.1.2 Build time and post-manufacturing operations of SLM Fabricated parts.....121

4.2 Model for surface roughness prediction.....124

4.2.1 Surface morphology and roughness analysis.....124

4.2.1.1 Surface roughness and morphology analysis using profilometer.....125

4.2.1.2 Surface Morphology Analysis through SEM.....130

4.2.2 New model for prediction of surface roughness.....136

4.2.2.1 Stair-step effect and surface roughness in Selective Laser Melting.....136

4.2.2.2 Mathematical formulation.....138

4.3 Model for build time prediction.....144

4.4 Multi-objective problem definition and algorithm implementation.....146

4.5 Results and discussion.....148

4.6 Conclusions.....155

5. Support structure optimisation for additive manufacturing.....157

5.1 Introduction.....157

5.1.1 Support Structures and build orientation.....160

5.1.2 Design of cellular support structures.....161

5.2 Design of optimal support structures for additive manufacturing.....166

5.2.1 Optimisation of part build orientation.....166

5.2.2 Design of support structures through 3D mathematical functions.....169

5.2.2.1 Effects of changing cell periodicity.....171

5.2.3 Method validation.....173
5.3 Evaluation of a complex shape structure as a case study.....175
5.4 Result and discussion on support structures for a complex structure.....178
5.5 Conclusions.....180

6. Multi-objective optimisation of parts and support structures.....181
6.1 Introduction.....181
6.1.1 Manufacturing optimisation of part with supports structures.....182
6.2 Three-objective optimisation.....185
6.2.1 Models used for the three-objective optimisation.....185
6.2.2 Performance objective functions for three-objective optimisation.....187
6.2.3 Case study definition.....192
6.4 Results and discussion.....194
6.5 Conclusions.....203

7. Conclusions.....205

Appendix.....211
Appendix A – Matlab code for multi-objective optimisation.....211
Appendix B – Program to generate graded support microstructures.....219
Appendix C – Publications.....223

Glossary.....279

Bibliography.....281

List of Tables

Table 2.1. Mechanical properties of materials processed by SLS.....64

Table 5.1. Comparison of material saving for different build orientations. *Values in respect to the original orientation.....179

Table 6.1. List of Pareto solutions for the first case study.....197

Table 6.2. List of Pareto solutions for the second case study.....200

List of Figures

2.1. Initial design and result in a) sizing optimization; b) shape optimization; c) topology optimization.....42

2.2. Example of topology optimisation for compression-only structure through ESO. Initial design (top) and final solution through three consecutive steps 44

2.3. Original and optimised engine nacelle hinges for A320 airliners.....44

2.4. Hexagonal honeycomb, example of lightweight bio inspired structure.....45

2.5. Example of 3D trusses flat panel.....46

2.6. Expansion-manufacturing process for honeycomb cores.....49

2.7. Corrugation-manufacturing process for honeycomb cores.....50

2.8. Heated press assembly for honeycombs panel.....51

2.9. Vacuum Bag Processing assembly for honeycombs panel.....51

2.10. Match Mould Processing assembly for honeycombs panel.....52

2.11. Illustration of the folding operation used to create the single layer pyramidal truss sandwich structures.....52

2.12. Example of multilayer tetrahedral structure manufactured through folded perforated aluminium sheets.....53

2.13. Collinear wires deposited in alternate direction (left), and core structure by bonded and cut wires (right).....54

2.14. Possible defects in truss cells produced by casting.....55

2.15. Direct production of air ducts.....59

2.16. T700 Blisk leading edge repaired through LENS technology.....61

2.17. Optimised engine nacelle hinges for A320 airliners.....62

2.18. Aligned composite structures made by an FDM like process and example of structural architecture components.....62

2.19. Selective Laser Sintering system schematic.....65

2.20. Selective Laser Melting: (a) Illustration of the machine; and (b) working principle of the system.....66

2.21. F1 car component built through SLM process.....67

2.22. Jet nozzle deposition during LENS sintering process.....67

2.23. Laser engineering net shaping: parts fabricated on Ti alloy.....68

2.24. LENS employed for gas turbine engine repair.....69

2.25. Parts manufactured by Electron Beam Melting.....70

2.26. Optimisation of a control arm that links the wheel to the body of the car.....76

2.27. Example of dominance on a two-objective minimisation problem; the solutions coloured in green form the Pareto front.....80

3.1. Qualitative comparison of production time and surface texture for traditional finishing processes.....95

3.2. Representation of 1D (top) and 2D (bottom) surface profiles.....99

3.3. Truncheon sample CAD model (a), and manufactured sample (b, c).....100

3.4. Experimental roughness in SLS process at different sloping angle; (a) upward-facing, and (b) downward-facing oriented data.....101

3.5. Filleting effect caused by flow of molten polymer for downwards oriented facets (a), but inhibited by surface tension to only partially smooth thick layers (b). For upward facing facets (c) filleting is minimised although surface tension may smooth sharp corners.....102

3.6. Angle between the building direction and STL file facet normal vectors.....103

3.7. Principal algorithm routines flowchart for surface roughness and energy prediction.....108

3.8. Artefacts to be manufactured by SLS: support for aluminium profile (a),tension latch (b).....108

3.9. Weighted average roughness function for the artefact shown in Figure 3.8a.....109

3.10. Solutions and Pareto front for the first case study.....110

3.11. First case study at different orientations; a) original oriented geometry, b) minimisation of surface roughness, c) minimisation of build process energy, d) compromise between the two objectives.....112

3.12. Solutions and Pareto front for the artefact for the second case study.....113

3.13. Second case study at different orientations; a) original oriented geometry, b) minimisation of surface roughness, c) minimisation of build process energy, d) compromise between the two objectives.....114

4.1. Manufactured sample geometry. During building the truncheon is oriented with the long axis vertical.....124

4.2. Experimental roughness at different sloping angle.....125

4.3. Profilometer surface profiles inclined at (a) 5°, (b) 10° and (c) 65°. The grey scale indicates surface height.....127

4.4. Schematic representation of a sliced profile. The dash dotted line represents the mean location of the surface.....128

4.5. Measured and predicted distance between consecutive step edges.....129

4.6. SEM picture of a horizontal surface (sloping angle 0°): a) a surface overview, b) detail profile, c) detail profile at high magnification.....130

4.7. SEM picture of slightly inclined surface (sloping angle 5°), (a) at low magnification, (b) at high magnifications, (c) detail of slightly inclined surface.....131

4.8. Schematic representation of heat diffusion during the laser sintering Process.....133

4.9. Transition between sample steps at a) 5°-10°, b) 30°-35° and c) 85°-90° sloped surfaces. The superimposed white lines mark the boundary between surfaces of the truncheon test piece with different sloping angles.....134

4.10. Presence of particles on highly sloped surface (sloping angle 90°).....135

4.11. Comparison of experimental roughness and simulated roughness in accord to Equation 4.2.....137

4.12. 3D Schematic representation of particles partially bonded at step edge.....139

4.13. Schematic representation: a) lateral and top view of λ fraction of partially bonded particles; b) cross section of the modelled surface.....139

4.14. Surface roughness calculated using Equation (4.4).....141

4.1. Comparison between measured roughness and roughness predicted through newly developed model using Equation (4.5).....142

4.16. Proposed geometries to be processed.....146

4.17. Solutions and Pareto front for the first case study.....149

4.18. First case study at different orientations: (a) original oriented geometry; (b) minimization of surface roughness; (c) minimization of build time.....150

4.19. Solutions and Pareto front for the second case study.....151

4.20. Second case study at different orientations: (a) original oriented geometry; (b) minimization of surface roughness; (c) minimization of build time.....152

4.21. Solutions and Pareto front for the third case study.....153

4.22. Third case study at different orientations: (a) original oriented geometry; (b) minimization of surface roughness; (c) minimization of build time.....154

5.1. Typical polymer and metal support structures in AM.....157

5.2. Support structures (centre) require considerable amount of material powder. The orange part is the part to be manufactured, the yellow part is the support required to sustain it.....158

5.3. Removal of laminated object manufacturing (LOM) support structure.....159

5.4. From the left, representation of level surfaces expressed by Equations (5.1), (5.2), (5.3) respectively.....163

5.5. Functionally graded geometry described by Equation (5.4), with k=0.04.....164

5.6. Example of support structures, with different cell size and graded structures, mathematically generated by Equation (5.5).....165

5.7. Schematic of first step optimisation, for optimal orientation to minimise support volume.....167

5.8. Examples of solid supports, generated for arbitrary orientations.....168

5.9. Schematic of second step optimisation, for the generation of a graded microstructure.....169

5.10. "test.stl" geometry oriented as originally (left), and optimally (right). In green, the associated solid support.....170

5.11. Segmentation of entire volume of the object into sub-volumes.....171

5.12. Discontinuities might appear at the interface between blocks with different cell sizes.....172

5.13. Schwartz cells with the same periodicity in z direction (kz1 = kz2).....173

5.14. Final support structure for "test.stl" geometry (left); manufactured geometry (right).....174

5.15. Truss structure geometry "cell.stl".....175

5.16. Solid support for original orientation.....176

5.17. Best (left) and worst (right) building orientation for "cell.stl" geometry.....177

5.18. Final support structure for "cell.stl" geometry.....177

6.1. Surface roughness at different inclination angles according to model (4.7).....185

6.2. “Cantilever.stl” test geometry.....187

6.3 Performance objectives for “Cantilever.stl” geometry; volume of support structures (top), build time (centre), weighted average roughness (bottom).....189

6.4. Orientation that minimise support for “Cantilever.stl” geometry.....190

6.5. Orientation that minimise built time and roughness for “Cantilever.stl” geometry.....191

6.2. Rotations around x axis, for: $0^o <= \theta_x <= 90^o$ and $\theta_y = 0^o$.....191

6.7. Artefacts to be processed.....192

6.8. 3D Pareto set for the first case study.....195

6.9. First case study at different orientations; a) minimisation of support structures, b) minimisation of build time; c) minimisation of surface roughness.....198

6.10. 3D Pareto set for the second case study.....199

6.11. Second case study at different orientations; a) minimisation of support structures, b) minimisation of built time; c) minimisation of surface roughness.....202

Author’s declaration

The PhD work has generated a number of papers which are incorporated within the content of the thesis. These papers, either published or submitted for publication during the period of research at University of Exeter towards a PhD, are listed, together with the chapters they appear in, as follows:

Chapter 3 includes work from the study *"Multi-objective Optimisation of Selective Laser Sintering Processes for Surface Quality and Energy Saving",* in Proceedings of the Institution of Mechanical Engineers, Part B: Journal of Engineering Manufacture, August 8, 2011, by G. Strano, L. Hao, R.M. Everson and K.E. Evans.

Chapter 3 includes work from the study *"Optimisation of Quality and Energy Consumption for Additive Layer Manufacturing Processes",* in 5th International Conference on Responsive Manufacturing - Green Manufacturing (ICRM 2010), Ningbo, China, 11-13 Jan. 2010, pp. 364 - 369, by G. Strano, L. Hao, R.M. Everson and K.E. Evans.

Chapter 4 includes work from the study *“Surface Roughness Analysis and Prediction in Selective Laser Melting”,* (accepted to Journal of Materials Processing Technology, November 2011) by G. Strano, L. Hao, R.M. Everson and K.E. Evans.

Chapter 4 includes work from the *study "Surface Roughness Analysis in Selective Laser Melting",* 5th International Conference on Advanced Research in Virtual and Rapid

Prototyping, Leiria, Portugal, Sept 28-Oct 1,2011, by G. Strano, L. Hao, R.M. Everson and K.E. Evans.

Chapter 5 includes work from the study *"A new approach to the design and optimisation of support structures in additive manufacturing",* (accepted to International Journal of Advanced Manufacturing Technology, December 2011) by G. Strano, L. Hao, R.M. Everson and K.E. Evans.

Chapter 6 includes work from the study *"Multi-objective optimisation of surface quality, manufacturing time and support structures for Selective Laser Melting"* (to be submitted to International Journal of Machine Tools and Manufacture, June 2012), by G. Strano, L. Hao, R.M. Everson and K.E. Evans.

Giovanni Strano

A mia madre Nuccia e mio padre Orazio,

e

a mio zio Gianni

a cui il mio pensiero é sempre rivolto

Acknowledgments

I wish to express the most sincere gratitude to my supervisors, Dr. Liang Hao and Prof. Kenneth Evans, who always offered invaluable support and guidance, and the highest example of professionalism that I wish to match one day.

My deepest gratitude is also due to Dr. Richard Everson, for his assistance in all the aspects of the research project, for his mentoring, and for his presence that has immensely contributed to my personal and professional development during my time at the University of Exeter.

There are not words to describe my gratitude to Dr. Martin Jenkins, for which my mere expression of thanks likewise would not suffice; his good advice, support and friendship have always encouraged my fervent enthusiasm and devotion to this project, and will continue beyond this project into the future.

Finally, I would like to thank EADS Airbus and Great Western Research for having funded this research.

Nomenclature

List of common abbreviations

AM	Additive Manufacturing
ASCII	American Standard Code for Information Interchange
CAD	Computer Aided Design
CAO	Computer-Aided Optimization
EA	Evolutionary Algorithm
EBM	Electron Beam Melting
FDM	Fused Deposition Modelling
FSW	Friction Stir Welding
HIP	Hot Isostatic Pressing
HOBE	Honeycomb Before Expansion
LENS	Laser Engineering Net Shaping
LFW	Linear Friction Welding
MO	Multi-Objective
MOOP	Multi-objective Optimisation Problems
MCDM	Multi Criteria Decision Maker
MOEA	Multi-Objective Evolutionary Algorithm
MOGA	Multi-objective Genetic Algorithm
NPGA	Niched Pareto Genetic Algorithm
NSGA-II	Non-dominated Sorting Genetic Algorithm II
PEEK	Polyether Ether Ketone Polymers
SEM	Scanning Electron Microscope

SL/SLA	Stereolithography
SLM	Selective Laser Melting
SLS	Selective Laser Sintering
SPEA-2	Strength Pareto Evolutionary Approach
STL	Standard Tessellation Language

Greek

α surface inclination angle with respect to platform base

λ particle fraction in the model for surface roughness prediction

ρ density of deposited powder in SLS process

θ_x inclination angle of a part with respect to axis *x*

θ_y inclination angle of a part with respect to axis *y*

θ vector of parameters in a multi-objective optimisation problem

Latin

A_i area of i*th* facet in a triangulated geometry

C_p specific heat capacity

D number of objectives in a multi-objective optimisation problem

E_h calculated energy for preheating operations during the SLS of one part

E_s calculated energy for laser sintering during the SLS of one part

E_{tot} calculated total energy for manufacturing of one part using SLS process

h distance between consecutive step edges in a stepped surface profile

L_t layer thickness

l latent heat of fusion

N number of layers of a part to be fabricated

R_a calculated surface roughness of a part to be fabricated

R_i calculated surface roughness of the i*th* facet in a triangulated geometry

s_s laser scan spacing

T_{dep} time required to deposit a layer of material during the SLM process of one part

T_p time required for moving the platform down of one step during the SLM process of one part

T_s time required for sintering operations during the SLM process of one part

T_{tot} calculated total build time for the manufacturing of one part using SLM process

T_z time required for non sintering operations during the SLM process of one part

V volume of one part to be fabricated using SLS or SLM process

V_s volume of support structures for one part to be fabricated using SLM process

v_s laser beam speed

W step width in a stepped surface

1. Introduction

1.1 Research background and rationale

1.1.1 Criteria and complexity in additive manufacturing

Additive Manufacturing (AM) allows the automatic construction of physical objects using a solid freeform fabrication process, by sequential "layer by layer" fusing or sintering of material with focused and localised material consolidation mechanisms, for instance, laser sintering and melting of powder materials to form three dimensional (3D) objects. This technology has demonstrated great potential to advance design and manufacturing and has shown higher flexibility than conventional manufacturing techniques for the production of small volume, complex and customised parts.

AM technology was traditionally used for prototyping purposes, but in recent years there has been a trend to use AM technology for small to medium volume production of high value parts. Nevertheless, some issues affect the process efficiency of AM technologies such as Selective Laser Sintering (SLS) and Melting (SLM), thus limiting their adoption as standard manufacturing processes for industrial production applications.

The surface quality of AM parts is generally poor when compared to conventional manufacturing techniques. This can have drastic consequences for the use of functional components, parts with high roughness will wear more quickly and they have higher friction coefficients. Roughness may also facilitate nucleation sites for cracks or

corrosion. Costs for refining the surface finish of complex components are very high since the polishing of these surface needs to be carried out manually due to the limited accessibility to the surfaces.

These limitations can be reduced by a robust roughness prediction approach to support the decision on optimal processing conditions during the process planning stage.

The mechanism governing the roughness of AM parts formed by SLS and SLM is a complex phenomenon to study; it is greatly influenced by part build orientation, but also by the combination of process parameters such as laser power, layer thickness, beam speed and hatch spacing. It is generally hard to distinguish the contribution that each single factor contributed, as a level of probability, and thus makes it difficult to model the dynamics of formation of surface roughness.

Some key AM technologies require the presence of support structures for the production of overhanging parts. These include Stereolithography (SLA) and Fused Deposition Modelling (FDM) for plastic part fabrication and SLM and Electron Beam Melting (EBM) for metal part fabrication. Support structures represent a serious issue for the manufacturing of complex shape components, particularly for metal parts; supports have to be removed by hand for each single manufactured object, and depending on the geometry complexity, the removal of some supports can be impossible or very time (and resources) consuming. As a consequence, the presence of supports increases the need for post-processing and tooling in the AM process. After the support removal, every surface that was supported presents a deteriorated surface quality, thus requiring additional surface refining operations.

Furthermore, supports are built of the same material of the part, and being sacrificial parts, they represent a process waste; an optimal design of support structures can significantly improve the overall AM process efficiency. Reducing the amount and

volume of the support structures allows considerable saving of the part manufacturing costs in terms of material, time and energy. This is particularly true for aerospace parts made from high-value metal alloys, such as titanium.

Higher process efficiency could be achieved by the minimisation of manufacturing time; this is particularly important at present, for powder based laser AM techniques such as SLS and SLM as very fine layer thickness is used in these processes. It can take a long time, from one to a few days, to build one single product, not including the time to be spent for support removal and surface refining. One of the main factors that affects the build time is the total number of layers to be sintered; this is proportional to the object's height which is determined by its orientation. Part build orientation also has a major influence on the amount of energy needed for SLS production. During the SLS process, preheating operations are required before the layer is sintered by laser, in order to minimize the amount of laser energy required for powder sintering, which thus minimises warping of the sintered layers. The amount of energy used for powder preheating is proportional to the number of sintered layers, and hence is directly influenced by the build orientation of the part.

Clearly there is significant complexity in the simultaneous optimisation and trade-off of contrasting performance and cost objectives for enhancing overall quality and process efficiency of AM production, such as surface quality, minimum support structures, build time and energy required for manufacturing. Most decisions on AM production still rely entirely on operator experience and for most cases the technology capability and economic benefits of AM production are not fully exploited, restricting the industrial implementation of Additive Manufacturing.

1.1.2 Multi-objective optimisation

The choice of optimal process parameters in AM generally needs a high level of expertise and experience from the machine operator. The choice of "wrong" process parameters such as part build orientation, or a non optimal design of support structures, can have drastic consequences on the performance of AM production, and more generally on the quality and sustainability of the manufacturing process.

AM production is normally used for making parts with complex geometry which necessitates the assessment of numerous processing options or choices. It is very hard for the decision makers to reach an optimal solution by purely relying on their own intuition or judgements. Very often, there is not a unique optimal solution to the problem, and it is necessary to explicitly evaluate multiple criteria; solving the problem means to choose the “most preferred” alternative from a set of possible choices. This scenario corresponds to Multi-objective (MO) optimisation problems, where there is a trade-off between two or more conflicting objectives such as profit or performance maximisation and cost minimisation.

Multi-objective optimisation problems can be found in various applications such as financial problems, product and process design, automotive and aircraft design. In a MO problem there will be many variables, or parameters of the optimisation problem, to obtain a solution to the problem. The performance of each solution is evaluated for each objective to be optimised. Considering a MO minimisation problem, it is desirable to have a small value for each objective. Once the solutions have been evaluated and mapped into the “objective space”, there will be some solutions that are wholly better than others. The solutions are called the “dominating” solutions; they have the property that, in moving from one solution to another, it is not possible to improve (minimise) one criterion without making the other criteria worse (bigger). This set of solutions is

known as a Pareto front, and it represents the optimal trade-offs between the competing objectives.

The aim of multi-objective optimisation is, given a number of objective functions, to evaluate the performance of each solution in each objective and, to find the optimal parameters that correspond to the members of the Pareto solutions. A wider overview of solutions methods and applications of MO is presented in Chapter 2.

Multi-objective optimisation can solve the multi-aspect complexity of the optimisation of additive manufacturing processes by providing support to the user, the MO decision support system providing guidance to achieve contrasting cost/performance objectives. The savings obtained create an impact on the diffusion of additive manufacturing technologies for industrial productions in high value industry sectors such as Aerospace.

1.2 Research objectives and contributions

1.2.1 Overall aim and objectives

This research aims to develop an effective decision support system to assist the AM operator in the choice of optimal parameters during the AM process planning stage for the efficient production of complicated parts.

The first objective of the research was to formulate accurate computational models for the prediction of surface roughness, build time, energy employed in the AM processes including Selective Laser Sintering (SLS) and Selective Laser Melting (SLM). The second objective of the research was to deliver simple, yet robust algorithms for the design of optimal support structures for SLM platforms. The third

objective was to develop a mathematical multi-objective optimisation technique to automatically determine the set of optimal trade-off part orientations that simultaneously achieved all the contrasting objectives. The technique used the predictive models to evaluate the performance objectives including surface quality, energy consumption and support structure minimisation which were typically contrasting and all greatly determined by the object's build orientation.

Hence, it was envisaged that an integrated computational prediction and optimisation tool could be derived to assist the operator in the "process planning" stage in order to achieve higher efficiency and sustainability through large savings of material, time and energy in AM.

1.2.2 Research methodology and development

This study adopted a mathematical modelling and multi-objective optimisation approach to determine the AM parameters required for the efficient production of complex parts.

New mathematical models have been developed to determine parts' surface roughness, estimated time and energy for manufacturing, and for the design of optimal cellular support structures. All the models have been formulated using data from literature and by experimental observations. Most of the models' validation has been performed through the manufacturing of samples by SLS and SLM platforms. Some of the developed models (i.e. surface roughness prediction, manufacturing time prediction, algorism of support structures for design) could be directly employed or easily adapted in other AM platforms.

1.2.3 Principal contributions

The main contributions of this research were:

- The development of a new computational methodology for the simultaneous optimisation of surface roughness and energy consumption in the SLS process. By determining the optimal trade-off set between the two objectives, known as the Pareto set, it provides a build orientation decision support system for SLS.

- To extend the use of prediction models that interpolate data from empirical observations, providing a phenomenological approach for the prediction of surface roughness. This overcomes limitations of classic models that derive surface roughness through geometrical considerations on the surface profile of the part.

- The formulation of computational models for SLS/SLM process performance in terms of required manufacturing time and energy.

- To derive a new model for accurate roughness prediction in SLM by considering the stair step effect and the presence of partially bonded particles on the top surface. It can achieve accurate roughness prediction for all the surface inclinations, where classic models fail.

- To derive a new algorithm for the generation and optimisation of support structures. The algorithm locates the building orientation requiring minimum support surfaces and then generates the support cellular structure for the optimal orientation. Furthermore, it uses a microstructure generation module for the easy

design and optimisation of tailored cellular structures which can provide a more robust support where the weight is concentrated and less support elsewhere.

- To provide an integrated multi-objective optimisation solution to maximise the efficiency and sustainability of the SLM process, identifying optimal build orientation and provide the best trade-off between contrasting performance objectives such as surface quality, minimum support structures and build time.

1.3 Thesis overview

Chapter 2 reviews the state of the art of advanced material structures and AM technology and introduces the multi-objective optimisation techniques. Advanced material structures such as cellular structures and complex shape components which can be developed by new topology optimisation shows great promise to save material and energy and enhance performance, especially for high value aerospace products but their manufacturing is constrained by the geometrical capability of conventional techniques. AM has emerged as an innovative technique capable of fabricating complex material structures and producing advanced aerospace products. It also discusses the current issues of AM techniques such as SLS, SLM, Laser Engineering Net Shaping (LENS), for production of aerospace (but also biomedical, automotive, consumer in general) parts. Within the scope of AM process optimisation, mathematical multi-objective optimisation is introduced and an overview of the main concepts and methods for conducting multi-objective optimisation is presented.

Chapter 3 focuses on the multi-objective optimisation of the SLS process and investigates a computational methodology for the simultaneous minimization of surface

roughness and energy consumption in the SLS process. It formulates prediction models for surface roughness and energy consumption objectives which are competing criteria and optimises their SLS build orientation of the parts as a key influential factor by locating the optimal trade-off set between these objectives. This research provides a consistent decision support system for the identification of optimal build orientations for SLS and presents its evaluation using two aerospace components. Overall, it describes the employment of a phenomenological model to predict the surface quality and the formation of an energy prediction model for SLS processed parts, which takes into consideration both the contribution of the energy required by the preheating operations and the energy required by the laser sintering.

Chapter 4 presents a multi-objective optimisation study for the SLM process to identify the best estimated trade-off between surface quality and build time. Firstly, it investigates the surface roughness and morphology of Steel 316L alloy parts made by SLM, using a surface profilometer and scanning electron microscope (SEM). Secondly, a new mathematical model is developed for the prediction of surface roughness. The model includes the presence of particles on top surfaces, in addition to the stair step effect, for the accurate prediction of surface roughness, avoiding the failure of the classic roughness prediction model which purely considers geometrical stair step profile. With the formulation of a build time prediction model, the chapter presents a computational technology to produce complete Pareto solutions set for the definition of an optimal part orientation for the minimization of build time and surface roughness, ensuring surface quality and, simultaneously, total process time saving.

In Chapter 5 a new approach is developed to design optimal support structures in metallic AM including SLM through defining best part build orientation and generating cellular support structures. This approach applies a new optimisation algorithm to use pure mathematical 3D implicit functions for the generation of the material efficient

cellular support structures, including graded supports. The implicit function approach for support structure design allows geometries to be simply designed by pure mathematical expressions and therefore easily defines and optimises different cellular structures, in particular to have graded structures providing more robust support where the object's weight is concentrated, and less support elsewhere. This new approach is promising to achieve significant materials savings for complex geometrical parts, thus increasing the sustainability and efficiency of metallic AM.

Chapter 6 presents the development of an integrated decision support system which utilises a multi-objective optimisation approach to analyse SLM production and determine comprehensive optimal parameters for production of complex shape metal parts. It implements the mathematical prediction models for surface roughness, build time, and the algorithms for designing cellular support structures. The multi-objective optimisation algorithms are employed to determine the optimal trade-offs between these conflicting objectives. This new development provides an effective tool to set up optimal SLM production parameters for enhanced manufacturing efficiency and sustainability through material, time and energy savings.

Chapter 7 discuss the outcomes of the research project has achieved, and the benefits introduced by the study developed. Furthermore a discussion on possible future developments is presented.

2. Background

This chapter reviews the state of the art of advanced material structures and AM technology such as cellular structures and complex shape components. AM is introduced as an innovative technique to fabricate complex material structures, and capable of expanding the limits of conventional manufacturing for the production of complex shape parts. The Chapter furthermore discusses the current issues of AM techniques such as SLS, SLM, Laser Engineering Net Shaping (LENS), for the production of aerospace (but also biomedical, automotive, consumer in general) parts.

The chapter presents an overview on the application of multi-objective optimisation for design and manufacturing processes.

Furthermore, the main concepts of mathematical multi-objective optimisation are introduced and an overview of the main concepts and methods for conducting mathematical multi-objective optimisation is discussed.

2.1 Advanced material structures in aerospace

In this section an overview on the principal material structures for lightweight applications in Aerospace is presented.

2.1.1 Aerospace materials and lightweight applications

There is an enormous choice of materials available in aerospace engineering nowadays, varying with applications, design and manufacturing. One of the keyword characteristics of aerospace functional components is lightness; even a small amount of weight saved might allow for more payload and reduce considerable fuel consumption over the operational life of an aircraft.

There has been a considerable evolution in the design of lightweight components, made possible through progress in the field of material science and manufacturing technologies in the last couple of decades. One major category of lightweight aerospace material is metal alloys, the most widespread being, aluminium, steel and titanium alloys. Aluminium alloys have a relative high strength to weight ratio, and are easy to work; they can be used in all the structural applications where, for instance, rather than pure strength, a resistance to buckling is needed, such as in wing skins. When high local strength is required (such as in wing lugs, engine mountings, join plates, door latches, bolts), the use of steel alloys is preferred. Initially steel was combined with other materials (such as aluminium) to produce structural parts, but due to the corrosion problems, and improvements in titanium and aluminium alloys, the amount of steel used in aerospace has been gradually reduced (Cutler and Liber 2005). Nevertheless, steel has better fatigue resistance than aluminium in those applications where constant pressurizations and depressurizations, temperature changes and stresses induced by vibrations can cause failure; also it is less susceptible than aluminium to the effect of notching that can propagate into cracks. Titanium alloys weight is typically between aluminium and steel alloys and, having excellent strength and resistance to corrosion even at high temperatures, is thus suitable for specialized pieces of structures close to the engine jet efflux. Despite its good mechanical proprieties, titanium is relatively difficult to refine and work, therefore very expensive.

In general, the design approach to lightweight metal alloys can vary significantly depending upon the required strength and temperature operational range of a given assembly. For structures which operate up to approximately 200° C, aluminium alloys can be effective in terms of moderate strength and weight, conventional titanium alloys are preferred at temperature up to 1000° C, due to higher temperature resistance and density; at higher temperatures, the strength and stability requirements imply the use of

even higher density super-alloys based on nickel, cobalt or iron (Ott 2002). As a result, the design and manufacture of lightweight components for extreme conditions of service (such as high temperature, low pressures) are compromised by the high alloy material densities.

To reduce weight, in many cases aircraft structures are made by polymer composite materials. A composite material consists of a construction of strands of strong fibers stuck together with an adhesive (resin or matrix). For military and commercial aircraft in the 21st century, composites are mostly used in the form of uni-directional tapes, were the straight fibre strands are all laid side by side and run in the same direction like a ribbon. These are supplied with a measured quantity of resin already squeezed around the fibers and are referred to as pre-preg (for pre-impregnated). Examples of the use of pre-preg materials can be seen in the wings and forward fuselage of the AV-8B Harrier II and the tail planes of the Airbus A-320. More recently, composite materials are being used extensively in combat aircraft like the Eurofighter Typhoon and Saab Grippen, in Helicopter structures and rotor blades and in fairing and control surface of airliners (Cutler and Liber 2005). Unlike metals, which have virtually the same strength in all directions, composites, such as a tape, have a different behavior depending of the applied force direction; it is much stronger when pulled in the direction of the fibers (longitudinal direction) than when pulled to the side (transverse direction). In many structures the loads are predominantly in one direction, so the designer can place most of his fibers in that same direction to maximise strength and minimize weight.

2.1.2 Lightweight structure components with complex and optimal geometries

Optimised lightweight components typically have high shape complexity; this makes their manufacturing more challenging, particularly by conventional methods. Complex shape geometries are typically generated by the so called "Topology Optimisation" process. Topology optimisation is a mathematical method that solves the problem of finding the best distribution of material, to achieve one or more desired proprieties (such as low weight under or high resistance) to specific loading conditions, and/or constraints on volume. A complete structural optimization study implies topology, shape and sizing optimization of the object; Figure 2.1 summarizes the main differences among the three types of optimisation.

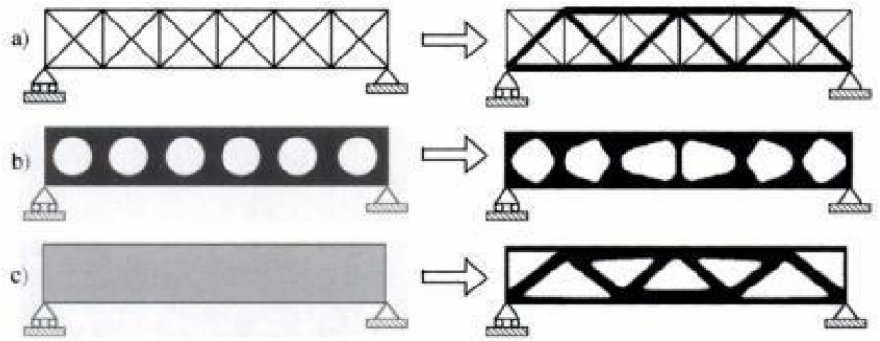

Figure 2.1. Initial design and result in a) sizing optimization; b) shape optimization; c) topology optimization (Bensoe and Sigmund 2003).

The criteria for structural optimality can be various, examples include Fully Stressed Design, the condition where all the elements within a design utilize their full strength; Minimum Compliance, minimizes the ease with which a structure may be deformed or

Minimum Weight, given a loading condition the design that has the least self weight. Many techniques have been developed for topology optimization, some of them are the *Homogenization Method* (Bendsoe and Kikuchi 1988), *Solid Isotropic Material with Penalization (SIMP)* (Bendsoe and Sigmund 2003), *Evolutionary Structural Optimization (ESO)* (Xie and Steven 1993).

As an illustrative example, a case studied run by (Xie et al. 2005) using the ESO method, uses the evolutionary design method to solve topology structural optimization, size, shape problems for static, dynamic, stability and heat transfer problems or a combination of these. In this method, an optimal topology is generated systematically by removing the material from the structure depending on the Von Mises stress or strain energy value of the single element of the entire domain. Each iteration includes a finite element analysis. The method stops when a predefined structural volume is reached. The element efficiency evaluated from sensitivity analysis is used as an index for the determination of the element detection.

For example, to achieve an optimum compression-only structure, elements with the highest tensile stresses will be removed first. Then the less compressive elements will be deleted from the structure as well. Figure 2.2 shows the optimization of a structure under gravity loading evolving in to structures which are predominantly in compression.

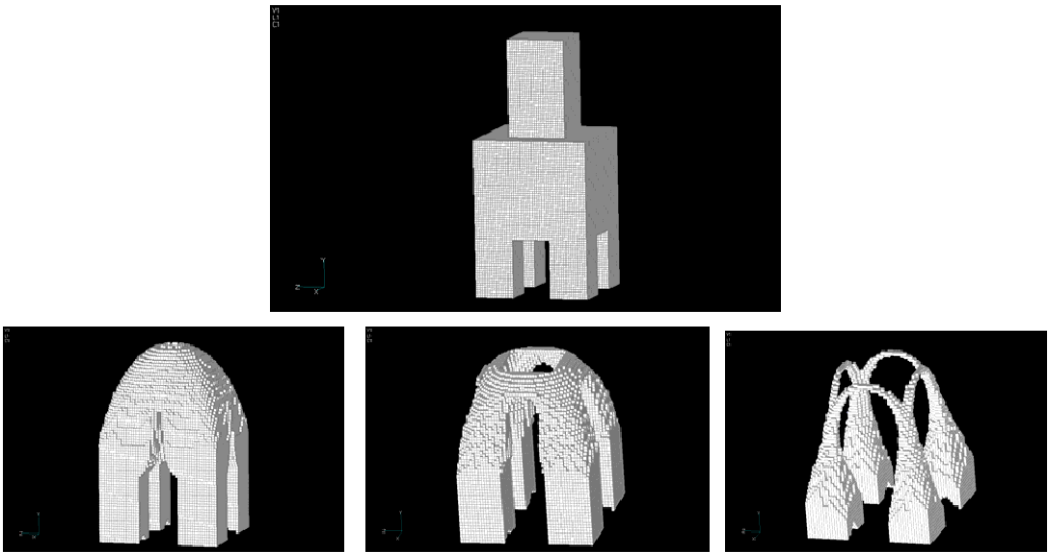

Figure 2.2. Example of topology optimisation for compression-only structure through ESO. Initial design (top) and final solution through three consecutive steps (Xie et al. 2005).

As discussed, the optimised geometries usually have a complex shape, and their manufacturing could be onerous by conventional manufacturing techniques. To give a further example, shown in Figure 2.3 is a complex shape part resulting from topology optimisation of engine nacelle hinges for A320 airliners. Results from topology optimisation have shown the final hinges to have their weight reduced by up to 60%, but providing the same strength and fatigue endurance of the original full dense part (Tomlin and Meyer 2011).

Figure 2.3. Original and optimised engine nacelle hinges for A320 airliners (Tomlin and Meyer 2011).

2.1.3. Lightweight cellular structures

Alternate structure approaches are required in order to further reduce the weight of traditional material structures; these materials have been referred to as cellular materials, also termed lattice structures. Some examples of traditional lightweight structures design are honeycombs, sandwich panels and truss structures. Honeycombs structures are an example of very light-efficient bio-inspired structures (Figure 2.4).

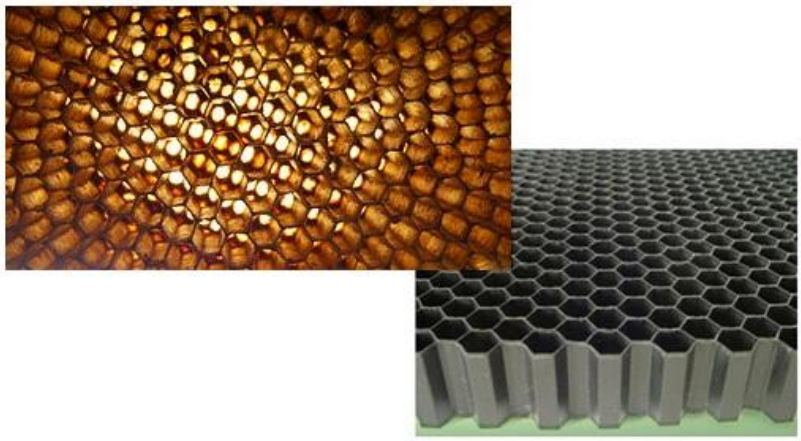

Figure 2.4. Hexagonal honeycomb, example of lightweight bio inspired structure (adapted from (Hoyland 2007) and (Trego 2010)).

They require complicated fabrication methods, especially to form them into non-planar shapes. Honeycomb cores are directional with regard to mechanical proprieties and their design must take this into consideration to take best advantage of them. Strength and stiffness (compression and shear) are proportional to honeycomb density; a large cell size can also produce a patterned outer surface of the panel, while a smaller cell size provides greater bonding area and better appearance, but higher costs. The heat transfer through the sandwich depends upon material core, metallic cores typically maximise

heat the flow characteristic. However, the close nature of the porosity in a honeycomb sandwich can trap moisture leading to corrosion (Hexweb 2000).

Three dimensional truss structures provide significant improvements in shear strength compared to honeycomb structures; furthermore the open cell core nature of truss panels allows fluids to pass through them, facilitating the heat flux exchange (Sypeck 2005). Panels of trusses such as the ones illustrated in Figure 2.5, have been produced from aluminium, steel and titanium, as well as for other non-metallic materials (Wallach and Gibson 2001; Li et al. 2008).

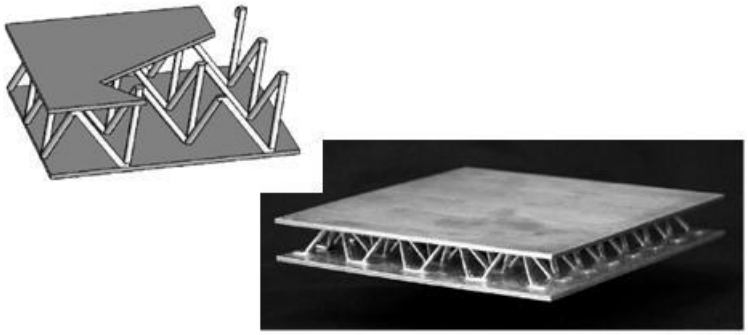

Figure 2.5. Example of 3D trusses flat panel (Wadley 2006).

The mechanical behaviour and the structure topology optimisation of truss structures have been investigated in a number of studies, typically referring to flat panel configurations under relatively simple loading conditions (Wallach and Gibson 2001).

2.1.4 Conventional manufacturing of complex aerospace components

Conventional manufacturing of metal parts can be accomplished by a large variety of processes, including casting, machining, forging, forming, joining and assembly. Beyond the choice of a specific manufacturing process, there is the desire to achieve a final functional part, at lowest possible costs of materials, time, and energy employed in the manufacturing. Considerable costs in manufacturing are represented by the necessity for machining, due to the quantity of material removed and scrapped; achieving near-net-shape quality parts, reduces the manufacturing costs, but also the energy and emissions associated with production and recycling of waste material.

Conventional processes such as casting or moulding, have been employed for centuries and they are still employed for the production of complex shape parts, otherwise difficult or uneconomical to make by other methods (Black and Kohser 2008). In a casting process a liquid is typically poured or injected into a preformed mould (or die), allowed to solidify (usually by cooling, but sometimes by heating or chemical curing), and then removed from the mould. Sometimes the mould is disposable (e.g. sand, ceramic) and then destroyed during removal of the formed part. One of the limitations of casting is the necessity for mould tools. Subtractive machining is used to obtain specific features into preformed blanks, by manipulating a fast-moving cutting tool relative to the work piece on a computer-controlled machine tool, such as lathe, mill, or grinder. The process limitations are the material waste, and the wear and tear of the machine tool. Another conventional technology used for manufacturing of near-net-shape parts is the Hot Isostatic Pressing (HIP). The process subjects the part to both elevated temperature and isostatic gas pressure from all directions, in a high pressure containment vessel. The pressurizing gas is inert (typically argon), so that the material does not chemically react. When castings are treated with HIP, the application

of heat and pressure eliminates internal voids and microporosity; this process also improves the fatigue resistance of a component. Alternatively, near-net-shape parts can be manufactured by Linear Friction Welding (LFW). In this process heat is generated through mechanical friction between a moving workpiece and a stationary component. Since no melt occurs, friction welding is not actually a welding process in the traditional sense, but a forging technique. Friction welding techniques are generally melt-free, this avoids grain growth in engineering materials. Also another advantage is that the motion tends to "clean" the surface between the materials being welded, which means they can be joined with less preparation. Also, friction welding allows dissimilar materials to be joined, this feature is particularly useful in aerospace structures, where aluminium alloys and Steel can be joined efficiently, otherwise impossible without using mechanical connections, due to the difference of melting point between the two materials. On the other hand, equipment costs can be high, and production is limited to relatively small and simple parts. A more affordable process is Friction Stir Welding (FSW); in the process a cylindrical-shouldered tool, with a profiled probe (nib or pin) is rotated at a constant speed and fed at a constant traverse rate into the joint line between two pieces of sheet or plate material, which are butted together. Frictional heat is generated between the wear-resistant welding tool, and the work pieces. The heat is such as to cause the stirred materials to soften without reaching the melting point, allowing the traversing of the tool along the weld line in a plasticised tubular shaft of metal. The process is slower than LFW; and the weld properties and process reliability are not fully understood, being a relative novel technology (Wiesner and Norris 2007).

2.1.5 Conventional manufacturing of lightweight cellular structures

Traditionally, there are two different methods to manufacture honeycomb cores, the expansion process and the corrugation process. In the expansion process, flat sheet of material such as an aluminium alloy, are cut from a roll on a rotating drum; the sheets are placed on top of each other, bent as desired and selectively bonded at alternate strips. These operations produce the so called HOBE (HOneycomb Before Expansion) block. To obtain the desired honeycomb cell configurations, the HOBE block is pulled apart to expand (Figure 2.6). The expansion requires high inter-sheets bond strengths, to allow sheet stretching; for low density honeycombs with thin sheets, the required bond strength is achievable with adhesives or by laser welding (Bitzer 1997).

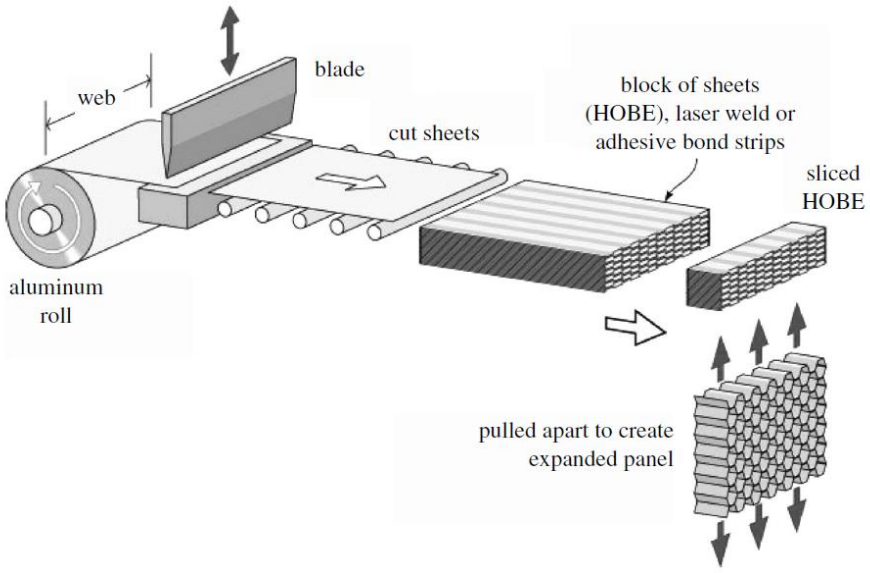

Figure 2.6. Expansion-manufacturing process for honeycomb cores (Wadley 2006).

However, as the sheet thickness increases, the manufacture of honeycombs requires the corrugation process in which the sheet is first corrugated, and then stacked. The sheets are adhesively bonded or welded together to form a block which is then sliced to the desired thickness (Figure 2.7). This process is considered to be more laborious in

comparison to the expansion-manufacturing approach, because the process of corrugating and stacking sheets requires more steps and time.

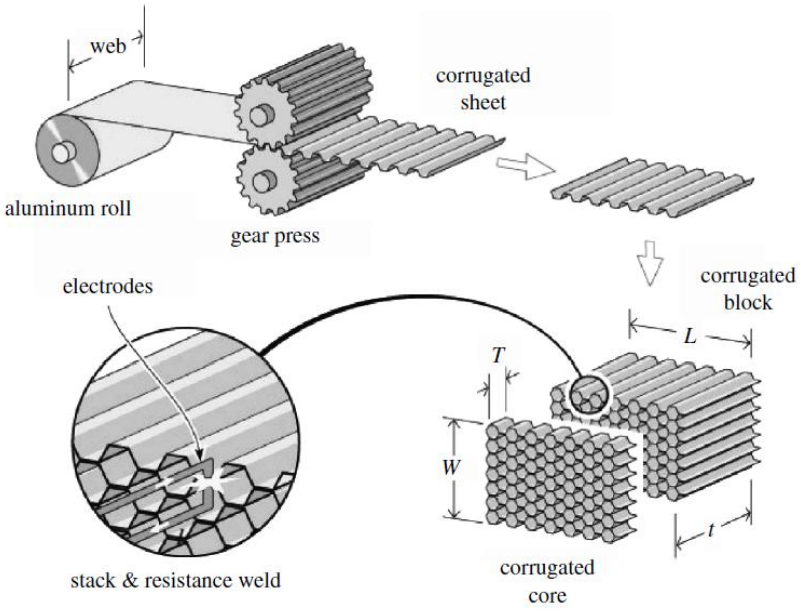

Figure 2.7. Corrugation-manufacturing process for honeycomb cores (Wadley 2006).

The consecutive step to the honeycomb core manufacturing is to attach a top and bottom sheet layer to produce the sandwich panel. Sandwich panels might be produced using three alternative well-established methods (Hexweb 2000): Heated Press, generally used for the production of flat panels; Vacuum Bag Processing, used for curved and complex form panels; Matched Mould Processing, used generally for batch production of finished panels. The Heated Press method simply applies a layer of adhesive film between the honeycomb core and the facing skin material, as represented in Figure 2.8.

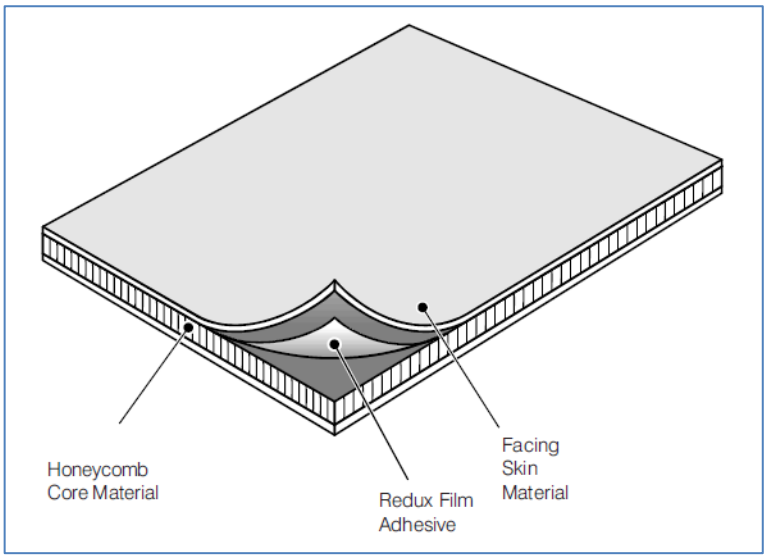

Figure 2.8. Heated press assembly for honeycombs panel (Hexweb 2000).

In the Vacuum Bag Process, the necessary consolidation is obtained using a vacuum, and curing in an oven Figure 2.9.

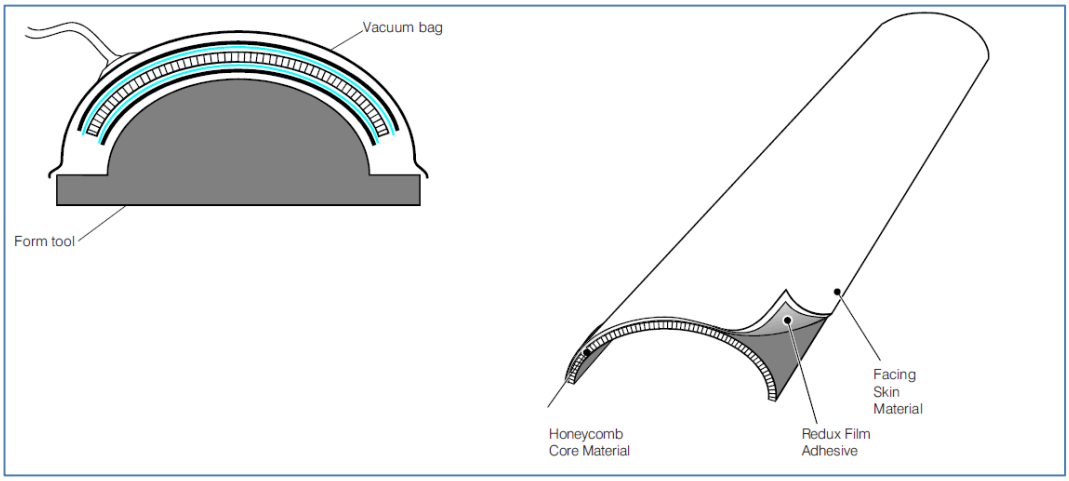

Figure 2.9. Vacuum Bag Processing assembly for honeycombs panel (Hexweb 2000).

The Match Moulding Process achieves higher levels of tolerance and surface finish. The heat and pressure are typically applied through heated tools with external mechanical pressure or non-heated tools placed in a press. Using a room temperature curing

adhesive cold bonding may be considered if the sandwich construction is too large to be processed using the above methods, or if heating equipment is unavailable (Figure 2.10).

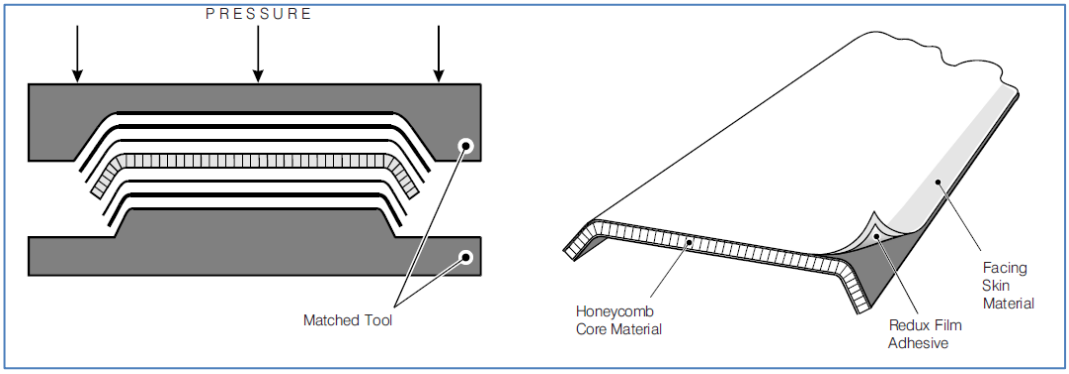

Figure 2.10. Match Mould Processing assembly for honeycombs panel (Hexweb 2000).

Truss structures can be manufactured in a number of different ways. One way is to fold perforated metal sheets in such a way that alternate nodes are displaced in and out of the sheet plane as represented in Figure 2.11 (Sypeck 2005).

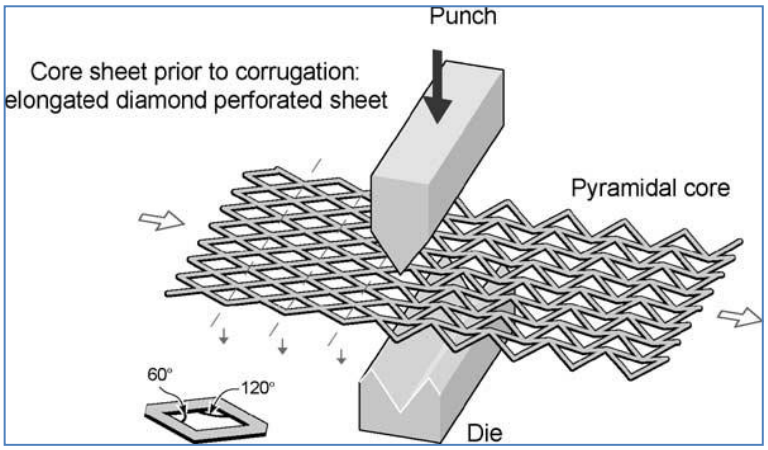

Figure 2.11. Illustration of the folding operation used to create the single layer pyramidal truss sandwich structures (Sypeck 2005).

When low density lattices are fabricated, this method produces a considerable waste of material during the perforation, therefore increasing the manufacturing cost. Cellular structures can be made from these metal structures by simply stacking and bonding layer of trusses panel (Figure 2.12) .

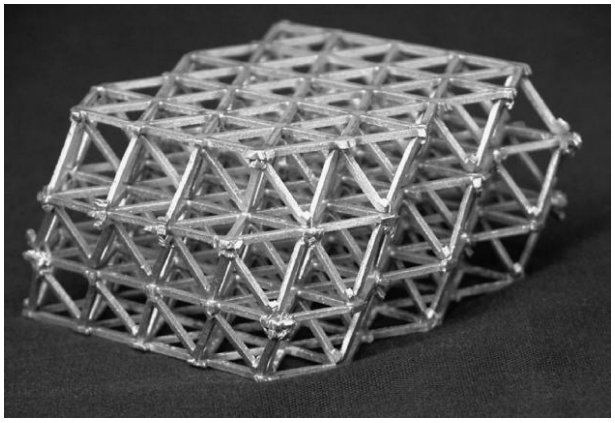

Figure 2.12. Example of multilayer tetrahedral structure manufactured through folded perforated aluminium sheets (Wadley 2006)

Alternatively, lattice truss structures can be fabricated by a wire layup process followed by transient liquid phase bonding or node fusion welding. Wire spacing and orientation is done by laying down collinear wires and to alternate the direction of successive layers (Figure 2.13). This approach maintains a good cell alignment throughout the structure at low densities.

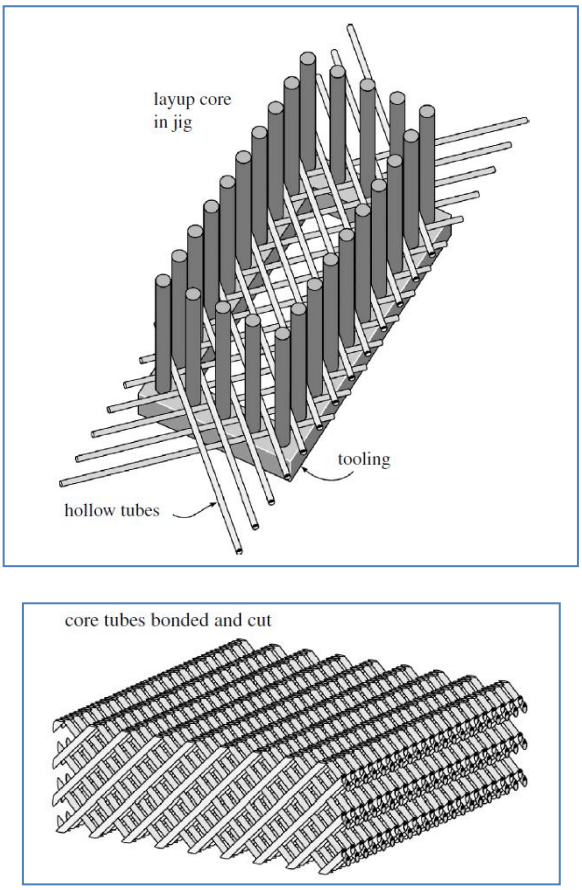

Figure 2.13. Collinear wires deposited in alternate direction (left), and core structure by bonded and cut wires (right) (Wadley 2006).

In order to bond the core structure with the top and bottom plate to produce a sandwich panel, several processes can be used such us laser, friction stir, electrical resistance and many other common welding methods; for Ti6Al4V alloy for instance, by applying a pressure of 5-10 Mpa to each of the truss face sheet nodes while panels are held at 850-930 °C (Wadley 2006).

These techniques produce efficient manufacturing of sandwich panels with relative low density, however very often higher density, non-planar complex shape structures are required and for the production of those parts, investment casting is best used.

Investment casting begins with the creation of a wax or polymer pattern of the lattice truss structure and face sheets typically made by injection moulding. The structure is coated with ceramic casting slurry, the pattern is then removed and the empty (negative) mould filled with liquid metal. After solidification the ceramic is removed, and the component is inspected to ensure that complete liquid metal infiltration has occurred and that casting porosity has not compromised structural integrity (Wadley 2006). The most significant constraint relates to the manufacturing of large thin wall structures. A NASA study (Ott 2002) has examined three-dimensional truss blocks as an alternative to bulk, fully dense, high-temperature static structures due to their strength, stiffness, and reduced weight, for aircraft gas turbine engines. The study evaluated Alloy 718 and MarM247 panels in order to identify potential defects produced by the casting process that may lead defects in the structure, shown in Figure 2.14.

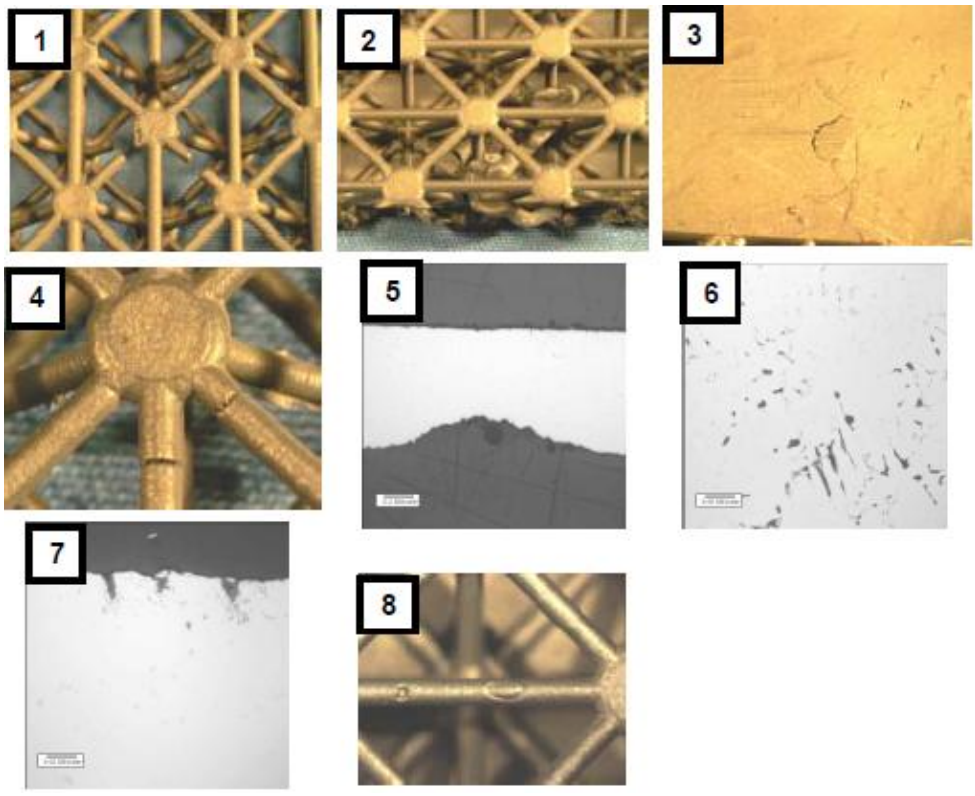

Figure 2.14. Possible defects in truss cells produced by casting (Ott 2002).

The defects depicted in Figure 2.14, are missing ligament sections (1), face sheet cracking (3), partial fill in face sheet (5), partial fill of truss ligaments (8) and may be due to inadequate fill and feeding during the casting process or a low pour temperature. Temperature can also affect metal-mold interaction (7) in casting surfaces adjacent to the mould. Local mould failure and leakage can lead to residual cast metal (2) within ligaments intersects. Porosity (6), which can be generated by inadequate feeding, can be responsible for the formation of ligament cracking (4).

2.2 Additive Manufacturing

This section introduce Additive Manufacturing as an innovative technique to fabricate complex material structures; the section introduces the current issues of AM techniques such as SLS, SLM, Laser Engineering Net Shaping (LENS), for production of aerospace (but also biomedical, automotive, consumer in general) parts.

2.2.1 Introduction to Additive Manufacturing

Additive Manufacturing (AM) allows the automatic construction of physical objects using solid freeform fabrication, by sequential "layer by layer" deposition of material utilising focused energy, often a laser. This technology has demonstrated great potential to advance design and manufacture and has demonstrated higher flexibility than conventional manufacturing techniques for the production of purpose made and customised parts. AM provides a more flexible way to produce objects. Starting from a sketch design, a CAD model of the object is then built through the use of a computer package, and sent to the AM platform to produce the artefacts in a few hours. This method, in comparison with conventional manufacturing techniques, enables an enormous amount of time to be saved in the design development cycle, since the production of prototypes enhances the assessment of object quality and characteristics in a quicker and more efficient way, than if only a drawing was used. Additive manufacturing technology was traditionally used for prototyping purposes, but recently there has been a trend to use AM technology for the production of parts. Following, an overview of the common features of AM is presented, from the initial design step to aspects related to part fabrication.

2.2.2 Technical aspects of Additive Manufacturing

The AM production of parts starts with a definition of the part geometry in a CAD model, afterwards converted into a compatible data format for the AM machine software as for example the STL (Standard Tessellation Language) format. This data format is used to create a mesh of the internal and external surfaces of the piece using basic geometrical elements like triangles. Some problems can arise with the STL file format as it does not contain topological data and many CAD vendors use tessellation algorithms that are not robust. Consequently, they tend to create polygonal approximation models which exhibit gaps (cracks, holes, punctures), inconsistent and/or incorrect normals, incorrect intersections, and facet degeneracy (Noorani 2006).

The STL file is then sent to the machine for the next operations such as orientation selection, support generation and slicing. Orientation allows choosing the optimal "growing" direction for the piece, which affects geometrical accuracy, surface finish, anisotropic properties, and time and costs of production. Some AM technologies (such as Selective Laser Melting (SLM), Electron Beam Melting (EBM) and Stereolithography (SL)) require the presence of support structure to sustain overhanging parts. After the object is built, the supports are sacrificed, thus they represent a waste of material, time and energy. Manufacturing costs of parts made by high-value metal alloys, such as titanium, can be reduced by minimising the volume of the supports. Also, the presence of support structures influences directly the complexity of post-manufacturing operations; minimising the volume of support can shorten this operation, thus improving process efficiency. Slicing is a critical stage; it can produce constant thickness layers, or adaptive thickness layers depending on the surface curvature. Adaptive slicing is most used in order to reduce the staircase effect of the surface as well as part fabrication time.

Following data preparation stages, the parts are fabricated in AM machines, and if necessary the parts are subjected to post-processing that consists of part removal, support removal, cleaning, post-curing and finishing. This step generally involves manual operations where an operator does the post-processing with extreme care. Otherwise, the part may be damaged and may need to be manufactured again (Noorani 2006).

2.2.3 AM for aerospace and defence applications

The aerospace industry has always been an active supporter of AM methodologies because parts for aircraft are normally made in small quantities and often complex to meet stringent requirements. Costs generally secondary to function. This is essentially the definition of a high value-added application - which is exactly the type of application that AM is most appropriate for at present. Minimizing weight, in order to save fuel cost, fly faster and more sustainably, and increasing payload are some of the most recurrent objectives of the Aerospace industry.

The SLS process has been used by Boeing Co. in their programme "Production on Demand" to produce air ducting (Figure 2.15) for the aerospace industry within hours (Levy et al. 2003).

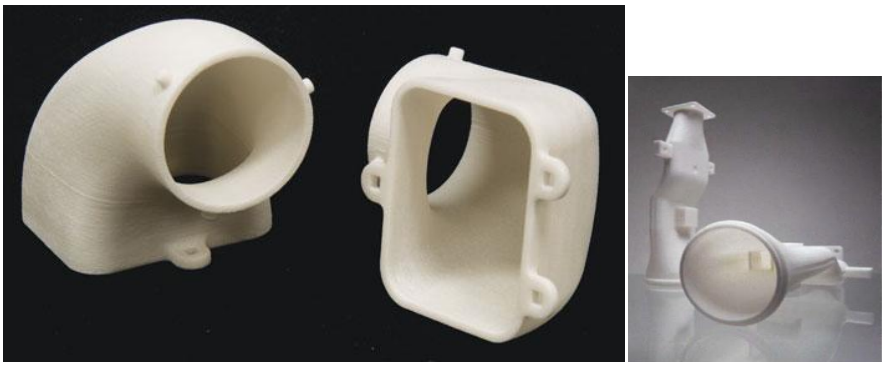

Figure 2.15. Direct production of air ducts (3DSystems 2012).

A significant area of interest is to be able using the AM process to fabricate jet engine components. For example, turbine blades have complex shapes and must meet extremely stringent performance specifications. Laser Engineered Net Shaping (LENS) technology can be used to improve blade finishes and repair damaged parts as shown in Figure 2.16. Furthermore, laser powder forming technologies can fabricate sensors within blades (Good 2007). Sensor integration in composite structures can be used to instruct smart devices on how to adjust the structure to improve performance and/or attenuate a detrimental loading condition and provide structural maintenance information. Sensors and electronic systems could also be embedded to provide remote monitoring of vehicle component condition and engine health (CastleIslandCo. 2011).

An “agile” rapid manufacture for low volume and rapid evolving design objects and repairing of “un-reparable” or delicate parts can be delivered through the LENS process at reduced cost (Hedges and Calder). LENS has been proposed for the production of wheels for tracked vehicles such as tanks with complex hollow features that optimize weight and inertia. The Mobile Parts Hospital (MPH) concept, as was deployed in a Iraq war could conceivably use LENS, three dimensional scanning and CNC equipment together to make replacement parts right at the point of action. The MPH compensates for the fact that much military equipment is as much as 40 years old or may have come from manufacturers that are no longer in business. Future versions of the MPH are being evaluated that will use LENS technology from Optomec to make fully-dense parts.

Figure 2.16. T700 Blisk leading edge repaired through LENS technology (Optomec 2012).

In many cases, for the production of functional components, such as parts for airframes, AM is employed to build complex freeform shapes with low mass, but sufficient load-bearing efficiencies. Great weight saving can be achieved through structural topology optimisation of the functional parts for AM. The topology optimisation of continuum structures is able to identify the best distribution of material, in order to achieve one or more desired proprieties at the same time, such as low weight or high resistance to specific loading conditions and/or constraints on volume. Recently, it has been shown to potentially allow up to 60% weight reduction in the production of steel and titanium engine nacelle hinges for A320 airliners as visible in Figure 2.17, ensuring the same strength and fatigue endurance when compared with the original full dense part (Tomlin and Meyer 2011).

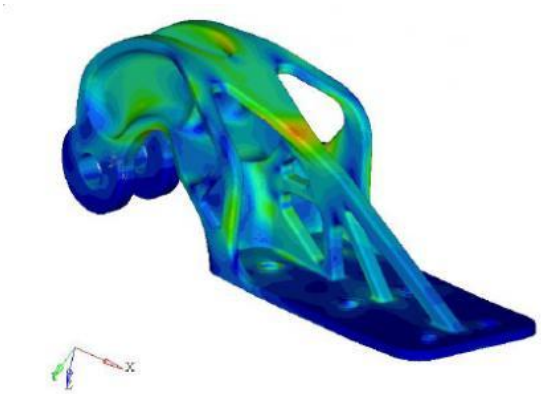

Figure 2.17. Optimised engine nacelle hinges for A320 airliners (Tomlin and Meyer 2011).

Furthermore, structural members of aircraft could be optimized for the requirements of a particular structure, or even a specific location within that structure. In (Rotheroe 2005) for instance, a family of internally-reinforced structural components with high strength-to-weight ratio (Figure 2.18), which would be manufactured using additive fabrication was described. Their external shape and internal geometry would be manufactured according to specific building requirements.

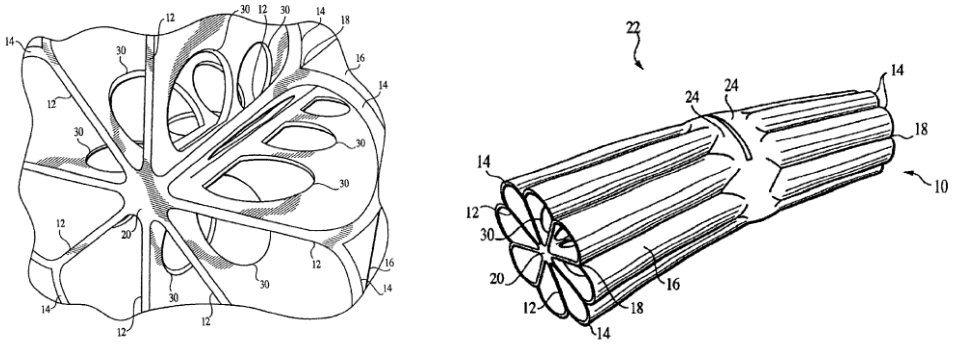

Figure 2.18. Aligned composite structures made by an FDM like process and example of structural architecture components (Rotheroe 2005).

Finally, in many cases military applications of AM can be expected to be either parallel with, or take advantage of their counterparts in the civilian world. For example, custom seats for aircraft, custom helmets and goggles, may all be adapted from ongoing military work to the automotive and sports sectors. Civilian versions might someday be used to make parts for such remotely-located machinery applications as oil rigs and mines.

2.2.4 State of art of main AM processes for aerospace applications

There are more than 25 different additive manufacturing techniques available, of which 70% are based on the application of a laser (Pera and Marinsek 1992). One way to classify AM systems, is by the initial form of its material, i.e. the material that the part is built from. In this manner, all ALM systems can be categorized into either liquid-based, solid-based or powder-based. A description of the most widely used technologies used in the production of functional components for the aerospace industry is now presented. They are *Selective Laser Sintering (SLS), Selective Laser Melting (SLM), Laser Engineering Net Shaping (LENS), and Electron Beam Melting (EBM).*

Selective Laser Sintering (SLS)

SLS uses a high power laser to fuse small particles of plastic, metal, or ceramic powder. After one cross-section is scanned, the powder bed is lowered by one layer thickness; the elevator is moved down (typically 0.02 mm - 0.1 mm). A new layer of material is deposited. The process is repeated until the part is completed. An inert atmosphere (nitrogen or argon) in the chamber is required to avoid oxidation. Figure 2.19 illustrates the main components of a SLS system.

Table 2.1 shows the polymer materials currently used for this process and their mechanical properties (3Dproparts, 2012).

	DuraForm® PA	DuraForm® EX	DuraForm® GF	DuraForm® HST	Injection Molded ABS	Injection Molded Polypropylene	Injection Molded Glass Reinforced Polypropylene
Material Details							
Description	Engineering Thermoplastic	Engineering Thermoplastic	Glass Bead-Filled Engineering Thermoplastic	Mineral Fiber-Reinforced Engineering Thermoplastic	General Purpose (Typical Values)	General Purpose (Typical Values)	20% Glass Fiber Reinforced (Typical Values)
Features	Excellent mechanical properties and surface finish	Exceptional toughness & impact resistance	Improved stiffness and thermal resistance	Best stiffness and thermal resistance	N/A	N/A	N/A
Stiffness							
Tensile Modulus (D638)	1586 MPa (230 ksi)	1517 MPa (220 ksi)	4068 MPa (590 ksi)	5643 MPa (818 ksi)	2340 MPa (339 ksi)	1780 MPa (258 ksi)	4170 MPa (605 ksi)
Flexural Modulus (D790)	1387 MPa (201 ksi)	1310 MPa (190 ksi)	3106 MPa (450 ksi)	4457 MPa (646 ksi)	2470 MPa (358 ksi)	1430 MPa (207 ksi)	3400 MPa (493 ksi)
Static & Dynamic Toughness							
Tensile Elongation at Break (D638)	14%	47%	1.4%	5%	27%	155%	6%
Notched Izod (D256)	32 J/m (0.60 ft-lb/in)	74 J/m (1.39 ft-lb/in)	41 J/m (0.77 ft-lb/in)	37 J/m (0.69 ft-lb/in)	232 J/m (4.35 ft-lb/in)	78 J/m (1.46 ft-lb/in)	92.4 J/m (1.73 ft-lb/in)
Drop Dart Imact - Total Energy (D3763)	3 J (2.21 ft-lb)	30 J (22.1 ft-lb)	N/A	N/A	23 J (17.0 ft-lb)	11 J (8.11 ft-lb)	N/A

Table 2.1. Mechanical properties of materials processed by SLS (source: 3Dproparts, 2012).

Compared to other AM methods, SLS can produce parts from a relatively wide range of commercially available powder materials, including polymers (nylon, also glass-filled or with other fillers, polystyrene, PEEK (Polyether ether ketone polymers), metals (steel, titanium, alloy mixtures, and composites) and green sand. However, it should be pointed out that SLS of metal parts requires burning the polymer and then subjecting the green metal part to the HIP process; so in-direct SLS is not widely used for

industrial applications, especially for aerospace applications. The SLS process does not need support structures, and high resolution can be achieved. Furthermore good mechanical properties and high complex geometries are possible. Powder in excess has to be removed and can be recycled after sieving. However, loose powder will deteriorate after recycling several times.

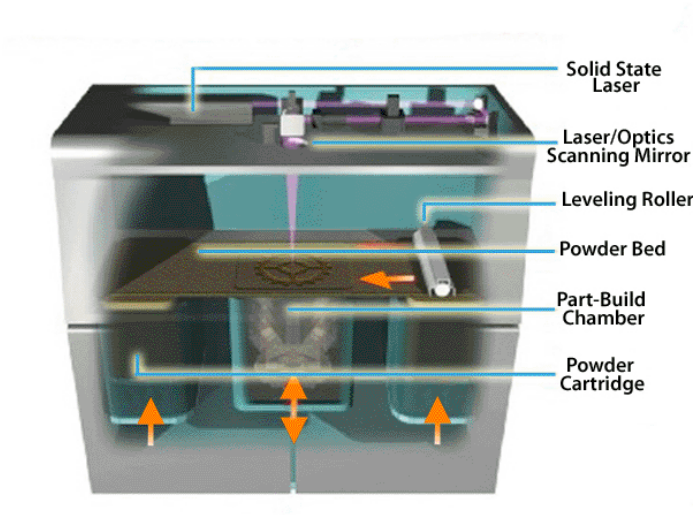

Figure 2.19. Selective Laser Sintering system schematic (LLC 2012)

Selective Laser Melting (SLM)

SLM is a powder based method, it requires a powerful laser in order to melt metal (stainless, cobalt alloy, titanium) powders and produce net-shape or near net-shape metallic components layer-by-layer.

The SLM production starts from the metal powder deposition, and leveling. The laser, utilising a mirror system, melts the particles according to the layer data and thereby melts and consolidates a new layer of material to the previous layer. The fusion happens in an inert gas filled chamber in order to reduce the metal oxidation in its interaction with the laser beam. The elevator moves down one step equal to the thickness of the layer (typically 0.02 – 0.1 mm), then the process repeats for a new

layer. After the production stage, the elevator is relieved and the sintered part is released. Figure 2.20 illustrates the main components of a SLM system.

During the build of overhanging parts, support structures are required; supports present typically a cellular structure topology to save material, since they are sacrificed after the build is completed, thus representing a process waste. The amount of support structures can increase the manufacturing costs of parts made by high-value metal alloys, such as titanium. Furthermore, support structures reduce the quality of surfaces that are in contact with the part and thus influence directly the complexity of post-manufacturing operations; minimising the volume of support can shorten this operation, thus improving process efficiency. Finally, the presence of support structures can limit the feasibility of building objects with complex shapes, because their removal can be impossible if they are internal surfaces.

Surfaces that have been supported, or not, are typically post-processed by mechanical treatments such as milling and threading in order to achieve good surface finishing and completion. These operations are typically long-time operations and expensive, since they have to be carried out by hand as a result of the shape complexity of parts typically produced. Figure 2.21 shows a F1 car component built through SLM process (CRPGroup 2012).

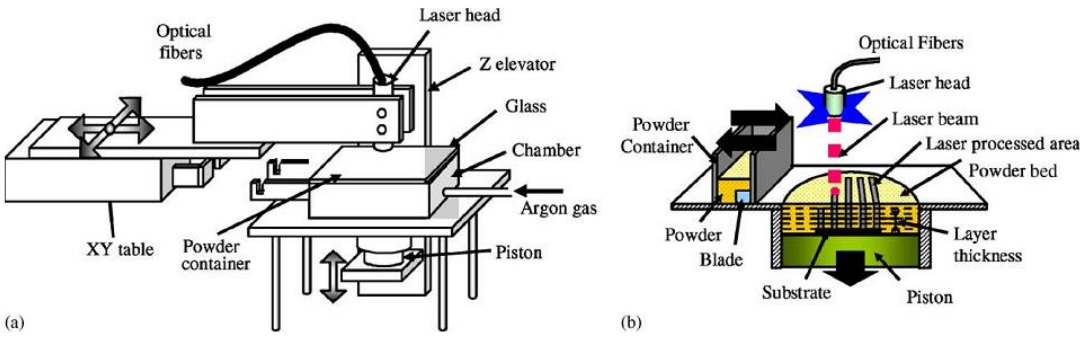

Figure 2.20. Selective Laser Melting: (a) Illustration of the machine; and (b) working principle of the system (Santos et al.).

Figure 2.21. F1 car component built through SLM process (CRPGroup 2012).

Laser Engineered Net Shaping (LENS)

In the LENS (also known as *Laser Consolidation*) process, instead of fusing material in a powder bed, the powder is delivered in a gas jet through nozzles (Figure 2.22).

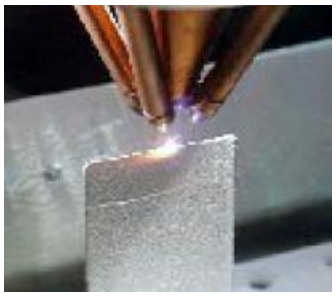

Figure 2.22. Jet nozzle deposition during LENS sintering process (Optomec 2012).

Most commonly used materials are titanium alloys, nickel alloys, steels, cobalt alloys and aluminum alloys. The powder feeder and the laser beam axis may also form an angle between them (usually from 0° to 45°), it has been shown that the maximum powder efficiency of the process is achieved when the powder arrives almost perpendicular to the substrate (Villar 1999). Figure 2.22 shows a particular of the jet nozzle deposition during the LENS sintering process (Optomec 2012). The metal

powder is fused in the focal zone of a high-energy laser beam and thus parts with complex geometries can be formed. The process occurs in closed chambers with controlled inert atmospheres Figure 2.23 shows the illustration of the process and some fabricated parts of the system used by Aeromet. The Aeromet machine uses a very high CO_2 power (410 W) laser for the fabrication of parts for the aeronautical industry.

Figure 2.23. Laser engineering net shaping: parts fabricated on Ti alloy (Hedges 2004).

Since there is no powder support during build, three-axis LENS machines cannot produce complex parts with overhangs. This restriction was overcome by applying 5-axis machines or by depositing separate support material around the part (Levy et al. 2003). By this process, fully dense parts with mechanical properties close, or even superior, to the conventionally processed material are usually achieved (Hedges and Calder 2006). Figure 2.24 shows an example of the application of LENS technology to repair a gas turbine engine stator.

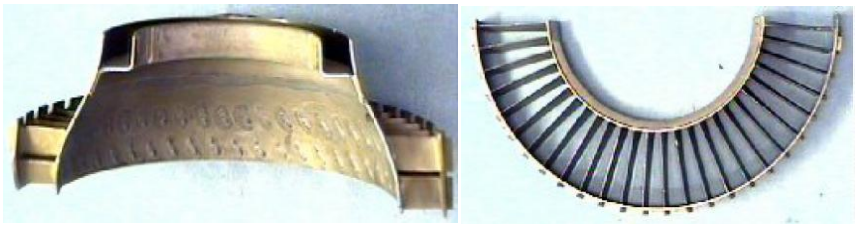

Figure 2.24. LENS employed for gas turbine engine repair (Optomec 2012).

Additionally, LENS technology has been recently employed for the manufacturing of porous and functionally graded structures for load bearing implants (Bandyopadhyay et al. 2009) and porous tantalum structures for bone implants (Balla et al. 2010).

Electron Beam Melting (EBM)

EBM technology manufactures parts by melting metal powder layer by layer with an electron beam in a high vacuum chamber. After the metal powder is deposited, pressed and leveled; the electron beam fuses the particles in a selective way bonding the molten material to the previous layer. The electron beam is controlled by electromagnetic coils, rather than optics as in other systems and moving mechanical parts, which provides for very good beam control and extremely fast beam translation. The fusion happens in an inert gas filled chamber in order to reduce the metal oxidation. The elevator moves down a step equal to the thickness of the layer and the process starts again for a new layer. The process repeats until the part is completed. Figure 2.25 shows an example of parts fabricated through Electron Beam Melting (Arcam 2012).

Figure 2.25. Parts manufactured by Electron Beam Melting (Arcam 2012).

Important characteristics of EBM are the necessity for a temperature of about 1000 ºC and a vacuum chamber, and thus precludes the building of large objects. Also, materials processed have to be conductive. Surface quality and the minimum feature size is larger than SLM. On the beneficial side, the high temperatures and the vacuum provide a clean environment that improves metal characteristics (DeGarmo et al. 2011).

2.2.5 Limits and challenges of AM for production in aerospace

AM has been increasingly used to produce small and medium size aerospace components. The potentialities of the process to produce reduced weight parts with complex shape, and to process a number of high-value engineering materials, such as titanium alloys, nickel-based stainless steels, high-strength aluminium alloys, has incentivised aerospace manufacturers to produce larger, and more complex parts. Nevertheless, there are some practical aspects that need to be considered, when large parts are built. Large volume components require a greater amount of powder and hence AM process platforms need to be stable and big enough to accommodate large size and

heavy weight. Also, very heavy components have to be removed safely and easily, with no risk for the operator, and for the part itself.

Furthermore, although a number of materials are already available, compared to the range of materials available to machining processes; there are only a few dozen AM materials commercially available today, (mainly plastics and metals). Plastic selection databases for conventional manufacturing methods include 40,000+ active grades of plastic alone (Maniscalco 2003). The narrowness of material choice can be justified by the relative short history of AM, but also because it is more difficult to design materials that interact so closely with the machinery as required in most of the AM platforms.

Although complex shape parts can be produced with significant time saving, the speed of AM fabrication of a part with reduced complexity, when compared to standard manufacturing methods, is much slower. By some estimates, existing mass production methods are 10 to 1,000 times faster (Sachs 2001). At present, some AM processes, such as SLS, allow the production of multiple parts, in numbers that depend on the part dimensions; nevertheless, especially for metal processes, it can take up to one day to sinter one single item, this does not include the time spent for support removal and surface refining.

Some important AM technologies require the presence of supports for the production of overhanging parts. Part supports are needed in the production of polymer parts (Stereolithography), as well as metal ones (Such as SLM, EBM). Other platforms such as SLS, do not need support, because the objects can be supported by the pre-heated powder bed. Another use of supports can be to constrain part distortion, particularly for large thin layer geometries. Support structures represent a serious limit in terms of complex shape manufacturing; supports have to be removed by hand for each single manufactured object, therefore introducing a need for special tooling in the AM process. Depending on the geometry complexity, supports can be hard or

impossible to remove. Furthermore, the bottom surface of the part, which is in contact with the base support, presents a reduce level of surface finishing and therefore requires expensive post production surface polishing operations. Finally, support structures are a sacrificial part of the build, and represent a wasted amount of material, energy and manufacturing time.

Many AM processes still have large deficiencies with respect to accuracy and repeatability (typically in the range of 0.1mm to 0.2mm, for 100mm), and surface finishing. Historically, when AM technologies were employed exclusively for the production of single prototypes, a poor surface finish was acceptable, and eventually corrected through post-manufacturing hand finish. Nevertheless, as there is a trend in the aerospace industry to employ AM for the production of functional parts in small-to-medium or even relatively large volume, the cost of expensive and time demanding surface finishing operations have to be taken into account in the estimation of the balance between economic cost and benefits.

2.3 Multi-objective optimisation

This section introduces the main concepts of mathematical multi-objective optimisation. Furthermore an overview of the selected methods for conducting mathematical multi-objective optimisation is presented.

2.3.1 Multi-criteria decision analysis for optimisation of industrial processes

The optimisation of manufacturing processes is one of the most important task of an enterprise; not only for saving costs, but also for maintaining competitiveness in a more

and more turbulent market (Weigert et al.). Modern manufacturing systems present have enhanced flexibility that involves a wide choice of process parameters, and objectives (i.e. built time, makespan, lead time, etc.). The priority among these parameters is usually established by the decision maker's experience and intuition, according to his commitments and preferences. Nevertheless, especially when the complexity of the systems and the number of contrasting objective increases, there is not a unique optimal solution, and it is necessary to properly structure the problem and explicitly evaluate multiple criteria. Solving the problem could correspond to choosing the "best" alternative from a set of available choices, and the "best" alternative could be interpreted as "the most preferred". Alternatively, the solution to the problem could be choosing a small set of good alternatives, or grouping the alternatives into different preference sets.

This scenario corresponds to a Multi Criteria Decision Maker (MCDM) problem, where the user has to consider multiple criteria to make the optimal choice. MCDM problems can be classified in different ways; some methods require the decision maker's preference at the start of the process, transforming the multi-criteria problem into a single criterion, these methods are called "prior accumulation of preferences". Other methods require preference information from the decision maker throughout the solution process, these methods are called "progressive articulation of preferences". Recently a particular methodology called Multi-objective mathematical programming problems, has become popular as a solution to MCDM problems in industrial design. Unlike other MCDM problems, in Multi-objective problems, the solutions typically are not known a priori, and are found by solving mathematical espressions.

2.3.2 Importance of multi-object optimisation in industrial design

The majority of the problems considered in the industrial manufacturing are with regards to improving the productive capacity without increasing costs, while ensuring short delivery times and satisfying production constraints. This problem is particularly complex, especially when the number of variables increases, and the time required to find a solution is short. As a consequence, the logistic and industrial processes require the use of flexible optimisation techniques to assist the decision maker during the choice of optimal solutions. These must not only satisfy the production constraint with contained costs, but also allow the prediction of risks, and costs of potential alternative scenarios. Furthermore, optimisation of engineering problems presents very often the necessity to copy with many (more or less) conflicting objectives which better define the various aspects of the problem, rather than just a single aspect.

Multi-objective optimisation problems (MOOP) can be found in various applications, financial problems, product and process design problems, automotive and aircraft design, and more generally in the presence of trade-offs between two or more conflicting objectives such as maximisation of profit or performances and minimisation of costs. There is wide literature available about applications of multi-objective optimisation in the area of mechanical engineering, industrial and manufacturing engineering, and supply and logistics management. A complete review of applications on state of the art and applications in production and operations management can be found in (Kadadevaramath and Mohanasudaram 2007) and (Wang et al. 2011).

Industrial example applications of multi-object optimisation can be found in process scheduling (Unilever), turbine design (Rolls Royce, Honda) micro chip design (Texas Instruments), robot movement (Honda), nuclear fuel reloading (Siemens), design of telephone networks (US West), games (Creatures), military pilot training (British Air

Force), vehicle routing (PinaPetroli), and coating of fluorescent lamps (Philips). Canon Inc. is working to transform virtual prototyping from a means of verifying prototype replacement to a means of proposing improvements at the design phase, which takes full advantage of optimization analysis (CAO: Computer-Aided Optimization), multi-objective optimization analysis, and robust optimization analysis for stable functionality and performance (CanonInc. 2011).

Examples of virtual prototyping at Canon include optimization analysis of the zoom lens barrels in compact cameras. Canon uses multi-objective optimization analyses to simultaneously optimize multiple design goals to ensure ease of assembly and disassembly, usability, safety, and drivability at the product-design stage. In particular, for the optimal design of the zoom lens barrels, two contrasting objectives have to be satisfied, zoom lens drive time and power consumption.

Another illustrative example of the potential for a multi-objective optimisation in industrial design is a recent case study by (Andersson et al. 2009) aimed at the design of an automotive control arm (Figure 2.26), made from aluminium extruded profile. The study aimed to find the best design with respect to cost, performance and manufacturability. For this purpose, performance was measured in terms of durability of the component, by considering the number of loading-unloading cycles it could withstand without fracturing and the deformations during the forming operations to not be allowed to exceed a certain limit. The optimised design reduced the material cost by 25% and increased the durability from 13000 to 1700000 load cycles, with respect to the constraint on the maximum allowed plastic strain during the forming operations.

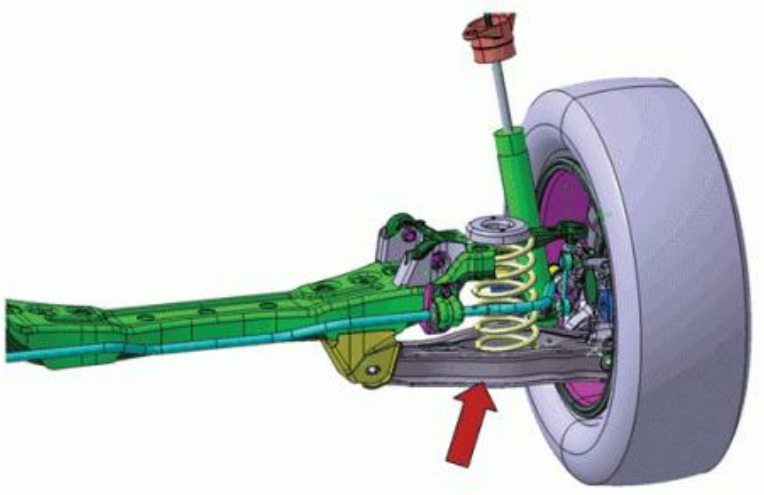

Figure 2.26. Optimisation of a control arm that links the wheel to the body of the car (Andersson et al. 2009)

Multi-objective optimisation problems have also been employed in the optimisation of supply chain networks. In (Strano G. et al. 2008) the MO was employed to optimise the capacity allocation problem in a big semiconductor company; more recently (Hnaien et al. 2010) a supply planning for two-level assembly systems under lead time uncertainties was considered. The objective was to find the release dates for the components at level 2 in order to minimize the expected component holding costs and to maximize the customer service level for the finished product.

Examples of multi-objective techniques for the optimisation of manufacturing process can be found in (Quiza Sardiñas et al. 2006). The study demonstrated the advantages of the multi-objective optimization approach over the single-objective one, for the optimal definition of the cutting parameters in turning processes, cutting depth, feed and speed. In the study, two conflicting objectives, tool life and operation time, were simultaneously optimized, in order to obtain the best trade-offs solutions to develop a micro-genetic algorithm. (Roy and Mehnen 2008) optimised the efficient machining of material with continuously varying properties, so called gradient material.

The problem needed advanced planning of cutting parameters; thus representing a dynamic optimisation problem. The optimisation algorithm developed adapted online to the dynamically varying hardness properties of the material. A model based detailed case study was presented where the optimisation identified good parameter set for the machining. Finally, the solutions were selected based on a desirability function and heuristics.

Following, the key concepts of multi-objective optimisation problems, and a review of a common approach to their solution are proposed.

2.3.3 Basic multi-objective optimisation concepts - dominance and Pareto front

The notion of "Pareto Optimality" (Coello 1999) is often used to define the concept of "optimal" in the presence of conflicting objectives. In the case of two or more conflicting objectives, very often there is no one overall optimal solution that is entirely better than the others. Rather, there exists a list of solutions to be intended as "best trade-offs" between the conflicting objectives. These solutions are called "Pareto Optimal" and they have the property that moving by one solution to another, it is not possible to increase the fitness of one objective without decreasing the fitness in at least one other objective.

In general, the solution of a multi-objective optimisation problem consists of locating the optimal trade-off curve (or surface) between the conflicting objectives. Following a mathematical description of the problem is proposed.

A general multi-objective optimisation problem seeks to simultaneously extremise D objectives:

$$y_i = f_i(\theta), \qquad i = 1, \ldots, D \tag{2.1}$$

where each objective depends upon a vector of θ of P parameters. Since any function to be maximised can be converted to one that is to be minimised, it is assumed that all the objectives are to be minimised. The multi-objective optimisation problem can thus be expressed as:

$$\textit{minimise} \quad y = f(\theta) = (f_1(\theta), \ldots, f_D(\theta)) \tag{2.2}$$

where $\theta = (\theta_1, \ldots, \theta_p)$ and $y = (y_1, \ldots, y_D)$.

In the case of a single objective optimisation, an optimal parameterisation is one which minimises the objective given the constraints. In the presence of more objectives to be minimised, parameterisations may exist for which performance on one objective cannot be improved without sacrificing performance on at least one other. Such parameterisations are called Pareto optimal and the set of all Pareto optimal parameterisations is the Pareto set.

In order to compare two multi-objective parameterisations, the concept of dominance is introduced. A parameter vector θ is said to strictly dominate another Ψ, if and only if, all the objectives corresponding to the parameter θ are no worse than those obtained with Ψ and at least one objective is better, that is:

$$f_i(\theta) \leq f_i(\Psi) \quad \forall\, i=1,...,D \quad \text{and} \quad f_i(\theta) < f_i(\Psi) \quad \text{for at least one} \quad i \qquad (2.3)$$

Less stringently, θ weakly dominate Ψ if the objectives corresponding to θ are all at least as good as those corresponding to Ψ:

$$f_i(\theta) \leq f_i(\Psi) \quad \forall\, i=1,...,D \qquad (2.4)$$

A set of solutions, in the form of parameterizations is considered a Pareto optimal (Srinivas and Deb 1994). The set of all Pareto-optimal solutions is referred to as the Pareto set and the image in objective space under $f(\cdot)$ of the Pareto set is known as the Pareto optimal front. Thus, the Pareto front represents all possible trade-offs between the competing objectives of a problem.

In Figure 2.27 an example of a two-objective minimization problem is illustrated for which 5 solutions are available. Solutions *a*,*b* are mutually non-dominating since none

of them dominates the other. Solutions c, *d* and *e* are also mutually non-dominating, however they are dominated by the solutions *a,b* that form the Pareto front.

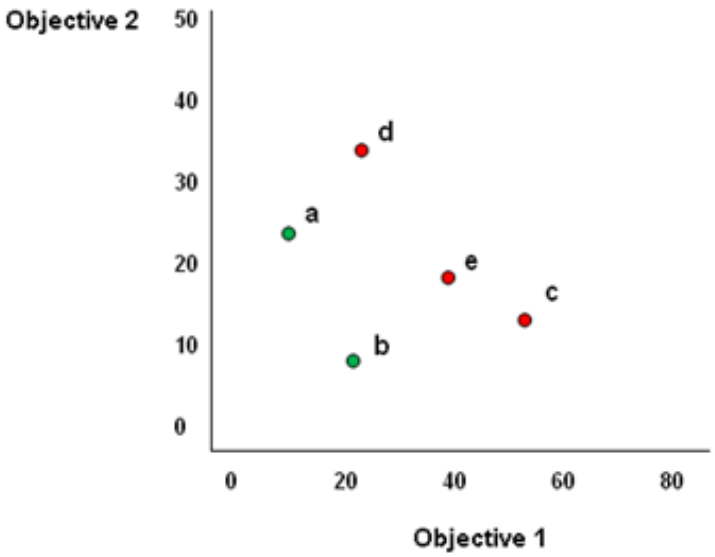

Figure 2.27. Example of dominance on a two-objective minimisation problem; the solutions coloured in green form the Pareto front.

2.3.4 Solution methods

There exist many methods to find a solution to a multi-objective optimisation problem, the most popular are now discussed.

Non-Pareto Based methods

The most intuitive approach to solve a MO problem with *D*-objectives is to combine the *D* functions into a single function that can be solved by a single-objective optimiser. This method provides an "aggregation" approach, by the "scalarization" of the objectives vector by the weighted sum, the "Min-Max", or the root mean square of the objectives. For example, if the objective is to minimise the production costs, and

maximise the strength of a machine component, the decision maker will allocate different weights to the two contrasting objectives, thus selecting a priori the most important. A list of definitions for some popular aggregation methods now follows.

Weighted sum (Baeck et al. 1997) – in the weighted sum method, the objectives $f_{1,\ldots,}f_D$ are weighted by $w_{1,\ldots,}w_D$, in the form :

$$f(\theta) = \sum_{i=1}^{D} w_i \, \theta_i \qquad (2.5)$$

An alternative approach to weighted-sum aggregation is goal attainment methods. In goal attainment methods each objective is associated with a goal or target value to be achieved. Unwanted deviations from this set of target values are then minimised in an achievement function that can be a vector or a weighted sum dependent on the goal programming variant used. A Goal Deviation measures the difference between the aspired and the actual objective, the optimum is reached when the target satisfies the decision maker. Some of the most popular goal programming approaches are:

Min-Max (Baeck T. et al. 1997) – this method minimise the maximum difference between D objectives $f_{1,\ldots,}f_D$ and and the user specified goals $g_{1,\ldots,}g_D$

$$f(\theta) = \max_{i=1,\ldots,D} f_i(\theta) - g_i \qquad (2.6)$$

A variant of the *Min-Max* method is the *weighted Min-Max* method, where the difference between objectives and goals is weighted by $w_{1,\ldots,}w_D$ *:*

$$f(\theta) = \max_{i=1,\ldots,D} w_i (f_i(\theta) - g_i) \qquad (2.7)$$

Global Criterion Method (Coello et al. 1998) – similar to the Min-Max method, but it minimises the relative distance of objectives to a target vector $g_{1,\ldots},g_D$

$$f(\theta) = \sum_{i=1}^{D}\left(\frac{g_i - f_i(\theta)}{g_i}\right)^p \tag{2.8}$$

where the coefficient *p* controls the bias towards minimising the objective f_i.

L_p *norm* – this method calculates the sum of the differences of objectives to goals. Similar to the previous method the coefficient *p* controls the bias towards minimising the objective with the highest value

$$f(\theta) = \left(\sum_{i=1}^{D}\left|g_i - f_i(\theta)\right|^p\right)^{1/p} \tag{2.9}$$

ε *constraint* (Ehrgott M. 2005) – in this method a single objective is minimised, constrained by the remaining objectives

$$f(\theta) = \min f_i(\theta) \tag{2.10}$$

subject to $f_j(\theta) \leq \varepsilon_j \quad j = 1,\ldots 1,D \quad j \neq i,$ where $\varepsilon \in \Re^D$.

Aggregation methods are essentially subjective, as the decision maker need to supply weights; furthermore, a translation of objectives into comparable lengths is usually required. The most limiting factor of aggregative approaches such as the weighted-sum aggregation function, has been illustrated by (Das and Dennis 1997). Das and Dennis

demonstrated that varying weights associated with a weighted sum aggregation function, was not able to identify all the non-dominated (or Pareto optimal) solutions, but only to locate those solutions lying on the convex part of the Pareto front. In addition, an even spacing of weighted intervals did not necessarily guarantee an even spacing of the Pareto optimal solutions across the front.

Goal attainment approaches such as Min-Max or Global Criterion Method, do not suffer from this limitation, however, similar to the weighted-sum approach, goal attainment might require multiple runs to acquire the Pareto front. Also the method is limited by the necessity to provide goal objectives a priori; choosing the "right" targets and weights is not easy, and if the targets and weights are not appropriate, the solution might not be the one in the best interest of the decision maker. Finally, one of the debated aspects of goal attainment techniques, is the fact that it does not allow trade-offs between goals. For example, if performances growth is the first priority goal, and costs reduction is the second, the formulation implies that not even the minimum performance can be sacrificed in order to obtain even a large saving in costs. For this reason, goal attainment techniques are often considered a "satisfying" approach to decision making, meaning that what is sought is a satisfactory solution rather than one that is truly optimal.

Pareto-dominance based methods

The techniques discussed so far can be very effective for the solution of problems characterised by linear equality constraints and linear objective functions. In general, optimisation problems can have nonlinear equality constraints; hence, they are non-convex optimization problems. They can also have some nonlinear optimization objectives; variables can vary discretely, and in general there can be several local optima, and one global optimal solution. Non-convex, nonlinear, combinatorial

problems are usually difficult to solve using traditional mathematical methods since these methods are designed to find local optima solutions. The approach to deal with these problems is typically based on the use of heuristic optimization techniques, such as Evolutionary Algorithms (EA). These heuristic techniques are well suited to dealing with non-convex combinatorial problems and can handle discontinuous search spaces. Moreover, they allow optimization of intricate non-differentiable objective functions. EAs are inspired by processes observed in the natural world. In EA, a population of candidate solutions is maintained, on which the reproduction process (through the use of "genetic operators") is applied to generate new solutions. Finally, a computational analogue of a natural selection process determines which individuals of the current population participate in the new population. Moreover, the drawback of these techniques is that they only find an approximation of the global optimal solution in a limited time. Following is a review of some EA techniques.

The study (Goldberg D.E. 1989) set up a milestone for the development in the field of evolutionary algorithms. Goldberg proposed a method of ranking solutions based on levels of non-domination. This means that individuals that are not dominated with respect to the rest of the population but would be assigned rank 1; the rest of the population would be classified as rank 2, and so on. The purpose of this operation is to maintain a population of non-dominating solutions that, step by step, would approximate better to the true Pareto front.

The following Multi-objective Genetic Algorithm (MOGA) proposed in (Fonseca and Fleming 1993), adopted Goldberg's approach to rank population; solution fitness is initially assigned as 1 plus the number of members by which the population is dominated. In addition, in MOGA a goal attainment strategy is introduced; non-dominated solutions are compared to predefined goal values for each objective, those non-dominated members that satisfy the goals are considered superior to those that do

not. The advantage of the MOGA on the weighted sum aggregation technique is that the Pareto front is investigated entirely, however, in the MOGA approach a knowledge a priori of the objective costs is still required.

Another EA approach is the NSGA algorithm, presented in (Srinivas and Deb 1994), all solutions of the same rank are initially given an identical fitness. In order to identify a population of rank 2, members in more crowded regions are penalised by dividing the individual fitness value by the number of neighbouring solutions found within a specified niche area. The derived population of rank 2, will have an initial fitness value that is less than the one assigned to the population of rank 1. This process continues until the entire population has been assigned a tailored fitness value. The main disadvantage of such an approach is the computational overhead associated with the repetition of Pareto ranking and fitness assignment.

A more efficient approach to population niching was proposed in the Niched Pareto Genetic Algorithm (NPGA) by (Horn et al. 1994). In the NPGA a tournament selection is made between members randomly selected from the whole population and then compared to a subset of the remaining population. The member that is found non-dominated is considered the "winner". In case both members are either non-dominated or dominated, the winner is considered to be the one with smallest neighbourhood, and it will be the one which will procreate in the next generation. This method overtakes the computational effort of population ranking and at the same time conserves the benefits of niching. However, it has to be noted that an effective tournament size parameter needs to be specified. Finally it should be considered that MOGA, NSGA and NPGA are all sensitive to correct regulation of fitness selection parameters such as the size of solution's neighbourhood.

In the last 20 years, the research into Multi-Objective Evolutionary Algorithms (MOEAs) has focused on reducing the time spent re-discovering previous good

solutions and preventing loss of good solutions (Zitzler et al. 2000), (Laumanns et al. 2001).

The updated version of NSGA, NSGA-II introduced by (Deb et al. 2002), adopts this philosophy by implementing the concept of "elitism". In this algorithm, the child solutions from one generation are combined with the previous generation, before performing ranking. In NSGA-II initially an archive *P* is assigned to all the members of the population. A member of *P* is then copied to a temporary archive *P'*. The copied member is compared to all the members of the original archive *P*. At the end of the comparison, the archive *P'* contains only non-dominated solutions corresponding to rank 1. All the members of rank 1 are copied to a new archive F_1 and consequently *P* is emptied from the members of F_1. The procedure repeats with a new layer of population to be identified and assigned to a new archive F_2 containing members of rank 2, and so on until the entire population has been ranked. The NSGA-II reduces the computational overhead in respect to the previous version of the algorithm. Also the algorithms target to eliminate the necessity to supply a suitable neighbourhood sharing factor by introducing an automated density calculation, the "crowding distance". Crowding distance is calculated by averaging the distance (in objective space) to the two nearest solutions either side of a given number.

A number of implementations of evolutionary algorithms alternative to NSGA-II have been developed as well, such as Strength Pareto Evolutionary Approach 2 (SPEA-2). Also other techniques based on Particle Swarm or Simulated Annealing, have become very popular standard approaches to solve multi-objective optimisation; a thorough review of techniques and application of multi-objective evolutionary algorithms can be found in (Deb 2001), (Coello et al. 2007), (Das and Panigrahi 2009), (Reckhouse W. 2010).

2.4 Conclusions

In this chapter the state of the art of advanced material structures in aerospace has been presented. Manufacturing and applications of cellular structures and complex shape components have been illustrated. The most popular AM technologies for the production of aerospace components have been reviewed. Additive manufacturing can represent an innovative technique for the fabrication of complex material structures, and is capable of overtaking the constraint of conventional manufacturing for the production of complex shape parts. In addition, the major limits to the diffusion of AM as a standard manufacturing process in Aerospace have been presented. The chapter has illustrated a wide range of industrial applications of multi-objective optimisation for the optimisation of design and manufacturing process.

Furthermore, the main concepts of mathematical multi-objective optimisation have been introduced, the concepts of dominance and Pareto front, and an overview of the main concepts and methods for conducting mathematical multi-objective optimisation is discussed. These concept and methods are analysed in the next chapter, where the multi-objective optimisation is applied to the manufacturing of polymer parts by the Selective Laser Sintering process, for the simultaneous objectives of energy saving and part's surface quality.

3. Multi-objective Optimisation of Selective Laser Sintering Processes for Surface Quality and Energy Saving

3.1 Introduction

Selective Laser Sintering (SLS) is one of the most mature Additive Manufacturing (AM) processes which can construct complex three-dimensional objects layer-by-layer with minimal material waste and tooling utilization. In recent years continuous technical and process control improvements have allowed SLS to be utilised for the manufacture of end-use parts, in particular with robust plastics such as Nylon 12 ((Levy et al. 2003), (Kim and Oh 2008)).

The surface finish of the SLS parts is one of the major requirements for functional end-use components; it considerably affects the amount of time spent on polishing and post-manufacturing operations of any SLS processed part, especially for parts subjected to aerodynamic or fluid flows such as air ducts used in aircraft. Roughness of AM processed parts is greatly affected by the "stair-stepping" effect, that is a stepped approximation of the edges of curves and inclined surfaces. Although thinner layer thicknesses can be used to reduce the stair-stepping effect and improve surface finish, it drastically increases the number of the layers and consequently the time for material layering, pre-heating and sintering, resulting in long processing time and high manufacturing cost and energy consumption. Surface roughness is greatly influenced by the part build orientation (Bacchewar et al. 2007), as the stair stepping effect depends on the surface inclination. Part build orientation also affects the amount of energy needed

for manufacturing during the SLS process. Preheating of powders is required before the layer is sintered by a laser, in order to minimize the amount of laser energy required for powder sintering, which thus minimises warping of the sintered layers. The amount of energy used for the powder preheating is dependent upon the number of sintered layers, and hence is directly influenced by the build orientation of the part. The research work in this chapter investigates a computational methodology, based on multi-objective optimization, for the simultaneous minimization of surface roughness and energy consumption in the SLS process, thus providing a decision support system for the identification of optimal build orientations as a "trade-off" between these two objectives.

3.1.1 Previous work on multi-object optimisation in AM

There have been a number of studies on multi-objective optimisation for various AM technologies. (Lan et al. 1997) investigated the optimisation of part deposition orientation for Stereolithography (SLA) parts based on surface quality, build time or complexity of support structures. Part orientation was selected to optimise surface quality by maximising the total area of perpendicular and horizontal faces, in order to minimise stair stepping on inclines. Aesthetically important faces were also considered by maximising the sum of upward facing surfaces and vertical faces, as they do not require the presence of any support structures that deteriorate their quality. In SLA, like other AM platforms, there is a long non-productive time spent for the material deposition on each layer, considerably longer than the time for layer sintering. When uniform slicing of the part was applied, the height of the part and the build time, were directly affected by the deposition orientation. For each part inclination, support structures were then optimised by minimising the number of supported points along the

length of the hanging profile. (Alexander et al. 1998) proposed a study on optimal orientation for better part accuracy and lower cost. Stair step effect was measured in terms of cusp height. The cusp height was calculated by geometrical consideration of the sliced profile of the part and was defined as the maximum normal distance between the triangular facet of the CAD model and the deposited part, considering a uniform slice deposition. The model for cost prediction has been generically developed for any AM platforms and takes into account the pre-build, build, and post-processing costs. (Cheng et al. 1995) presented a multi-objective approach for determining an optimal part build orientation for SLA. The two objectives, namely part accuracy and build time, were combined in a weighted sum for optimisation. Part accuracy was calculated using different weight factors for different types of surface geometries, and based on their experience they considered various contributions of fabrication errors, such as slicing effects, tessellation, distortion, stair stepping, etc. Minimisation of build time was achieved by reducing the number of slices. More recently, (Singhal et al. 2009) applied multi-objective optimisation to simultaneously optimise part average surface roughness, build time and support structure for both SL and SLS processes. In their study the multi-criteria optimization problem was solved by minimising the weighted sum of the three different objectives, using a conventional optimization algorithm based on a trust region method (More and Sorensen 1983) to find an optimum. All of the above methods employ a weighted-sum of several objectives approach, without considering their minimization simultaneously. From the point of view of multi-objective optimisation, although the conversion of a multi-objective functional into a scalar optimisation by a combination of the different objective has been very popular in the past, as (Das and Dennis 1997) show, this method only finds a single solution on the Pareto set for a particular weighting of the objectives. Varying the weighting obtains solutions across the entire Pareto set only when the set is convex, and even for convex

sets, an evenly distributed set of weights fails to produce an even distribution of solutions from all parts of the Pareto front.

To overcome these limitations, multi-objective optimization for problems with four or more objectives can be addressed by one of the recently developed evolutionary algorithms; see (Deb 2001) for a review. The NSGA-II evolutionary algorithm for multi-objective optimisation was used in (Pandey et al. 2004) for the optimisation of the parts fabricated by Fused Deposition Modelling (FDM) in order to find an estimate of the Pareto trade-off between average surface roughness and build time. A tessellated CAD data file was used as input. An analytical expression based on geometrical observation of the stair stepping effect was used to formulate the surface roughness model; the build time and other non-productive times specific to the FDM technology (such as lowering the platform after deposition of each layer) were based on a model previously developed by Alexander et al (Alexander et al. 1998). A crucial point necessary to achieve high surface quality for the manufactured part is a mathematical model to predict accurately the surface roughness.

3.1.2 Importance of surface finish in industrial design and applications

In industrial applications surface finishing has critical aesthetic and functional importance. It is usually employed to improve appearance, corrosion resistance, wettability, solderability, tarnish resistance, chemical resistance, wear resistance, hardness, electrical conductivity, and control the surface friction. In applications that involve sliding components, for instance in automotive and aerospace applications, specific roughness of fraction of micrometres is often required (Vorburger and Raja 1990). In ship building, where hull surfaces and propellers are fabricated, the surface

roughness is often preferred to be of the order of several micrometres for hydraulically smooth surfaces on high-speed ships (Townsin et al. November 1981). In wind tunnel applications a difference of a few micrometres in surface roughness can lead to considerable changes of aerodynamic characteristic at lower Mach numbers, especially on axial force such as pitching moment, and its derivative coefficients (Daneshmand et al. 2006).

Also surface morphology of end-use parts play a fundamental role in various applications. In the area of surface science, the presence of steps on a surface profile can greatly influence chemical reactions that can take place on it (Vorburger and Raja 1990). Surface finishing also has considerable influence on the into resistance and corrosion of metal surfaces; a coarse polished surface for coastal/marine applications can favour accumulation of chloride ions, thereby initiating a corrosion attack (Honess 2006) that will affect the morphology, and deteriorate mechanical performance.

Commonly, the term roughness is referred to as the average deviations of the profile from the mean plane, throughout the sample surface area. In a few practical applications, directionality of eventual ridges in the surface have functional importance; patterns with vertically aligned ridges minimise the possibility for entrapment of harmful species. In addition the natural washing effect is maximised; rainwater is in fact beneficial to the cleaning of stainless steel and a patterned or directional surface facilitates water run-off, where the presence of spare, not aligned crevices, contribute to accumulate airborne contaminants. Also, a more uniform surface pattern is preferred for aesthetic functionality.

3.1.3 Issues in surface finish of AM parts

Poor surface quality caused by the "stair step" effect represents a very important issue in AM production and compromises the complex geometrical benefits of AM process, especially when conventional manufacturing processes such as moulding or machining can provide better surface quality. Low surface quality can lead to long and expensive post-finishing operations, often executed by hand due to the shape complexity of the AM parts produced thus creating a barrier to using the AM processes for industrial production.

A polishing operation is time-consuming, and generally the cost of consumables is very high because the small surface area of abrasive used tends to wear out rapidly. Furthermore, the cost rises very rapidly when trying to decrease surface roughness below a set value; Figure 3.1 shows the qualitative relation between production time and resulting surface texture for traditional finishing processes, therefore the cost of over finishing a component should be taken into account. Complex shape parts, such as the ones produced through AM, are strongly dependant on the shape complexity and dimensions, fittings and components such as elbows, are nowadays still polished by the "off-hand" method, where quality of finish and time rely on the skill and experience of the operator. Spindle lathes or backstand abrasive polishing machines are used with the operator manipulating the component, whereby excellent finishing can be achieved on any number of complex shape parts, but for each component the best route has to be found, in order to ensure that finishing matches the needs.

Surface finish of internal inaccessible surfaces, depending on shape complexity, is not always possible. This limitation has to be mitigated by pre-polishing internal surfaces and then welding, fabricating and assembly are carried out, requiring additional manufacturing procedures, time and cost.

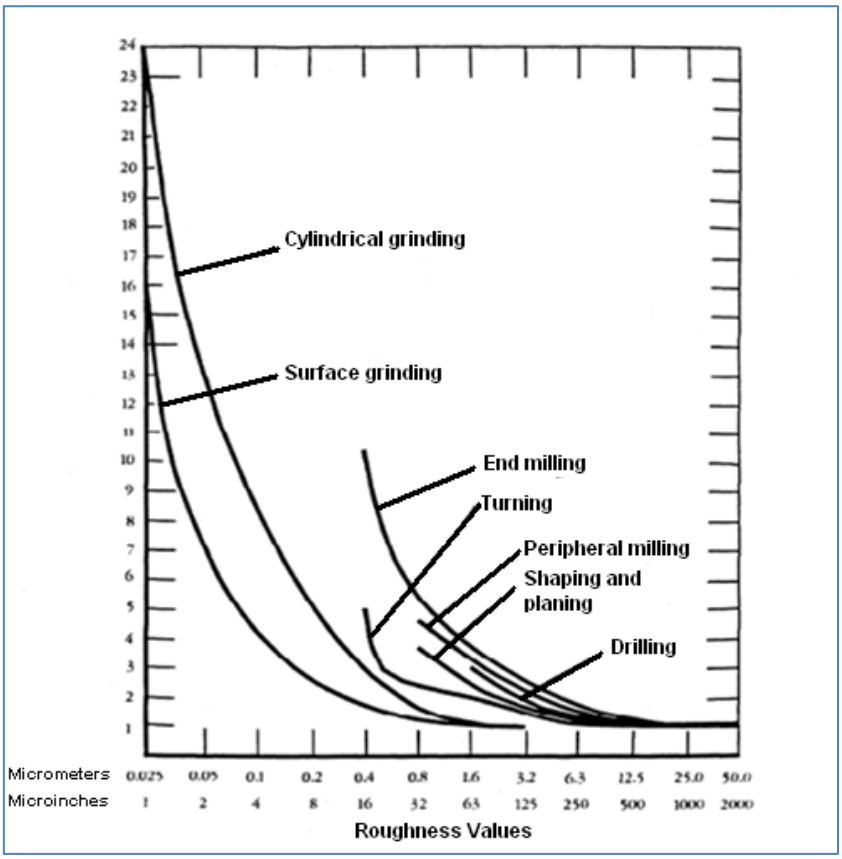

Figure 3.1. Qualitative comparison of production time and surface texture for traditional finishing processes (Inst 1972).

3.1.4 Models for roughness prediction of AM parts

Following is proposed a review of research on models for the prediction of surface roughness of AM parts.

3.1.4.1 Theoretical models based on geometrical considerations

In the past a number of studies have been conducted to predict the surface roughness of parts processed through different ALM platforms. In (Reeves and Cobb 1997), a "truncheon" test geometry was introduced to investigated the effect of stair-step on surface roughness at different sloping angles. Furthermore, a model was presented to predict the surface roughness for SLA parts by introducing two different expressions to predict the roughness of upward and downward-facing surfaces considering the layer thickness, surface angle and layer profile. (Campbell et al. 2002) carried out a comparison between theoretical roughness obtained from a trigonometrically derived equation, on the stair step profile, and empirical roughness measured on several different AM platforms. It was found that the model was able to predict roughness for only a partial range of surface inclinations with respect to the build direction. More recently, (Luis Pérez et al. 2001) proposed a geometrical roughness model to predict the average surface roughness of ALM parts and compared the theoretical and the actual surface roughness of SLA prototypes. In their model some corrections were considered to be necessary, especially for surfaces sloped close to $0°$ and $90°$.

3.1.4.2 Models based on experimental data interpolation

Models based on the pure description of the stair step profile could fail to accurately predict the surface roughness of ALM parts, because surface roughness might be influenced also by other process parameters. (Bacchewar et al. 2007) investigated the

contribution of build orientation, laser power, layer thickness, beam speed and hatch spacing on surface roughness of SLS parts. In the case of upward oriented surfaces, build orientation and layer thickness were confirmed to be significant parameters; downward oriented surfaces were also influenced by laser power. An alternative phenomenological model was presented to interpolate data from empirical observations of test samples; theoretical and real distributions were compared through the SLA fabricated test parts (Ahn et al. 2009). This roughness prediction approach exhibits the potential to include the sum of the all contributing factors to the part surface roughness, but faces difficulty in distinguishing among all of the most influencing factors. Also, the interpolation of empirical roughness is based on a discrete number of measurements. In order to achieve high resolution, a large number of measurements are required. The following research extends the phenomenological approach to predict surface roughness of SLS parts. Experimental surface roughness data have been collected and interpolated for a range of deposition orientations in order to predict the overall part roughness.

3.2 Models for multi-object optimisation of SLS processes

This section introduces the model for prediction of surface roughness developed by experimental work on SLS manufactured samples.

3.2.1 Computational model for surface roughness prediction

Considering a surface profile of length *L*, the one-dimensional definition of surface roughness R_a is

$$R_a = \frac{1}{L}\int_0^L |f(x)|dx \tag{3.1}$$

Where *f(x)* is the deviation of surface height at *x* from the mean height over the profile, assuming that the overall profile is level (Figure 3.2). If the height f_i is measured at *N* locations along the profile length *L*, the roughness is numerically calculated as:

$$R_a \approx \frac{1}{N}\sum_{i=1}^{N}|f_i| \tag{3.2}$$

The definition of surface roughness is readily extend to a two-dimensional surface profile of area A, as the average magnitude of the surface profile from the mean plane, again assuming that the mean plane is level (Figure 3.2). In this case, with *NxM* measured deviations $f_{i,j}$ the roughness is approximated as:

$$R_a \approx \frac{1}{NM}\sum_{i=1}^{N}\sum_{j=1}^{M}|f_{ij}| \tag{3.3}$$

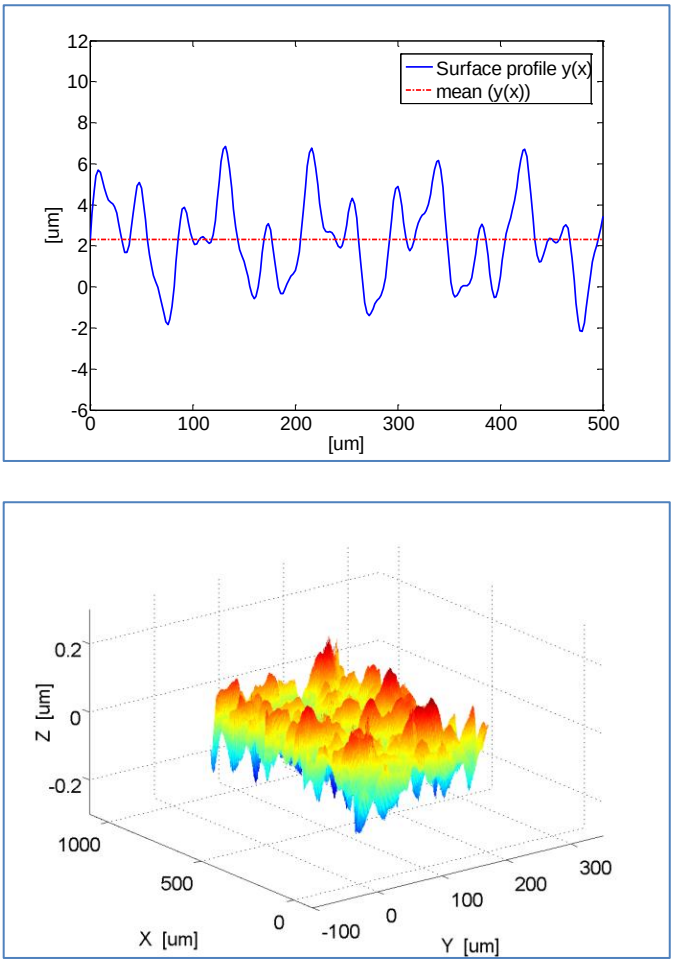

Figure 3.2. Representation of 1D (top) and 2D (bottom) surface profiles.

Following a characterisation of the surface roughness of SLS processed parts is presented, at different orientations. For this purpose surface characterisation on manufactured samples was conducted at different inclination angles by the use of a surface profilometer.

3.2.2 Effects of sloping angles on the surface roughness of SLS polymer parts

In order to characterise the actual surface roughness distribution in a SLS processed part, a "truncheon" test part shown in Figure 3.3 was fabricated. This geometry has been adapted from the one used in previous work by (Reeves and Cobb 1997), because it allows the surface roughness for each inclination angle to be measured. The truncheon has been designed to measure roughness, defined as the mean absolute deviation from the average surface height, at all angles in the range from 0° to 90° by a 5° step, for both the upward and downward-facing surfaces.

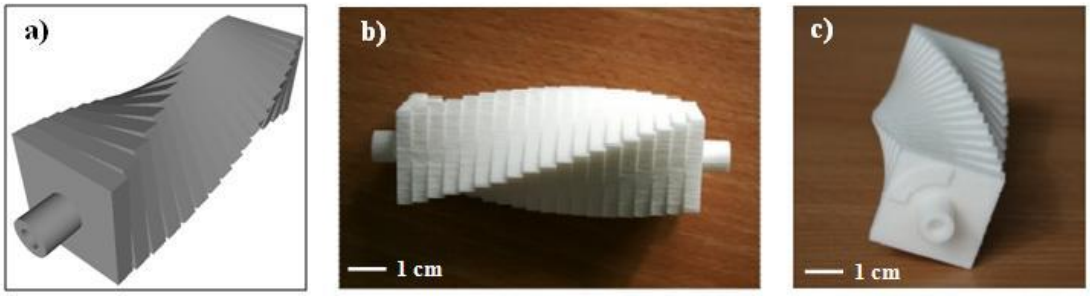

Figure 3.3. Truncheon sample CAD model (a), and manufactured sample (b, c).

The truncheon sample was made from Duraform polyamide powder material sintered by a SLS Sinterstation® 2000 platform, manufactured by DTM Corporation (DTM), now 3D Systems. The SLS process parameters were: layer thickness fixed at 0.1 mm; the hatch spacing at 0.15 mm; the beam scan speed at 12.5 $mm \cdot s^{-1}$ and the laser power at 4 W. Surface roughness measurements on the sample were carried out using a surface profilometer Talyscan 150 system (Taylor Hobson Ltd). For each inclination, the surface roughness of the sample was collected on a surface of 10mm x 2 mm, with a scanning spacing fixed at 5 μm and scanning speed at 2500 $\mu m \cdot s^{-1}$.

a)

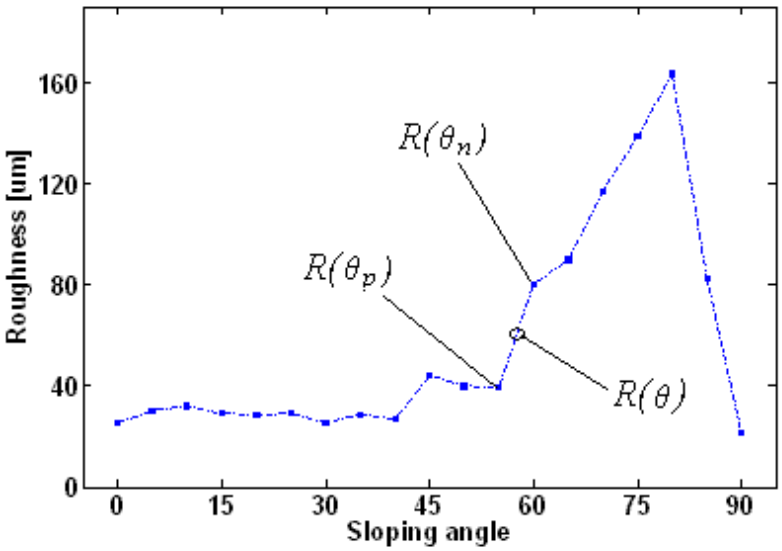

b)

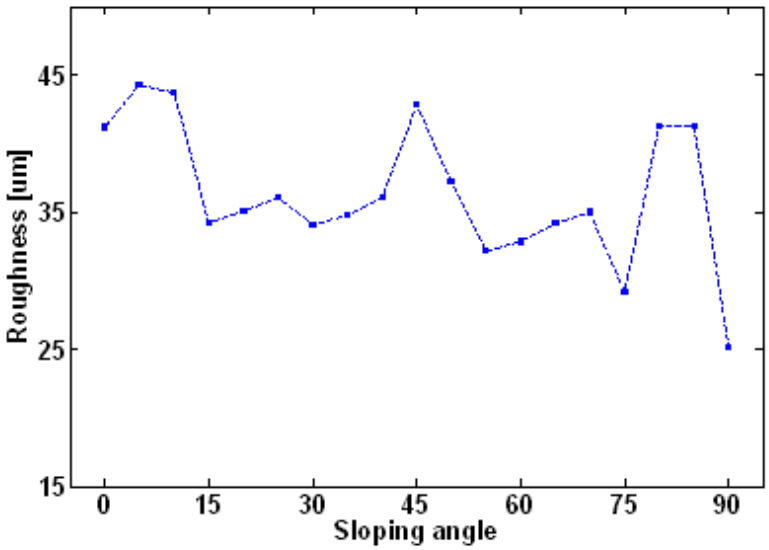

Figure 3.4. Experimental roughness in SLS process at different sloping angle;

(a) upward-facing, and (b) downward-facing oriented data.

The experimental data sample in Figure 3.4 shows the roughness as a function of the surface sloping angle θ. The data confirm the trend reported on a similar geometry by (Bacchewar et al. 2007); upward-facing surfaces present the highest values of surface

roughness in the range of angles between 60° and 85°, where peak values are up to three times higher than those in the range 0° to 60°. Smaller peaks can be observed in the experimental measures of downward-facing oriented surfaces; these can be the result of the "filleting effect" that affects the downward oriented surfaces during the SLS of polymer powders.

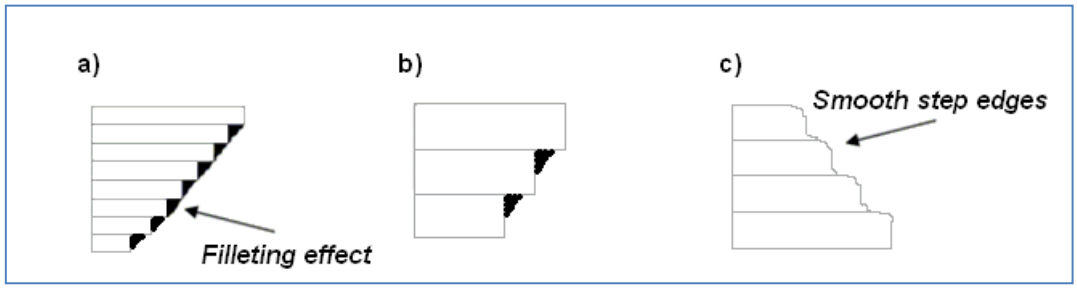

Figure 3.5. Filleting effect caused by flow of molten polymer for downwards oriented facets (a), but inhibited by surface tension to only partially smooth thick layers (b). For upward facing facets (c) filleting is minimised although surface tension may smooth sharp corners.

The filleting effect is generated by the gravity and surface tension forces on the molten polymer which tends to drop down due to the action of gravity, thus filling the gaps between layers sintered consecutively and providing a “compensation” to the stair stepping effect before solidification. Figure 3.5(a) schematically shows this effect. Nevertheless, at higher layer thickness, the filleting effect was observed not to be significant in improving the surface finish (Bacchewar et al. 2007); this is because, for high layer thickness, gravity is not sufficient to produce complete filleting because of the counteracting effect of surface tension which inhibits the spread of molten polymer as represented in Figure 3.5(b). On upward oriented surfaces the filleting effect is observed not to be geometrically influential on surface profiles (Bacchewar et al. 2007). This is because the absence of gravity's action; although surface tension may slightly

reduce the roughness by smoothing the sharp stair-step corners as shown in see, Figure 3.5(a).

3.2.3 Mathematical formulation

Although different values could be expected depending upon the scan direction, the surface roughness has been observed to be independent of the measured direction (Kruth et al. 2005). Consequently, for each facet it can be assumed that the roughness function depends upon θ, the angle between the fabrication direction $\vec{z} = (0,0,1)$ and the vector normal to the surface facet $\vec{n}$ as shown in Figure 3.6.

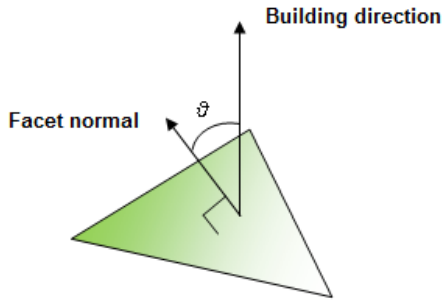

Figure 3.6. Angle between the building direction and STL file facet normal vectors.

If the surface geometry is defined by K facets, the roughness value $R_i(\theta)$ $(i=1,\ldots,K)$ for the ith facet, at any surface angle, can be calculated by interpolating the measured roughness function as follows:

$$R_i(\theta) = R(\theta_p) + \frac{R(\theta_n) - R(\theta_p)}{\theta_n - \theta_p}(\theta - \theta_p) \qquad (3.4)$$

Where $R(\theta_p)$ and $R(\theta_n)$ are the measured roughness values at the sample angles adjacent to θ; see Figure 3.4.

The roughness objective is defined as the average roughness of the surface facets weighted by the facet area, A_i:

$$R_a = \frac{\sum_{i=1}^{K} R(\theta_i) A_i}{\sum_{i=1}^{K} A_i} \qquad (3.5)$$

3.2.4 Model for energy prediction

The energy employed in the manufacturing process influences the overall cost of SLS parts and sustainability of the SLS process. The SLS process involves a moving laser beam irradiating a polymer powder to sinter the individual powder particles. Before the sintering process, layer by layer, an amount of energy is employed to preheat the deposited powder, in order to reach a temperature just below the melt temperature (for *Nylon12*, typically *178 C*^{o}). The laser power provides the energy to locally heat the powder, until the polymer reaches the liquid phase. After the laser scan is over the scanned pool solidifies thus sintering powder particles to the previous sintered material layer.

The proposed energy prediction model, takes into consideration both the contributions of energy E_h required by the preheating operations, and energy E_s required by the laser sintering of the part.

The volume of the powder spreads out during the preheating operation, $V_{p,}$ is determined by the height of the object to be sintered; hence it is defined by the build orientation chosen. The term V_p can be therefore expressed as $V_p = V_p(\theta_x,\theta_y)$, as a

function of the orientation angles θ_x and θ_y around the *X* and *Y* axes respectively. Considering C_p the specific heat capacity (*nylon 12 = 1640 kJ/kg*), *l* the latent heat of fusion *(nylon 12 = 120 kJ/kg)*, ρ the green density of the powder *(nylon 12 = 590 kg/m^3)* and $V_p(\theta_x,\theta_y)$ the volume of the total preheated powders, the energy required for preheating operations can be calculated by the following expression:

$$E_h(\theta_x,\theta_y) = (C_p \cdot \Delta T + l) \cdot \rho \cdot V_p(\theta_x,\theta_y) \quad (3.6)$$

Where ΔT is the difference between the temperature of *178 C^o (Nylon 12* melting point) and the environmental temperature and is considered as constant in the model. The applied energy for part sintering E_s presented in eq. (3.6) can be calculated from the model developed by (Gibson and Shi 1997). If *P* represents the power available from the laser beam at the powder bed surface; S_s the scan spacing, distance between two adjacent parallel scan vectors; B_S the scan beam speed; A_a the area of each slice; and *N* total number of layers, then the energy E_s applied for the entire part is given by:

$$E_s = \sum_{i=1}^{N} \frac{P}{B_s \cdot S_s} \cdot A_{ai} = \frac{P}{B_s \cdot S_s} \cdot \sum_{i=1}^{N} A_{ai} \quad (3.7)$$

The total amount of energy required for the manufacturing of the piece E_{tot}, is calculated as sum of the two terms in eq. (3.6) and (3.7):

$$E_{tot}(\theta_x,\theta_y) = E_h(\theta_x,\theta_y) + E_s \quad (3.8)$$

3.3 Multi-objective problem definition and algorithm implementation

Suppose there are D objectives $f_i(\theta)$ $(i= 1,\ldots,D)$, a general multi-objective minimisation problem can be written as:

$$minimise \quad F = f(\theta) = (f_1(\theta), ..., f_D(\theta)) \tag{3.9}$$

subject to: $c(\theta)=0, h(\theta)\leq 0$

where each objective depends upon a vector of θ of P parameters, and the vectors $c(\theta)= c_1(\theta), ...,c_D(\theta)$ and $h(\theta)= h_1(\theta), ..., h_D(\theta)$ are, respectively, equality and inequality constraints of the problem.

In this study the objectives considered are the weighted average roughness and the total energy required for SLS. The decision variables for the problem are θ_x and θ_y, the rotation angles around the x and y axes respectively, in a range between $0°$ to $180°$ by 5° steps. Thus, the complete problem of optimal part orientation can be summarized as follows:

$$min \quad F(\theta_x,\theta_y)=(R_a(\theta_x,\theta_y), E_{tot}(\theta_x , \theta_y)) \tag{3.10}$$

subject to the constraints: $0 <\theta_x \leq 180°$ and $0 <\theta_y \leq 180°$.

Each component geometry is defined by the Standard Tessellation Language (STL) used as the input file for the optimisation system. The STL file, which provides a description of the surface geometry, is imported into the Matlab environment where the multi-objective optimisation is performed (see code in Appendix A). At the beginning, an STL file containing the geometry surface information is imported; then the algorithm

starts rotations around the two axis routines, for each rotation step each of the objectives is calculated and stored. Once the entire domain has been investigated including all the possible orientations, the Pareto set of solutions is calculated and plotted. Finally the geometry both with the original orientation and with any of the Pareto-optimised orientations is shown.

Multi-objective optimisation is often performed using a Genetic Algorithm (GA) (Deb 2001) in which a population of individuals, each representing a possible solution, is mutated and combined with other individuals to improve the overall fitness of the population. GAs and related methods are employed to search for large solution spaces for global optima, and are seldom able to search the entire space due to computational limitations. In this problem, however, the solution space is two-dimensional (θ_x, θ_y,) and it is therefore possible to search the entire space without resorting to approximate methods. This has the combined benefit of exploring the entire space and thus locating the global Pareto front with certainty (given the resolution of the search domain), and is computationally more efficient than GA approaches which are stochastic searchers.

Figure 3.7 illustrates a schematic of the main algorithm routine, details of the Matlab code are reported in Appendix A. The computational time required by the system to perform the optimization varies with the number of facets defining the STL geometry, and it is expected to be less than that required by a GA based optimisation. To give an idea of the computational overhead to process the two geometries, the first and second case studies have *21,054* and *11,438* facets respectively, the longer simulation took about *5 minutes* on a *Pentium ® 4 2.00 GHz CPU, 512 Mb RAM,* computer.

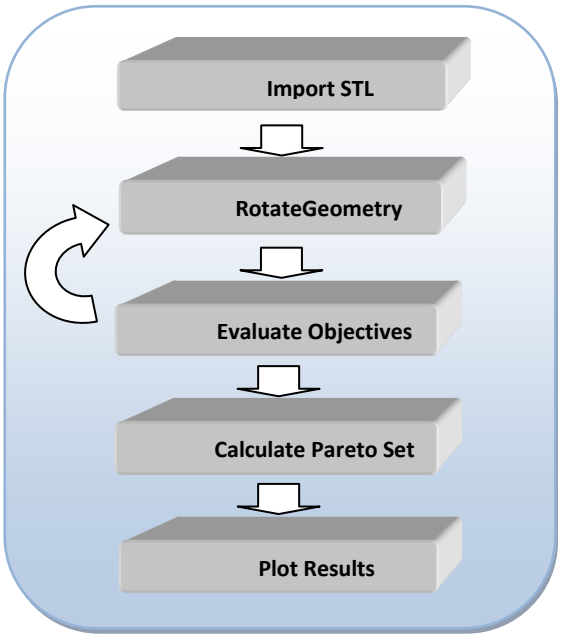

Figure 3.7. Principal algorithm routines flowchart for surface roughness and energy prediction.

3.4 Results and discussion

The problem has been solved for two different industrial case studies shown at arbitrary orientations in Figure 3.8; they are two real aerospace components, Figure 3.8a shows a support for aluminium profiles manufactured from Polyamide Plastic (Boutet S.A.), while Figure 3.8b shows a tension latch manufactured from Polyamide Plastic (POM) (Aerotecnica S.A).

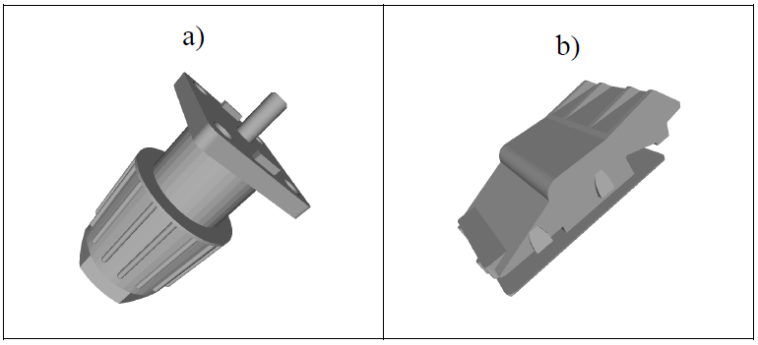

Figure 3.8. Artefacts to be manufactured by SLS: support for aluminium profile (a), tension latch (b).

The prediction of the average surface roughness for the first case study, is shown in Figure 3.9. The figure represents the value of predicted average roughness for each material deposition orientation. For a given inclination the roughness has been calculated by taking into account the contribution of each single mesh element and its surface area. The vertical orientation of the facet has also been taken into account, as, depending whether upward or downward oriented, facets present a different roughness due to the filleting effect.

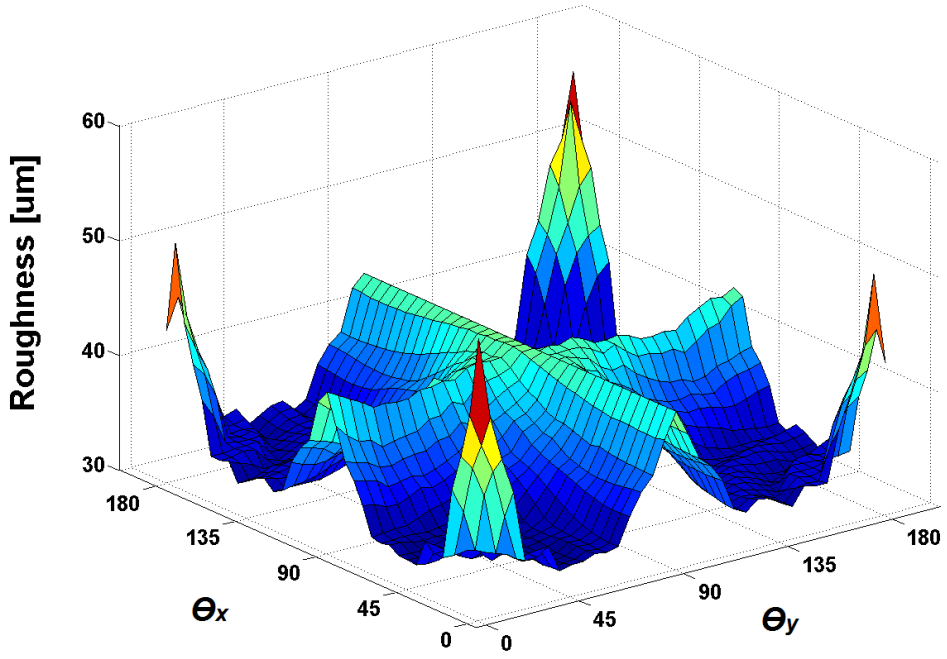

Figure 3.9. Weighted average roughness function for the artefact shown in Figure 3.8a.

The roughness function has a high degree of symmetry with respect to rotation angles of 90º around both axes. A similar characteristic has been observed for the energy objective function. The symmetry occurs when artefacts with significant geometric symmetry are processed; therefore it can be argued that, by reducing the search domain

to 0° - 90°, a significant reduction in the algorithm computational time could be achieved.

The result from the optimisation of the first case study is presented in Figure 3.10. The large heavy dots highlight the complete set of Pareto solutions, solutions which define the set of best compromises between the surface roughness and energy saving objectives (Equation 3.10). Also shown as small light dots are non-Pareto-optimal solutions at other orientations; each of these is worse on at least one objective than a Pareto optimal solution.

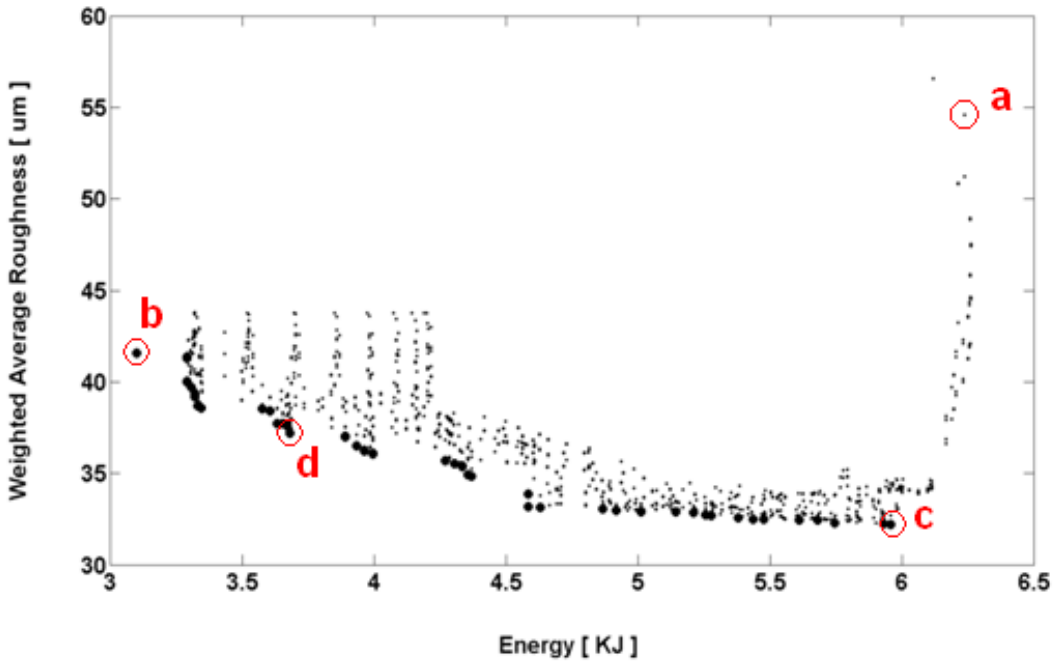

Figure 3.10. Solutions and Pareto front for the first case study.

Orientations which yield low energy and low roughness in the Pareto curve ones are preferred, and the Pareto front shows that energy expenditure beyond *~4.6KJ* tends to produce very small improvements in surface roughness. The non-dominated solutions have roughness values of about 5*0%* less than those of the worst orientation visible on the top right of the Figure 3.10. By choosing the solutions at the bottom left of the

Figure 3.10, it is also possible to save the total amount of energy used in the manufacturing process by a factor of two when compared to the worst case. Thus, a SLS operator can choose the optimal orientation for part building based on the part requirements and the predicted results of the surface roughness and energy consumption, rather than relying on the pure experience and skill of the operator.

Figure 3.11 shows a comparison between the original oriented geometries and three solutions chosen from the Pareto set of solutions in Figure 3.10; Figure 3.11(b) shows the orientations that minimise the surface roughness objective; Figure 3.11(c) shows the orientations that minimise the total energy employed in the build process. Figure 3.11(d) represents a compromise between surface quality and energy saving chosen at arbitrary points on the Pareto set. The four selected solutions are also highlighted in Figure 3.10 by red circles. It is noticeable that solutions that minimise the roughness objective, calculated as a weighted average, are the ones that orientate the artefact such that mesh triangles with the biggest area, are orientated at an angle characterised by lower roughness in Figure 3.4.

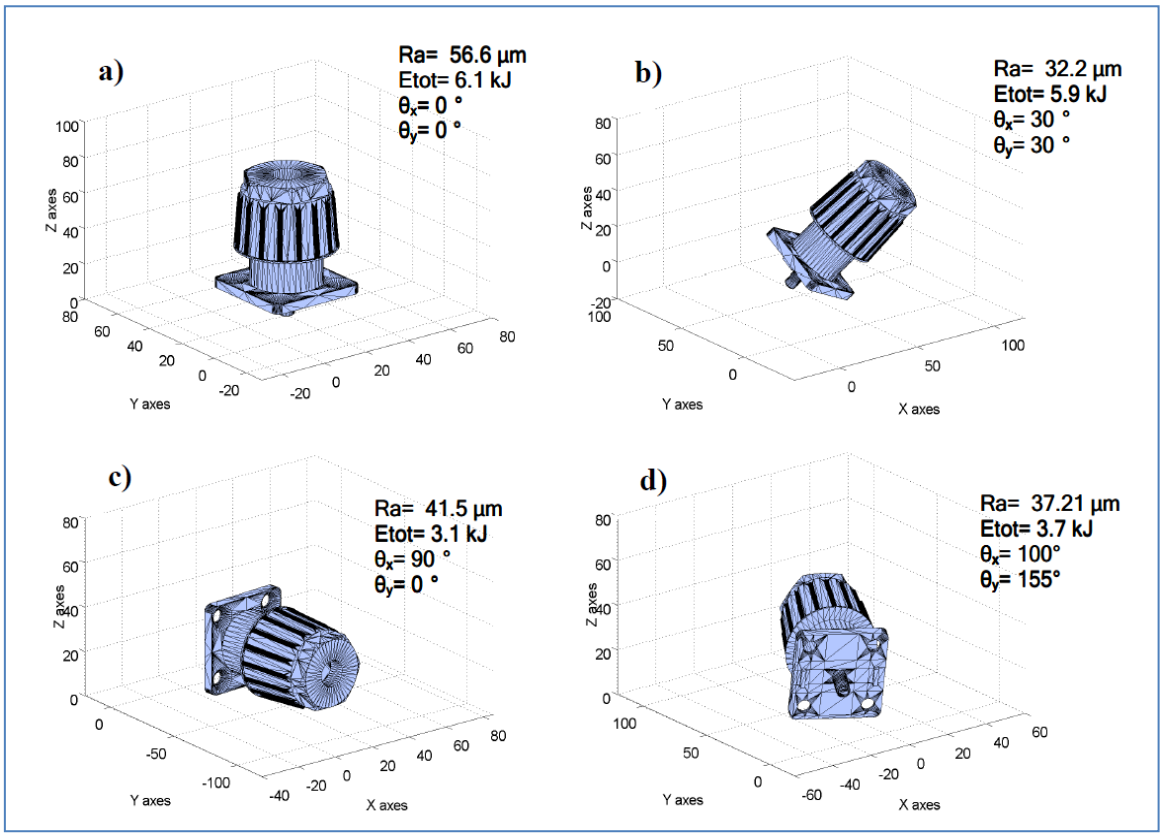

Figure 3.11. First case study at different orientations; a) original oriented geometry, b) minimisation of surface roughness, c) minimisation of build process energy, d) compromise between the two objectives.

Furthermore, solutions that minimise the energy are the ones that minimise the height of the artefact in the build position, this in fact allows minimising the number of the layers of powders to be deposited, and consequently the energy for pre-heating operations.

The multi-objective optimization in Figure 3.12 shows the optimization of the second case study.

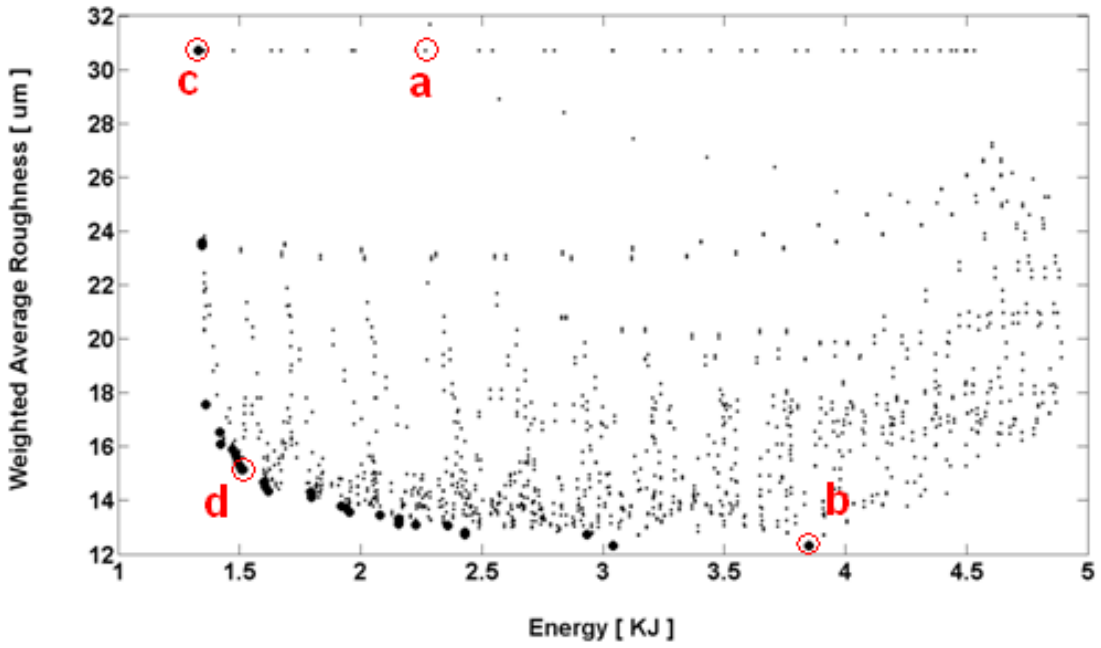

Figure 3.12. Solutions and Pareto front for the artefact for the second case study.

Figure 3.13 shows a comparison between the original orientated geometries and three solutions chosen from the Pareto set of solutions in Figure 3.12. Figure 3.12(b) shows the orientations that minimise the surface roughness objective and Figure 3.12(c) the orientations that minimise the total energy employed in the build process. Figure 3.12(d) represents a compromises between surface quality and energy saving chosen at arbitrary points on the Pareto set. The four selected solutions are also highlighted in Figure 3.10 by red circles. Similarly to the first case, it is confirmed that solutions that minimise the surface roughness objective are the ones that maximise the amount of mesh surface, at sloping angles characterised by lower roughness values. Also, solutions that minimise the energy are the ones that minimise the height of the artefact in the build position.

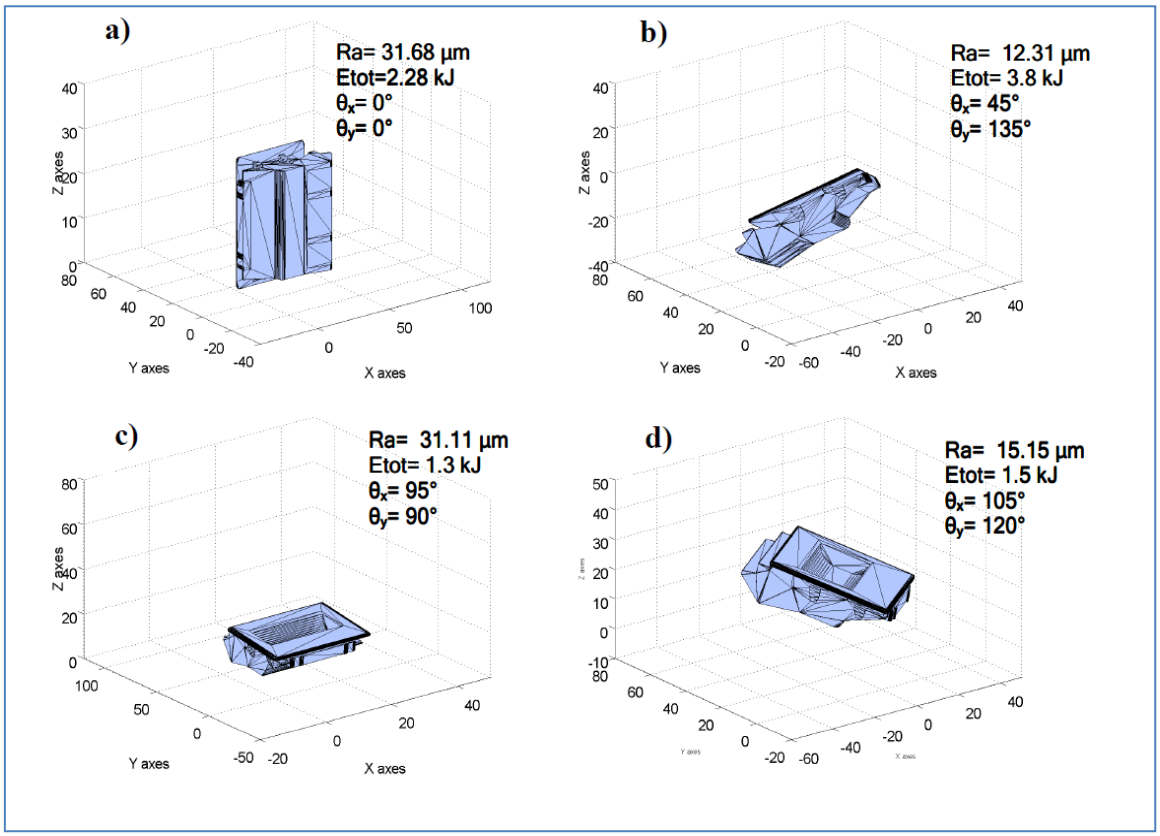

Figure 3.13. Second case study at different orientations; a) original oriented geometry, b) minimisation of surface roughness, c) minimisation of build process energy, d) compromise between the two objectives.

3.5 Conclusions

A computational model has been developed for the process optimization of part manufacturing through Selective Laser Sintering. The multi-objective computational optimization provides the operator with the Pareto set of solutions which define the best compromises between the surface quality of the part and the manufacturing process efficiency, through the minimization of energy employed in the manufacturing process.

For this purpose, a surface roughness prediction model has been developed by using an interpolation of measured data on a SLS manufactured geometry sample. Such a model interpolates different sets of data from downward and upward oriented surfaces, in order to include the filleting effect that has been experimentally observed in the layer-by-layer sintering of polymer powder.

The modelling approach using experimental data extends the empirical observations of surface roughness to the SLS technology platform, and provides for a more complete and accurate description of the stair step effect over the entire range of possible inclination angles. The model for manufacturing process efficiency takes into consideration both the contributions of the energy required for the preheating operations and the energy required for the laser sintering of the part. The optimisation problem has been solved by an exhaustive search algorithm; the computational time required is expected to be less than that required by a GA based optimisation and the global optimum has been found in a reasonable time, given the search domain resolution. Further reductions of computational time for symmetrical parts are possible. Furthermore, the methodology and the mathematical approach presented are generally applicable not only to AM manufacturing of metal parts but also to other powder bed based AM platforms such as Selective Laser Melting (SLM) and Electron Beam Melting (EBM). The following chapter extends the multi-objective optimisation

approach presented for the simultaneous optimisation for manufacturing time and surface quality for metal part manufactured by the SLM process.

4. Multi-objective Optimisation of Selective Laser Melting Processes for Manufacturing Time and Surface Quality

4.1 Introduction

In recent years Selective Laser Melting (SLM) has become accepted as a viable automated direct manufacturing process for end-use parts, with a large number of potential applications in the aerospace, automotive and medical industries. One of the main challenges in Additive Manufacturing (AM) is to reduce the time required for the building process and at the same time maintain the surface quality of the parts, as this affects the process costs and the quality of manufactured parts.

The surface roughness is greatly influenced by the “stair-step” effect, stepped approximation of curved and inclined surfaces. Furthermore, surface quality and dimensional accuracy is limited by “balling” phenomenon that occurs during the laser sintering and the resulting into formation of discontinuous tracks.

As with any manufacturing process, the cost of the part is directly related to the manufacturing time. Production time and costs influence the possibility of using SLM and other AM technologies for industrial applications. Layer by layer deposition and consolidation takes a considerable time which can be much longer than conventional manufacturing techniques. Also, due to limited surface quality of SLM parts, complex and long-time post manufacturing operations need to be carried out, thus introducing additional costs in the process.

Both surface quality and build time are significantly affected by the build orientation of the parts; this important process parameter often relies on the experience and skill of the operator and there is therefore no consistent method available to provide an optimal solution.

This chapter investigates a computational technology for the definition of an optimal part orientation for the minimization of build time and surface roughness, ensuring surface quality and, simultaneously, total process time and cost savings. A computational model based on a multi-objective optimization technique has been developed to predict and optimise the build time and surface quality objectives, using process parameters such as build time for each layer and weighted average surface roughness of the part. In order to accurately predict the surface roughness of SLM manufactured part, an analysis of surface morphology has been conducted, and a novel mathematical model has been developed. The output of the computational optimisation includes the estimated set of Pareto solutions, which define the set of best compromises between the chosen objectives, thus permitting the operator to select the best trade-off between final surface quality and build time.

4.1.1 Surface roughness in Selective Laser Melting process

SLM still faces an apparent limitation in terms of surface quality when compared to some alternative metal manufacturing processes such as machining. Surface quality is greatly influenced by the "stair step" effect. This effect is present, to a greater or lesser degree, in all AM processes as consequence of the additive deposition and fabrication of layers. Despite the fact that layer thickness can be reduced to improve the surface finish, obtaining a good surface finish presents a very important issue in SLM production. Furthermore, a smooth surface is limited by the "balling" phenomenon that occurs

during laser sintering. The balling effect limits the SLM process resolution because it causes the formation of discontinuous tracks (Mumtaz and Hopkinson 2009), therefore limiting the formation of very sharp geometries. Also it is responsible for a non-uniform deposition of material on the previous layers, thus inducing a possible porosity and delamination between layers that is detrimental to the functional performance of parts, such as fatigue life for aerospace components and longevity for medical devices. During the process planning of SLM production, important benefits and improvements can be achieved by predicting the surface roughness in advance.

In the past, a number of studies have been conducted to predict the surface roughness of parts processed through different AM platforms. A theoretical model was presented to predict the surface roughness for Stereolithography (SLA) parts by introducing two different expressions to predict the roughness of upward and downward-facing surfaces considering the layer thickness, surface angle and layer profile (Reeves and Cobb 1997). The phenomenon of "print-through" on down-facing planes was capable of providing low roughness for a limited range of angles. The phenomenon was responsible for partially curing the resin at the interface of down facing layers, which continued to cure during the subsequent scanning of the next layer. However, complementary processes for surface smoothing were considered necessary. More recently, (Luis Pérez et al. 2001) proposed a geometrical roughness model to predict the average surface roughness of ALM parts; prototypes were fabricated using SLA to compare the theoretical and the actual surface roughness. In their model some corrections were established as necessary for the characterisation of surfaces sloped closely to $0°$ and $90°$.

All the previous models based the prediction of surface roughness on the geometrical description of the stair-stepped profile of sloped surfaces. Such models could fail to accurately predict the surface roughness of AM parts, because surface

roughness might be influenced by other process parameters as shown in (Bacchewar et al. 2007). An alternative approach to roughness prediction has been used in (Ahn et al. 2009); the model interpolated data from empirical observations of test samples; theoretical and real distributions were compared through the fabrication of test parts manufactured by SLA. The phenomenological approach to the roughness prediction exhibits the potential to include the sum of the all contributing factors to the part surface roughness. On the other side, it faces a difficulty in distinguishing among the most influential of the factors. Also, the interpolation of empirical roughness is based on a discrete number of measurements, which means that a large number of measurements is required to achieve a high resolution. The research presented in (Strano et al, 2011) has adopted the phenomenological approach to the production of parts by SLS and used a mathematical multi-objective optimisation technique to simultaneously maximise surface quality and energy saving through an optimal part build orientation. Experimental roughness data were collected and interpolated for a range of deposition orientations, and a phenomenological model for the evaluation of the surface was used in the optimisation procedure. Data collected on downward-oriented surfaces presented a more homogeneous trend than that of upward ones. This was thought to be the result of gravity and surface tension forces on the molten pool during the sintering process: on downward oriented surfaces the molten polymer tends to drop down due to the action of the gravity, thus filling the gaps between layers sintered consecutively and providing "compensation" to the stair stepping effect before solidification.

There is little research reported on the experimental study and computational prediction of the surface roughness of SLM parts. In order to accurately predict the surface roughness, this study analyses the stair step and balling effect contributions to the surface roughness of SLM processed parts at different orientations. Surface characterisation by surface profilometer and scanning electron microscope (SEM)

revealed that the presence of partially-bonded particles on the top surfaces has affected the surface roughness significantly when the layer thickness is comparable to particle size. Classical models for roughness prediction, based on purely geometrical consideration of the stair step profile, fail to describe the observed trend of the experimental data. A new mathematical model has been developed to include the presence of particles on top surfaces, in addition to the stair step effect, for the accurate prediction of surface roughness. Results show that surface roughness predicted by this model has good agreement with the experimentally observed roughness. In addition to solving the multi-objective optimisation problem, this chapter investigates the key contributing factors influencing surface morphology, and a theoretical model for roughness prediction that provides valuable information to improve the surface quality of SLM parts, thus minimising the need for surface finishing.

4.1.2 Build time and post-manufacturing operations for SLM fabricated parts

As with any manufacturing process, the cost of the part in AM is directly related to the manufacturing time. Although complex shaped parts can be produced with significant time saving, the speed of AM fabrication of a part with reduced complexity, compared to standard manufacturing methods, is much slower. In (Sachs 2001) it is estimated that existing mass production methods are 10 to 1,000 times faster. At present, especially for metal processes such as SLM, it can take up to one day to sinter a single item, this does not include time spent for support removal and surface refining. Therefore, production time and costs influence the use of SLM and other AM technologies for large scale industrial applications.

In the SLM process, the build time is greatly influenced by the built orientation as this determines the object height and therefore the total number of layers to be sintered. An additional cost in SLM manufacturing is represented by the amount of time and resources spent during surface refining operations in post manufacturing.

After a geometry with complex shape is manufactured, the mechanical polishing of structured surfaces can be particularly laborious and very often requires a combination of different approaches, such as chemo mechanical polishing, abrasive flow machining and laser polishing (Gessenharter et al. 2003). Mechanical polishing employs pin type and wheel type polishing tools. In order to achieve full contact with one side of the structure the pin tools have to be tilted, therefore it can only be used for the polishing of external surfaces. For the polishing of inner faces, the abrasive flow machining process is particularly suited; the process uses an abrasive medium consisting of a polymer fluid, abrasives with a defined grain size, and additives, that is pressed along the contours at a specific pressure and temperature. In abrasive flow machining, the material removal rate is in direct proportion to the speed of the abrasive medium (Szulczynski and Uhlmann 2002). One limitation of this technique is that the rounding of edges cannot be avoided, this can worsen geometrical accuracy of the part. Finally, laser polishing is performed by focussing a laser beam perpendicularly on the workpiece. Depending on the power of the laser beam the surface of the workpiece is evaporated, i. e. material is removed, or slightly melted. Material is no longer removed and due to surface tension of the melted material a smoothing effect can be achieved.

The example reported in (Gessenharter et al. 2003), shows the complexity of the polishing of metal parts, and the necessity of using various different equipment tools/strategies to achieve the desired surface quality in parts with structured geometry. This also has a great influence on the cost of the end-use product, because of time, manpower, and consumables needed. Thus, during the process planning of SLM

production, important benefits and improvements can be achieved by predicting the surface roughness in advance.

4.2 Model for surface roughness prediction

This section describes the development of a novel theoretical model for the prediction of surface roughness of SLM manufactured parts. The model is derived starting from experimental surface analysis on SLM manufactured samples.

4.2.1 Surface morphology and roughness analysis

A "truncheon" test part was designed to measure roughness surfaces inclined to the horizontal at “slopes” in the range 0° to 90° at 5° intervals (see Figure 4.1). This geometry was used in previous work (Reeves and Cobb 1997), (Campbell et al. 2002), (Ahn et al. 2009), because it allows the surface roughness for each inclination angle to be easily measured. Two sample parts were fabricated with a Selective Laser Melting machine M270 by EOS; the process parameters were: layer thickness 20 µm, beam scan speed 900 mm/s, hatch spacing (distance between consecutive laser scans) 100 µm, and laser power 195 W.

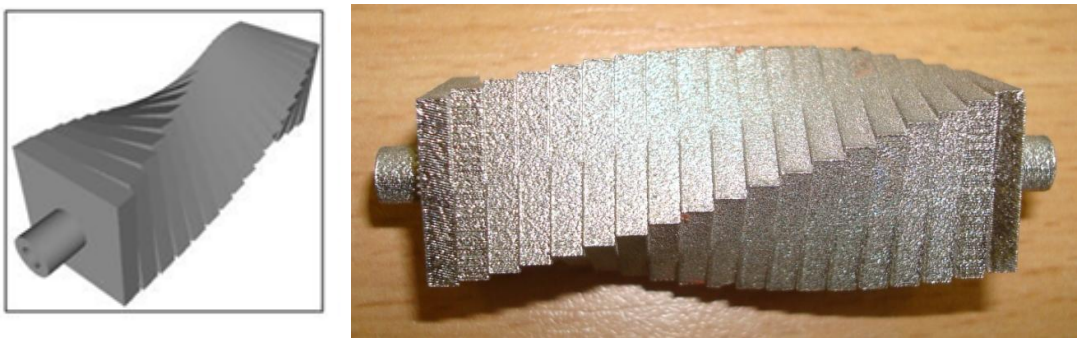

Figure 4.1. Manufactured sample geometry. During building the truncheon is oriented with the long axis vertical.

The analysis of the sample surface was carried out using a surface profilometer (Talyscan 150, Taylor Hobson Ltd). For each inclination, surface roughness was measured using a stylus gauge on a surface of 10 mm x 1 mm, with a scan spacing fixed at 5 µm and scanning speed of 2500 $\mu m \cdot s^{-1}$. To further investigate the surface morphology, at microscopic scale, the sample was treated with isopropanol and analysis carried out using a SEM (S-3200N, Hitachi).

4.2.1.1 Surface roughness and morphology analysis using the profilometer

Data were collected from two measurements on each upward oriented side of two manufactured "truncheon" samples, giving a total of four independent datasets. Figure 4.2 shows the variation in average surface roughness with the sloping angle, with error bars indicating the standard deviation at each angle across the datasets.

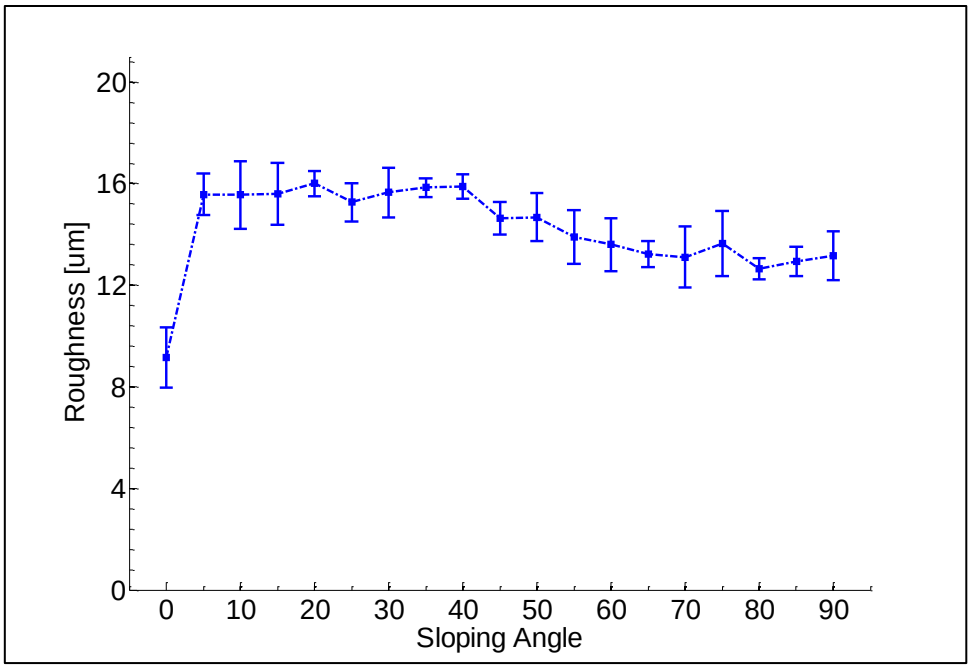

Figure 4.2. Experimental roughness at different sloping angle.

The datasets presented similar trends: for each of them the horizontal surface (0° inclination) had lowest roughness, as expected. Surface roughness at 0° horizontal surface is mainly the result of molten tracks on the surface due to laser melting, which tends to completely fuse the powders and generate relatively smooth surfaces; it may be possible to be further reduce roughness here by surface re-melting (Kruth et al. 2010). As the inclination angle increases from 0°, higher surface roughness results from the stair-step effect. It is important to notice that on inclined surfaces, unlike on horizontal ones, laser re-melting is not possible with SLM technology, since material can only be sintered horizontally. The trend of measured roughness is mainly constant in the range of 5°-45°, with a relatively slow decrease in the range 50°-90°.

A further investigation of the upward surfaces reveals the presence of patterns with vertically aligned reliefs for surfaces at low sloping angles. Figure 4.3 illustrates a number of two-dimensional surface profiles at different inclinations of 5°, 10° and 65°. The white, regularly space, parallel streaks at low sloping angles (Figure 4.3a, Figure 4.3b) correspond to elevated ridges, separated by the distance between stair steps.

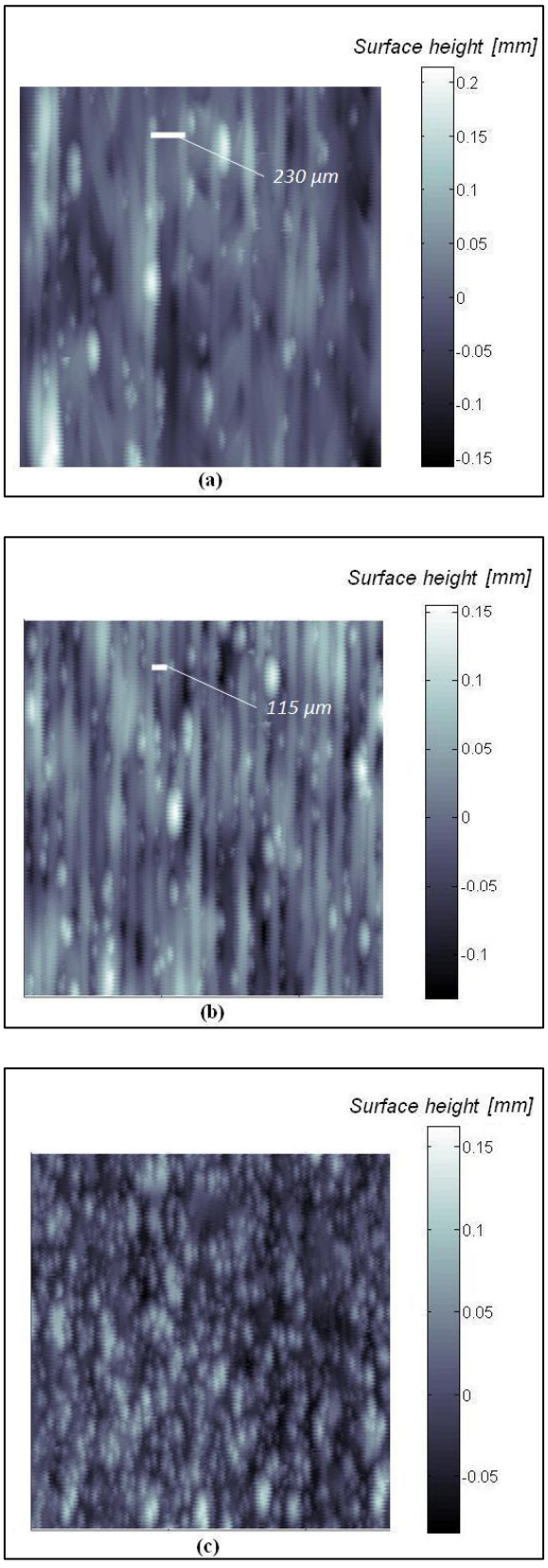

Figure 4.3. Profilometer surface profiles inclined at (a) 5°, (b) 10° and (c) 65°. The grey scale indicates surface height.

For each inclined surface, we compared the distance between consecutive ridges on the scanned surface, and h the distance between consecutive step edges, derived trigonometrically from the stepped profile of surface inclined by angle α (see Figure 4.4) were compared.

$$h = \frac{L_t}{\sin(\alpha)} \tag{4.1}$$

where L_t is the layer thickness and W the step width.

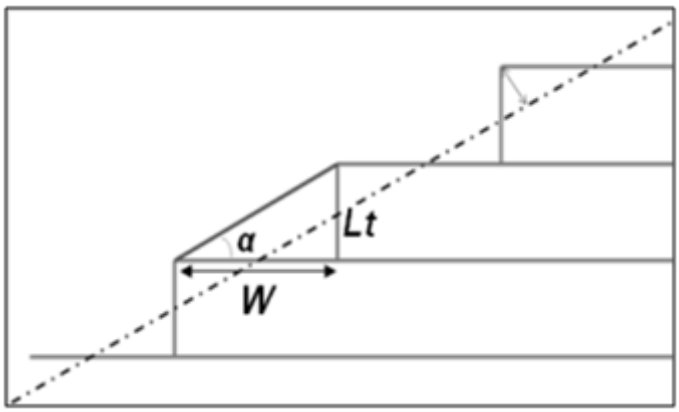

Figure 4.4. Schematic representation of a sliced profile. The dash dotted line represents the mean location of the surface.

Figure 4.5 shows that there is a good correlation between predicted and measured h, for the range of angles up to 50°; for this range of angles, in fact, the stair step generates the waviness characterised by the parallel ridges observed on the surface.

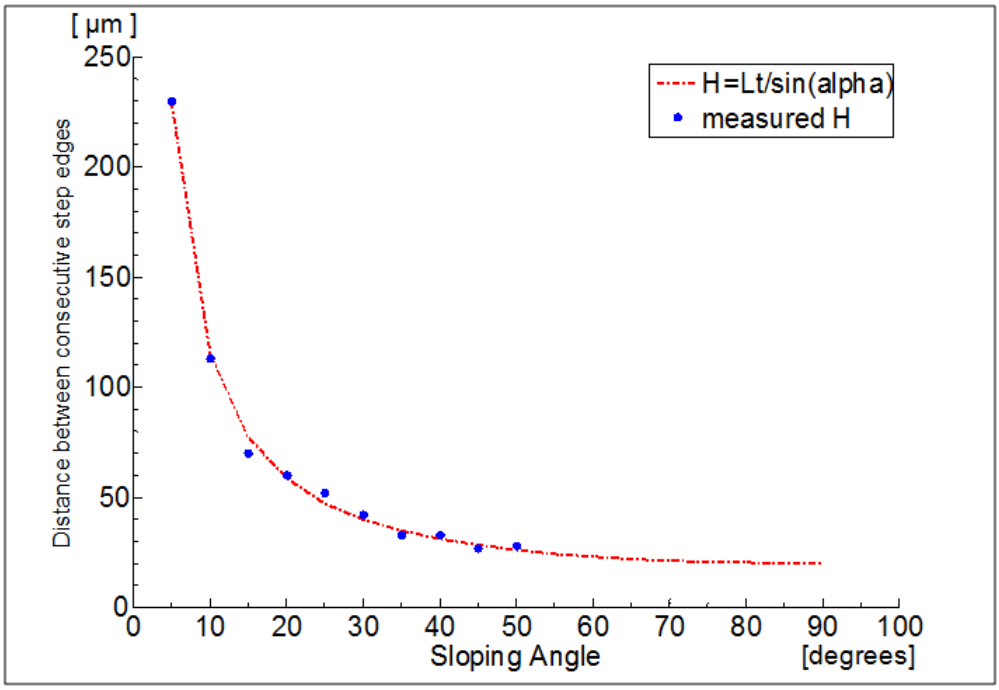

Figure 4.5 Measured and predicted distance between consecutive step edges.

At sloping angles bigger than 50°, the effect of the stair step into the formation of vertical ridges could not be clearly observed and are therefore not plotted. Particularly, at sloping angles greater than 65°, no vertical line patterns were observed; instead, the surface was characterised by the presence of isolated high peaks (Figure 4.3c). In order to characterise the surface morphology at higher sloping angles, and to investigate the contribution of other effects to surface roughness, a surface morphology analysis was carried out by SEM.

4.2.1.2 Surface Morphology Analysis using SEM

SEM analysis has been carried out for a number of different orientations of the SLM part. Figure 4.6 shows the profile of a horizontal surface, normal to the build direction (α = 0). There are few spare, unsintered particles on the surface, because the small layer thickness (20 μm) and the high power (195 W) supplied by the laser beam, meant that the powder was fully melted and fused into a relatively smooth and uniform layer.

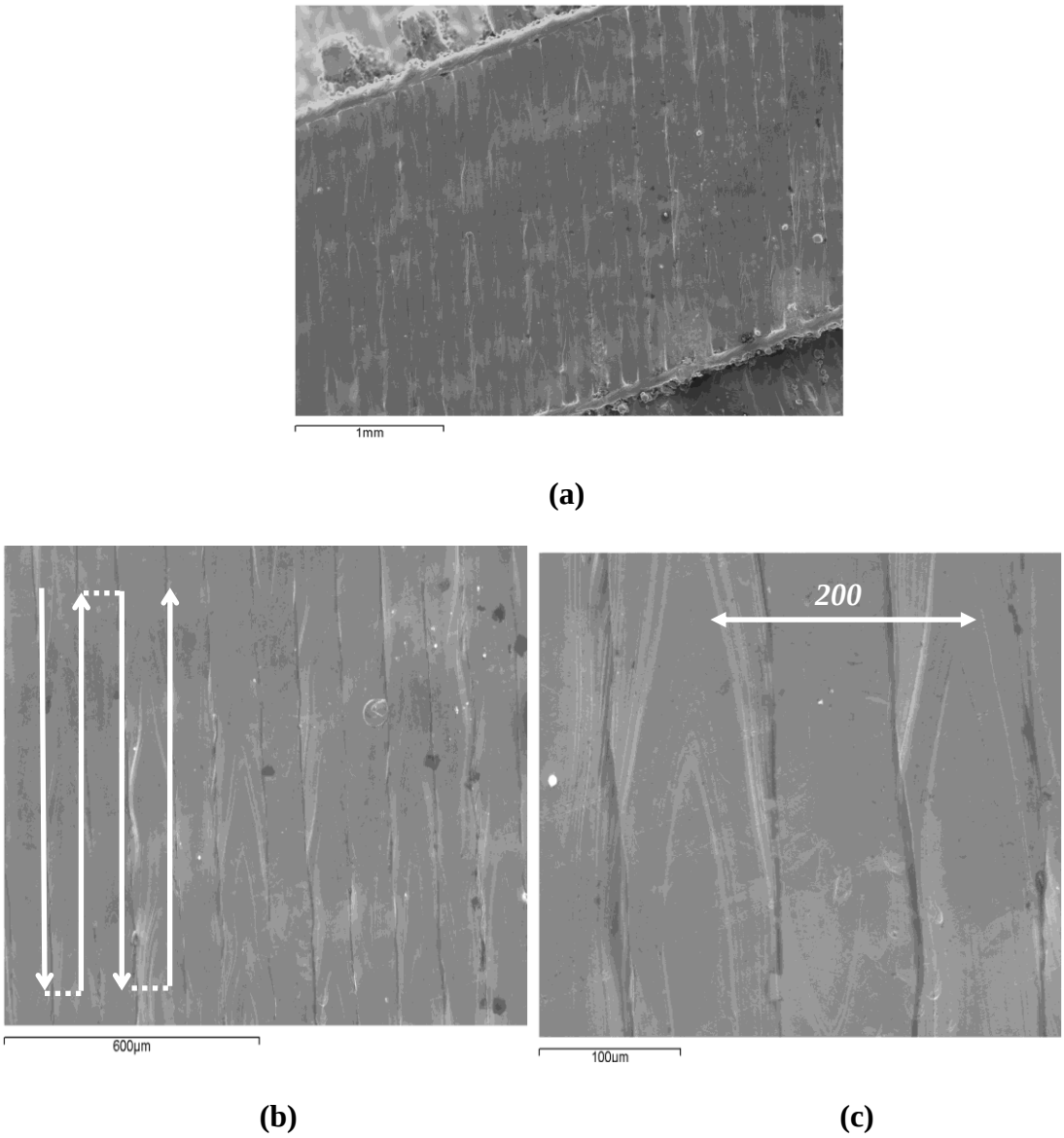

Figure 4.6. SEM picture of a horizontal surface (sloping angle 0°): a) a surface overview, b) detail profile, c) detail profile at high magnification.

In Figure 4.6b the effects of scan direction and strategy (highlighted by the arrows) are visible; for each scan line there are noticeable bullet-shaped marks oriented in the sense of the moving laser beam, it was presumed to be due to slower cooling in the centre of each track. The distance between the centres of these marks within the same orientation was about 200 μm, (Figure 4.6c) as a result of the chosen hatch spacing (100 μm) and laser beam diameter (100 μm).

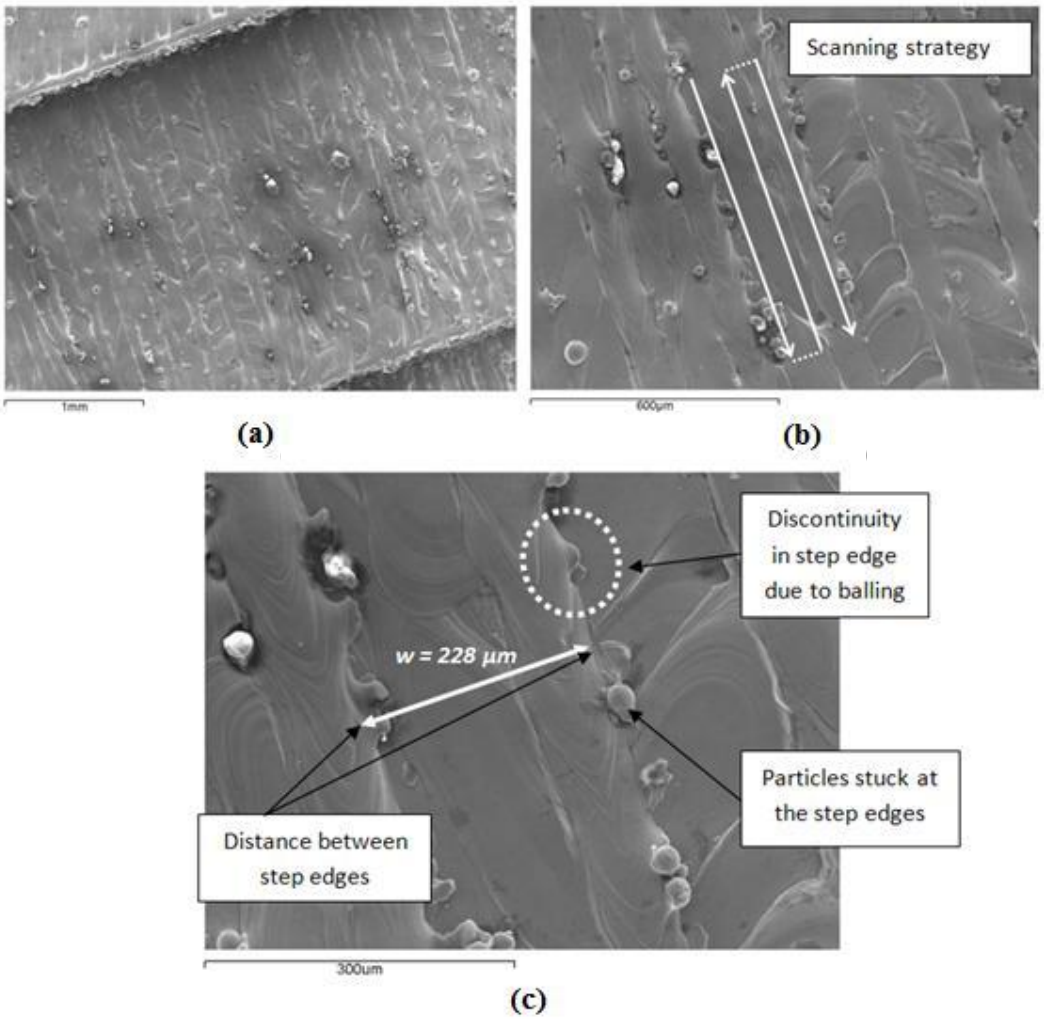

Figure 4.7. SEM picture of slightly inclined surface (sloping angle 5°), (a) at low magnification, (b) at high magnifications, (c) detail of slightly inclined surface.

The surface of the second sample step, with sloping angle of 5° is presented in Figure 4.7. The stair-step is visible at intervals of approximately 230 μm (Figure 4.7c); this confirms the observations made through stylus equipment and the values calculated using Equation (4.1).

When the build incline increases, the SEM micrographs illustrates the lack of sharpness of the step edges, due to discontinuities along step edges and the presence of partially bonded particles stuck at the edge borders (Figure 4.7c).

The formation of discontinuous borders is partially determined by the balling effect that occurs during the laser sintering of the metal powder. Balling is the breakup of the molten pool into small entities. During the laser sintering of metal powders, the high thermal gradient between different volumes of the molten material generates a difference in surface tension within the pool, which produces Marangoni convection (Steen and Mazumder 2010). The general pattern of the flow field is that the material is pulled radially outwards to the surface(Chan and Mazumder 1987). The pool breaks into smaller spherical entities; the detached drops of material scatter on both sides of the pool(Mumtaz and Hopkinson 2009), and, having solidified, they appear as irregularities along the single scan tracks.

During the sintering of the step represented in Figure 4.7c, in order to cover the entire step width ($W = Lt / tan(\alpha) = 228\ \mu m$), three scan tracks were overlapped, starting from the left and moving to the right (Figure 4.7b). The balling produced by each scan is almost entirely removed by the following scan, so the only balling effect is visible only at the final scan of each edge (Figure 4.7c).

Furthermore, partially-bonded particles stuck at step edges are visible in Figure 4.7c. During the laser melting, the heat on the edge borders is not sufficient to fully sinter particles so particles do not merge completely with the layer, tending to stick to the surface at the step edges as shown in Figure 4.7 and Figure 4.8. As the sloping angle

increases, the concentration of particles stuck to edges has been observed to increase. This is because as the sloping angle increases, step edges with adhered particles are closer to each other, leading to higher concentration of particles on the surface area. Figure 4.8 shows the variation of particle concentration between consecutive layers.

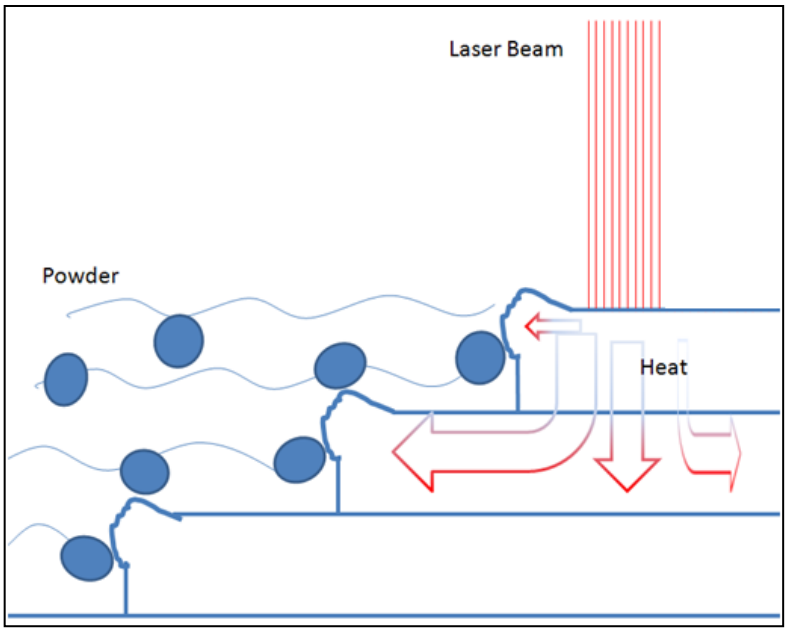

Figure 4.8. Schematic representation of heat diffusion during the laser sintering process.

Figure 4.9 shows the surface morphology on consecutive sample steps, respectively between 5°-10°, 30°-35°, 85°-90° sloped surfaces. Particle concentration increases considerably when the surface at 5° is compared to the one sloped at 10°; as predicted by Equation (4.1). When the surface is inclined at 10°, step edges are closer to each other, than when the surface is inclined at 5°. This explains the higher concentration of particles at 10°. At small sloping angles ($\alpha < 35°$) the number of particles per unit area is expected to be proportional to the distance between step edges, h, because particles

are found principally at step edges. At larger sloping angles the variation in particle concentration is not so marked because $h = L_t/cos(\alpha)$ varies more slowly with α.

No waviness is seen on the surfaces sloped at 85° and 90°, where no stair step is expected. Figure 4.10 shows a particular effect on the 90° inclined surface: a high number of partially bonded, clustered particles are present on the surface, and partially bonded particles can be considered the main cause of surface roughness at 90°.

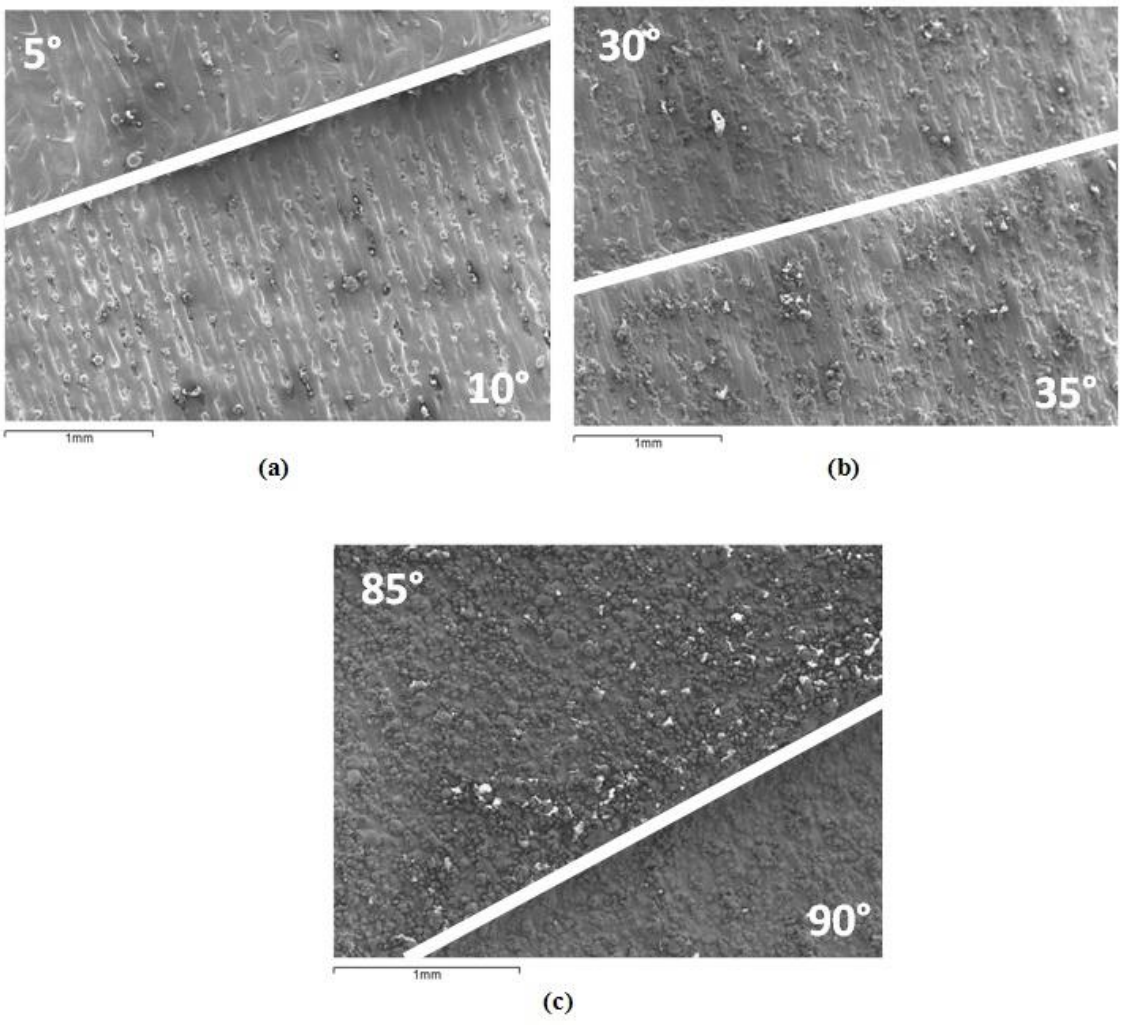

Figure 4.9. Transition between sample steps at a) 5°-10°, b) 30°-35° and c) 85°-90° sloped surfaces. The superimposed white lines mark the boundary between surfaces of the truncheon test piece with different sloping angles.

The trend of measured roughness on the "truncheon" sample can be explained as the effect of increasing presence of particles with surface inclination. At very low sloping angles the presence of particles along step edges does not considerably influence the morphology because the distance between consecutive step edges is much bigger than the particle size. This means that a few particles stuck on the step edges do not make a major contribution to the surface roughness. As the sloping angle increases edges become closer to each other causing the particle concentration to increase. The presence of particles that partially fill the spaces between edges cannot be ignored, and in fact, it affects the measured roughness, causing it to be larger than expected from merely the stair stepping effect. The presence of partially bonded particles results in the high surface roughness at 90°sloping angle even though there is no stair-step presence.

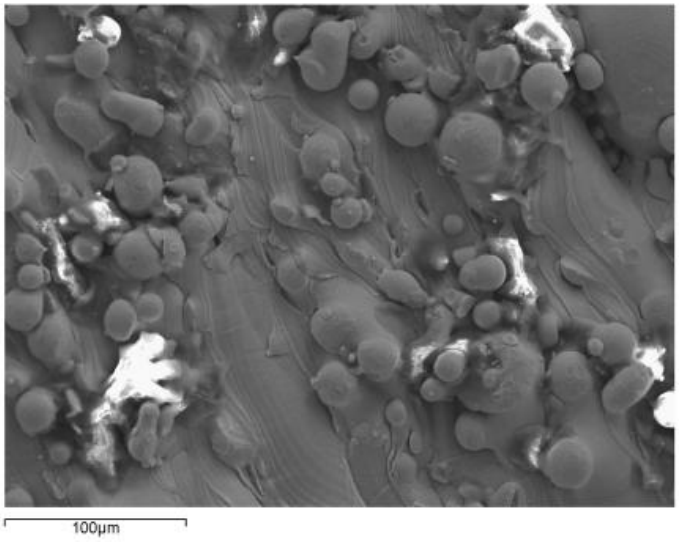

Figure 4.10. Presence of particles on highly sloped surface (sloping angle 90°).

4.2.2 New model for the prediction of surface roughness

This section describes the development of a novel theoretical model for the prediction of surface roughness for SLM manufactured parts. The model describes not only the stair-step effect between consecutive layers, but also the presence of partially bonded particles at step edges.

4.2.2.1 Stair-step effect and surface roughness in selective laser melting

The SLM process starts with a CAD model of the object that has to be built; slicing the geometry involves a level of approximation, described by the stair-step effect (see Figure 4.4).

The surface roughness R_a for the inclined surface represented schematically in Figure 4.11, can be defined as:

$$R_a = \frac{1}{L}\int_0^L |y(x)|dx = \frac{1}{4} L_t \cos(\alpha) \qquad (4.2)$$

where L_t is the layer thickness and α the surface slope angle.

It is evident that an improved surface finish is achievable through the choice of a smaller layer thickness.

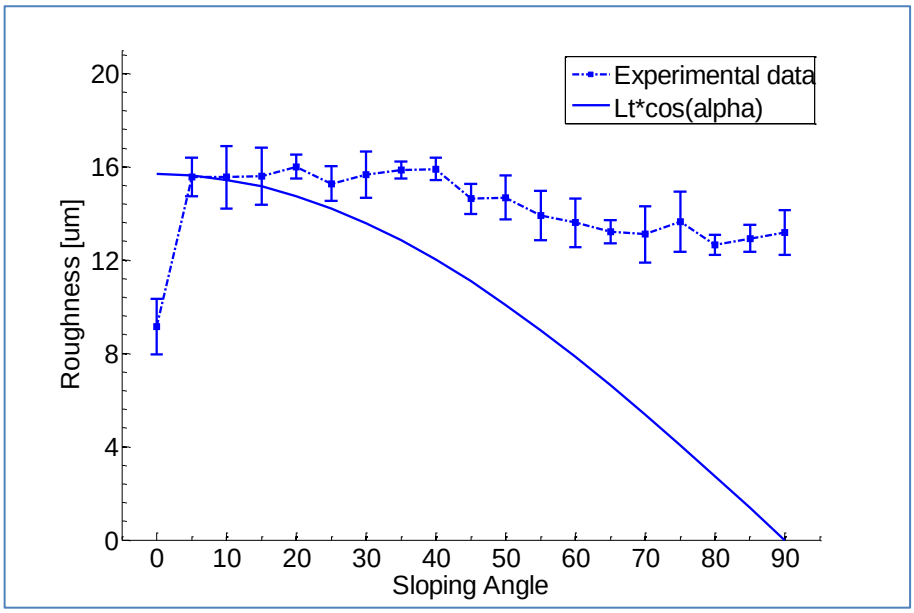

Figure 4.11. Comparison of experimental roughness and simulated roughness in accord to Equation 4.2.

Roughness is expected to decrease as the surface inclination increases, according to the cosine term in Equation (4.2). However, comparison between the experimental data collected and the theoretical roughness predicted by considering only the stair-step effect (Figure 4.11), shows that the stair-step model inadequately describes the measured variation in surface roughness for almost the entire range of incline angles. In particular, experimental roughness does not decrease as much as predicted by the cosine function. The SEM analysis shows that the additional roughness is due to the presence of particles stuck at the step edges.

In these experiments a small layer thickness (L_t = 20 μm) has been chosen, relative to the average particle diameter of 20μm, so the effect of partially bonded particles is readily apparent. When sloping angles are in the range of (5°-15°), the width of each step (228μm -74μm) is bigger than the average particle diameter therefore the surface keeps the characteristic stepped profile, and the stair step effect is well described by Equation (4.2). For higher sloping angles, the width of each step becomes

smaller, compared with the particle size, so that the presence of partially bonded particles can significantly influence the surface profile. For instance, at very high sloping angles (80°-90°) the roughness due to the stair step effect is expected to be a minimum, and theoretically null at 90°, which corresponds to the situation when layers are overlapped on top of each other (however a minor residual roughness is expected because of the limits on the repeatability of the process accuracy). Nevertheless, as observed with SEM analysis (Figure 4.10), the surface presents a high concentration of particles that increase the actual surface roughness to a value of 14 μm.

4.2.2.2 Mathematical formulation

A novel model is presented to describe the effect of partially bonded particles on the surface roughness. As illustrated in Figure 4.12 and Figure 4.13, layers are considered to have depth L_t which form steps of width *w*, corresponding to an ideal surface sloping at angle $\alpha = tan^{-1}(L_t/w)$. For simplicity the partially bonded particles are modelled as if they had a square cross-section (shown as black in Figure 4.13) and it is assumed that a fraction λ along unit length of step edge has partially bonded particles adhering to it. In Figure 4.13(a) the particles are shown schematically as a single block, but, of course, the partially bonded region may be distributed in any fashion along the stair step. Figure 4.13(b) shows a cross section of the modelled surface perpendicular to the laser direction (which moves in and out of the paper) and oriented so that the ideal surface is horizontal.

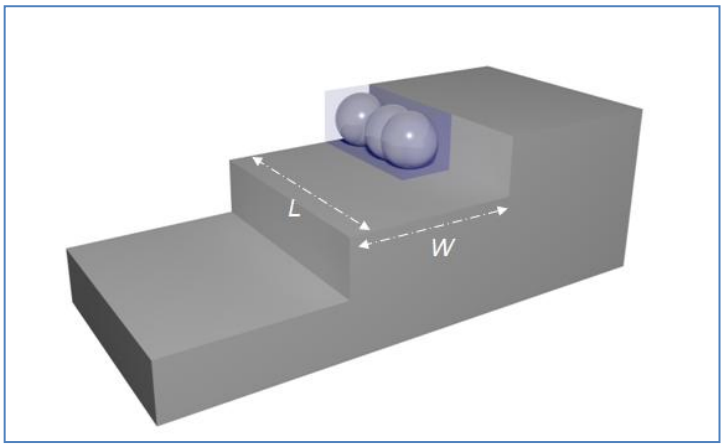

Figure 4.12. 3D Schematic representation of particles partially bonded at step edge.

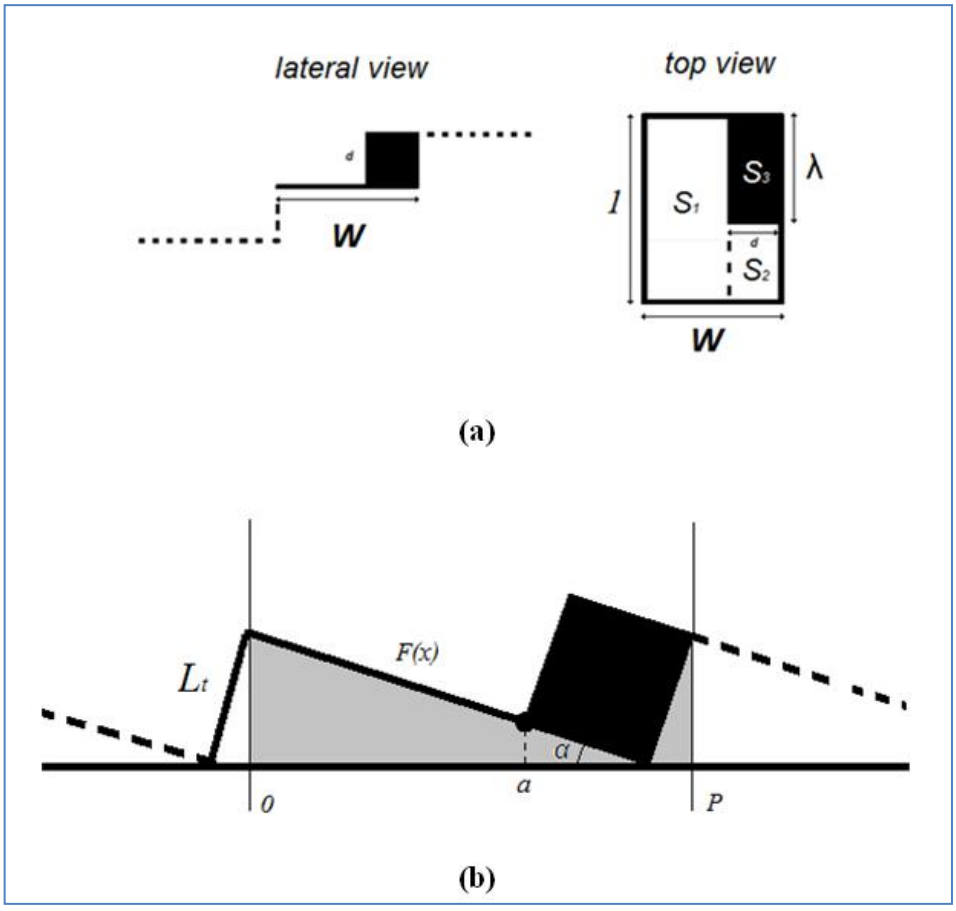

Figure 4.13. Schematic representation: a) lateral and top view of λ fraction of partially bonded particles; b) cross section of the modelled surface.

The height of the surface is denoted as *F(x,y)*, so that the roughness may be calculated as:

$$R(\alpha,\lambda) = \iint_S \left|F(x,y) - \overline{F}\right| dxdy \tag{4.3}$$

where $\overline{F}$ is the average height of the surface above some fiducial level. Considering a single period of the step between 0 and *P* (as shown in Figure 4.13b) and unit length of track, the integral for the roughness may be split into three integrals over the regions S_1, S_2 and S_3:

$$\begin{aligned} R(\alpha,\lambda) &= \iint_S \left|F(x,y) - \overline{F}\right| dxdy \\ &= \iint_{S1} \left|F(x,y) - F\right| dxdy + \iint_{S2} \left|F(x,y) - \overline{F}\right| dxdy + \iint_{S3} \left|F(x,y) - \overline{F}\right| dxdy = \\ &= \frac{1}{P}\int_0^a \left|F(x) - \overline{F}\right| dx + \frac{1-\lambda}{P}\int_a^P \left|F(x) - \overline{F}\right| dx + \frac{\lambda}{P}\int_a^P \left|F'(x) - \overline{F}\right| dx \end{aligned} \tag{4.4}$$

where *F(x)* is the one-dimensional profile describing the stair step and *F'(x)* is the one-dimensional profile describing the step and the partially bonded particles. The average height is calculated as

$$\overline{F} = \frac{1}{P}\int_0^a F(x)dx + \frac{1-\lambda}{P}\int_a^P F(x)dx + \frac{\lambda}{P}\int_a^P F(x)dx \tag{4.5}$$

Figure 4.14 shows the surface roughness as function of the sloping angle α and of particle fraction λ. When $\lambda = 0$, the surface roughness is described by a cosine function which purely describes the stair step effect (4.2).

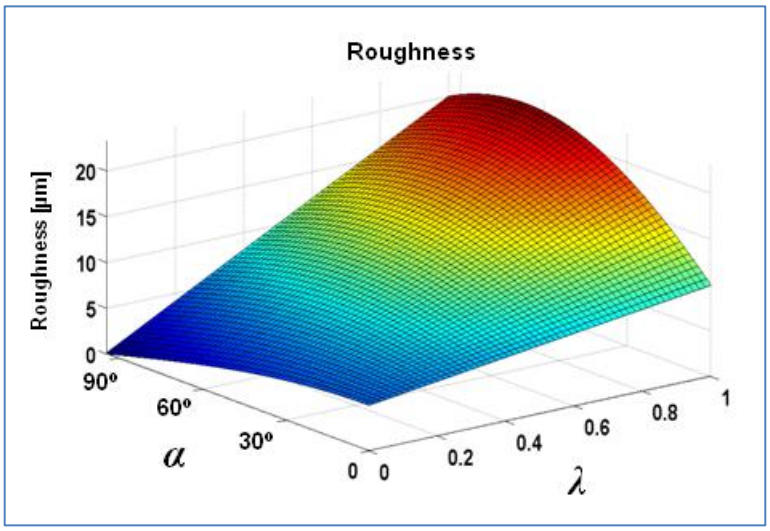

Figure 4.14. Surface roughness calculated using Equation (4.4).

However, as the concentration of particles λ increases, the roughness of greatly inclined surfaces increases markedly; indeed when λ is large the trend of diminishing roughness with increasing α at low λ is reversed.

The average experimentally measured $R_a(\alpha_n)$ at angle α_n is compared with the prediction model by minimising the following error function:

$$\min_{\lambda,c} E(\lambda,c) = \sum_{n=1}^{N} \left| \overline{R_a}(\alpha_n) - c \cdot R(\alpha_n,\lambda) \right| \qquad (4.6)$$

with $\quad 0 \le \lambda \le 1$

to determine the optimum λ and scale factor c. Figure 4.15 shows the best model fit ($\lambda'=0.15$) which describes the experimental data to within the sample-to-sample variation. Since λ is expected to increase with α it has been tried also fitting the experimental data by minimising the average error between $R_a(\alpha_n)$ and $c \cdot R(\alpha, \Lambda(\alpha_n))$ with $\lambda(\alpha_n)$ a flexible non-decreasing function of α; however the use of non-decreasing λ did not provide significantly better results and we therefore prefer the more parsimonious model using an average value of λ.

The comparison between measured roughness, and predicted roughness $R(\alpha_n, \lambda')$ with λ solution of Equation (4.6), is presented in Figure 4.15.

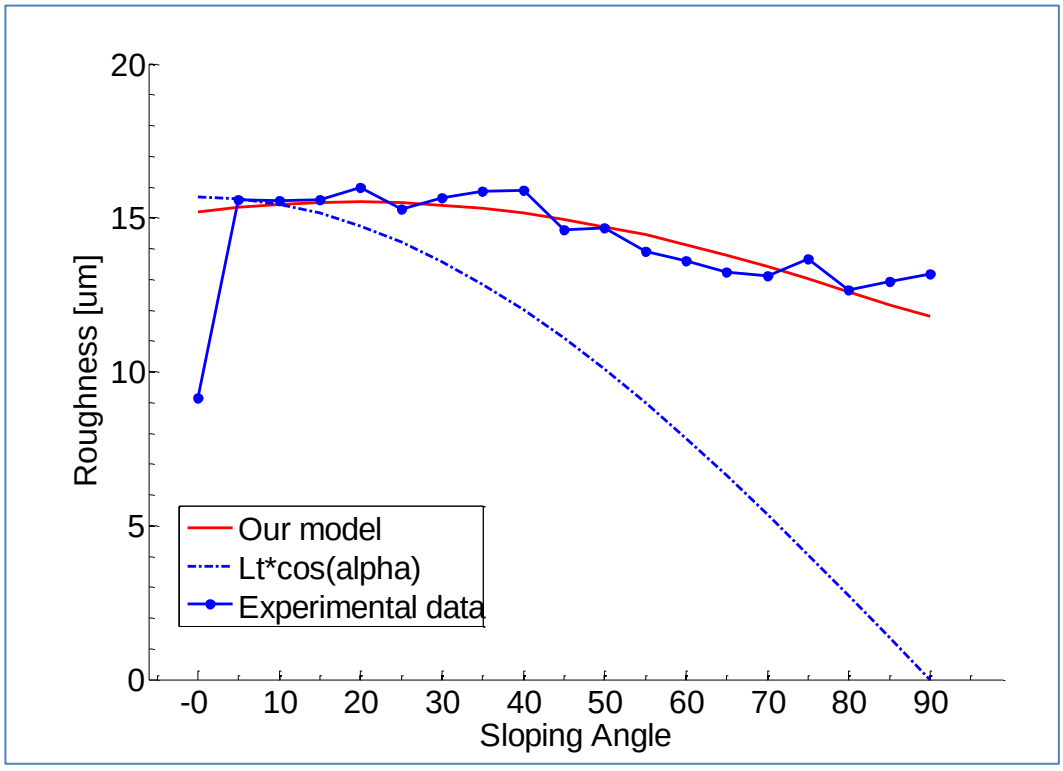

Figure 4.15. Comparison between measured roughness and roughness predicted through newly developed model using Equation (4.5).

Data predicted through the developed model presents a better matching with the experimental data, than the one based on pure geometrical consideration on the stair step profile with no particle presence. At low slope angles, the stair step effect represents the main contribution to surface roughness; at higher slope angles, the increasing presence of partially bonded particles on the surface compensates for the gaps between layers and results in a rough surface. Conventional models that do not include particle presence fail to predict surface roughness, especially at high slope angles. The new model succeeds in describing this phenomenon to predict the surface roughness within the broad range of slope angles between 0° to 90°.

For each facet it can be assumed that the roughness function depends upon the slope angle θ, and the angle between the perpendiculars to the build deposition to the surface facet $\vec{n}$ as shown in Figure 3.6.

If the surface geometry is defined by K facets, the roughness value $R_i(\theta)$ $(i=1,\ldots,K)$ for the ith facet, at any surface angle θ_i, can be calculated using the Equation (4.4), with of $\lambda = \lambda'$, solution of Equation (4.6).

The roughness objective is defined as the average roughness of the surface facets weighted by the facet area, A_i:

$$R_a = \frac{\sum_{i=1}^{K} R(\theta_i) A_i}{\sum_{i=1}^{K} A_i} \qquad (4.7)$$

4.3 Model for build time prediction

As with any manufacturing process, the cost of the part is directly related to the manufacturing time. Production time and costs influence the feasibility of using SLS/SLM and other AM technologies for industrial applications. Layer by layer deposition and consolidation takes considerable time which can be much longer than conventional manufacturing techniques. In this chapter a fixed layer thickness has been considered; even though adaptive slicing is expected to further reduce build time and enhance surface quality.

In the proposed model for build time prediction, the total time to build the part has been characterized by the time for "non-sintering" operations T_z, and the time for “sintering” operations T_s. The time for non-sintering operations T_z, is the sum of time for moving the platform elevator down one step T_p, and the time to deposit a new material layer T_{dep}. Therefore T_z is proportional to the total number of layers N. The time for sintering operations T_S is gives by the sum of T_{Si} the time spent to sinter the i-th deposited layer.

Consequently, the build time T_{tot} for the entire piece is given by the following expression:

$$T_{tot} = N \cdot T_Z + T_S \tag{4.8}$$

with:

$$T_Z = T_{dep} + T_p \tag{4.9}$$

$$T_S = \sum_{i=1}^{N} T_{Si} \tag{4.10}$$

Furthermore, the time T_{si} required to melt the i-th layer of powder, can be expressed as a function of A_i the area of the i-th object slice to be sintered, v_s beam scan speed, and s_s scan spacing;

$$T_S = \sum_{i=1}^{N} T_{Si} = \sum_{i=1}^{N} \frac{A_i}{v_s \cdot s_s} \tag{4.11}$$

If v_s and s_s are constant, T_s can be expressed as:

$$T_s = \frac{1}{v_s \cdot s_s} \cdot \sum_{i=1}^{N} A_i \tag{4.12}$$

Finally, substituting the expressions (4.10) (4.11) (4.12), into (4.9), the expression of the total build time T_{tot} for the entire piece can be expressed as:

$$T_{tot} = N \cdot (T_{dep} + T_p) + \frac{1}{v_s \cdot s_s} \cdot \sum_{i=1}^{N} A_i \tag{4.13}$$

Term $\sum_{i=1}^{N} A_i$ is the volume V of the object, and as such the expression for the total manufacturing time can be rewritten as:

$$T_{tot} = N \cdot (T_{dep} + T_p) + \frac{V}{v_s \cdot s_s} \tag{4.14}$$

As might be expected the build time is therefore a constant plus a factor proportional to the maximum height of the object when oriented for building.

4.4 Multi-objective problem definition and algorithm implementation

The multi-objective optimisation problem has been solved for three different geometries, all defined by the Standard Tessellation Language (STL) used as the input file for the optimisation system. The STL file, which provides a description of the surface geometry, is imported into the Matlab environment where the multi-objective optimisation is performed. The three proposed geometries are shown in Figure 4.16, their surfaces are described by adaptive triangle meshes. Figure 4.16a represents an oil pump shell, Figure 4.16b a generic mechanical part with complex shape, and Figure 4.16c a spar component. All the structured geometries present a high level of shape complexity, and normally their manufacturing by conventional techniques requires considerable time and resources.

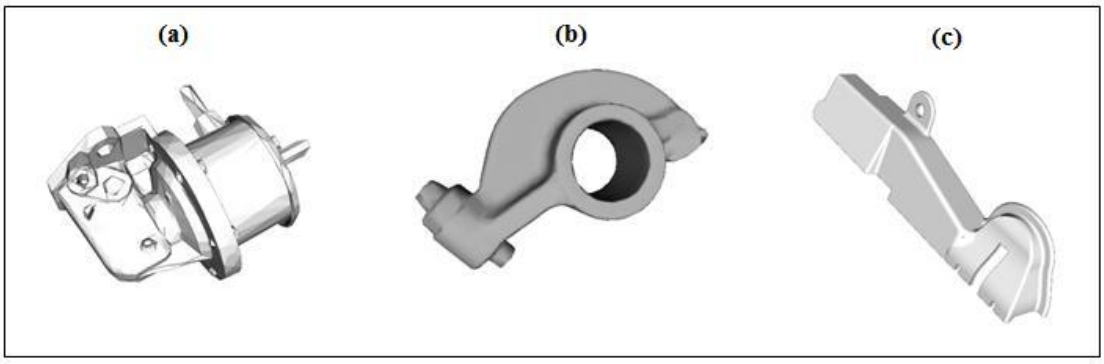

Figure 4.16. Proposed geometries to be processed.

In this case study, the objectives considered are the weighted average roughness and build time calculated by the expressions (4.7) and (4.14). The decision variables for the problem are θ_x and θ_y, rotation angles around the X and Y axes respectively. The rotation

angles are kept in a range between *0°* to *180°* by *5°* steps. Thus, the complete problem of optimal part orientation can be summarized as follows:

$$min\ F(\theta_x,\theta_y)=(R_a(\theta_x,\theta_y),\ T_{tot}(\theta_x,\theta_y)) \quad (4.15)$$

subject to the constraints*:* $0 < \theta_x \leq 180°$ and $0 < \theta_y \leq 180°$

At the beginning, an STL file containing the geometry surface information is imported, then the algorithm starts the rotations around the two axis routines, for each rotation step and each of the objectives is calculated and stored. Once the entire search domain has been investigated including all the possible orientations, the Pareto set of solutions is calculated and plotted.

In this problem, the solution space is sampled at 5 degrees, this resolution makes it possible to search the entire space without resorting to approximate methods such as Genetic Algorithms (GA). The exhaustive search was expected to give a more computationally efficient method of search than a GA, and to provide an approximation of the Pareto front which is limited only by the search domain resolution. However, a solution space with higher resolution, would increase the number of solutions to be identified, therefore might justify the use of a GA solver.

4.5 Results and discussion

The results from the optimisation of both the parts are presented. The result from the optimisation of the first case study are presented in Figure 4.17, where the heavy dots highlight the complete set of Pareto solutions, while the light dots are the non-Pareto-optimal solutions at other orientations; each of these is worse on at least one objective than a Pareto optimal solution, which are therefore to be preferred. Obviously, the orientations which yield low roughness and manufacturing time in the Pareto curve, are to be preferred, on the contrary, the non-Pareto-optimal solutions on the top right of the figure, represent the worst orientations. The Pareto solution that lies on the right end of the Pareto front, if compared to the worst solutions on top right of the figure, allows a reduction in surface roughness of about 15%. The manufacturing time, is expected to be considerably reduced by the choice of the solution at the top left of the Pareto front. Figure 4.18 shows the comparison between the original oriented geometry and two solutions chosen from the Pareto set of solutions in Figure 4.17. Figure 4.18b shows the orientation that minimise the surface roughness objective, Figure 4.18c the one that minimise the total manufacturing time. The solutions that minimise surface roughness objective, calculated as weighted average roughness, are the ones that orientate the artefact such that mesh triangles with larger areas are oriented at angles characterised by lower roughness. As expected, the solution that minimise the build time are the ones that minimise the height of the artefact in the build position. In fact, considering the expression of the build time (4.14), the term $N \cdot T_z$ is directly proportional to the number of layers N, the object's height.

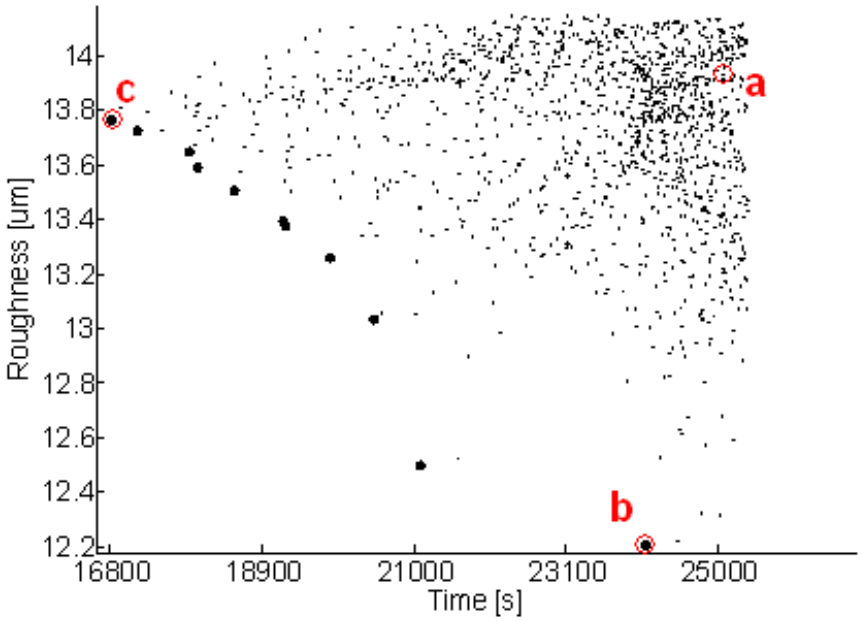

Figure 4.17. Solutions and Pareto front for the first case study.

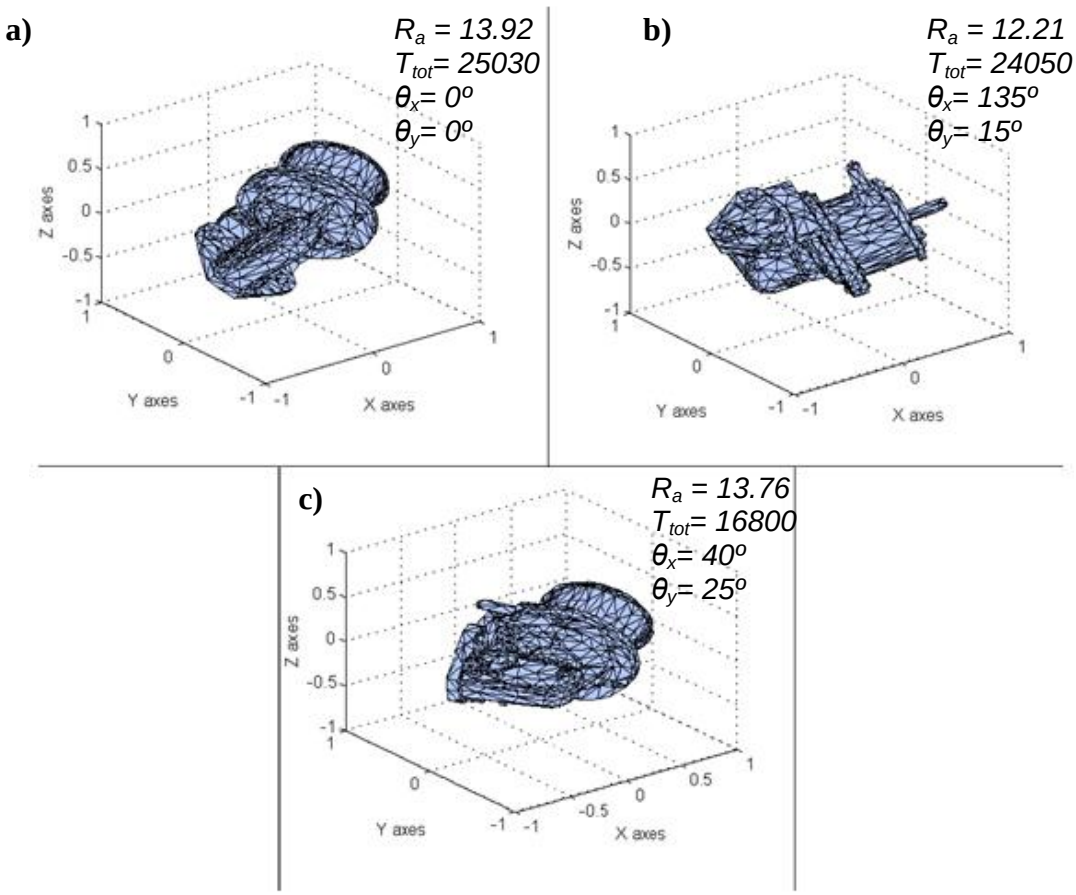

Figure 4.18. First case study at different orientations: (a) original oriented geometry; (b) minimization of surface roughness; (c) minimization of build time.

The Pareto set obtained from the optimisation of the second case study is presented in Figure 4.19. Figure 4.20 shows a comparison between the original oriented geometry and two solutions arbitrarily chosen from the Pareto set of solutions in Figure 4.19. Figure 4.20b shows the orientation that minimises the surface roughness objective, Figure 4.20c the one that minimises the total manufacturing time. Similar to the previous case study, the orientation that minimise the surface roughness is the one that minimises the amount of surface exposed at inclinations characterised by higher surface roughness. The minimisation of the build time is ensured by horizontal part positioning,

in order to minimise the height and therefore the number of material layers to be deposited.

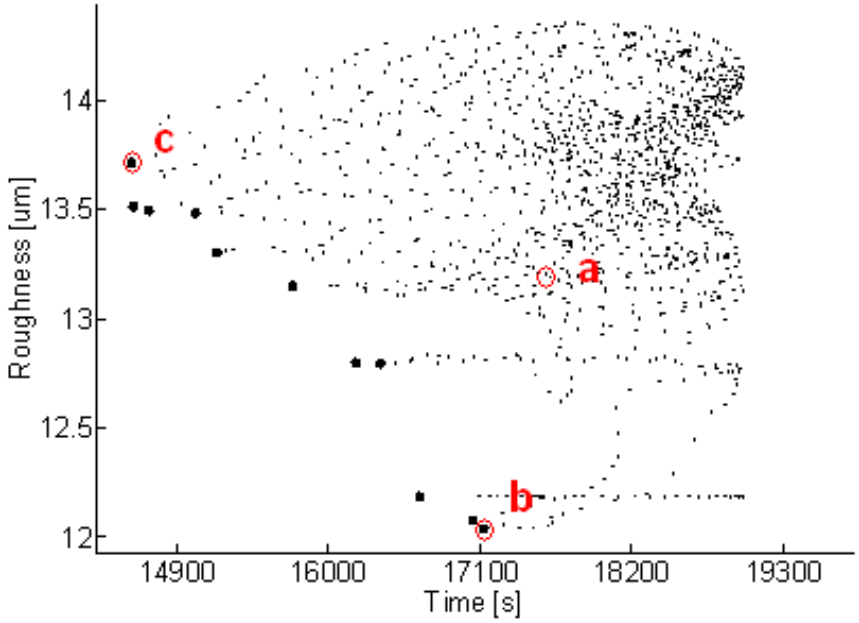

Figure 4.19. Solutions and Pareto front for the second case study.

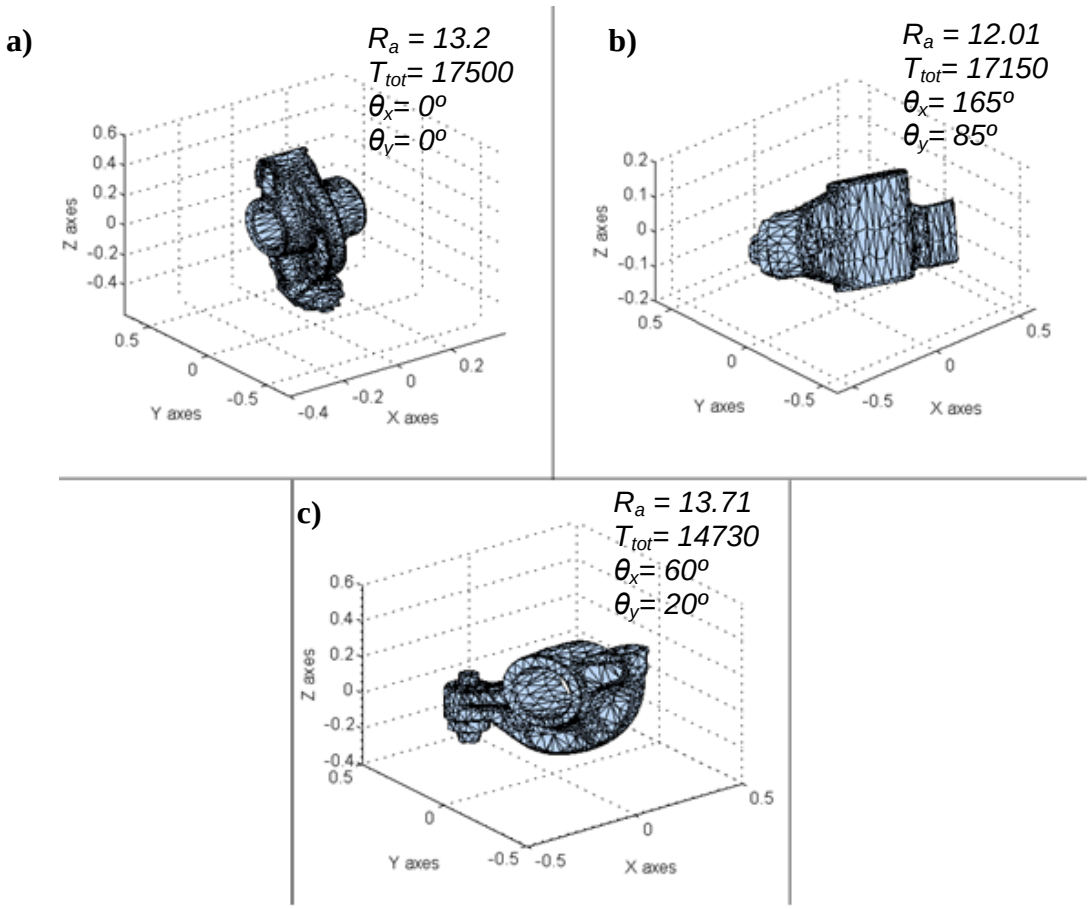

Figure 4.20. Second case study at different orientations: (a) original oriented geometry; (b) minimization of surface roughness; (c) minimization of build time.

The results from the optimisation of the third case study are presented in Figure 4.21 and Figure 4.22. Unlike the previous two cases study, the Pareto dominant solutions are concentrated on almost vertically aligned Pareto front.

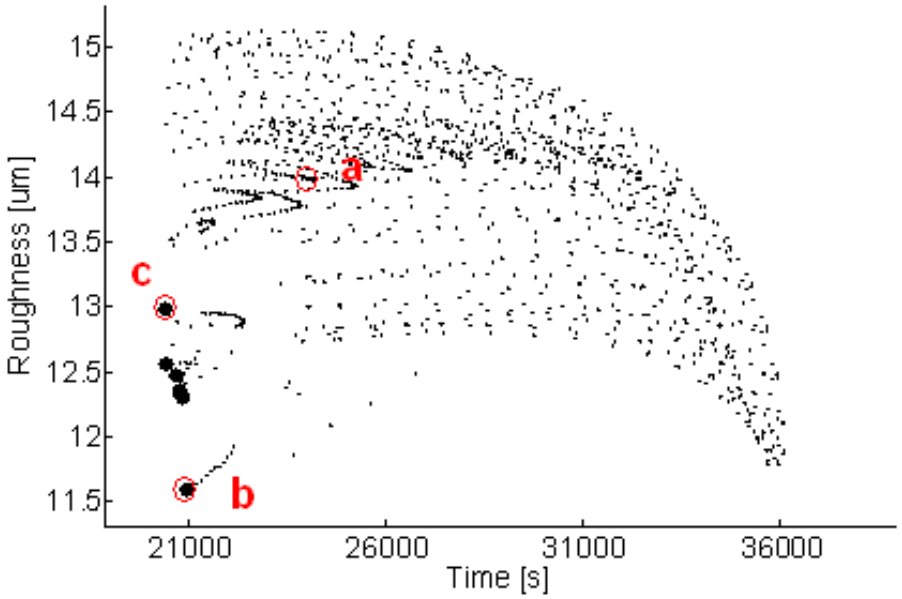

Figure 4.21. Solutions and Pareto front for the third case study.

In this case, the orientation that yields build time and roughness at the bottom of the Pareto curve, is to be preferred because moving away from the bottom, produces an increase in roughness for relative a small gain in build time.

The bottom solution allows approximately a 30% roughness decrease when compared to orientations at the top left of the figure. Similar to the previous cases, Figure 4.22 shows a comparison between the original oriented geometry and two solutions chosen from the Pareto set of solutions in Figure 4.21. Figure 4.22b shows the orientation that minimise the surface roughness objective, Figure 4.22c the one that minimise the total manufacturing time.

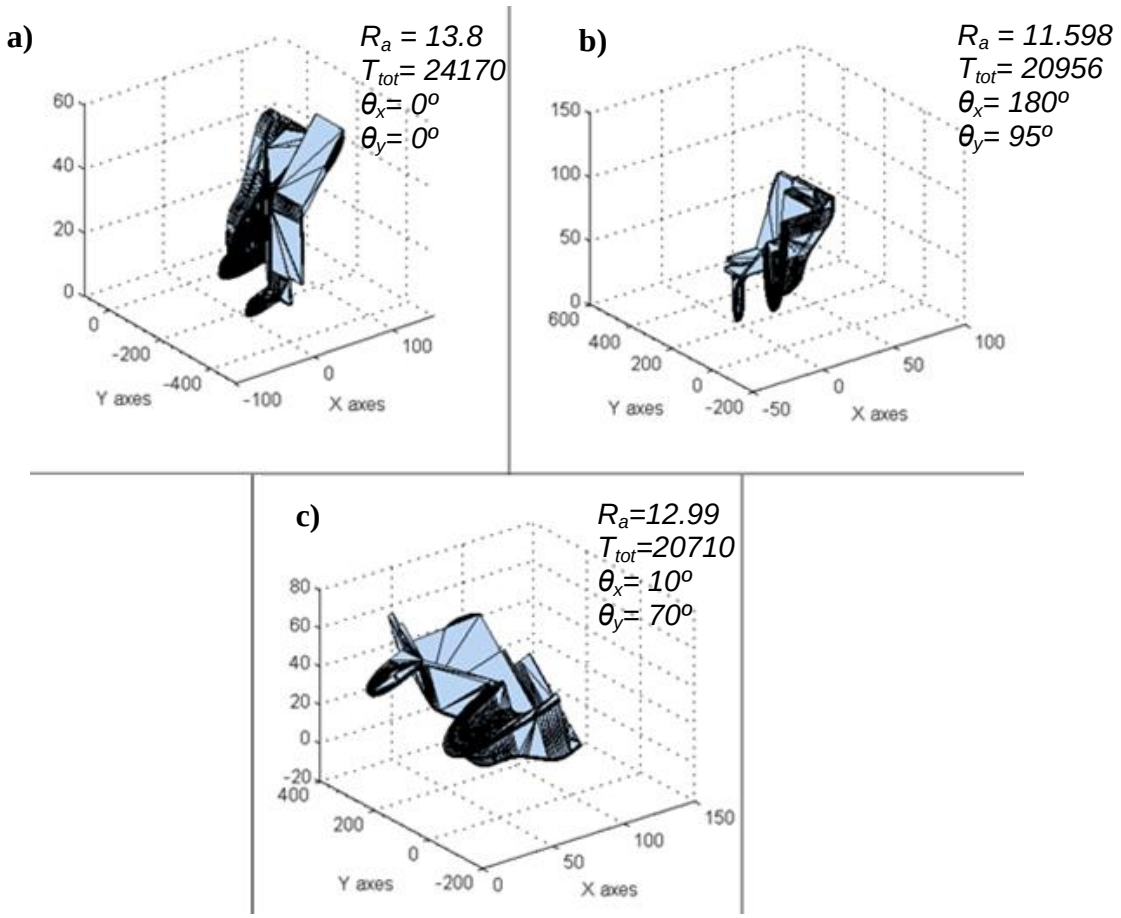

Figure 4.22. Third case study at different orientations: (a)original oriented geometry; (b) minimization of surface roughness; (c) minimization of build time.

4.6 Conclusions

In this chapter, a decision support system for optimal part orientation in SLM processes has been presented. A model based on the multi-objective optimisation technique has been developed in order to find the Pareto set of solutions which define the best compromise between the weighted average surface roughness and build time. The optimisation has been performed for three different case studies.

A model for build time and roughness prediction has been developed. To develop the model for surface roughness prediction, an investigation of surface morphology has been conducted for Steel 316L alloy parts made by SLM. In order to characterise the actual surfaces at different sloping angles, truncheon samples have been produced and an analysis has been conducted at different scales, by surface profilometer and scanning electron microscope (SEM).

Empirical observations of measured roughness by profilometer were different from those predicted through the classic model based on pure geometrical consideration on the stair step profile, due to the presence of partially bonded particles on the surface. In particular, SEM analysis confirmed an increasing density of spare particles positioned along the step edges, as the surface sloping angle increases; during the laser melting of each layer step, the heat applied at edge borders bind them to the step edge. When layer thickness is comparable to particle diameter, the particles stuck along step edges can fill the gaps between consecutive layers, thus affecting the actual surface roughness.

A new mathematical model for the prediction of real surface roughness at different sloping angle has been formulated; the model takes into consideration the increasing presence of particles on the top surface, in addition to the stair step effect.

Unlike a straightforward stair-step model, this model accounts for the observed roughnesses over the full range of surface angles.

The multi-objective optimisation for the simultaneous minimization of build time and surface roughness was solved by an exhaustive searching algorithm that rotated the geometries around the *x* and *y* axes, for three different complex shape geometries. The computational time required was expected to be less than that required by a GA based optimisation; the global optimum (given the search domain resolution) has been found in a reasonable time.

This chapter showed the importance of considering particle presence in the formulation of theoretical models, for an accurate prediction of surface roughness in the SLM manufacturing in steel. Furthermore, results show that, by simply orienting the artefact as described by solutions lying on the Pareto front, significant surface roughness improvements and manufacturing time savings can be achieved. The operator, without prior knowledge or experience can choose from among a set of optimal compromises between the two objectives, depending on his preference. A bad choice of a random orientation, might end up in a part surface deteriorated by the stair step effect and other factors, and/or resulting in a longer manufacturing time and therefore affecting production cost.

The next chapter describes a novel technique for the optimisation of support structures design. Support structures in fact, together with build time and surface quality, represent the most challenging barriers to a more efficient AM of metal parts.

5. Support structure optimisation for additive manufacturing

5.1 Introduction

The additive manufacturing (AM) of parts through technologies such as Selective Laser Melting (SLM) and Electron Beam Melting (EBM), requires the presence of external support structures, because materials employed in those processes, typically metals (Aluminium, Steel, Titanium, Copper, Nickel-based alloys), do not provide sufficient support for an overhanging object (Figure 5.1). Support structures are typically hollow or cellular structures that are sacrificed after the object's build, thus representing a waste in the AM process (Figure 5.2).

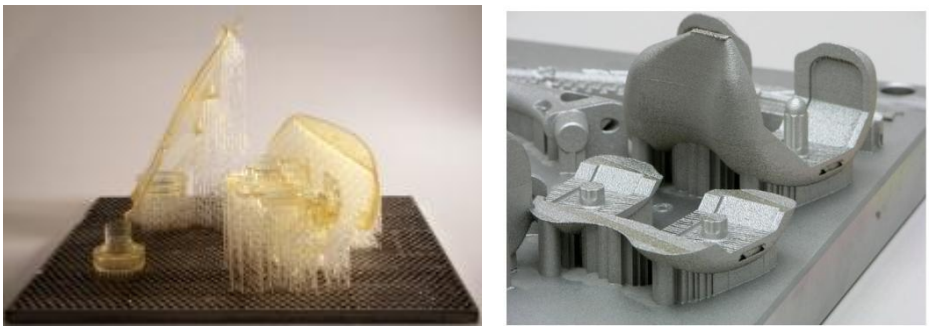

Figure 5.1. Typical polymer and metal support structures in AM.

Support structures introduce a number of issues that limit the efficiency of AM processes:

- The fabrication of sacrificial supports requires time, energy and material, as its supported functional object does. The amount of material wasted by fabricating support structures affects the manufacturing costs, especially when high-value metal alloys such as titanium are employed, for instance in the production of aerospace components.

- The presence of support structures increases both the time required for the part manufacturing, and the time and complexity of post-manufacturing operations. In fact, support removal and surface polishing are usually carried out by expensive hand polishing (Figure 5.3).

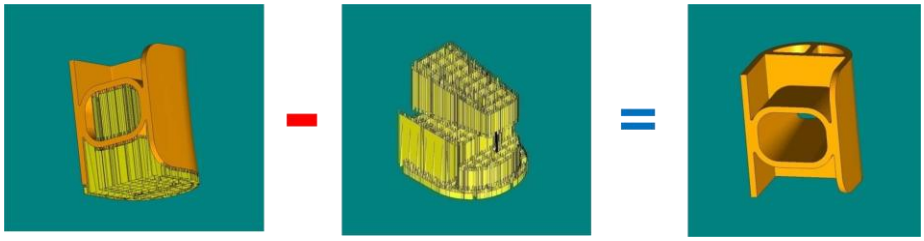

Figure 5.2. Support structures (centre) require considerable amount of material powder. The orange part is the part to be manufactured, the yellow part is the support required to sustain it.

Minimising the amount of supported surfaces can shorten this operation, thus improving post-process efficiency. Consequently, design and optimised material efficient support structures are demanded to improve the sustainability and efficiency of metallic AM.

Figure 5.3. Removal of laminated object manufacturing (LOM) support structure (Cubic Technologies, Inc.).

In this chapter, an alternative approach to the optimal design and generation of support structures in AM is developed, using the SLM process as a typical case study. In order to minimise the amount of support required by the part build by the SLM process, a two-step optimisation algorithm is implemented. As a first step, the best orientation to minimise the volume of support is determined from all the possible orientations; secondly, once the optimal orientation is identified, a further optimisation step performs a support microstructure optimisation in order to further reduce the support volume. The design of the microstructure topology for the supports is performed by 3D surfaces generated by pure mathematical expressions. This approach presented a high flexibility for design cellular structures with different densities, thus reducing the limitation presented by solid modelling software commercially available today.

5.1.1 Support structures and build orientation

For a given object, one of the more effective ways to reduce the amount of support needed is to orientate the object into an optimal building position. Depending on the artefact built orientation, the amount of bottom surface that need support can change dramatically. A previous study (Allen and Dutta 1995) investigated the optimal orientation to minimise support structures for Stereolithography (SLA) process, an AM process for plastic parts. The support was simulated to identify where the part became unstable, overhangs appeared, and components that were separated initially and connected later to the rest of the part. Also, the surface area of the support structure that was in contact with the object was minimised to improve the quality of the surface finish. When two different orientations of an object shows the same amount of support structure, the orientation with lower centre of mass was chosen, since it was more stable. In their research work, supports did not present cellular structures; instead they were treated as solid blocks of materials. An effective way to significantly minimise the amount of material volume for supports could be support design with an internal cellular structure. Support structures in fact have been typically designed as hollow or cellular structure to save materials and energy. A support design approach using cellular structures was presented by (Putte et al. 1997), where some airier support structures were designed, in order to overcome the disadvantages of supporting structures made of solid standing walls. In most of the support structure generation packages commercially available today, the supports' cellular structure design is implemented by combining a number of basic cell elements. For instance the support generation software developed by a company named Materialise locates and group close surfaces with same inclination, and implements a list of rules to determine the appropriate type of supports, such as blocks for large surface areas; lines for narrow surfaces; points for very small

features; gussets for overhanging parts; and web support for circular areas (Swaelens et al. 1995).

5.1.2 Design of cellular support structures

There are several ways to design cellular structures, each method has its own advantages and disadvantages.

The combination of different element structures allows the possibility for users to tailor the support topology by providing choice from different cell types. However, some drawbacks to this method need to be acknowledged. Very often the operation of optimal support is initially approximated, and users need to refine it manually relying on their own experience. Also, unavoidable limits to the surface continuity at the junctions between struts and node fillets are introduced, when different cell types are in contact. This is a problem common to many solid modelling software applications, and it can lead to local concentrations of stress that can degenerate into a structure collapse (Gabrielli 2009). Furthermore, the presence of sharp edges or cavities can facilitate the non uniform distribution of heat during the laser melting process, causing distortion. An additional drawback is the impossibility to develop a regularly graded support structure, which would lead to an optimal distribution of cellular structure density according to the object's weight distribution. Clearly, an optimal distribution of support structure density, that provides more robust support where the object weight concentrates, and reduced density elsewhere, would enhance the ability to achieve an optimal reduction of support volume.

Traditionally cellular structures were created using traditional commercial CAD packages. However these packages have been proven to be unsuitable for potentially

large complex micro-architectures due to the vast number of Boolean operations needed (Wang et al. 2005). Alternatively, voxel modelling presents a more straightforward way to perform Boolean operations. However, this method requires high resolution volumes to sufficiently represent geometries using voxels.

A relatively simple image-based approach to the generation of cellular structures is presented in (Starly 2006). In this work the bounding geometry, defined using a CAD model was sliced into a number of binary images. Each slide was then treated with a Boolean operator to introduce a number of simple unit cells. This slice-based approach avoided the need for handling triangulated surfaces for the creation of an STL file. However, this was likely limited to 3D printing where image-based slices may be used. As with any purely voxel-based method, it also results in a poorly defined geometry at the boundaries (Hao et al. 2011).

Another approach to the generation of micro-architectures is through the use of implicit functions. This technique has been employed in (Gabrielli 2009) and more recently in (Pasko et al. 2010). This approach use a set of periodic implicit functions, such as the Schoen Gyroid (Schoen 1970), to create microstructures. By introducing functional variations to the equations it was possible to functionally grade the microstructure. However, there were no methods given to precisely control the grading, such as the minimum and maximum volume fractions. Furthermore, this method provided a compact representation of the complex structures, and through the use of an appropriate iso-surfacing algorithm, a straightforward way to produce triangulated surfaces.

In the method introduced in this chapter the generation of 3D solid geometries is performed by implicit functions expressed in the form: $f(x,y,z) = 0$, where $f : \Re^3 \rightarrow \Re$. Implicit functions provide a flexible way to design complex cellular structures; also, they provide a compact representation for these structures.

The periodical surfaces that are presented in this work are the "Schwartz" equations (Schwarz 1890), and two others generated by the combination of trigonometric functions, known as "Gyroid", and "Diamond" equations (Figure 5.4).

"Schwartz" level surface equation:

$$cos(x) + cos(y) + cos(z) = 0 \quad (5.1)$$

"Gyroid" level surface equation:

$$cos(x)sin(y) + cos(y)sin(z) + cos(z)sin(x) = 0 \quad (5.2)$$

"Diamond" level surface equation:

$$sin(x)sin(y)sin(z) + sin(x)cos(y)cos(z) +$$

$$cos(x)sin(y)cos(z) + cos(x)cos(y)sin(z) = 0 \quad (5.3)$$

The surfaces generated through 3D pure mathematical expressions, are triangulated in the Matlab environment (see code in Appendix B) to generate a 3D solid structure; the mesh is then transferred into STL file format specification, in order the support to be processed by the AM machine.

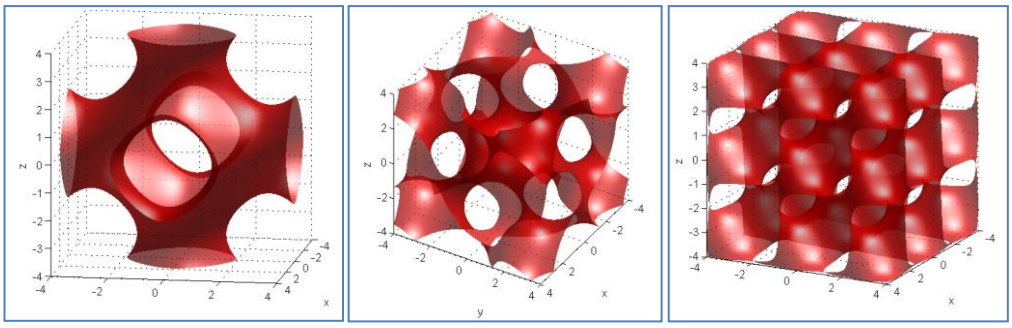

Figure 5.4. From the left, representation of level surfaces expressed by Equations (5.1), (5.2), (5.3) respectively.

By modifying an isosurface equation it is possible to generate functionally graded materials with varying porosity. One possibility for instance, is adding a linear term *kx* to the trigonometric terms of the expression of the Gyroid. In this way it is possible to grade the microstructure along the vertical direction, and the modified expression of the Gyroid becomes:

$$cos(x)sin(y) + cos(y)sin(z) + cos(z)sin(x) + k \cdot z < 0 \qquad (5.4)$$

Figure 5.5 plots the Equation (5.4), with value $k=0.04$.

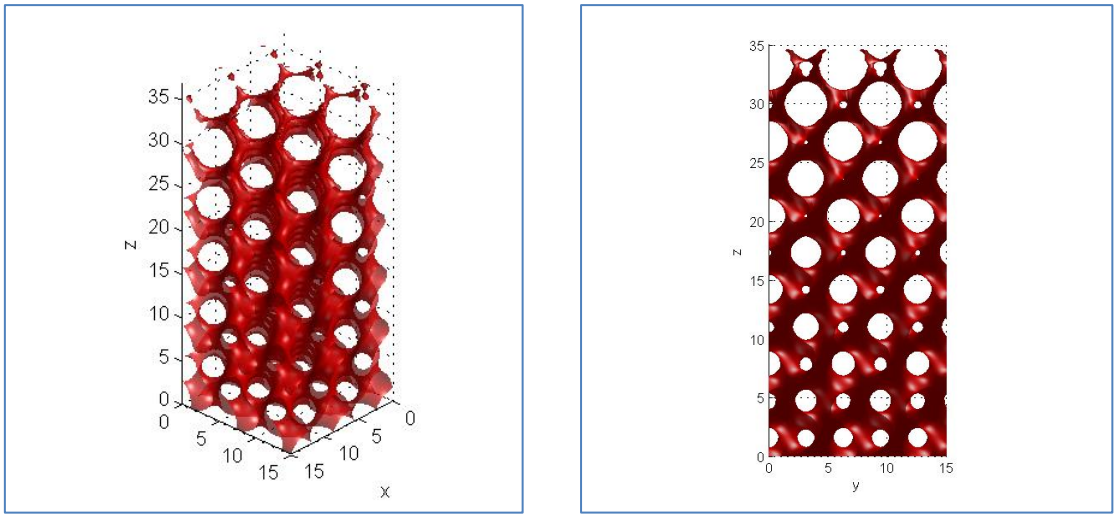

Figure 5.5. Functionally graded geometry described by Equation (5.4), with k=0.04.

From the perspective of the support application, grading the support geometry might present the advantage of reducing the number of contact points between the support and the bottom surface of the part to be supported. This could facilitate considerably the support removal during post-manufacturing, and also the polishing operations, since

fewer points on the surface are touched by the support, creating less deterioration of surface quality. It is important to acknowledge that, on the other hand a too coarse microstructure in contact with the part surface, might facilitate part distortion induced by the laser melting.

Following, as an illustrative example, in Figure 5.6 the application of a Gyroid equation for the potential application of support for a square cantilever plate is given. Three different geometries have been generated, through the modified Gyroid equation.

$$cos(k_1 \cdot x)sin(k_1 \cdot y) + cos(k_1 \cdot y)sin(k_1 \cdot z) + \\ + cos(k_1 \cdot z)sin(k_1 \cdot x) + k_2 \cdot z < 0 \quad (5.5)$$

The first geometry using the values $k_1=0.5$, $k_2=0$ (big cell size); the second using the values $k_1=1$, $k_2=0$ (small cell size); and the third geometry, that is vertically graded, using the values $k_1=1$, $k_2=0.08$.

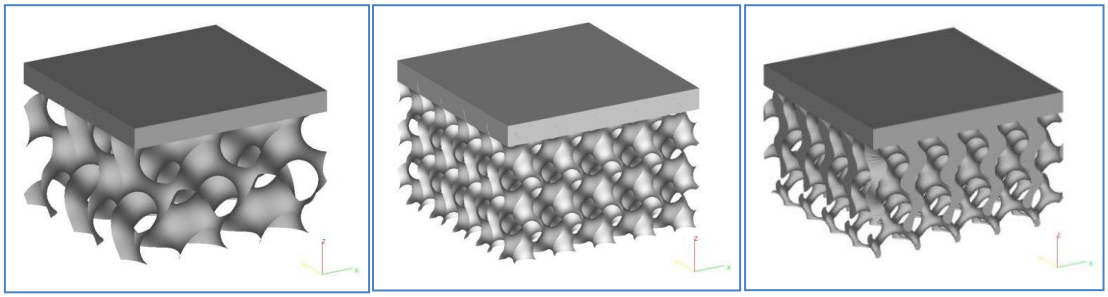

Figure 5.6. Example of support structures, with different cell size and graded structures, mathematically generated by Equation (5.5).

5.2 Design of optimal support structures for additive manufacturing

A novel approach to the optimal design of support structures for AM fabricated objects is now detailed.

5.2.1 Optimisation of part build orientation

For a given object, the amount of support structure is directly determined by the build orientation. In fact, depending on the artefact build orientation, the amount of bottom surface that needs support changes sensitively.

Following the procedure is described that was developed to locate the best orientation to minimise the volume of support, among all the possible orientations. The optimisation is performed by an algorithm implemented in Matlab code (Appendix B). Following, the structure of the algorithm that executes the orientation optimisation, i.e. the first step of the total support structure optimisation is schematically proposed, as is shown in Figure 5.7. The geometry of the object is defined by the Standard Tessellation Language (STL) used as the input file for the optimisation system. The STL file, which provides a description of the surface geometry, is imported into the Matlab environment.

The initial step allows for users to choose: *1)* the distance *"z_base"* between the platform base and the lowest point on the bottom surface of the part; *2)* the parameter *"slop_deg"*, threshold angle of inclination respect with the platform bed, that is used to select the bottom surfaces that are to be supported. Surfaces that are sloped less than the threshold are considered to need support. The next step is to input the geometry, either in the form of ASCII, or binary STL file. The geometry is then rotated around the *x* and

y axes, with a default resolution of *5* degrees. Higher resolutions can be easily specified by the user; however this would increase the number of possible orientations (theoretically infinite resolution), and consequently the algorithm iterations and the total computational time required for the optimisation. For each rotated geometry, the facets that need to be supported are selected, in accordance with the inclination angle specified initially by a threshold value *"slop_deg"* in the preferences.

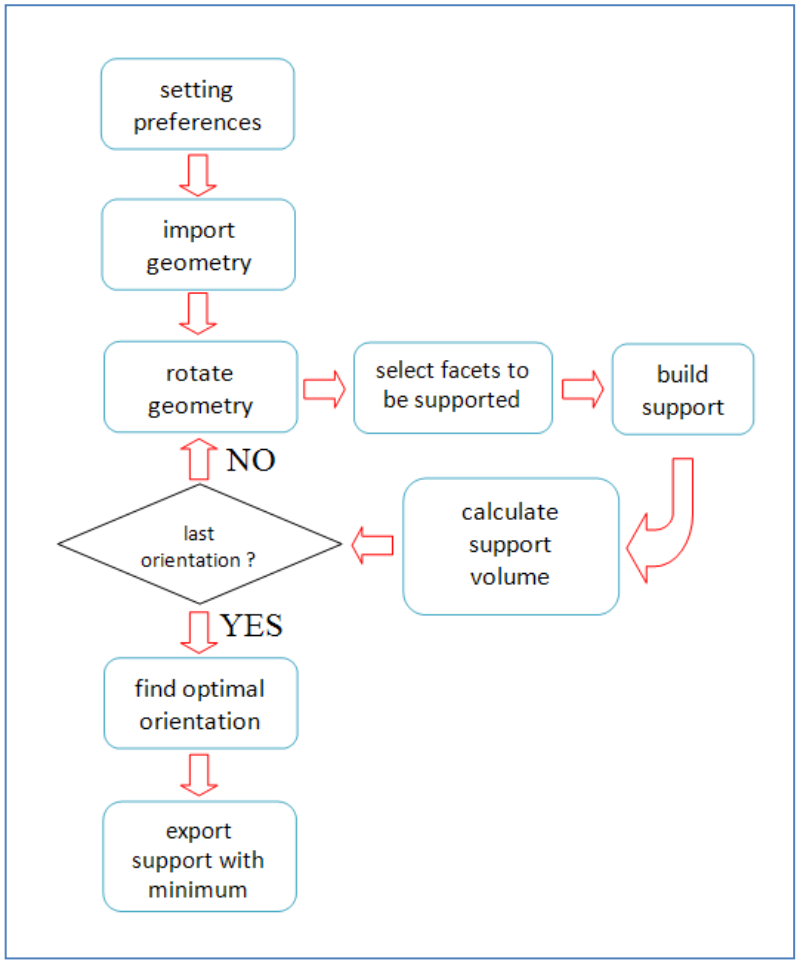

Figure 5.7. Schematic of first step optimisation, for optimal orientation to minimise support volume.

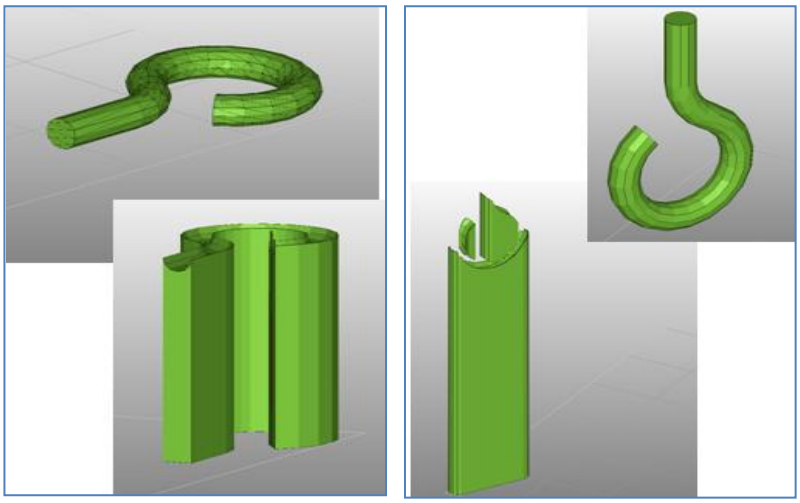

Figure 5.8. Examples of solid supports, generated for arbitrary orientations.

The support is built for the selected surfaces and the relative support's volume is calculated and stored. Figure 5.8 shows two examples of solid supports generated for the "hook.stl" geometry file, at arbitrary chosen orientations, with the threshold value "*slop_deg*" set at *85*°. The threshold value of 85° has been chosen arbitrarily, in order that the support structure (green colour in the figure) is emphasised.

The algorithm iterates until the supports for all the orientations are calculated. Once all the possible orientations are investigated, the orientation that requires minimum support volume is identified, and the relative support volume exported in the form of an STL file for eventual visualisation/manipulation.

5.2.2 Design of support structures using 3D mathematical functions

A second algorithm described is now described which is used for the design of optimal cellular structures, to act as support for AM platforms. The proposed method provides a function to tailor the volume fraction of support structure to generate more robust support where needed; thus it enhances the efficient employment of support structures. Following Figure 5.9 describes the structure of the algorithm to design graded support structures.

The algorithm first starts by importing the STL geometry oriented optimally as a result of the first stage optimisation. For the example each algorithm step on a simple 3D geometry file, "test.stl" is illustrated.

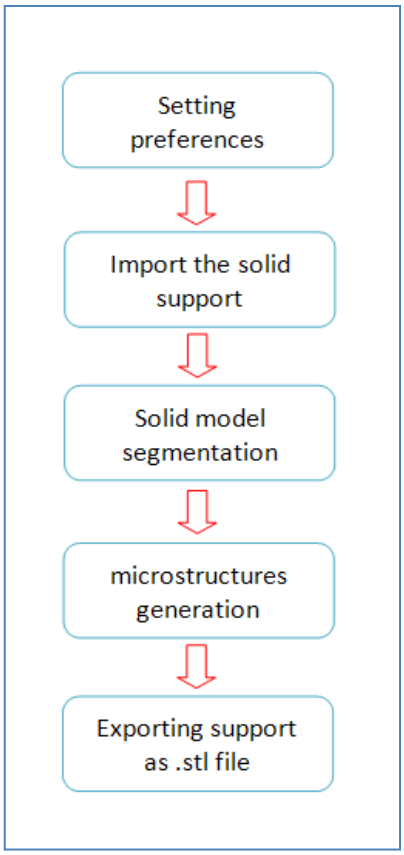

Figure 5.9. Schematic of second step optimisation, for the generation of a graded microstructure

Figure 5.10 shows the "test.stl" geometry in the original orientation (left), and the optimal orientation (right) that minimise the volume of support. For illustration purposes, a choice to fully support all the downward oriented surfaces has been carried out, by setting the threshold *"slop_deg = 90°"*. Also, in the preference settings, a distance from the platform base of the machine has been set to *2 cm*. The choice of "*slop_deg"* and *"z_base"* has been done arbitrarily. The optimally oriented "test.stl" geometry and the associated solid support are visible in Figure 5.10.

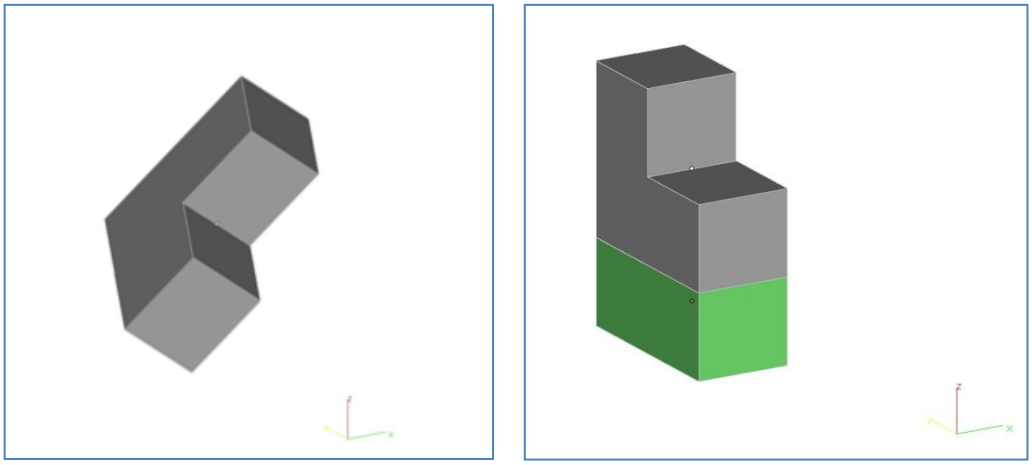

Figure 5.10. "test.stl" geometry oriented as originally (left), and optimally (right). In green, the associated solid support.

Once the "test.stl" has been imported, the solid volume is segmented; in Figure 5.11 two sub-volume blocks have been identified, as represented by different colours.

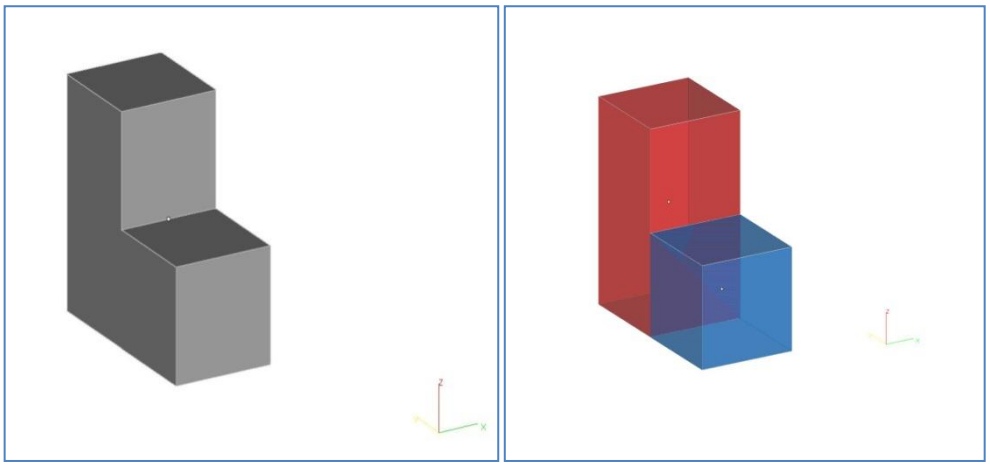

Figure 5.11. Segmentation of entire volume of the object into sub-volumes.

For each block, an associated microstructure support is generated through the use of implicit functions, and using cells with a different volume fraction. The use of implicit functions in fact allows the volume fraction to be specified by simply introducing a variation of the original equations. One possibility is changing the periodicity of the trigonometric terms of the equation, by adding a term *k*. For instance, the modified expression of the Schwartz equation becomes:

$$cos(k_x \cdot x) + cos(k_y \cdot y) + cos(k_z \cdot z) = 0 \quad (5.6)$$

5.2.2.1 Effects of changing cell periodicity

Changing the cell periodicity will generally affect the cell size. The continuity of the implicit trigonometric function is generally not conserved after having merged the support with different cells size, as observed in Figure 5.12. The detail of the support

microstructure (in the figure, the red square at the right), highlights a typical discontinuity that can appear at the interface between blocks with different cell sizes.

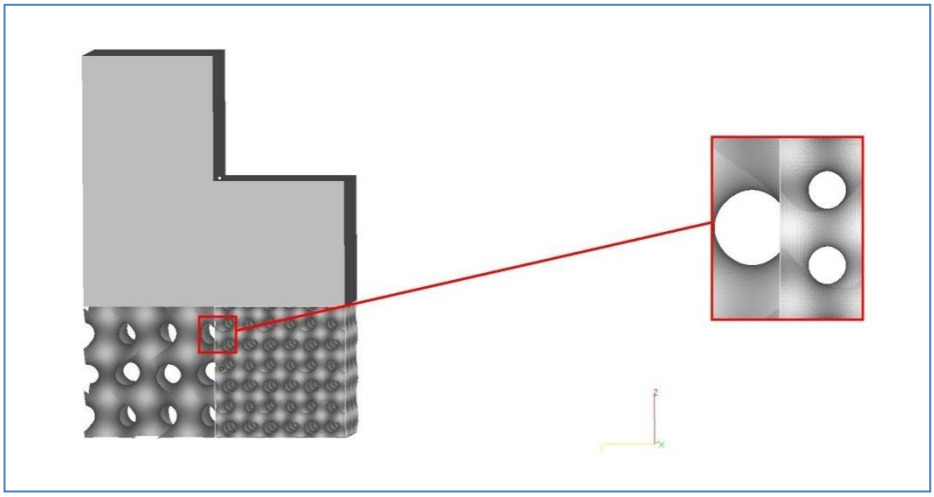

Figure 5.12. Discontinuities might appear at the interface between blocks with different cell sizes.

However, from the structural point of view, the formation of discontinuities is not expected to represent a serious issue in the specific application of support structures. When a discontinuity appears, there are no transverse load conditions that could yield to stress concentrations that would degenerate into a structure collapse, because each sub-volume of the object displaces a vertical load which is vertically sustained by the corresponding support block below. In fact, the use of minimal surfaces allows the stress to be distributed into the structure homogeneously, due to the absence of cavities or peaks that would otherwise locally concentrate the stress (Gabrielli 2009).

In order to limit the number of discontinuities at interfaces between blocks of different cell types, the periodicity along one or more directions can be conserved. For

instance, the two different Schwartz cells represented in Figure 5.13 have been produced assuming the same periodicity along the *z* direction, fixed at $k_{z1} = k_{z2}=0.75;$ and using the values k_{x1} = 0.75, $k_{x2}=1.5$, and k_{y1} = 0.75, $k_{y2}=1.5$ for the *x*, and *y* axis respectively.

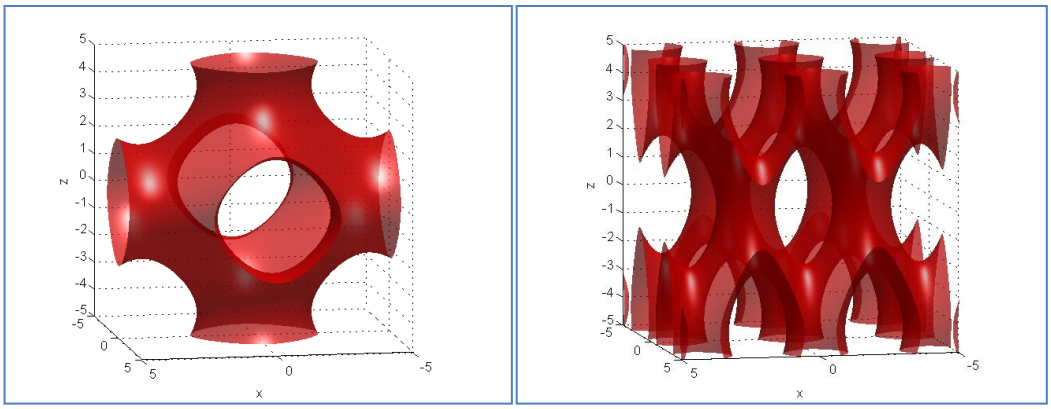

Figure 5.13. Schwartz cells with the same periodicity in z direction ($k_{z1} = k_{z2}$).

5.2.3 Method validation

The method proposed in this chapter has been validated by prototyping the "Test.stl" part in its optimal orientation, and its support (Figure 5.14). As seen in the figure, the support presents a graded volume fraction, given by the combination of the different periodic microstructures. In order to limit surface discontinuities, the periodicity on *z* direction has been conserved, by specifying $k_{z1} = k_{z2}$. The manufactured artefact and its support are shown in Figure 5.14 (right). The artefact has been manufactured, for prototyping purpose, by an EOSINT P 800 Selective Laser Sintering Machine (EOS GmbH, 2011).

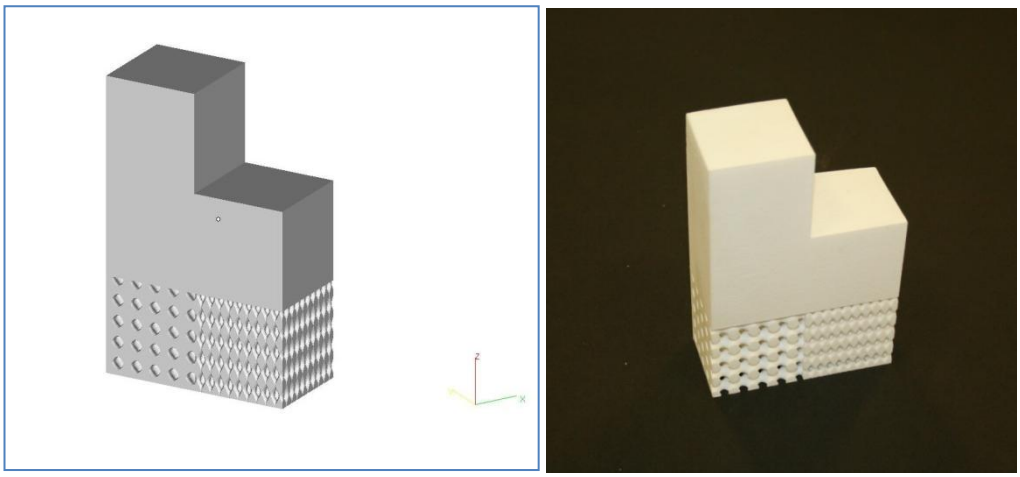

Figure 5.14. Final support structure for "test.stl" geometry (left); manufactured geometry (right).

The STL file with the support for the entire part is finally exported for visualisation/manipulation. The diagram in Figure 5.9 summarises the algorithm routines discussed.

5.3 Evaluation of a complex shape structure as a case study

A more complex shape geometry shown in Figure 5.15 is used as a case study to evaluate a new support structure design and optimisation algorithm. The geometry “cell.stl”, represents a cylindrical truss cell core, typically employed for the production of lightweight aerospace applications. The limits of conventional manufacturing processes for the manufacturing of truss structures have been previously discussed in Section 2.1; in this context it is briefly stated that the manufacturing of a complex geometry such as the “cell.stl” would be typically impossible without welding the single trusses and the welding would produce weak junctions where cracks and corrosion could occur.

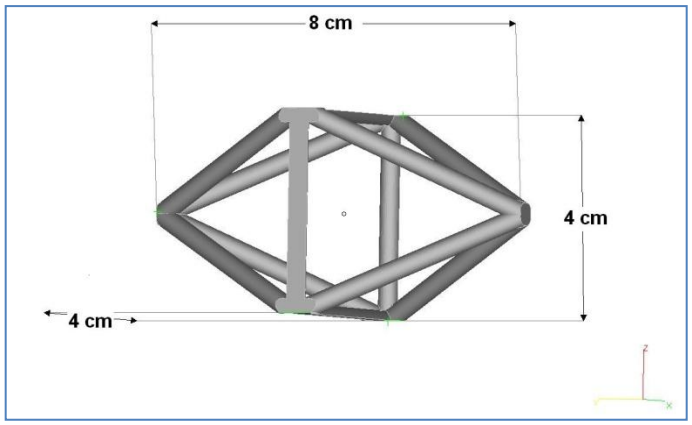

Figure 5.15. Truss structure geometry "cell.stl".

In the parameters set for the optimisation, it has been set to support all the downward surfaces inclined less than *35*° are supported in accord with the actual standards on EOS

M270 machine (EOS GmbH, 2011). The height between the platform base and the part has been set to zero. The support microstructure has been generated by using the Schwartz equation. The solid support for the original orientation generated by the algorithm is shown in green in Figure 5.16; the support affects a large portion of the object surface, this is because in the original orientation, almost all the trusses are horizontal or inclined less than 35°.

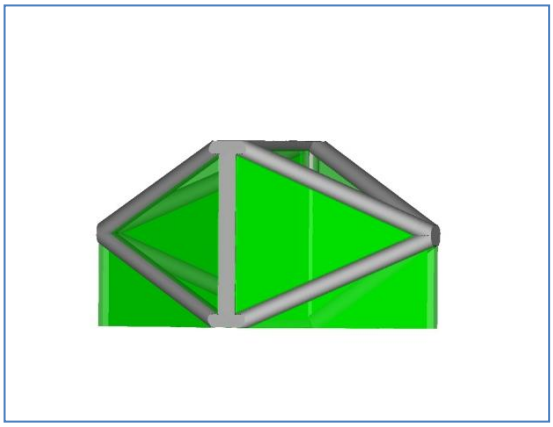

Figure 5.16. Solid support for original orientation.

In Figure 5.17, the best orientation, with minimal amount of support needed, is shown at the left, and for the purpose of comparison, the worst orientation, with maximum amount of support needed, is shown at the right, respectively.

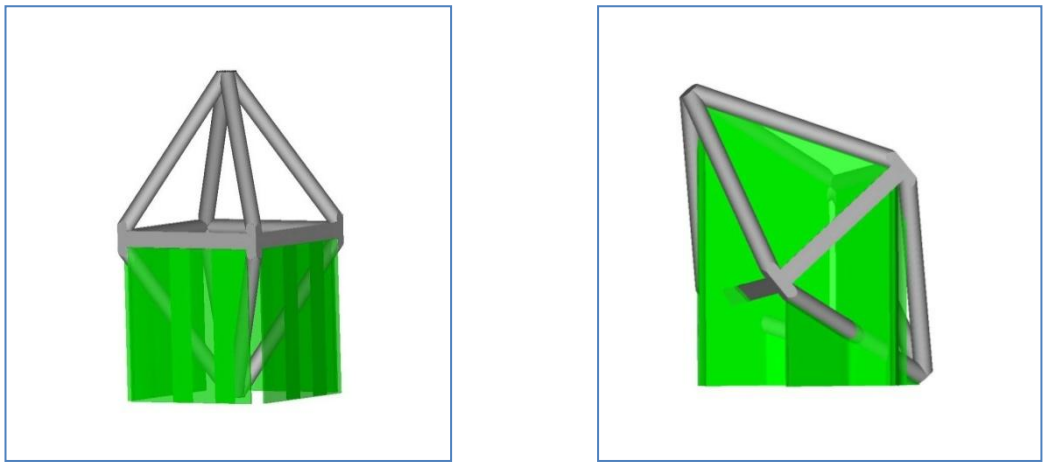

Figure 5.17. Best (left) and worst (right) building orientation for "cell.stl" geometry.

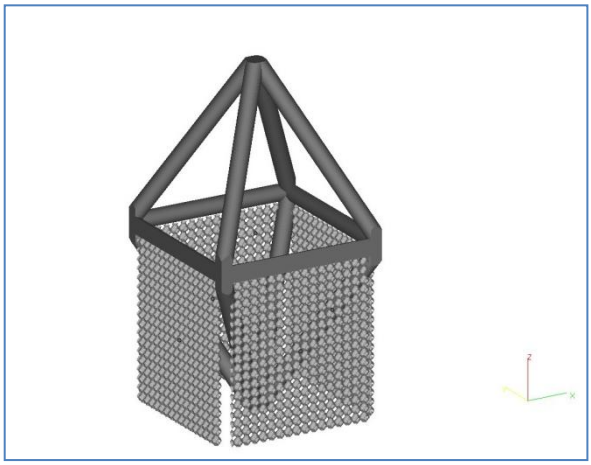

Figure 5.18. Final support structure for "cell.stl" geometry.

The final support structure generated for the “cell.stl” is shown in Figure 5.18; unlike for the “test.slt” case study, the support does not have a graded microstructure. This is because of the part symmetry that puts weight distribution with equal intensity on each of the supported trusses.

5.4 Result and discussion on support structures for a complex structure

The solid support for the original orientation (Figure 5.16) affects a large portion of the object surface, because in such orientation almost all the trusses are horizontal or inclined less than 35° with respect to the platform bed, thus they require support. As a consequence of building the geometry with this orientation, a large portion of the object surface will be deteriorated, because of contact with the support, and expensive and long time operations of surface finishing will be required during the post-manufacturing stage (Frank and Fadel 1995), (Pham and Demov 2001). Furthermore, the volume of support will require the sintering of a large amount of material powder, which has extra costs in itself, and will also increase time and energy for the manufacturing process. In addition, due to the complex shape of the geometry the operation of support removal could be difficult, especially without running into the risk of damaging any trusses. Table 5.1 shows a comparison of material savings for different build orientations; the best orientation shown at the left of Figure 5.17, allows a 45% saving of support with respect to the original orientation, and a 55% saving with respect to the worst orientation. In the optimal orientation, most of the part volume is displaced in such a way as to support itself. Only four trusses need an external support structure, thus enhancing easier support removal, and minimising the amount of bottom surface deteriorated by contact with the support.

Built orientation	**Support volume [mm3]**	**Material saving***
Original *(θ_x=0°; θ_y=0°)*	142.795	-
Best *(θ_x=0°; θ_y=90°)*	81.059	+ 43 %
Worst *(θ_x=50°; θ_y=10°)*	172.723	- 21 %

*Table 5.1. Comparison of material saving for different build orientations. *Values In respect to the original orientation*

The implicit functions approach for the design of a periodical microstructure, allows easy specification of the support structure for the optimally oriented part Figure 5.18. The topology described by the Schwartz equation provided a further 50% material saving with respect to the full dense support shown in Figure 5.17 (left). Furthermore, the use of trigonometric functions for the definition of cellular structures, might facilitate the stress distribution in the structure homogeneously, due to the absence of cavities or peaks that would locally concentrate the stress and thus avoid support structure collapse.

5.5 Conclusions

This chapter has presented a new approach to the design and optimisation of support structures in Additive Manufacturing platforms such as Selective Laser Melting (SLM). This optimisation provides functions to minimise support structures through both the definition of an optimal part build orientation and the definition of optimally graded cellular structures. A Matlab algorithm that performs a two-step optimisation has been developed. Firstly, the part orientation that requires the minimum support has been located among all the possible orientations; secondly the cellular support structures for the optimal orientation is generated, through pure mathematical 3D implicit functions. The implicit function approach for cellular support design is found to be very versatile because it allows geometries to be simply defined by mathematical expressions. The method has been validated through the manufacturing of a real artefact and associated supports. Optimisation evaluation results on a truss part with complex shape geometry demonstrated that significant materials saving, up to 45% for this case, can be achieved by optimal part positioning, and further reductions can be obtained by designing cellular structures defined by implicit mathematical functions. This newly developed design and optimisation approach of cellular support structures exhibits great potential to achieve a higher efficiency for the SLM process, and consequently deliver time, material and energy savings. Results achieved in this chapter are utilised for the multi-objectives optimisation of SLM fabricated parts, discussed in the next chapter. The next chapter presents the simultaneously optimisation of build time, surface quality and support structures for SLM fabricated parts.

6. Multi-objective optimisation of parts and support structures

6.1 Introduction

Part production by the metallic Additive Manufacturing (AM) technique, such as Selective Laser Melting (SLM), typically requires the use of sophisticated software to assist the product development cycle including product design and process planning stages. The product design stage is typically carried out by employing a design software workstation (for instance employing CAD software tools), in order to develop geometric modelling, and eventual analysis. The next step, the process planning, includes the choice of important process parameters, such as the determination of the optimal building orientation and the generation of support structures. This represents an important decision making process to deliver improved efficiency for part production using SLM. The SLM machine user needs to specify key important process parameters and currently this choice typically relies on the user experience.

In Chapter 4 it has been discussed how the build direction of a part affects its surface finish, and the time needed to build it in the SLM process. The definition of an optimal build orientation that simultaneously satisfies all the operator's criteria is not often possible. The minimisation of the build time, is typically satisfied by orientations that lower the object height (minimum number of layers); on the other hand, such orientations might not match with the ones that provide the best surface finish.

The definition of an optimal orientation becomes even more complicated when further performance objectives need to be satisfied, for instance the necessity to minimise the volume of support structures. In Chapter 5 the importance of limiting the amount of support to achieve significant material and energy savings has been shown, since the supports are typically wasted after the object built. Furthermore, positioning the part optimally can minimise the amount of downward-oriented surfaces to be supported, therefore the support needed. However, minimising the part optimally (for instance vertically for a long beam geometry) could negatively affect surface finish and build time (displacing the part vertically increases the object height, therefore the build time). This chapter discusses three-objective optimisation to achieve the best trade-off solutions between, surface roughness, build time and support structures, in the SLM process. Following is a review of the multi-objective optimisation studies when consider the presence of support structures in AM.

6.1.1 Manufacturing optimisation of parts with support structures

A number of studies have investigated and developed multi-objective optimisation approaches for various AM technologies. The recent multi-objective optimisation developments have been reviewed in a recent publication (Strano et al. 2011) and this chapter provides an overview on those developments including the presence of support structure among the objective functions. (Lan et al. 1997) determined part deposition orientation for Stereolithography (SL) parts based on surface quality, build time and complexity of support structures. Surface quality was evaluated by maximising the total area of perpendicular and horizontal faces, in order to minimise stair stepping.

Aesthetically important faces were also considered by maximising the sum of upward facing surfaces and vertical faces, as they do not require the presence of any support structures that reduce their quality. Considering uniform slicing of the part, this work showed that the build height of the part and consequently the build were directly affected by the build orientation. For each determined build orientation, support structures were then optimised by minimising the number of supported points along the length of the hanging profile. (Cheng et al. 1995) presented a multi-objective approach for determining an optimal part build orientation for SL. The two objectives, namely part accuracy and build time, were combined in a weighted sum for optimisation. Part accuracy was calculated using different weight factors for different types of surface geometries, and based on their experience they considered various contributions of fabrication errors, such as slicing effects, tessellation, distortion and stair stepping. Minimisation of build time was achieved by reducing the number of slices. More recently, (Singhal et al. 2009) have applied multi-objective optimisation to simultaneously optimise part average surface roughness, build time and support structure for SL and Selective Laser Sintering (SLS) processes. In their study the multi-criteria optimization problem was solved by minimising the weighted sum of the three different objectives, using a conventional optimization algorithm based on a trust region method (More and Sorensen 1983).

In a previous study (Cheng et al. 1995) the surface finishing objective was prioritised over the build time; the deterioration on surface finish due to stair-step effect and support, was considered by multiplying each surface by a weighting factor; the areas multiplied by weights are summed, and the orientation with the lowest sum corresponded to the highest surface quality. When evaluations lead to similar orientations, the orientation with shortest build time (proportional to the number of layers) was chosen. Multi-objective optimisation for build time and surface finishing

were also presented in the reports (Sreeram and Dutta 1994) and (Bablani and Bagchi 1995), where the objective was to minimise a combination of the number of slices required to build the part (which determinates the build time), and the surface area that will suffer from the staircase effect, *0°* and *90°* inclination angle are excluded as no stair step is expected to occur.

There is little research on multi-objective optimisation for the SLM process. Following, a computational methodology based on multi-objective optimisation, for the simultaneous minimisation of surface roughness, build time, and amount of support structures for the SLM process, is discussed. The multi-objective optimisation predicts these three objective functions based on various build orientations and presents them in the form of 3D Pareto fronts, showing the front as best "trade-off" between the surface roughness, build time and volume of support. Two parts exhibiting different complex shape geometries are used as case studies in this chapter.

6.2 Three-objective optimisation

The multi-objective optimisation for simultaneous build-time, surface quality and support structures, for SLM fabricated parts is presented.

6.2.1 Models used for the three-objective optimisation

In MO problems, the objective functions are employed to evaluate the multiple-contrasting criteria in order to derive the "best" trade-off solution between them.

The models used for the evaluation of the surface quality and build time objective, are expressed by Eq. (4.7) and (4.14) respectively, presented in Chapter 4.

The model for surface roughness considers both the effect of the stair-step and the presence of particles on top surfaces, and produces a description of the roughness at different inclination angles as shown in Figure 6.1;

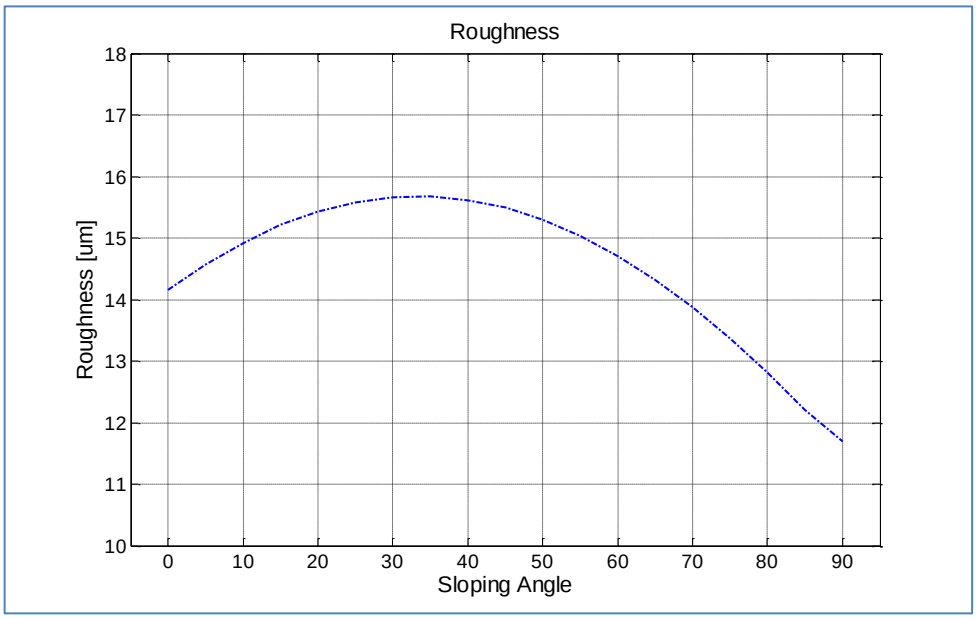

Figure 6.1. Surface roughness at different inclination angles according to model (4.7)

The model for build time prediction, similarly to the model expressed in Equation (4.14), sums the time spent to sinter the object, and the time for "non-sintering" layer recoating operations. When support structures are sintered, an additional term V_s needs to be considered in the expression, to indicate the volume of material required by the support. The final expression for build time estimation, in presence of support structures is given as;

$$T_{tot} = N \cdot (T_{dep} + T_p) + \frac{V}{v_s \cdot s_s} + \frac{V_s}{v_s \cdot s_s} \tag{6.1}$$

The terms T_{dep} and T_p time to deposit a new material layer and the time for moving the platform elevator down N steps, respectively. The terms v_s and s_s are the laser beam speed and scan spacing respectively.

The evaluation of support structures has been performed through the method discussed in Chapter 5. The settings for the support structure generation were: threshold angle "*slop_deg* = 35°", and *"z_base = 5mm "*.

Before performing the optimisation for the two case studies, an analysis of the performance objective functions - surface roughness, build time and support structures - is proposed, for the "Cantilever.stl" test geometry (Figure 6.2).

6.2.2 Performance objective functions for three-objective optimisation

Figure 6.3 illustrates the three objective functions, support structures, manufacturing time, and surface roughness for the "Cantilever.stl" geometry (Figure 6.2). For a given a set of angles (θ_x,θ_y), the values of the performance functions have been expressed as percentages; for example, a "*0%* Support volume" indicates the orientation that ensures the minimum amount of support possible, a "100% Support volume" indicates the one that produces the maximum amount of support. Due to the geometrical symmetry of the part around the x and y axes, the three objectives have been calculated for all the orientations defined by $0° \le \theta_x \le 90°$ and $0° \le \theta_y \le 90°$. In fact, as in Chapter 3, Paragraph 3.4, the objective functions calculated for parts with symmetries, presents periodicity with respect to rotation angles of *90º* in both axes.

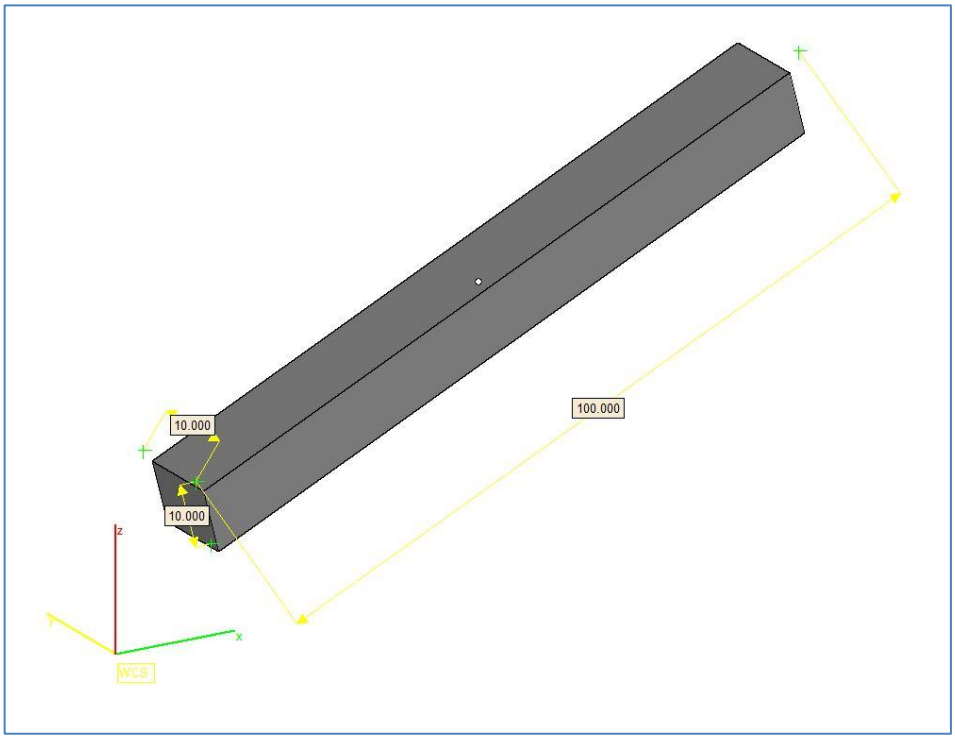

Figure 6.2. "Cantilever.stl" test geometry.

Since the solution domain is two-dimensional, halving the range of rotation angles, has reduced by *4* times the solution domain, thus by *4* times the computational time if the search domain is uniformly discretised and searched exhaustively.

The function that describes the volume of support presents minimum values for all the orientations defined by $0° \leq \theta_x \leq 90°$ and θ_y=*90º*. All those orientations correspond to the ones that position the cantilever vertically as shown in Figure 6.4. As visible in the figure, when the cantilever is oriented vertically, a minimal amount of support (coloured in green) is required.

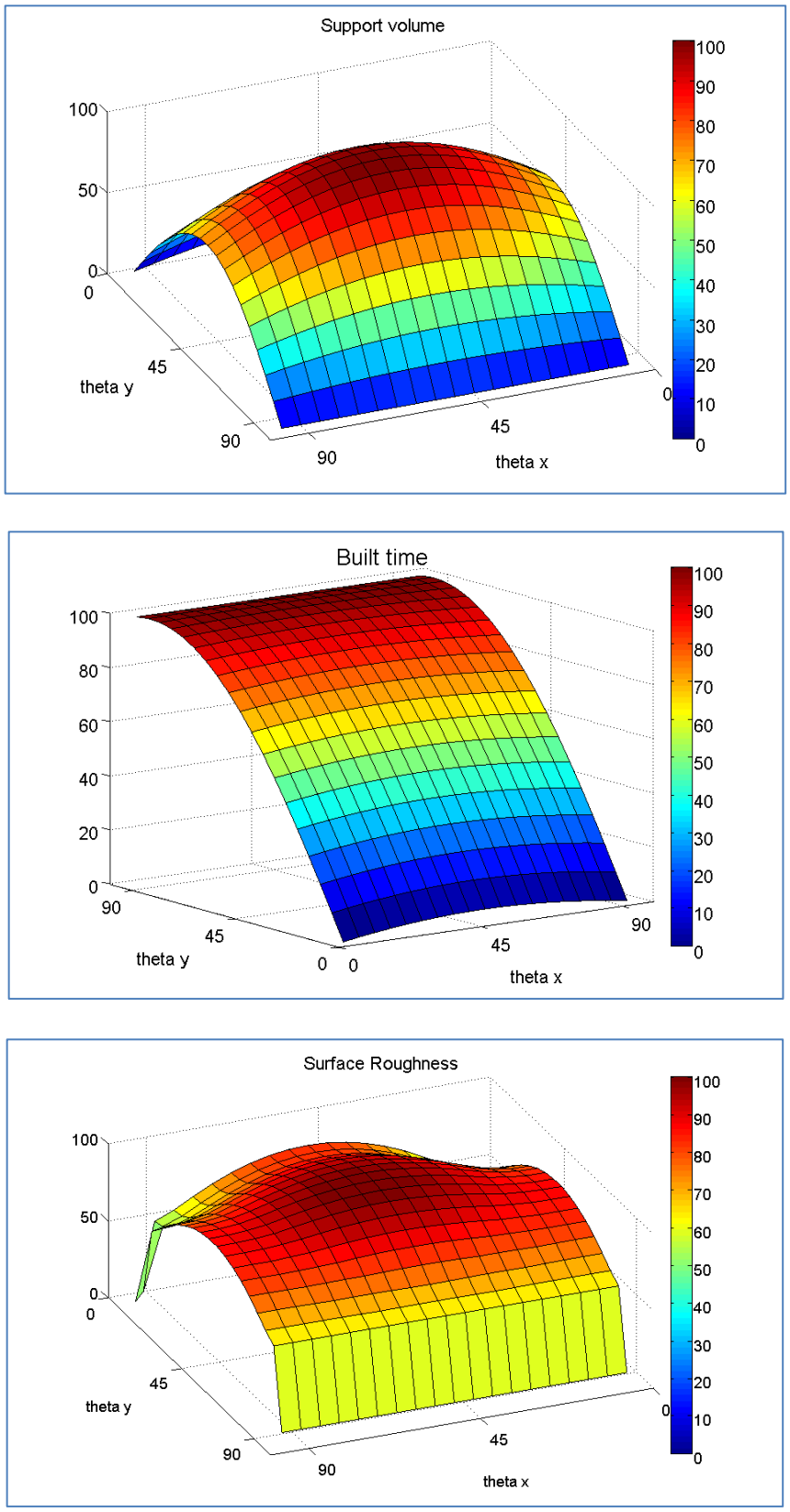

Figure 6.3 Performance objectives for "Cantilever.stl" geometry; volume of support structures (top), build time (centre), weighted average roughness (bottom).

The build time function presents maximum values for these orientations. This can be explained by observing that the term $N \cdot (T_{dep} + T_p)$ in the expression 6.1 - proportional to the number of layers *N* (therefore to the object height) – which is maximised when the cantilever is positioned vertically.

By moving along the values that correspond to $0° \leq \theta_x \leq 90°$ and θ_y=*90º*, the build time function presents a constant (maximum) value. When positioned vertically, the part is expected to have low surface roughness (7%). In fact, in this orientation the major part of the part surface is exposed at *90º* with respect to the build direction. In accord with the model for roughness prediction (4.7) both surface inclined at *0º* and *90º* are characterised by lower surface roughness (*8μm* and *14 μm* respectively) than at any other inclination angle.

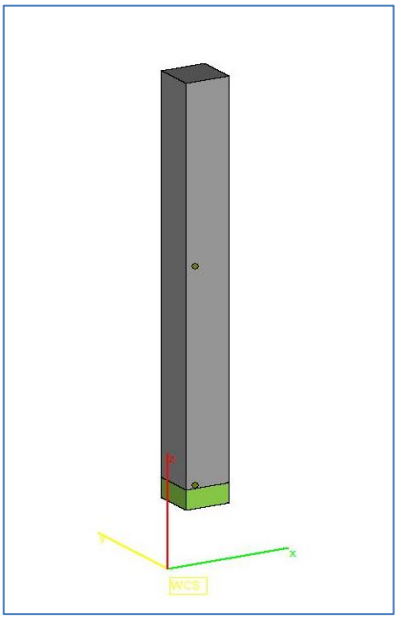

Figure 6.4.Orientation that minimise support for "Cantilever.stl" geometry.

Figure 6.5 shows the orientations that minimise the build time (θ_x=0º, θ_y=90ºor θ_x= θ_y=90º); as evident, in these orientations the object's height is at minimum. It is noticeable that, moving along the values of the build time function that correspond to $0° \le \theta_x \le 90°$ and θ_y=0º, the function value presents a slightly parabolic trend, having a peak at θ_x=45º, θ_y=0º. In fact, all these values correspond to a horizontal object positioning (θ_y=0º), and to a symmetrical rotation around the *x* axis, with a peak at θ_x=45º as shown in Figure 6.6.

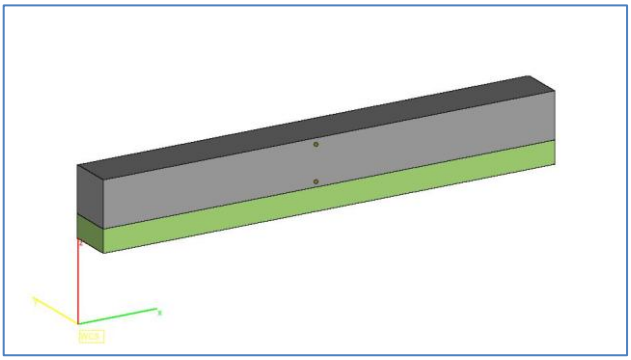

Figure 6.5. Orientation that minimise built time and roughness for "Cantilever.stl" geometry.

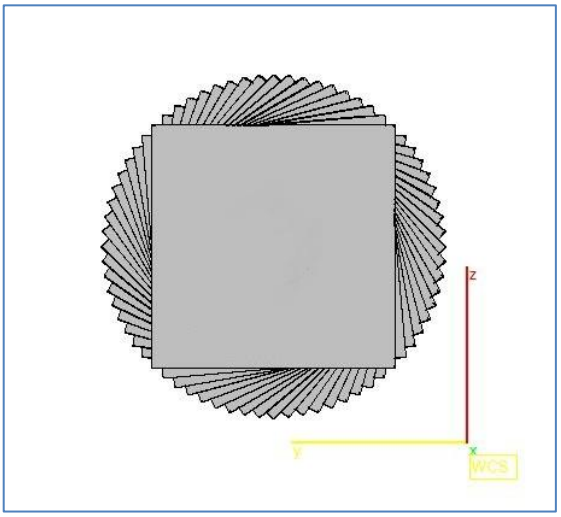

Figure 6.6. Rotations around x axis, for: 0º<= θ_x<=90º and θ_y=0º

When the cantilever is oriented as in Figure 6.5, the surface roughness function presents a minimum value. This is verified because, similarly to the previous orientation, all the part surfaces are exposed at 0^o (Roughness $=8\mu m$) or 90^o (Roughness $=14\ \mu m$), but in horizontal position the flat surface at the top has a larger extension, and it reduces the weighted average roughness calculated according to (4.7). As expected, a larger amount of support is required when the part is positioned horizontally.

6.2.3 Case study definition

The multi-objective optimisation problem is performed for the two geometries shown in Figure 6.7. Figure 6.7a represents an oil pump shell, Figure 6.7b a generic mechanical part with complex shape. Both part geometries present a high level of shape complexity, and normally their manufacturing by conventional techniques requires considerable time and resources.

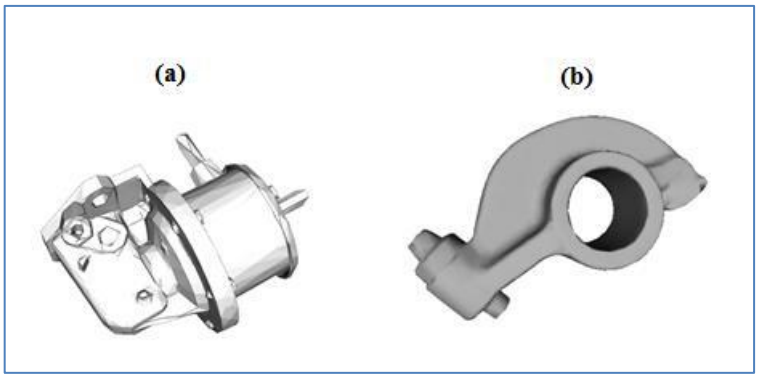

Figure 6.7. Artefacts to be processed.

In this case study, for each part geometry, the objectives considered are the weighted average roughness, the build time, and volume of support.

The multi-objective exhaustive grid searcher discovers the "non-dominated" solutions with respect to all objectives; i.e. moving from one solution to another, it is not possible to improve one criterion without making at least one of the other criteria worse. In this case study, the solutions are the orientations that simultaneously satisfy three objectives, thus the Pareto set of solutions will be represented by a 3D surface.

The decision variables for the multi-objective optimisation problem are θ_x and θ_y, rotation angles around the *X* and *Y* axes respectively. Since the parts do not present evident symmetries, the search domain has been extended for ($\theta_{x,}\ \theta_y$) from*0°* to *180°*, in order to cover all the possible orientations.

The complete problem of optimal part orientation can be summarized as follows:

$$min \qquad F(\theta_x,\theta_y) = (R_a(\theta_x,\theta_y), T_{tot}(\theta_x,\theta_y), V_{Supp}(\theta_x,\theta_y)))$$

$$subjected\ \ to \quad \begin{cases} 0° \le \theta_x \le 180° \\ 0° \le \theta_y \le 180° \end{cases}$$

with $R_a(\theta_x, \theta_y)$ and $T_{tot}(\theta_x, \theta_y)$ defined as in (4.7) and (4.14) respectively; and $V_{Supp}(\theta_x,\theta_y)$ volume of support structures generated by the method described in Chapter 5.

The three-objective optimisation is performed in the Matlab environment (Appendix). At the beginning, an STL file containing the geometry surface information is imported; then the algorithm starts the rotations around the two axis routines, for each rotation step each of the objectives is calculated and stored. Once the entire search domain has been discretised and investigated including all the possible orientations (given the domain resolution), the 3D Pareto set of solutions is calculated and plotted. Finally the geometry both with the original orientation and with any of the Pareto-optimised orientations is shown.

In the proposed optimisation problem, there are three objectives to evaluate $R_a(\theta_x, \theta_y)$, $T_{tot}(\theta_x, \theta_y)$, $V_{Supp}(\theta_x,\theta_y)$ in a two-dimensional (θ_x,θ_y) solution space. It is therefore possible to search the entire space with an exhaustive grid search and without resorting to approximate methods. This has the combined benefits of exploring the entire space and thus locating the global Pareto front with certainty (given the search domain resolution), and is expected to be computationally more efficient than GA approaches, which are stochastic searchers.

6.4 Results and discussion

In this section, the results from the multi-optimisation of the two geometries in Figure 6.7 are presented, in the form of Pareto solutions defining the best compromises between the surface roughness, build time, and support volume objectives; therefore, permitting the operator to select the best trade-off between them.

The results from the optimisation of the first case study are presented in Figure 6.8. The red dots highlight the complete set of Pareto solutions, while the blue dots are the non-Pareto-optimal solutions at other orientations. When three objectives are simultaneously optimised, the Pareto set describes a three-dimensional surface boundary, in Figure 6.8 highlighted in red. The blue dots in the Figure are the non-Pareto-optimal solution at other orientations. Obviously, the orientations which yield low roughness, manufacturing time and support volume, in the Pareto surface, are the preferred solutions; on the contrary, the dominated represents the worst orientations.

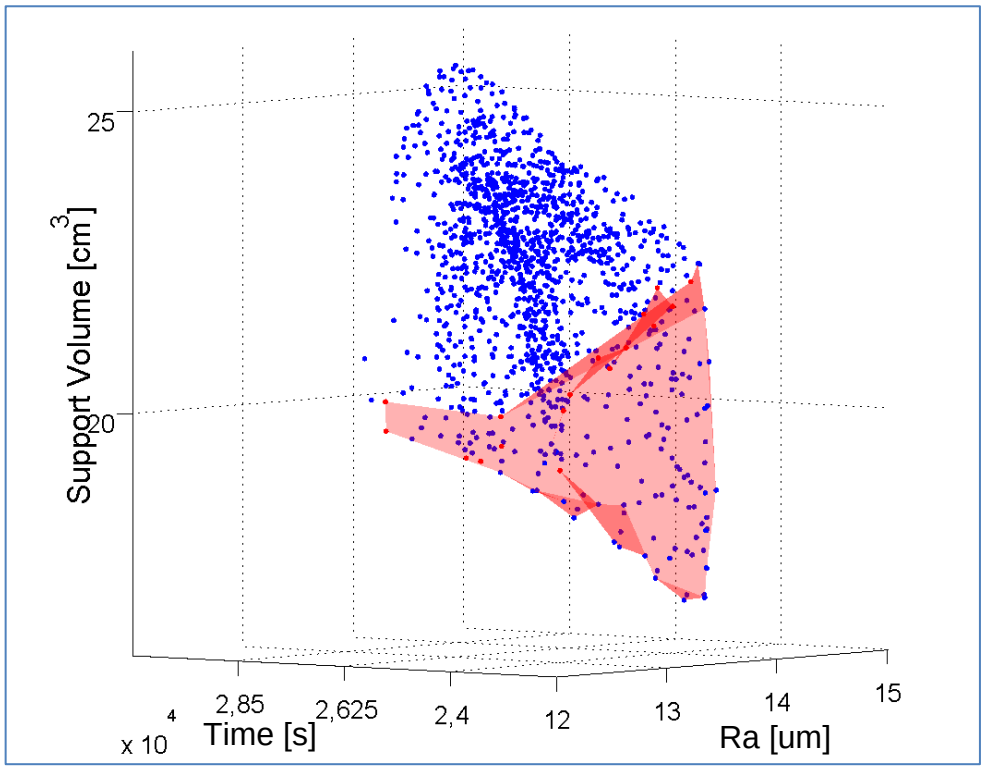

Figure 6.8. 3D Pareto set for the first case study.

For an easier consultation of the Pareto solution, Table 6.1 lists the complete set of Pareto solutions from the optimisation of the first case study, ordered by volume of support required. In order to facilitate the user into the choice of the orientation that best fulfils his requirements, the results have been expressed as normalised percentage values of the objectives calculated within the range of the Pareto front. For example, if the AM user's requirement is to have the highest surface quality possible (lowest surface roughness), then the optimal orientation is given by the set of (θ_x,θ_y) that provide "*0%* Surface Roughness" (second column of Table 6.1). On the other hand, if the requirement is the quick production of a spare prototype, or to speed up the production of large parts, the best option of (θ_x,θ_y) could be the ones that are as close as possible to "0% Build Time" (third column of Table 6.1). An attractive aspect of the decision support system introduced, is the possibility for the user to choose between a very long list of intermediate possibilities; the achievement of a good surface finish that

does not exclude support material saving, or build time. The AM operator does not have a “black or white” choice, but can opt for a number of “grey” solutions that better suit with the requirements. It is also important to notice that, the solutions provided in Table 6.1, are all Pareto optimal, therefore all better than any other “random” solution.

Supp. Vol.	*Surf. Rough.*	*Built Time*	Θ_x	Θ_y
0.0	98.1	71.5	45.0	160.0
0.9	100.0	63.3	45.0	165.0
6.2	95.7	79.2	45.0	155.0
9.6	99.3	57.0	40.0	170.0
9.9	97.0	54.8	45.0	170.0
12.2	96.8	70.2	50.0	160.0
12.8	93.6	78.5	50.0	155.0
15.3	90.5	86.1	45.0	150.0
16.8	88.4	85.8	50.0	150.0
19.5	93.3	85.7	40.0	150.0
21.1	94.2	46.2	45.0	175.0
24.0	79.2	92.0	50.0	145.0
24.8	96.1	45.5	50.0	175.0
26.3	82.4	92.0	45.0	145.0
27.5	92.2	78.8	55.0	155.0
27.8	85.9	84.8	55.0	150.0
28.9	76.2	91.3	55.0	145.0
32.1	70.7	97.0	50.0	140.0
32.1	68.1	96.5	55.0	140.0
32.3	91.4	37.9	45.0	180.0
33.1	93.6	34.5	50.0	180.0
37.8	59.0	100.0	55.0	135.0
39.5	54.9	67.8	30.0	35.0
41.7	46.5	95.5	130.0	5.0
42.4	43.5	62.9	35.0	35.0
42.9	41.0	96.6	135.0	5.0
45.5	49.9	61.7	30.0	30.0
47.3	92.4	30.5	150.0	105.0
48.6	17.9	56.0	35.0	30.0
52.7	0.7	91.5	135.0	10.0
55.2	91.9	29.5	150.0	100.0
57.2	91.0	24.0	145.0	100.0
57.4	16.3	50.0	40.0	30.0
57.7	47.4	49.3	35.0	25.0
58.0	91.2	22.4	145.0	105.0
61.4	0.0	86.3	135.0	15.0
62.6	46.2	42.5	40.0	25.0
69.6	62.9	35.4	40.0	20.0
70.3	90.0	18.2	140.0	100.0
71.0	90.8	14.2	140.0	105.0
72.8	59.0	35.4	45.0	25.0
75.7	66.5	27.8	45.0	20.0
80.0	58.8	38.9	50.0	30.0
81.7	76.5	20.9	45.0	15.0
85.4	72.7	20.0	50.0	20.0
85.7	90.0	12.1	135.0	100.0
86.6	88.9	5.9	135.0	105.0
87.5	80.6	12.6	50.0	15.0
90.7	70.6	27.6	55.0	25.0
92.9	77.5	13.9	55.0	20.0
94.7	85.0	4.3	55.0	15.0
99.6	89.5	1.6	60.0	15.0
100.0	87.2	0.0	130.0	105.0

Table 6.1. List of Pareto solutions for the first case study.

a) **b)**

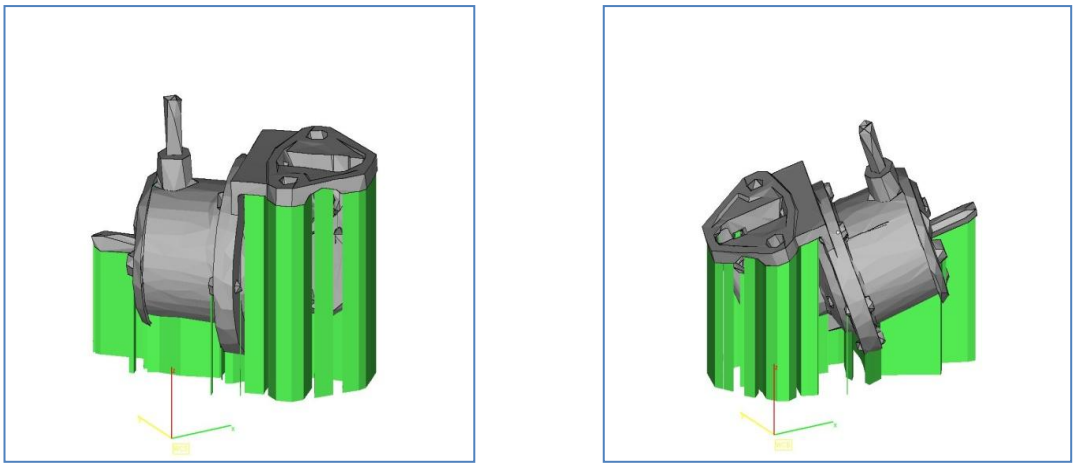

c)

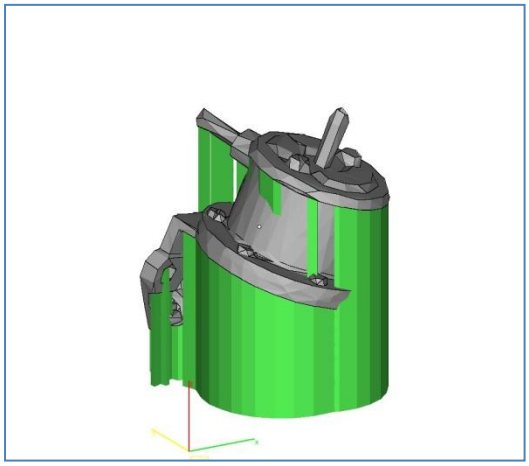

Figure 6.9. First case study at different orientations; a) minimisation of support structures, b) minimisation of build time; c) minimisation of surface roughness.

Figure 6.9 shows three solutions chosen from the Pareto set in Table 6.1; Figure 6.9a shows the solutions that minimise the support structure, Figure 6.9b the orientation that minimises the build time, and Figure 6.9c the orientation that minimises the surface roughness. It is noticeable that the solution that minimises the build time is the one that minimises the height of the object in the build position, this in fact minimises the number of layers to be deposited. The orientation that minimises the support structures positions the part horizontally; this is different to that observed in the cantilever test

geometry, where the support was minimised by positioning the part vertically (Figure 6.9(a)). This can be explained by the articulated complexity of the object, which presents many geometrical features such as hanging parts and hollow structures. In fact, the orientation that increases the object's height (Figure 6.9c) is the one that minimise the surface roughness, that is the one that orientates the artefact such that the mesh triangles with the biggest areas, are orientated at angles characterised by lower roughness in Figure 6.1.

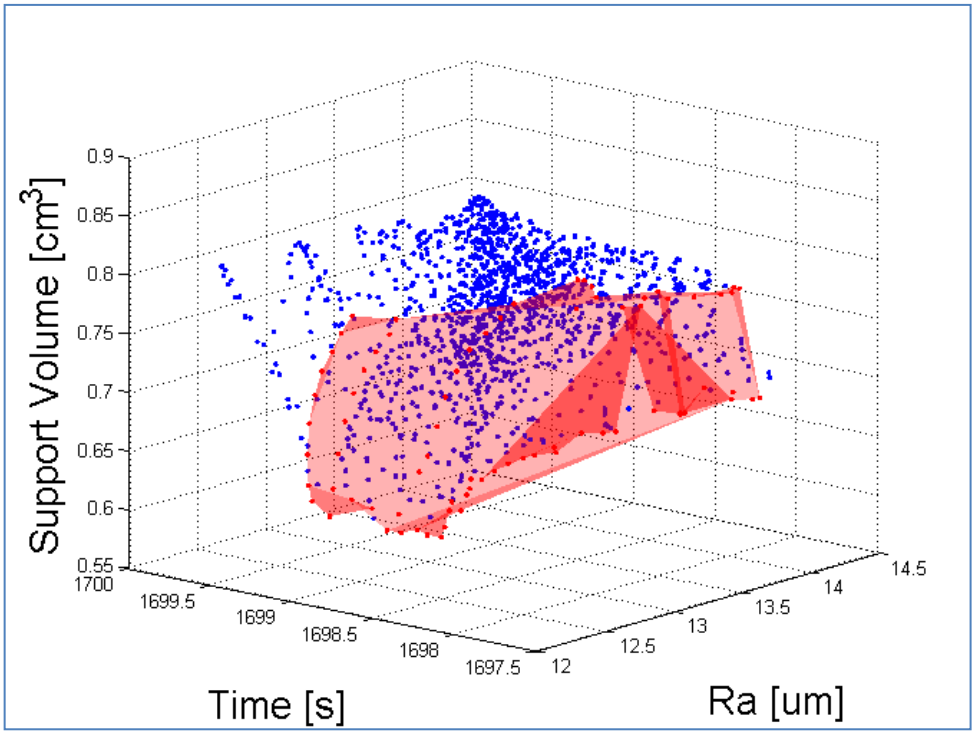

Figure 6.10. 3D Pareto set for the second case study..

Figure 6.10 shows the results from the optimisation of the second case study; the surface coloured in red in the figure represents the three-dimensional Pareto set, best trade-offs between the three objectives.

Supp. Vol.	*Surf. Rough.*	*Built Time*	Θ_x	Θ_y
0.0	99.3	59.0	170.0	5.0
0.4	94.0	58.5	175.0	5.0
2.8	87.9	57.9	180.0	5.0
3.0	77.4	55.4	10.0	180.0
3.1	81.4	54.4	5.0	180.0
6.6	76.6	55.9	15.0	180.0
10.0	88.3	50.9	180.0	180.0
11.4	75.2	60.9	20.0	180.0
11.6	94.6	47.1	175.0	180.0
11.9	76.5	57.8	10.0	5.0
14.0	100.0	45.2	170.0	180.0
15.8	74.4	56.2	15.0	5.0
17.3	73.1	60.8	25.0	180.0
20.0	71.7	60.3	20.0	5.0
21.7	77.1	8.5	180.0	90.0
23.6	68.4	61.4	25.0	5.0
23.9	70.4	59.4	30.0	180.0
27.3	64.5	62.0	30.0	5.0
28.0	78.7	3.1	180.0	85.0
29.0	75.5	43.9	180.0	95.0
30.6	60.1	62.5	35.0	5.0
31.5	75.9	8.5	175.0	90.0
33.5	55.1	62.8	40.0	5.0
33.8	78.9	1.8	175.0	85.0
35.0	73.0	44.4	175.0	95.0
36.0	49.7	61.0	45.0	5.0
37.7	43.8	62.8	50.0	5.0
39.7	43.9	62.3	55.0	5.0
43.5	40.8	70.1	45.0	10.0
44.2	74.1	8.5	170.0	90.0
44.6	34.0	70.7	50.0	10.0
44.9	78.3	0.8	170.0	85.0
45.8	30.0	71.3	55.0	10.0
45.9	70.0	44.8	170.0	95.0
49.6	21.6	88.2	70.0	15.0
51.1	18.3	86.1	65.0	15.0
51.8	24.8	81.1	50.0	15.0
52.1	16.8	84.1	60.0	15.0
52.3	16.9	82.4	55.0	15.0
53.5	13.7	100.0	70.0	20.0
56.0	4.4	97.6	65.0	20.0
56.0	71.7	8.5	165.0	90.0
56.3	77.2	0.0	165.0	85.0
57.1	66.4	43.9	165.0	95.0
57.8	0.0	95.5	60.0	20.0
58.7	7.9	93.7	55.0	20.0
58.9	16.6	92.0	50.0	20.0
66.5	75.3	0.2	160.0	85.0
66.6	68.7	8.5	160.0	90.0
67.1	62.2	43.6	160.0	95.0
75.4	72.9	0.3	155.0	85.0
75.4	65.1	8.5	155.0	90.0
75.6	57.5	43.3	155.0	95.0
82.6	52.2	43.8	150.0	95.0
82.7	69.8	1.0	150.0	85.0
82.7	61.0	8.5	150.0	90.0
87.9	28.9	80.5	150.0	110.0
89.2	46.6	43.1	145.0	95.0
89.4	37.2	63.5	145.0	100.0
89.5	28.4	72.3	145.0	105.0
89.7	56.3	8.5	145.0	90.0
90.3	66.1	0.2	145.0	85.0
91.8	20.6	81.7	145.0	110.0
94.2	12.0	82.4	140.0	110.0
94.5	20.6	72.0	140.0	105.0
94.8	30.2	63.4	140.0	100.0
94.9	42.0	43.3	140.0	95.0
95.5	54.0	8.5	140.0	90.0
95.7	5.5	93.4	130.0	115.0
96.1	64.1	2.3	140.0	85.0
96.4	6.1	91.8	135.0	115.0
96.5	3.2	83.1	135.0	110.0
97.6	0.3	84.0	130.0	110.0
97.6	16.0	72.1	135.0	105.0
98.3	31.6	63.3	135.0	100.0
99.8	36.5	63.2	125.0	100.0
100.0	34.2	63.2	130.0	100.0

Table 6.2 .List of Pareto solutions for the second case study.

Similar to the previous case study, Figure 6.11(a) shows the solution that minimises the support structure, Figure 6.11b the orientation that minimises the build time, and Figure 6.11c the orientation that minimises the surface roughness. The supports are minimised when the part is vertically positioned. Furthermore, in Figure 6.11c the part is orientated in a way that most of the part surface is inclined at very low *(0°-15°)* or very high *(80°-90°)* sloping angles; this ensure that surface roughness is reduced to lowest values over the possible range of inclinations as described by Figure 6.1.

a) **b)**

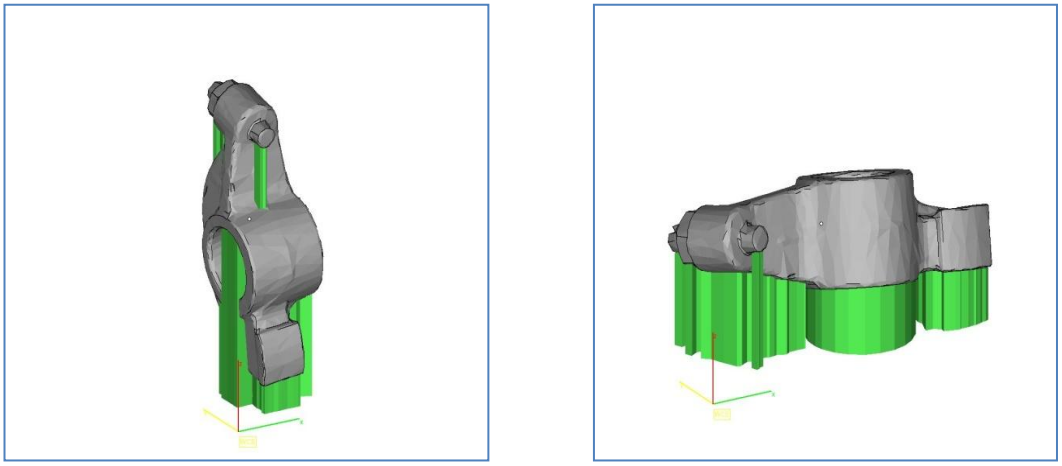

c)

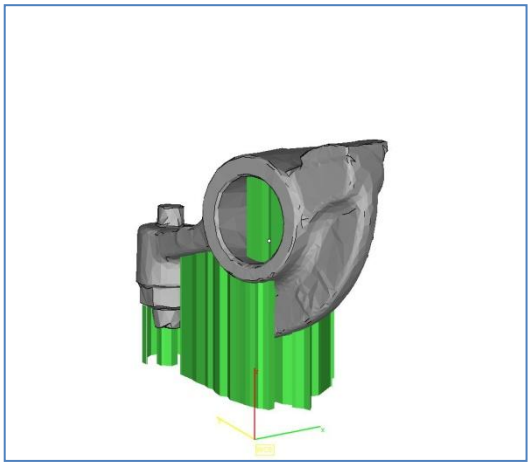

Figure 6.11. Second case study at different orientations; a) minimisation of support structures, b) minimisation of built time; c) minimisation of surface roughness.

6.5 Conclusions

AM is currently the best option for short series production of customized products. The future diffusion of AM production will increasingly interest home users, small enterprises, and large modern industries looking to develop customized and hi-tech products to take advantage of mass production with lower factor cost.

However, many consider AM technologies to be in their early stage; in fact, AM process efficiency can be compromised by the wrong choice of process parameters, which can affect surface quality. and can negatively reflect into additional costs, and time resources, thus preventing the establishment of AM as an alternative to conventional manufacturing processes.

The decision support system presented in this research is the response those mentioned challenges. This chapter has presented an integrated computational approach to perform the multi-objective process optimization of SLM production, which is potentially employable to assist users with varying experience in the field. The system provides to the AM operator with the best compromise between surface quality, build time, and volume of support structure. Results on two complex shape geometries demonstrate the potential of the system proposed. A considerable waste in terms of materials (and energy), and time employed for their construction can be reduced by using the computationally determined optimal parameters.

7. Conclusions

This thesis has addressed the complicated aspects that affect the use of Additive Manufacturing (AM) technologies as an efficient and effective industrial production process. Currently within AM technologies, the assessment of optimal parameters choice relies almost purely on the level of expertise of the operator.

As discussed in Chapter 2, one of the most important problems is the limited surface quality, typically generated by the discrete deposition and fusion of material, that characterises all the additive manufacturing technologies. The possibility of predicting the surface quality during the process planning stage, can save precious time and resources to refine the surface in post-manufacturing operations.

The mechanism governing the roughness of AM parts formed by SLS and SLM is a complex phenomenon to study; it is evidently influenced by the stair-step effect, but also very significantly by different process parameters. It is generally hard to distinguish the contribution of each of them, consequently it is difficult to formulate models generally valid to describe roughness for all the AM platforms.

This research has investigated the mechanism that characterises the surface morphology of AM fabricated parts. An initial approach to the surface roughness modelling has been presented in Chapter 3. The model interpolates roughness data on a SLS manufactured geometry sample; by interpolating different sets of data from over the entire range of possible inclination angles, the model provides a complete and accurate description of the part's average surface roughness. This approach has the advantage of including the effects of all the main process parameters generating surface roughness. Another advantage of this approach is that, although applied to SLS case study, the model has general formulation, thus it allows the prediction of surface quality

of any AM manufacturing platforms. The main drawback is that, since the model interpolates empirical roughness measured on a discrete number of measurements, a large number of measurements is required to achieve high resolution (Strano et al. 2011).

The necessity of having a high quality surface finish is particularly serious in the production of metal parts, typically performed by SLM; improving the surface roughness by a few microns requires an increasing amount of time, and often the combination of different surface polishing techniques. With the purpose of overcoming the drawbacks of current models, Chapter 4 has presented a novel model for the prediction of surface roughness of SLM parts.

The development of the new model for surface roughness prediction, started with the investigation of the surface morphology of Steel 316L alloy parts, manufactured by Selective Laser Melting (SLM).

The analysis revealed that roughness measured by profilometer was different from that predicted through the classic model based on pure geometrical consideration on the stair step profile. Furthermore, SEM analysis revealed the presence of partially bonded particles on the surface. An explanation of this phenomenon has been proposed.

The information acquired through surface analysis has been utilised in the formulation of the novel model, which introduces the effect of particles on the upper surface, in addition to the stair step effect. The developed model predictions showed good agreement with experimental observed roughness.

There is an interest currently in characterising the balling effect generated by a combination of process parameters (i.e. scan speed, laser power, hatch spacing). Future research could investigate the effects that process parameters have on balling formation once the dynamics of balling have been fully explored. The model that this research has

developed could then represent an important link between inputted process parameters and the final surface roughness, currently missing in other models.

Further research could aim to assess the capability of predicting surface roughness by simply observing an image of surface profile. By the automatic detection of the fraction of particles on the step edges, the model could provide a method for the analysis of surface roughness quicker than performed by scanning the surface by profilometer.

One of the future aims of AM is to replace the traditional manufacturing approach with a more sustainable manufacturing method that is, by minimising the carbon footprint in new product development and production. In AM processes such as SLS, the amount of energy employed for the part sintering can be significantly reduced by optimally orientating the part. The energy saving objective typically contrasts with surface quality requirements, the orientation that minimises the manufacturing energy does not necessary yield low surface roughness (i.e. high surface quality) at present.

In Chapter 3 a computational model based on multi-objective optimisation has been presented. Results provide the operator with the Pareto front of solutions which define the best compromise between the surface quality of the part and the manufacturing process efficiency. This way, the operator with no a priori knowledge or experience can choose from among a set of optimal compromises between the two objectives, depending on preference. A poor choice of random orientation might end up in a part surface deteriorated by the stair step effect and other factors, and/or in a higher manufacturing footprint and production cost.

Computationally, the global Pareto front has been estimated by using an exhaustive research grid over the solution space. This has been thought to be more efficient than a GA solver because the grid resolution of the research domain (5 degrees increments) has allowed researching the entire domain exhaustively in reasonable

computation time. However, an increase in the solution space resolution might justify the use of a GA solver.

Further development of this research could aim to perform the same computation with a higher resolution domain; although this would take increasing computational time, for symmetrical parts computational time can be reduced of 75% by performing the search only on one fourth of the research domain, as shown in Chapter 3.

During the SLM sintering of a part, the time required to manufacture an object, increases directly with the number of powder layers to be deposited. Long manufacturing time is one of the major limitations to the large scale diffusion of SLM for industrial production. In fact, in many advanced industry sectors (i.e. Aerospace, Biomedical) the SLM is being progressively replaced by the faster EBM technology. When high surface quality has to be achieved, the thin layer thickness required can yield to a higher number of layers, thus longer manufacturing time.

The work presented in Chapter 4 has extended the multi-objective optimization technique to predict and optimise the build time and surface quality objectives. The results showed that, by simply orientating the artefact using solutions lying on the Pareto front, significant surface roughness improvements and manufacturing time savings can be achieved.

The additive manufacturing (AM) of parts using technologies such as Selective Laser Melting (SLM) and Electron Beam Melting (EBM), require the presence of external support structures; the amount of material wasted by fabricating support structures affects the manufacturing costs, time required for the part manufacture, and the time and complexity of post-manufacturing operations. Minimising the amount of supported surfaces can shorten this operation, thus improving post-process efficiency and sustainability.

In Chapter 5, an innovative approach to the optimal design and generation of support structures in AM is proposed, using the SLM process as a case study. The method first locates the best orientation to minimise the volume of support; and second performs a support microstructure optimisation to further reduce the support volume.

This research has produced an innovative technique for the design of microstructure topology for supports. The technique generates 3D surfaces by pure mathematical expression. This approach presents high flexibility in order to design cellular structures with different densities, thus improving on the limitations presented by solid modelling software commercially available today. Benefits introduced in the case study truss part demonstrated that up to 45% material saving can be achieved by simply an optimal part positioning. Further reductions were obtained by replacing full dense support with cellular structures defined by implicit mathematical functions. This newly developed design and optimisation approach of cellular support structures exhibits great potential to obtain a higher efficiency in the SLM process, and consequently deliver time, material and energy savings.

Further work could investigate the optimal support topology to sustain a given object. The developed method allows a combination of virtually an infinite number of different cell topologies, however, the supports of interest are those that have minimal contact with the surface, and a minimum weight (material to be sacrificed). Simultaneous achievement of these properties is not always possible, often the thinner supports (reduced contact with surface) collapse during the melting process due to thermal stress in the material and thicker supports would increase process wastes. The proposed method for support design, provides important information on where a more robust support is needed, according to the object's weight distribution. This information could be integrated into multi-objective optimisation for optimal support structure configuration to satisfy minimal weight, contact points, and robust support at same time.

The algorithms for designing cellular support structures has been integrated into the developed models for SLM surface roughness and build time to create an expert system based on multi-objective optimisation, and thus provide guidance to the operator during the process planning stage of metal parts.

Further research, could aim to extend the methodology and the mathematical approach to optimisation, to enhance process efficiency of other additive manufacturing platforms, such as Electron Beam Melting, which currently represent one of the most advanced additive manufacturing technologies in the Aerospace and Biomedical industries.

Appendix A

Matlab code for multi-objective optimisation

```
clc
clear all
close all

string= 'rocker-arm.stl';
[F,V,N]= stlread(string);
%http://www.mathworks.com/matlabcentral/fileexchange/22409-
stl-file-reader

tolerance= 0.0001;
Z_base = -2;

%%%% Calculating area of the part%%%
[m,n]= size(V);
index=1;
for k=1:3:m
    sides = pdist(V(k:(k+2),:));
    SemiP = sum(sides)/2;
    Total_Area(index) = sqrt( SemiP * (SemiP-sides(1)) *
(SemiP-sides(2)) * (SemiP-sides(3)) );
    index = index + 1;
end

%%% Rotation %%
[m,n]= size(N);
delta=pi/36;
k1=1;
for i=0:delta:pi

        ang1=i;
        R1 = [1 0 0; 0 cos(ang1) -sin(ang1); 0 sin(ang1)
cos(ang1)];  %%  around X axis

        k2=1;
for j=0:delta:pi
            ang2=j;
            R2 = [cos(ang2) 0 sin(ang2); 0 1 0; -sin(ang2) 0
cos(ang2)];  %%  around Y axis
            VRot = (R1*R2*[V'])';
            NRot = (R1*R2*[N'])';
            VRot(:,1) = VRot(:,1) + min(VRot(:,1));
```

```
            VRot(:,2) = VRot(:,2) + min(VRot(:,2));
            VRot(:,3) = VRot(:,3) + min(VRot(:,3));

%%% Support Volume Objective
            Volume(k1,k2) =
Build_Supp_Fast(F,VRot,NRot,Z_base);

%%% Roughness Objective
for k=1:size(NRot,1)      % for each facet
                [h,phi,r] = cart2sph(NRot(k,1), NRot(k,2),
NRot(k,3));
                diff(k) = abs((pi/2) - phi)*(180/pi);   %
increase difference of a delta and convert it in degree
if (diff(k) > 180)
                    diff(k)= 360 - diff(k);
end
if (diff(k) > 270)
                    diff(k)= 180 - (diff(k)-180);
end
                Rf(k) = Rfeval(diff(k))*Area(k);
% evaluate the facet roughness for the new orientation
end
            Ra(k1,k2) = sum(Rf)/sum(Total_Area);    %
evaluate the Weighted Average Roughness for this orientation

%%% Time Objective %%%
            MaxZ = max(VRot(:,3));
            MinZ = min(VRot(:,3));
            Height(k1,k2) = (MaxZ - MinZ);
            Time(k1,k2)= 10*Height(k1,k2);

            k2=k2+1;

end
   k1=k1+1
end

Matrix = Volume;
[Minimum, temp] = min(min(Matrix));
index2 = temp;
[temp, index1] = min(min(Matrix'));
ang1= (index1*delta) - delta;
ang2= (index2*delta) - delta;
STLrot(string,ang1,ang2);
RotX= 180/pi*(ang1)
RotY= 180/pi*(ang2)

figure, imagesc(Volume)
figure, imagesc(Ra)
```

```
figure, imagesc(Time)

% % % % Export the Support STL
R1 = [1 0 0; 0 cos(ang1) -sin(ang1); 0 sin(ang1) cos(ang1)];
%%  around X axis
R2 = [cos(ang2) 0 sin(ang2); 0 1 0; -sin(ang2) 0 cos(ang2)];
%%  around Y axis
VRot = (R1*R2*[V'])';
NRot = (R1*R2*[N'])';
Volume_min = Build_Supp_Fast(F,VRot,NRot,Z_base);
```

List of functions

```
function Roughness = Rfeval (angle)


MyRoughness =
[13.7336000000000,14.2372469272847,14.6661767202004,15.016859
4159498,15.2864432461502,15.4727484062414,15.5742669617944,15
.5901640774249,15.5202780245514,15.3651175901258,15.125856157
5676,14.8043221320234,14.4029856696842,13.9249419252943,13.37
38913182774,12.7541177161528,12.0704660790955,11.328322270183
6,10.6872000000000;];


Rdata = [MyRoughness fliplr(MyRoughness)];


% step = 90/length(UpData) ;  % sample step in degree
step = 5;

if (angle<step)
    angle2=step;
    Rangle2=Rdata(2);
    Roughness =  ((Rangle2)/((angle2)*step))*((angle));
else
    angle1 = floor(angle/step);
    angle2 = angle1 + 1;
    Rangle1 = Rdata(angle1); %% switch to next vector value
as the 1st value
    Rangle2 = Rdata(angle2);
    Roughness = Rangle1 + ((Rangle2-Rangle1)/((angle2-
angle1)*step))*((angle-angle1*step));
end


%
% figure
% hold on
% plot(Rdata);
% plot(angle/step, Roughness,'+');
```

```
function  Volume = Build_Supp_Fast (F,V,N,Z_base)

Z_base = min(V(:,3)) + Z_base;

%% Select upward oriented triangles %%
[I] = find(N(:,3)>=0);
Fd = [F(I,1) F(I,2) F(I,3)];
for i=1:length(I)
     index = I(i);
     Vu((i*3)-2,:)= V((index*3)-2,:);
     Vu((i*3)-1,:)= V((index*3)-1,:);
     Vu((i*3),:)= V(index*3,:);
end

[I] = find(N(:,3)<=0);
for i=1:length(I)
     index = I(i);
     Vd((i*3)-2,:)= V((index*3)-2,:);
     Vd((i*3)-1,:)= V((index*3)-1,:);
     Vd((i*3),:)= V(index*3,:);
end


Nd = [N(I,1) N(I,2) N(I,3)];

Vd_z = [Vd(:,1), Vd(:,2), Z_base*ones(size(Vd,1),1)];


% %% Build up the Edge array for projected downward oriented
facets
[n,m]=size(Vu);
V_Id = Vert2Pts(Vu);

for i=3:3:size(Vu,1)
    Edges_Id(i-2,:) = [V_Id(i-2,:) V_Id(i-1,:)];
    Edges_Id(i-1,:) = [V_Id(i-1,:) V_Id(i,:)];
    Edges_Id(i,:)   = [V_Id(i,:) V_Id(i-2,:)];
end

for i=3:3:size(Vu,1)
    Edges(i-2,:) = [Vu(i-2,:) Vu(i-1,:)];
    Edges(i-1,:) = [Vu(i-1,:) Vu(i,:)];
    Edges(i,:) = [Vu(i,:) Vu(i-2,:)];
end

BorderId = findBorder2(Edges_Id);

% Rearrange Borders
NewBorderId(1,:)=BorderId(1,:);
```

```
for i=1:size(BorderId,1)
    index1=find(BorderId(:,1)==NewBorderId(i,2));
    NewBorderId(i+1,:)=BorderId(index1(1),:);
end

%% reconstruct Borders
for i=1:size(BorderId,1)
    index=find(V_Id==NewBorderId(i,1));
    Border(i,1:3)= Vu(index(1),1:3);
    index=find(V_Id==NewBorderId(i,2));
    Border(i,4:6)= Vu(index(1),1:3);
end

% clear F V N Edges Edges_Id Fd Nd V_Id  I i index m n string
tolerance


Border_z = [ Border(:,1:2) Z_base*ones(size(Border,1),1)
Border(:,4:5) Z_base*ones(size(Border,1),1)  ];

%% Connect the base to the downward oriented surface, using
the minimal
%% number of triangles

for i=1:size(Border,1)
    Vl1((i*3)-2,:) = [Border(i,4:6)];
    Vl1((i*3)-1,:) = [Border(i,1:3)];
    Vl1((i*3),:)   = [Border(i,1:2) Z_base];
    Vl2((i*3)-2,:) = [Border_z(i,1:3)];
    Vl2((i*3)-1,:) = [Border_z(i,4:6)];
    Vl2((i*3),:)   = [Border_z(i,4:5) Border(i,6)];
end

VL = [ Vl1; Vl2 ];

Ftot = [reshape( 1:length(Vu), 3, length(Vu)/3)';
        length(Vu) + reshape((1:length(Vd_z)),3,
length(Vd_z)/3)';
        length(Vu) + length(Vd_z) + reshape(1:length(VL), 3,
length(VL)/3)'];

Vtot = [Vu; Vd_z; VL ];

%% Export the support STL file
Ntot= STL_Export(Vtot, Ftot, 'prova.stl','solid');
%% http://www.mathworks.fr/matlabcentral/fileexchange/24400-
stlexport
```

```
Volume = SurfaceVolume(Vtot, Ftot, Ntot) - SurfaceVolume(V,
F, N) ;
end



function Id = Vert2Pts(Vert)

Id = zeros(size(Vert, 1), 1);            % Space for the
Vertex ids
D = dist2(Vert, Vert);                      % All the
pairwise distances (squared)

i = 1;                                  % Next id to assign
for n = 1:size(Vert, 1);
if Id(n) > 0
continue;                          % Already assigned its id
end

%     close = find( D(n,:) < tol);      % Indices of all
Vertertices closer to Vert(n,:) than sqrt(tol)
close = find( D(n,:) ==0);
Id(close) = i;                        %Give them all the same
id
i = i + 1;
end

end



function Mnew = findBorder2 (E)


%% Flip vertices
for j = 1:size(E,1)
if(E(j,1) > E(j,2))
      E(j,1:2) = fliplr(E(j,1:2));
      E(j,3) = 1;
end
end

%% Order the array
[M,I] = sortrows(E);

%% Eliminate duplicates
vett = zeros(1,size(M,1));
k = 1;
```

```
for i = 1:size(M,1)-1
    j = size(M,1)-i;
if (M(j,1:2) == M(j+1,1:2))
       vett(j:j+1) = 1;
       k = k + 1;
end
temp = find(vett == 0);
Mnew = M(temp,:);
end

%% Flip back the vertices
for i = 1:size(Mnew,1)
if (Mnew(i,3) == 1)
       Mnew(i,1:2) = fliplr(Mnew(i,1:2));
end
end

Mnew=Mnew(:,1:2);
```

Appendix B

Program to generate graded support microstructures

```
clc
clear all
close all
delete *.png

string = 'Lshape_big.stl';
[F,V,N]= stlread(['C:\Documents and Settings\Administrator\My
Documents\MATLAB\Function to STL\Freesteel Slice\dist\'
string]);
STL_Export(V, F, 'imported.stl', 'solid');
Rx = [1 0 0; 0 cos(pi/2) -sin(pi/2); 0 sin(pi/2) cos(pi/2)];
%%  around X axis
V = Rx*V'; V = V';


V(:,1) = V(:,1) - min(V(:,1)); V(:,2) = V(:,2) - min(V(:,2));
V(:,3) = V(:,3) - min(V(:,3));
STL_Export(V, F, 'to_slice.stl', 'solid');

Min = min(V(:,3));
Max = max(V(:,3));
step = (Max - Min)/50;
str= ['slice -z ' num2str(Min) ',' num2str(Max) ','
num2str(step) ' ''to_slice.stl'' -o output.png']
dos(str);
Sliced_STL_list = dir('C:\Documents and
Settings\Administrator\My Documents\MATLAB\Function to
STL\Freesteel Slice\dist\*.png');

for i=1:length(Sliced_STL_list)
    Sliced_STL = imread(['C:\Documents and
Settings\Administrator\My Documents\MATLAB\Function to
STL\Freesteel Slice\dist\' Sliced_STL_list(i).name]);
    [index1, index2] = find(Sliced_STL(:,:,1)==0);
    Section_Area(i)=length(index1);
End

% plot(linspace(Min,Max,length(Sliced_STL_list)),
Section_Area,'*');
```

```
% xlabel('Heigth')
% ylabel('Area of the slice')

%%%%%%%%%%%%%%% Finding Minima to grade support %%%%%%%%%%
k=1;
for i=1:length(Section_Area)
if (Section_Area(i)~=0)
       y(k)=Section_Area(i);
       k=k+1;
end
end
x = 1:length(y);
figure
plot(x, y,'*');
xlabel('Heigth')
ylabel('Area of the slice')


k=1;
minima=[];
for i = 2:length(y)-1
if (  y(i)-y(i-1) < 0 && y(i)<0.9*y(i-1) )
if ( y(i)-y(i+1) <= 0 )
        min_xval(k)=i;
        diff1(k) = y(i)-y(i-1);
        k=k+1;
end
end
end

%%%%%%%%%%%%%%% Constructing support %%%%%%%%%%%%%%%

%% Rotate solid

Rx = [1 0 0; 0 cos(-pi/2) -sin(-pi/2); 0 sin(-pi/2) cos(-
pi/2)];  %%  around X axis
V = Rx*V'; V = V';

V(:,1) = V(:,1) - min(V(:,1)); V(:,2) = V(:,2) - min(V(:,2));
V(:,3) = V(:,3) - min(V(:,3));
Xmax = max(V(:,1)); Xmin = min(V(:,1));
Ymax = max(V(:,2)); Ymin = min(V(:,2))+1;
Zmax = max(V(:,3)); Zmin = min(V(:,3));


%%% chopping the 3D geometry in N+1 parts
N= 2;
vect_base_real=1;
vect_base = [1 N length(y)];
```

```
for i=2:length(vect_base)-1
    vect_base_real(i) = vect_base(i)*Ymax/length(y);
end
vect_base_real = [vect_base_real Ymax];

%%%% Volume of each part%%%%
for i=1:length(vect_base)-1
    Supp_vol(i)=sum(y(vect_base(i):vect_base(i+1)));
end

V_zero = V;
V_zero(:,3) = zeros(size(V,1),1);

for i=1:length(vect_base_real)-1
    I = find(V(:,2) <= vect_base_real(i+1));
%     figure, plot(V(I,1),V(I,2))
if (mod(length(I),3)==1)
        I(length(I))=[];
elseif (mod(length(I),3)==2)
           I( (length(I)-1): (length(I)) )=[];
end
end
         V_cut = V(I,:);
         index = 1;
for k=1:3:length(I)
                sides = pdist(V_cut(k:(k+2),:));
                SemiP = sum( sides)/2;
                Area(index) = sqrt( SemiP * (SemiP-sides(1))
* (SemiP-sides(2)) * (SemiP-sides(3)) );
                index = index + 1;
end
    Supp_Area(i) = sum(Area) ;
end

for j=0:length(Supp_Area)-2
    i=length(Supp_Area)-j;
    Supp_Area(i) = Supp_Area(i)-Supp_Area(i-1);
end

Supp_weigth = ((Supp_vol)./(Supp_Area));
Supp_weigth = (Supp_vol)./diff(vect_base_real);
Supp_weigth = Supp_weigth/max(Supp_weigth)*2;

V=[]; F=zeros(2,3);
for i=1:length(vect_base_real)-1
% Supp_weigth(i)=2
    string = ['cos(' num2str(Supp_weigth(i)) '*x)*sin('
num2str(Supp_weigth(i)) ...
```

```
'*y)+cos(' num2str(Supp_weigth(i)) '*y)*sin('
num2str(Supp_weigth(i)) ...
'*z)+cos(' num2str(Supp_weigth(i)) '*z)*sin('
num2str(Supp_weigth(i)) '*x)']%% X Y Z range in mm

xyz=ezimplot3(string,[Xmin Xmax vect_base_real(i)
vect_base_real(i+1) 0 20]); %% X Y Z range in mm

close all

figure
    p = patch(xyz{1},xyz{2},xyz{3},1);
    Vmicro=get(p,{'vertices'});
    Fmicro=get(p,{'faces'});
    STL_Export(Vmicro{:,:}, Fmicro{:,:}, [num2str(i) '.stl'],
     'solid');
    V=[V; Vmicro{:,:}];
    F=[F; max(max(F)) + Fmicro{:,:}];

end
F(1:2,:)=[];
STL_Export(V, F, 'micro.stl', 'solid');
```

Appendix C

Publications

Journal of Materials Processing Technology 213 (2013) 589–597

Contents lists available at SciVerse ScienceDirect

Journal of Materials Processing Technology

journal homepage: www.elsevier.com/locate/jmatprotec

Surface roughness analysis, modelling and prediction in selective laser melting

Giovanni Strano*, Liang Hao, Richard M. Everson, Kenneth E. Evans

College of Engineering, Mathematics and Physical Sciences, University of Exeter, Exeter, EX4 4QF, United Kingdom

ARTICLE INFO

Article history:
Received 5 November 2011
Received in revised form 21 October 2012
Accepted 16 November 2012
Available online xxx

Keywords:
Additive manufacturing
Surface roughness prediction
Surface analysis
Mathematical modelling

ABSTRACT

Selective Laser Melting (SLM) is an increasingly employed additive manufacturing process for the production of medical, aerospace, and automotive parts. Despite progresses in material flexibility and mechanical performances, relatively poor surface finish still presents a major limitation in the SLM process.

In this study an investigation of surface roughness and morphology is presented for Steel 316L alloy parts made by SLM. In order to characterise the actual surfaces at different sloping angles, truncheon samples have been produced and an analysis has been conducted at different scales, by surface profilometer and scanning electron microscope (SEM). The surface analysis has showed an increasing density of spare particles positioned along the step edges, as the surface sloping angle increases. When layer thickness is comparable to particle diameter, the particles stuck along step edges can fill the gaps between consecutive layers, thus affecting the actual surface roughness.

Classic models for roughness prediction, based on purely geometrical consideration of the stair step profile, fail to describe the observed trend of the experimental data. A new mathematical model is developed to include the presence of particles on top surfaces, in addition to the stair step effect, for the accurate prediction of surface roughness. Results show that surface roughness predicted by this model has a good agreement with the experimentally observed roughness. The paper investigates the key contributing factors influencing surface morphology, and a theoretical model for roughness prediction that provides valuable information to improve the surface quality of SLM parts, thus minimising the need of surface finishing.

1. Introduction

Selective Laser Melting (SLM) is an emerging additive manufacturing (AM) process for the production of end-use parts with complex shapes, for medical, aerospace, automotive applications. Its widespread use in recent years has been permitted by an increasing availability of processing materials and mechanical performance of the resulting SLM parts (2003) (Wohlers, 2011). The SLM process enables the direct melting of powders of a number of metals, such as titanium, steel, chrome cobalt, aluminium alloys, and building of net-shape parts through a "layer by layer" approach. For each layer a scanning laser beam supplies the energy to locally melt a layer of deposited metal powder and fuse it onto a previously melted layer.

SLM still faces an apparent limitation in terms of surface quality if compared to some alternative metal manufacturing processes such as machining. Surface quality is greatly influenced by the "stair step" effect, which is the stepped approximation by layers of curves and inclined surfaces. This effect is present, to a greater or lesser degree, in all additive layer manufacturing (ALM) processes as consequence of the additive deposition and fabrication of layers. Despite the fact that layer thickness can be reduced to improve the surface finish, obtaining good surface finish presents a very important issue in SLM production: poor surface quality could lead to long and expensive post-finishing operations, often executed by hand due to the shape complexity of the parts produced, thus compromising the advantages of using the additive manufacturing processes for industrial production. Furthermore, a smooth surface is limited by the "balling" phenomenon that occurs during laser melting. The balling effect limits the SLM process resolution because it causes the formation of discontinuous tracks (Mumtaz and Hopkinson, 2009), therefore limiting the formation of very sharp geometries. Also it is responsible for a non-uniform deposition of material on the previous layers, thus inducing a possible porosity and delamination between layers that is detrimental to the functional performance of parts, such as fatigue life for aerospace components and longevity for medical devices. During the process planning of SLM production, important benefits and improvements can be achieved by predicting the surface roughness in advance.

Previous studies have attempted to predict the surface roughness of parts processed on different ALM platforms. Reeves and Cobb (1997) presented a model to predict the surface roughness for Stereolithography (SLA) parts by introducing two different expressions to predict the roughness of upward and

* Corresponding author. Tel.: +44 0 1392 723740; fax: +44 0 1392 263620.
E-mail address: g.strano@exeter.ac.uk (G. Strano).

0924-0136/$ – see front matter © 2012 Elsevier B.V. All rights reserved.
http://dx.doi.org/10.1016/j.jmatprotec.2012.11.011

downward-facing surfaces by considering the layer thickness, surface angle and layer profile. The phenomenon of "print-through" on down-facing planes is capable of providing low roughness for a limited range of angles, although complementary processes for surface smoothing were considered necessary. Campbell et al. (2002) presented a comparison between theoretical roughness obtained from a trigonometrically derived equation, on the stair step profile, and empirical roughness measured on several different ALM platforms. The model was able to predict roughness for a partial range of surface inclinations with respect to the build directions. More recently, Luis Pérez et al. (2001) has proposed a geometrical roughness model to predict the average surface roughness of ALM parts; prototypes were fabricated using SLA to compare the theoretical and the actual surface roughness. In their model some corrections were established necessary, for the characterisation of surfaces with sloped close to 0° and 90°.

Models based on the pure description of the stair step profile frequently fail to accurately predict the surface roughness of ALM parts, because surface roughness is influenced also by other process parameters. Bacchewar et al. (2007) has investigated the contribution of build orientation, laser power, layer thickness, beam speed and hatch spacing on surface roughness of Selective Laser Sintering (SLS) parts. In the case of upward oriented surfaces, build orientation and layer thickness were confirmed to be significant parameters; downward oriented surfaces were also influenced by laser power. Ahn et al. (2009) presented an alternative phenomenological model which interpolates data from empirical observations of test samples; theoretical and real distributions were compared through the fabrication of test parts manufactured by SLA. This roughness prediction approach exhibits the potential to include the sum of the all-contributing factors to the part surface roughness, but faces difficulty in distinguishing among the most influential of the factors. Also, the interpolation of empirical roughness is based on a discrete number of measurements, which means that a large number of measurements is required to achieve high resolution. Strano et al. (2011) adopted the phenomenological approach to the production of parts by SLS and used a mathematical multi-objective optimisation technique to simultaneously maximise surface quality and energy saving through an optimal part build orientation. Experimental roughness data were collected and interpolated for a range of deposition orientations, and a phenomenological model for the evaluation of surface was used in the optimisation procedure. Data collected on downward-oriented surfaces presented a more homogeneous trend than that of upward ones. This was thought to be the result of gravity and surface tension forces on the molten pool during the sintering process: on downward oriented surfaces the molten polymer tends to drop down due to the action of the gravity, thus filling the gaps between layers sintered consecutively and providing "compensation" to the stair stepping effect before solidification.

There is little research reporting on the experimental study and computational prediction of the surface roughness of SLM parts. This study has firstly analysed the surface morphology and roughness at different inclinations of the upward surfaces of SLM parts in order to identify the major contributions to surface roughness. Following this, a new mathematical model is proposed to predict the real surface characteristics in the SLM process. Using a surface profilometer and scanning electron microscope, the surface roughness and morphology analysis of a steel 316L alloy sample made by SLM shows the importance of considering the effect of lack of sharpness in the step edges and the presence of partially-bonded particles on the top surfaces, which significantly affect the surface roughness when the layer thickness is comparable to the particle size. The new surface roughness model is developed to include the presence effect of irregularities such us the presence of particles on top surfaces.

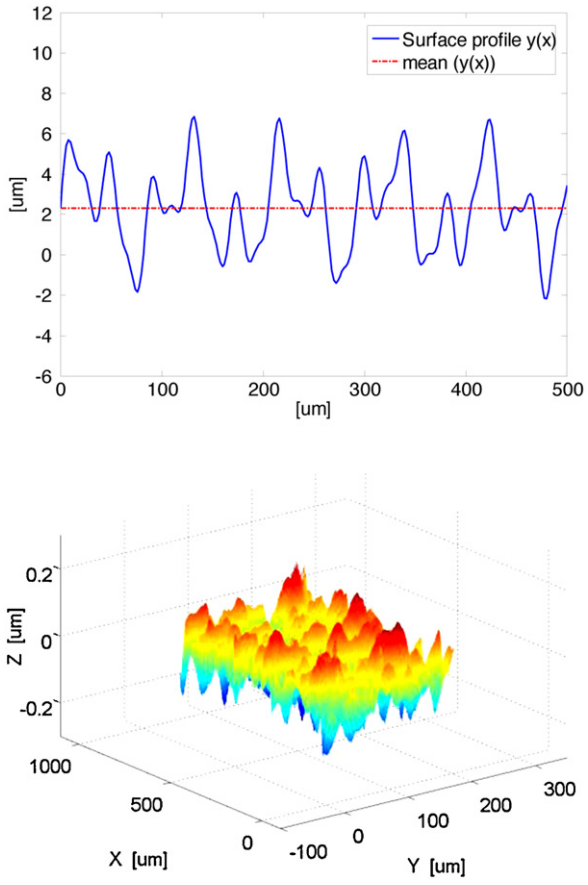

Fig. 1. Representation of 1D (top) and 2D (bottom) surface profiles.

2. Surface morphology and roughness analysis

2.1. Surface roughness

Considering a surface of profile of length L, the one-dimensional definition of surface roughness R_a is

$$R_a = \frac{1}{L}\int_0^L |f(x)|\ dx \tag{1}$$

where $f(x)$ is the deviation of surface height at x from the mean height over the profile, assuming that the overall profile is level (Fig. 1). If the height f_n is measured at N locations along the profile length L, the roughness is numerically calculated as:

$$R_a \approx \frac{1}{N}\sum_{i=1}^{N} |f_n| \tag{2}$$

The definition of surface roughness is readily extend to a two-dimensional surface profile of area A, as the average magnitude of the surface profile from the mean plane, again assuming that the mean plane is level (Fig. 1). In this case, with NxM measured deviations $f_{i,j}$ the roughness is approximated as

$$R_a \approx \frac{1}{NM}\sum_{i=1}^{N}\sum_{j=1}^{M} |f_{ij}| \tag{3}$$

In the following, an analysis of the stair step and balling effect contributions to the surface roughness of SLM processed parts, at different orientations is presented. For this purpose surface characterisation by surface profilometer and scanning electron

Table 1
Chemical composition of 316L steel powder used in the experiments.

Element (wt%)	C	Cr	Cu	Fe	Mn	Mo	Nb	Ni	N	O	P	Si
316L	0.03	17.2	N/A	Bal.	1.8	2.6	N/A	11.2	Trace	Trace	Trace	0.75

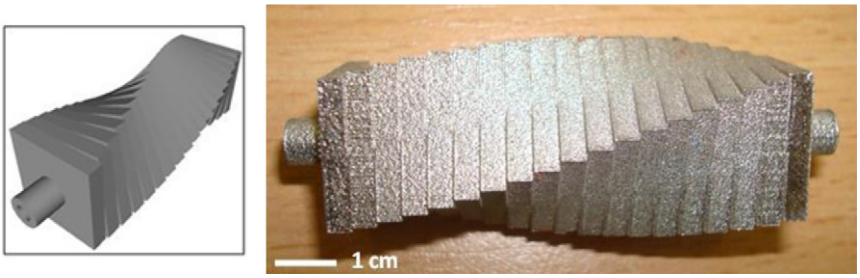

Fig. 2. Manufactured sample geometry. During building the truncheon is oriented with the long axis horizontal.

microscope (SEM) on manufactured samples was conducted for surfaces at different inclination angles to the deposition layers

2.2. Sample preparation and experimental procedure

A "truncheon" test part was designed to measure roughness surfaces inclined to the horizontal at "sloping angles" in the range 0°–90° at 5° intervals (see Fig. 2). This geometry was used in previous works (Reeves and Cobb, 1997; Campbell et al., 2002; Ahn et al., 2009), because it allows the surface roughness for each inclination angle to be easily measured. The material for the experiments was austenitic steel 316L supplied by Sandvick Osprey with particles diameter 20 μm and standard deviation of 8 μm (Sandvik Osprey Ltd., 2012). The material had the chemical composition listed in Table 1.

Two sample parts were fabricated with a Selective Laser Melting machine M270 by EOS (EOS GmbH, 2012); the process parameters were: layer thickness 20 μm, beam scan speed 900 mm/s, hatch spacing (distance between consecutive laser scans) 100 μm. The steel powder was melt by used for the material melting was a Yb (Ytterbium) fibre laser with wavelength 1060–1100 nm; the laser beam had Gaussian profile, a beam diameter of 100 μm and a maximum power output of 195 W (EOS GmbH, 2012).

The analysis of the sample surface was first carried out using a surface profilometer (Talyscan 150, Taylor Hobson Ltd). For each inclination, surface roughness was collected with a stylus gauge on a surface of 10 mm × 1 mm, with a scanning spacing fixed at 5 μm and scanning speed at 2500 μm/s. Secondly, to further investigate the surface morphology at microscopic scale, the sample was treated using isopropanol and surface analysis was carried out using a SEM (S-3200N, Hitachi).

2.3. Surface roughness and morphology analysis using profilometer

Data were collected through two measurements on each upward oriented side of the first two manufactured "truncheon" samples, giving a total of four independent datasets.

Fig. 3 shows the variation in average surface roughness with sloping angle, with error bars indicating the standard deviation at each angle across the datasets. The datasets presented similar trends: for each of them the horizontal surface (0° inclination) had lowest roughness, as expected. Surface roughness at 0° horizontal surface is generated by the rippling effect that occurs during the laser melting process. When the laser moves there is a temperature gradient between the laser beam and the solidifying zone, this generates a shear force on the liquid surface that is contrasted by surface tension forces (Kamran and Neil, 2010; Dutta Majumdar et al., 2011). As the laser has moved the temperature will uniform and the gravity and surface curvature counteract the external shear force, thus tending to restore the surface height of the melt pool to the free level (Ramos et al., 2003). However, due to quick melt pool solidification time, this relaxation process is often not fully achieved, instead a residual rippling on the surface is formed. However, it has been shown in (Kruth et al., 2010; Fischer et al., 2003) that it is possible to reduce the roughness generated by rippling effect, by surface remelting.

As the inclination angle increases from 0°, higher surface roughness results from the stair-step effect. It is important to notice that on inclined surfaces, unlike on horizontal ones, laser remelting is not possible with SLM technology, since material can only be sintered horizontally.

The trend of measured roughness is mainly constant in the range of 5°–45°, with a relatively slow decrease in the range 50°–90°.

Fig. 4 shows a number of two-dimensional surface profiles at different inclinations of 5°, 10° and 65°. The white, regularly space, parallel streaks at low sloping angles (Fig. 4a and b) correspond to elevated ridges, separated by the distance between stair steps.

For each inclined surface, the distance between consecutive ridges on the scanned surface, was compared with *h* the distance

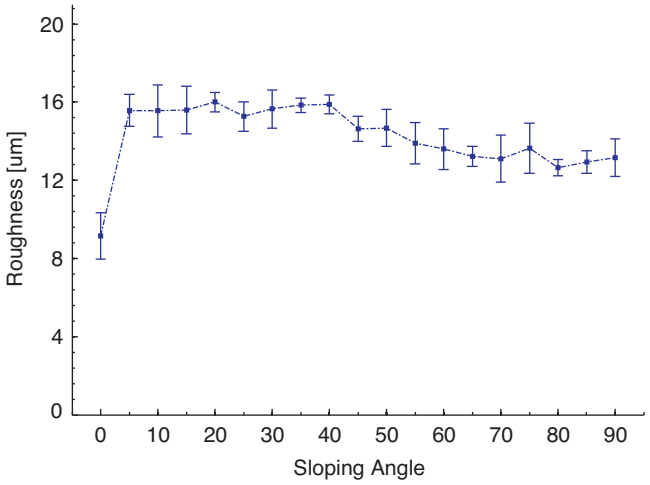

Fig. 3. Experimental roughness at different sloping angle.

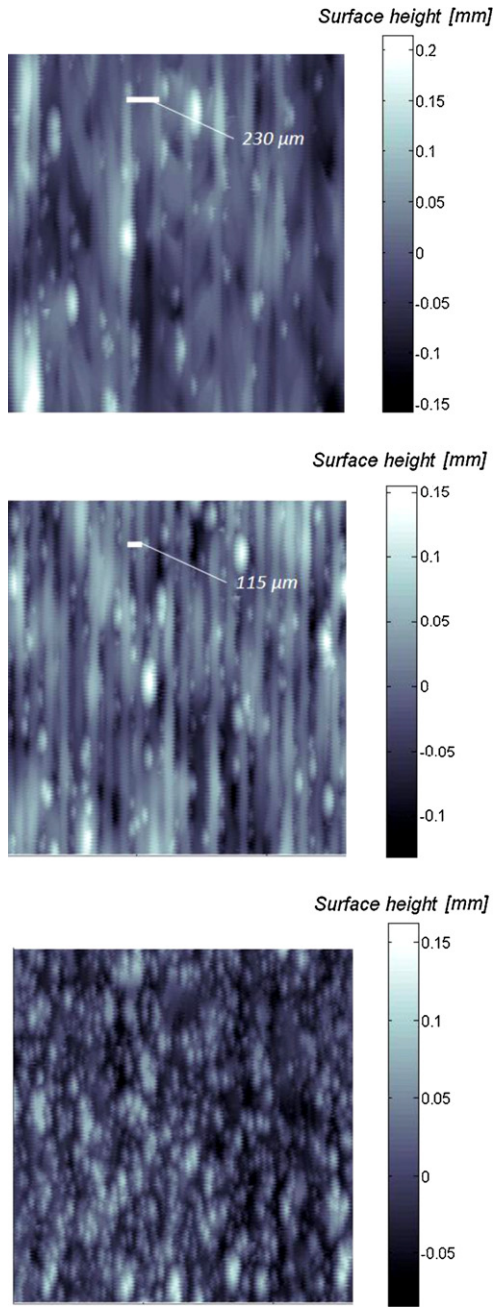

Fig. 4. Profilometer surface profiles inclined at (a) 5°, (b) 10° and (c) 65°. The grey scale indicates surface height.

between consecutive step edges, derived trigonometrically from the stepped profile of surface inclined by angle α (see Fig. 5):

$$h = \frac{L_t}{\sin(\alpha)} \tag{4}$$

where L_t is the layer thickness and W the step width.

Fig. 6 shows that there is a good correspondence between predicted and measured h, for the range of angles up to 50°. Clearly, for this range of angles, the stair step effect influences relevantly the surface morphology. In fact, the stair step is responsible for the waviness characterised by the parallel ridges observed on the surface.

The effect of the stair step into the formation of vertical ridges could not be clearly observed at sloping angles bigger than 50°. Particularly, at higher sloping angles greater than 65°, no vertical lines

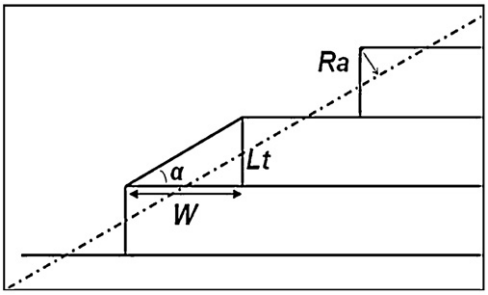

Fig. 5. Schematic representation of sliced profile. The dash dotted line represents the mean location of the surface.

pattern were observed; instead, the surface was characterised by the presence of isolated high peaks (Fig. 4c). In order to characterise the surface morphology at higher sloping angles, and to investigate the contribution of other effects to surface roughness, a surface morphology analysis was carried out by SEM.

2.4. Surface morphology analysis through SEM

SEM analysis has been carried out for a number of different inclinations of the SLM part. Fig. 7 shows the profile of horizontal surface, normal to the build direction (alpha = 0). There are few spare, partially-sintered particles on the surface, because the low layer thickness (20 μm) and the high power (195 W) supplied by the laser beam, mean that the powder is fully melted and fused into a relatively smooth and uniform layer. In Fig. 7b the effects of scan direction and strategy (highlighted by the arrows) are visible; for each scan line there are noticeable bullet-shaped marks oriented in the sense of the moving laser beam, presumebly due to slower cooling in the centre of each track. The distance between the centres of these marks with same orientation is about 200 μm, (Fig. 7c) as a result of the chosen hatch spacing (100 μm) and laser beam diameter (100 μm).

The surface of the second sample step, with sloping angle of 5° is presented in Fig. 8. The stair-step is visible at intervals of about 230 μm (Fig. 8c); this confirms the observations made through stylus equipment and the values calculated through Eq. (4).

When the build inclination increases, the SEM micrographs show the lack of sharpness of the step edges, due to discontinuities along step edges and the presence of partially bonded particles stuck at the edge borders (Fig. 8c).

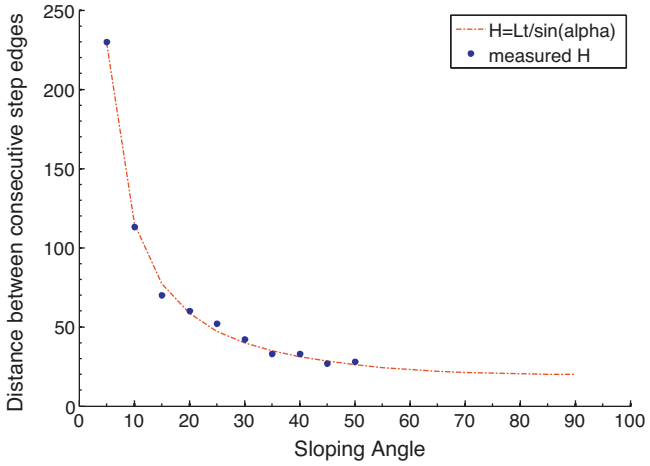

Fig. 6. Measured and predicted distance between consecutive step edges.

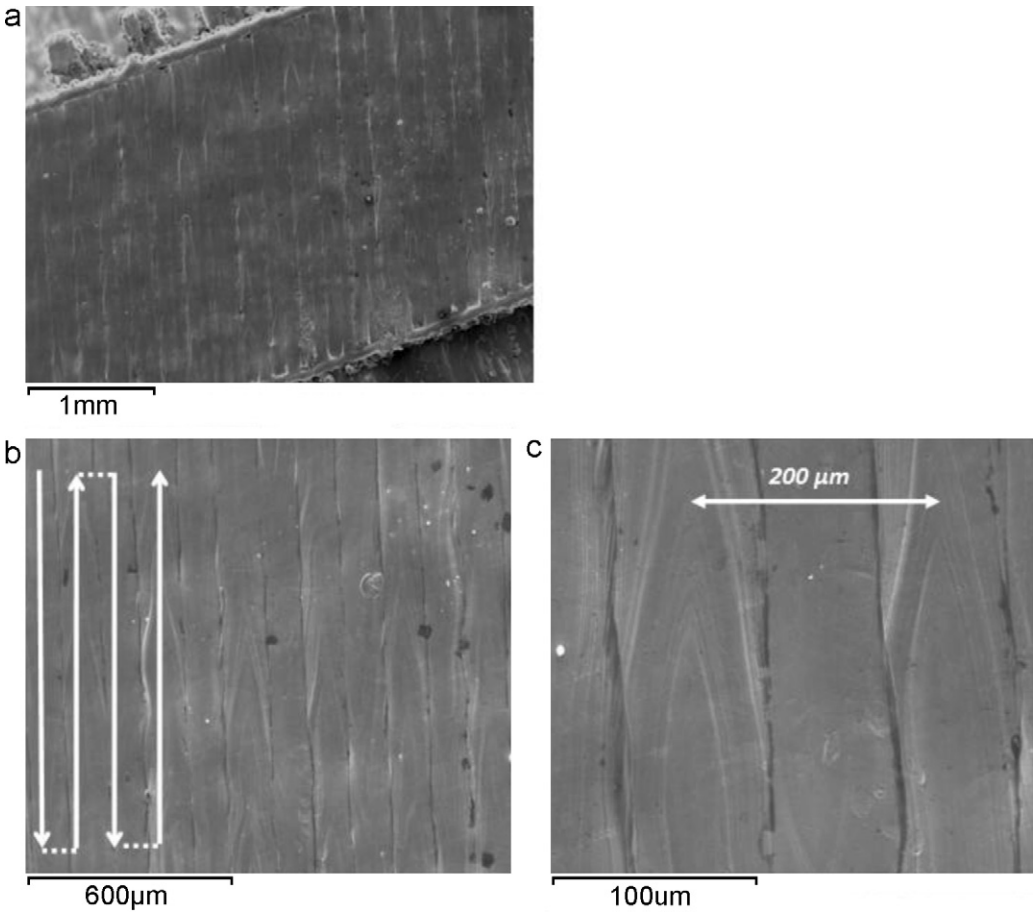

Fig. 7. SEM picture of a horizontal surface (sloping angle 0°): (a) an surface overview, (b) detail profile, (c) detail profile at high magnifications.

The formation of discontinuous borders is partially determined by the balling effect that occurs during the laser melting of the metal powder. Balling is the breakup of the molten pool into small entities. During the laser melting of metal powders, the high thermal gradient between different volumes of the molten material generates a difference in surface tension within the pool, which produces Marangoni convection (Steen and Mazumder, 2010). The general pattern of the flow field is that the material is pulled radially outwards to the surface (Chan and Mazumder, 1987). The pool breaks into smaller spherical entities; the detached drops of material scatter on both sides of the pool (Mumtaz and Hopkinson, 2009), and, having solidified, they appear as irregularities along the single scan tracks. Balling is a severe impediment on the interlayer connection, it decreases part density and increases surface roughness. A reduction in thermal variation across the melt pool reduces the strength of any potential Marangoni convection (Niu and Chang, 1999; Gu and Shen, 2007; Xiao and Zhang, 2007). Low viscosity within the melt pool favourites balling (Agarwala et al., 1995) as well as cold power beds, due to poor wetting (O'Neill et al., 1998); increasing the powder bed temperature can increase wetting therefore reducing balling phenomenon.During the melting of the step represented in Fig. 8c, in order to cover the entire step width ($W = Lt/\tan(\alpha) = 228$ µm), three scan tracks were overlapped, starting from the left and moving to the right (Fig. 8b). The balling produced by each scan is almost entirely removed by the following scan, so the only balling effect is visible only at the final scan of each edge (Fig. 8c).

Furthermore, partially-bonded particles stuck at step edges are visible in Fig. 8c. During the laser melting, The heat on the edge borders is not sufficient to fully sinter particles so particles do not merge completely with the layer, tending to stick to the surface at the step edges as shown in Figs. 8 and 9. As the sloping angle increases, the concentration of particles stuck to edges has been observed to increase. This is because as sloping angle increases, step edges with adhered particles are closer to each other, leading to higher concentration of particles on the surface area. Fig. 10 shows the variation of particles concentration between consecutive layers.

Fig. 10 shows the surface morphology on consecutive sample steps, respectively between 5° and 10°, 30°–35°, 85°–90° sloped surfaces. Particle concentration increase considerably when surface at 5° is compared to the one sloped at 10°; as predicted by Eq. (4), when surface is inclined at 10°, step edges are closer to each others, than when surface is inclined at 5°. This explain the higher concentration of particles at 10°. At small sloping angles (alpha < 35°) the number of particles per unit area is expected to be inversely proportional to the distance between step edges, h, because particles are found principally at step edges. At larger sloping angles the variation in particle concentration is not so marked because $h = L_t/\cos(\alpha)$ varies more slowly with α.

No waviness is seen on the surfaces sloped at 85°and 90°, where no stair step is expected. Fig. 11 shows a particular effect on the 90° inclined surface: a high number of partially bonded, clustered particles is present on the surface, and partially bonded particles can be considered the main cause of surface roughness at 90°.

The trend of measured roughness on the "truncheon" sample can be explained as the effect of increasing presence of particles with surface inclination. At very low sloping angles the presence of particles along step edges does not considerably influence the morphology because the distance between consecutive step edges is much bigger than the particle size. This means that a few

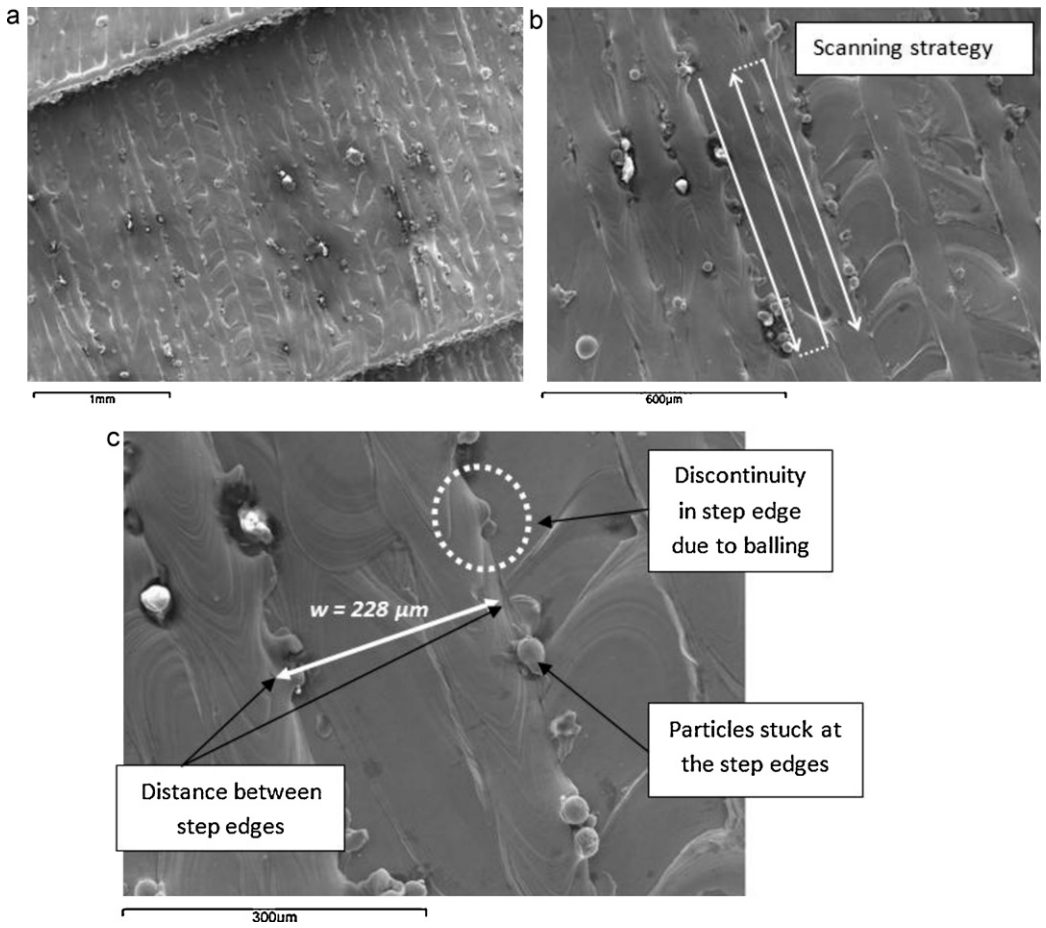

Fig. 8. SEM picture of slightly inclined surface (sloping angle 5°) (a) at low magnification, (b) at high magnifications, (c) detail of of slightly inclined surface.

particles stuck on the step edges do not make major contribution to the surface roughness. As the sloping angle increases edges become closer to each other causing the particle concentration to increase. The presence of particles that partially fill the spaces between edges cannot be ignored, and in fact, it affects the measured roughness, causing it to be larger than expected from merely the stair stepping effect. The presence of partially bonded particles results in the high surface roughness at 90° sloping angle even though there is no stair-step presence.

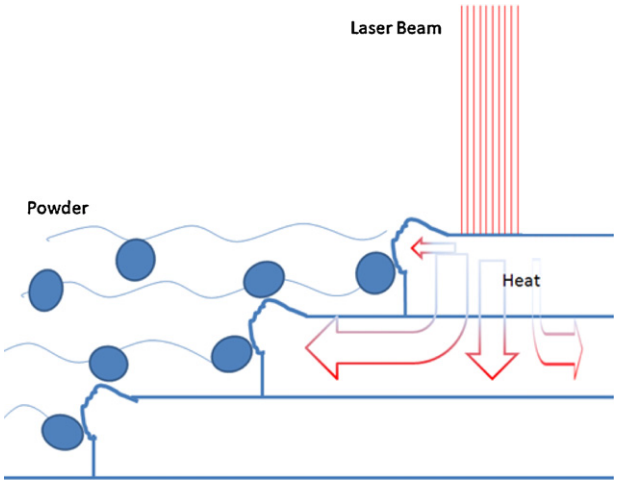

Fig. 9. Schematic representation of heat diffusion during laser melting process.

3. New model for surface roughness

3.1. Stair-step effect and surface roughness in selective laser melting

Selective laser melting (SLM) process starts with a CAD model of the object that has to be built; slicing the geometry involves a level of approximation, described by the "stair step" effect (see Fig. 5).

The surface roughness R_a for the inclined surface represented schematically in Fig. 5, can be defined as:

$$R_a = \frac{1}{L}\int_0^L |y(x)|\ dx = \frac{1}{4}L_t \cos(\alpha) \tag{5}$$

with L_t layer thickness and α surface sloping angle.

It is evident that an improved surface finish is achievable through the choice of a lower layer thickness.

Also roughness is expected to decrease as the surface inclination increases, according with the cosine term in Eq. (5). However, comparison between the experimental data collected and the theoretical roughness predicted by considering only the stair-step effect (Fig. 12), shows that the stair-step model inadequately describes the measured variation in surface roughness for almost the entire range of inclination angles. In particular, experimental roughness does not decrease as much as predicted by the cosine function. As the SEM analysis presented above shows this additional roughness is due to the presence of particles stuck at the step edges.

In these experiments a small layer thickness (L_t = 20 μm) has been used, relative to the average particle diameter (20 μm), so

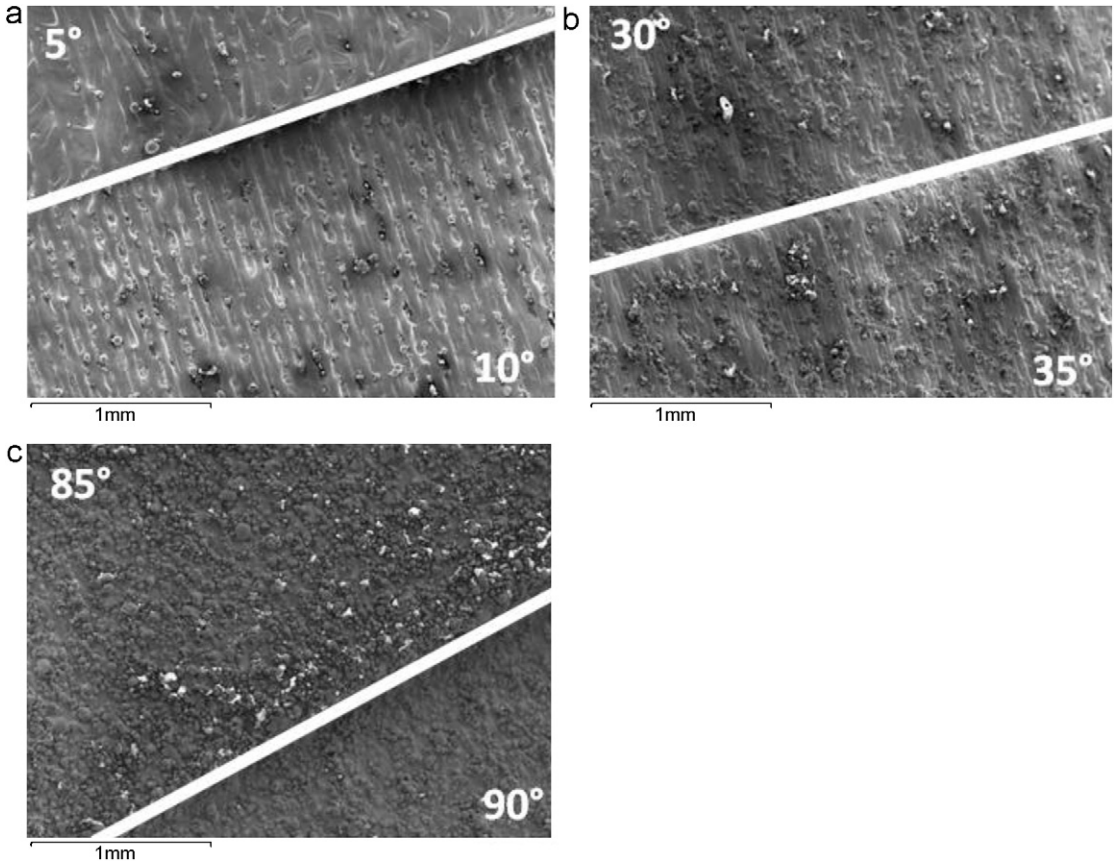

Fig. 10. Transition between sample steps at (a) 5°–10°, (b) 30°–35° and (c) 85°–90° sloped surfaces. The superimposed white lines mark the boundary between surfaces of the truncheon test piece with different sloping angles.

the effect of partially bonded particles is readily apparent. When sloping angle are in the range of (5°–15°), the width of each step (228 μm–74 μm) is bigger than the average particle diameter therefore the surface keep the characteristic stepped profile, and the stair step effect is well described by Eq. (5). For higher sloping angles, the width of each step becomes smaller, comparable with the particle size, so that the presence of partially bonded particles can significantly influence the surface profile. For instance, at very high sloping angles (80°–90°) the roughness due to the stair step effect is expected to be minimum, theoretically, null at 90°, which corresponds to the situation when layers are overlapped on the top of each other (however a minor residual roughness is expected to be because of the limits on the repeatability of the process accuracy). Nevertheless, as observed with SEM microscope analysis (Fig. 11), the surface presents a high concentration of particles that increase the actual surface roughness to a value of 14 μm.

3.2. Novel model

Here is presented a novel model to describe the effect of partially bonded particles on the surface roughness. As illustrated in

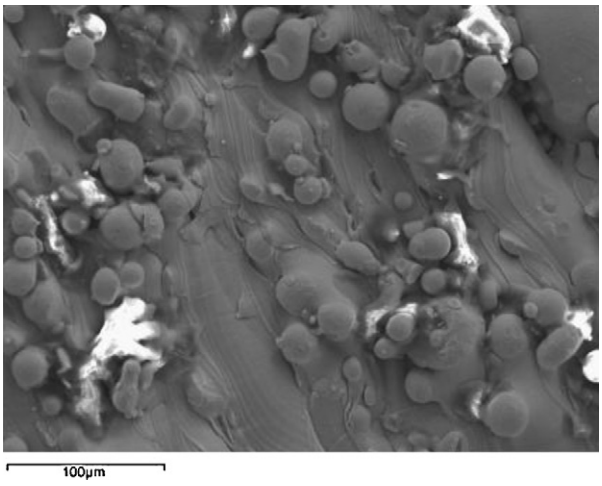

Fig. 11. Presence of particles on highly sloped surface (sloping angle 90°).

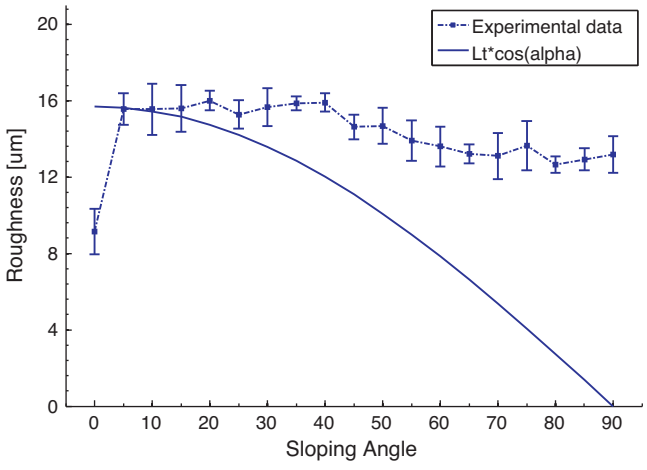

Fig. 12. Comparison of experimental roughness and simulated roughness in accord to Eq. (5).

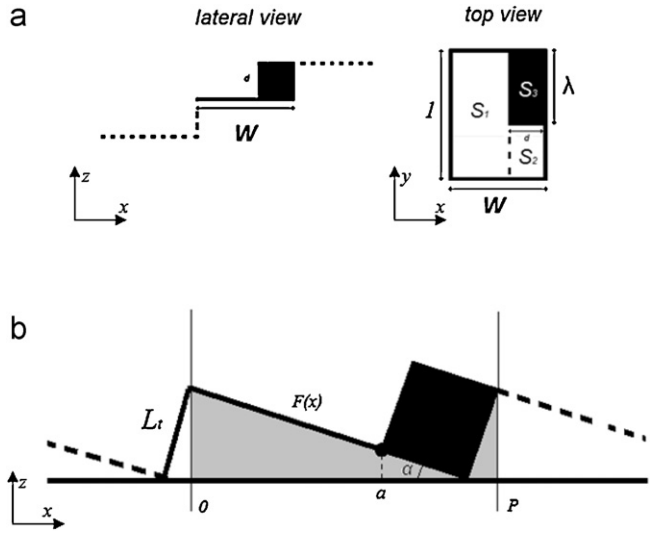

Fig. 13. Schematic representation: (a) lateral and top view of λ fraction of partially bonded particles; (b) cross section of the modelled surface.

Figs. 13 and 14, layers of depth L_t is considered, which form steps of width w, corresponding to an ideal surface sloping at angle $\alpha = \tan^{-1}(L_t/w)$. For simplicity the partially bonded particles are modelled as if they had a square cross-section (shown as black in Fig. 13) and it is assumed that a fraction λ along unit length of step edge has partially bonded particles adhering to it. In Fig. 13a the particles are shown schematically as a single block, but, of course, the partially bonded region may be distributed in any fashion along the stair step. Fig. 13b shows a cross section of the modelled surface perpendicular to the laser direction (which moves in and out of the paper) and oriented so that the ideal surface is horizontal.

The height of the surface is denoted as $F(x,y)$, so that the roughness may be calculated as:

$$R(\alpha, \lambda) = \leftrightarrow \int_S \int |F(x,y) - \bar{F}|\, dx\, dy \tag{6}$$

where $F(\bar{x}, y)$ is the average height of the surface above some fiducial level. Considering a single period of the step between 0 and P (as shown in Fig. 13b) and unit length of track, the integral for the roughness may be split into three integrals over the regions S_1, S_2 and S_3:

$$\begin{aligned} R(\alpha,\lambda) &= \int_s \int |F(x,y) - \bar{F}| dxdy = \int_{s1} \int |F(x,y) - F| dxdy \\ &+ \int_{s2} \int |F(x,y) - \bar{F}| dxdy + \int_{s3} \int |F(x,y) - \bar{F}| dxdy \\ &= \frac{1}{P} \int_0^a |F(x) - \bar{F}| dx + \frac{1-\lambda}{P} \int_a^P |F(x) - \bar{F}| dx \\ &+ \frac{\lambda}{P} \int_a^P |F'(x) - \bar{F}| dx \end{aligned} \tag{7}$$

where $F(x)$ is the one-dimensional profile describing the stair step and $F'(x)$ is the one-dimensional profile describing the step and the partially bonded particles. The average height is calculated as:

$$\bar{F} = \frac{1}{P} \int_0^a F(x)\, dx + \frac{1-\lambda}{P} \int_a^P F(x)\, dx + \frac{\lambda}{P} \int_a^P F(x)\, dx \tag{8}$$

Fig. 15 shows the surface roughness as function of the sloping angle α and of particle fraction λ. When λ = 0 the surface roughness is described by a cosine function which purely describes the stair step effect (Eq. (1)). However as the concentration of particles λ increases, the roughness of highly inclined surfaces increases markedly; indeed when λ is large the trend of diminishing roughness with increasing α at low λ is reversed.

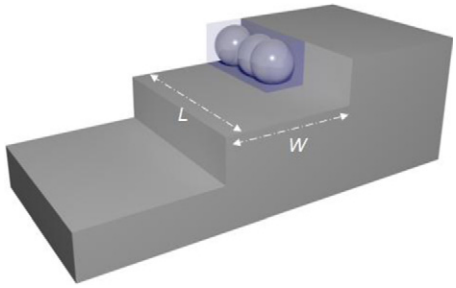

Fig. 14. Representation in 3D of the proposed model.

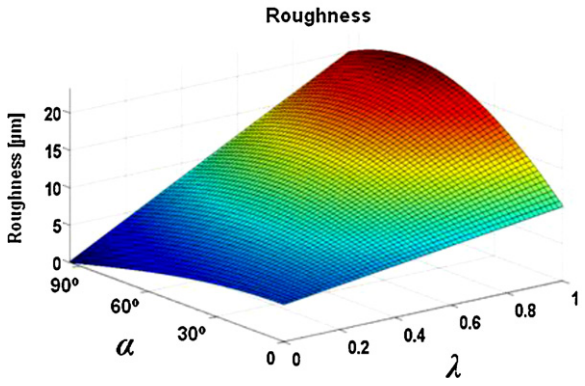

Fig. 15. Surface roughness calculated as in Eq. (7).

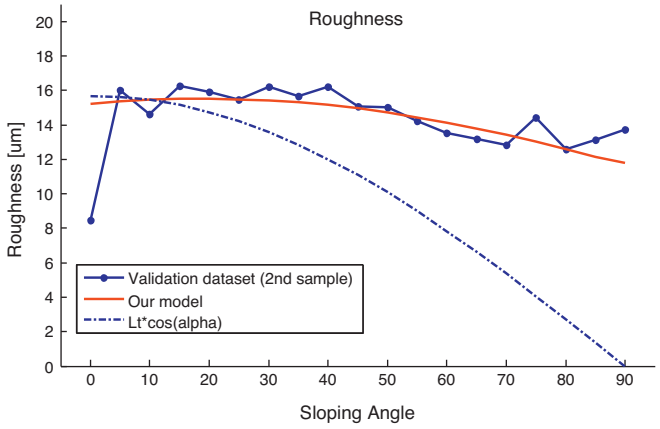

Fig. 16. Comparison between measured roughness on validation dataset (second sample) and roughness predicted through newly developed model based on Eq. (6).

The average experimentally measured $R_a(\alpha_n)$ at angle α_n from two out of the four independent datasets (first sample),was compared with the prediction model by minimising the following error function:

$$\min_{\lambda,c} E(\lambda, c) = \sum_{n=1}^{N} \left| \overline{R_a}(\alpha_n) - c \cdot R(\alpha_n, \lambda) \right| \quad \text{with } 0 \le \lambda \le 1 \tag{9}$$

to determine the optimum λ and scale factor c. Fig. 16 shows the best model fit (λ = 0.13) which describes the experimental data to within the sample-to-sample variation.

Since λ is expected to increase with sloping angle α, experimental data were firstly fit by minimising the average error

between $R_a(\alpha_n)$ and $c\ R(\alpha,\ \lambda(\alpha_n))$ with $\lambda(\alpha_n)$ a flexible non-decreasing function of α. However the use of non-decreasing λ did not provide significantly better results and therefore the more parsimonious model using an average constant value of λ, was preferred.

In order to validate the model, the measured roughness on the remaining two independent datasets (second sample), and predicted roughness $R(\alpha_n, \lambda')$ with λ' solution of Problem (9), were compared as shown in Fig. 16.

Data predicted through the developed model present a better matching with the experimental data, than the one based on pure geometrical consideration on the stair step profile and no particle presence. At low sloped angles, the stair step effect represents the main contribution to surface roughness; at higher sloping angles, the increasing presences of partially bonded particles on the surface compensate the gaps between layers and result in the rough surface. Conventional models that do not include particles' presence, fail to predict surface roughness, especially at high sloping angles. The new model proposed succeeds in describing this phenomenon to predict the surface roughness on the broad range of sloping angles between 0° and 90°.

4. Conclusions

An investigation of surface roughness and morphology has been conducted for Steel 316L alloy parts made by Selective Laser Melting (SLM). In order to characterise the actual surfaces at different sloping angles, truncheon samples have been produced and an analysis has been conducted at different scales, by surface profilometer and scanning electron microscope.

Empirical observations of measured data by profilometer were different from the those predicted through the classic model based on pure geometrical consideration on the stair step profile, due to the presence of partially bonded particles on the surface. In particular, SEM analysis confirmed an increasing density of spare particles positioned along the step edges, as the surface sloping angle increases; during the laser melting of each layer step, the heat applied at edge borders bind them to the step edge. When layer thickness is comparable to particle diameter, the particles stuck along step edges can fill the gaps between consecutive layers, thus affecting the actual surface roughness.

A new mathematical model for the prediction of real surface roughness at different sloping angle has been formulated; the model takes into consideration the increasing presence of particles on top surface, in addition to the stair step effect. Model validation showed that, unlike a straightforward stair-step model, this model accounts for the observed roughnesses over the full range of surface angles.

This study shows the importance of considering particle presence in the formulation of theoretical models, for an accurate prediction of surface roughness in the SLM manufacturing of steel.

Acknowledgements

The authors would like to thank Great Western Research and EADS Innovation Works UK for funding support; 3T RPD Ltd for samples fabrication and X-AT laboratory at the University of Exeter for the access to surface roughness measurement equipment. Also, Mr. Matthew Johns for drawing the sketch of the model proposed in 3D Studio MAX.

References

Agarwala, M., Bourell, D., Beaman, J., Marcus, H., Barlow, J., 1995. Direct selective laser sintering of metals. Rapid Prototyping Journal 1 (1), 26–36.
Ahn, D., Kim, H., et al., 2009. Surface roughness prediction using measured data and interpolation in layered manufacturing. Journal of Materials Processing Technology 209 (2), 664–671.
Bacchewar, P.B., Singhal, S.K., et al., 2007. Statistical modelling and optimization of surface roughness in the selective laser sintering process. Proceedings of the Institution of Mechanical Engineers, Part B: Journal of Engineering Manufacture 221 (1), 35–52.
Campbell, R.I., Martorelli, M., et al., 2002. Surface roughness visualisation for rapid prototyping models. Computer-Aided Design 34 (10), 717–725.
Chan, C.L., Mazumder, J., 1987. Spectroscopic studies of plasma during laser material interaction. Journal of Applied Physics 2, 4579–4586.
Dutta Majumdar, et al., 2011. International Materials Reviews 56, 341.
EOS, GmbH. EOS Stainless steel PH1 material data sheet. Available from http://www.eos.info/en/home. html (accessed 09.07.2012).
Fischer, P., Romano, V., Weber, H.P., Karapatis, N.P., Boillat, E., Glardon, R., 2003. Sintering of commercially pure titanium powder with a Nd:YAG laser source. Acta Materialia 51 (6), 1651–1662.
Gu, D., Shen, Y., 2007. Balling phenomena during direct laser sintering of multi-component Cu-based metal powder. Journal of Alloys and Compounds 432 (1–2), 163–166.
Kamran, M., Neil, H., 2010. Selective laser melting of Inconel 625 using pulse shaping. Rapid Prototyping Journal 16 (4), 248–257.
Kruth, J.P., Badrossamay, M., et al., 2010. Part and material properties in selective laser melting of metals. 16th International Symposium on Electromachining (ISEM XVI) , Shanghai, China.
Luis Pérez, C.J., Vivancos Calvet, J., et al., 2001. Geometric roughness analysis in solid free-form manufacturing processes. Journal of Materials Processing Technology 119 (1-3), 52–57.
Mumtaz, K., Hopkinson, N., 2009. Top surface and side roughness of Inconel 625 parts processed using selective laser melting. Rapid Prototyping Journal 15 (2), 96–103.
Niu, H.J., Chang, I.T.H., 1999. Instability of scan tracks of selective laser sintering of high speed steel powder. Scripta Materialia 41 (11), 1229–1234.
O'Neill, W., Sutcliffe, C.J., Morgan, R., Hon, K.K.B., 1998. Investigation of short pulse Nd:YAG laser interaction with stainless steel powder beds, 47–60.
Ramos, J.A., Bourell, D.L., Beaman, J., 2003. Surface over-melt during laser polishing of indirect-SLS metal parts. Materials Research Society 758, 53–61.
Reeves, P.E., Cobb, R.C., 1997. Reducing the surface deviation of stereolithography using in-process techniques. Rapid Prototyping Journal 3 (1), 20–31.
Sandvik Osprey Ltd., Powder Group, 316L Material, data sheet, available from http://www.smt.sandvik.com/osprey (accessed 09.04.12).
Steen, W.M., Mazumder, J., 2010. Laser material processing. Springer-Verlag London Limited 2010.
Strano, G., Hao, L., et al., 2011. Multi-objective optimization of selective laser sintering processes for surface quality and energy saving. Proceedings of the Institution of Mechanical Engineers Part B: Journal of Engineering Manufacture.
Xiao, B., Zhang, Y., 2007. Laser sintering of metal powders on top of sintered layers under multiple-line laser scanning. Journal of Physics D: Applied Physics 40, 6725–6734.
Wohlers, T., 2011. Wohlers Report 2011 – Additive Manufacturing State of the Industry. Wohlers Associates Inc., Fort Collins, CO, USA.

Int J Adv Manuf Technol
DOI 10.1007/s00170-012-4403-x

ORIGINAL ARTICLE

A new approach to the design and optimisation of support structures in additive manufacturing

G. Strano · L. Hao · R. M. Everson · K. E. Evans

Received: 28 December 2011 / Accepted: 17 July 2012

Abstract Support structures are required in several additive manufacturing (AM) processes to sustain overhanging parts, in particular for the production of metal components. Supports are typically hollow or cellular structures to be removed after metallic AM, thus they represent a considerable waste in terms of material, energy and time employed for their construction and removal. This study presents a new approach to the design of support structures that optimise the part built orientation and the support cellular structure. This approach applies a new optimisation algorithm to use pure mathematical 3D implicit functions for the design and generation of the cellular support structures including graded supports. The implicit function approach for support structure design has been proved to be very versatile, as it allows geometries to be simply designed by pure mathematical expressions. This way, different cellular structures can be easily defined and optimised, in particular to have graded structures providing more robust support where the object's weight concentrate, and less support elsewhere. Evaluation of support optimisation for a complex shape geometry revealed that the new approach presented can achieve significant materials savings, thus increasing the sustainability and efficiency of metallic AM.

Keywords Additive manufacturing · Support structures optimisation · Selective laser melting · Cellular structures design

G. Strano (✉) · L. Hao · R. M. Everson · K. E. Evans
College of Engineering, Mathematics and Physical Sciences,
University of Exeter,
Exeter EX4 4QF, UK
e-mail: g.strano@exeter.ac.uk

Published online: 02 August 2012

1 Introduction

The additive manufacturing (AM) of parts through technologies such as selective laser melting (SLM) and electron beam melting requires the presence of external support structures because materials employed in those processes, typically metals (aluminium, steel, titanium, copper and nickel-based alloys), do not provide sufficient support for a overhanging object. Support structures are typically hollow or cellular structures that are sacrificed after the object's build, thus they represent a waste in the AM process. The fabrication of these sacrificial supports requires time, energy and material, as its supported functional object does. The amount of material wasted by fabricating support structures affects the manufacturing costs, especially when high-values metal alloys such as titanium are employed, for instance in the production of aerospace components. Furthermore, the presence of support structures increases both the time required for the part manufacturing and the time and complexity of post-manufacturing operations. In fact, support removal and surface polishing are usually carried out by expensive hand polishing. Minimising the amount of supported surfaces can shorten this operation, thus improving post-process efficiency. Consequently, design and optimise material-efficient support structures are highly demanded to improve the sustainability and efficiency of metallic AM.

In this paper, we introduce an alternative approach to the optimal design and generation of support structure in AM using SLM process as a typical case study. In order to minimise the amount of support required by the part built by SLM process, we implement a two-step optimisation algorithm. As first step, the best orientation to minimise the volume of support is located, among all the possible orientations; secondly, once the optimal orientation is identified, a second step optimisation performs a support

microstructure optimisation in order to further reduce the support volume. In order to design of the microstructure topology for the supports, we employ 3D surfaces generated by pure mathematical expression. This approach presented high flexibility to design cellular structures with different densities, thus overtaking limitation presented by solid modelling software commercially available today.

1.1 Support structures

For a given object, one of the more effective ways to reduce the amount of support needed is to orientate the object into an optimal building position. Depending of the artefact built orientation, in fact, the amount of bottom surface that needs the supports change sensitively. A previous research [1] investigated the optimal orientation to minimise support structures for stereolithography process, an AM process for plastic parts. In this study, the support was simulated to identify where the part became unstable, overhangs appeared and components that were separated initially and connected later to the rest of the part. Also, the surface area of the support structure that was in contact with the object was minimised to improve the quality of the surface finish. When two different orientations of an object shows the same amount of support structure, the orientation with the lower centre of mass was chosen, since it was more stable. In this research work, supports do not present cellular structures; instead they were treated as solid blocks of materials. An effective way to significantly minimise the amount of material volume for supports could be a support design with an internal cellular structure. Support structures in fact have been typically designed as hollow or cellular structure to save materials and energy. A support design approach using cellular structures was presented in [9], where some airier support structures were designed, in order to overcome the disadvantages of supporting structures made of solid standing walls. In most of the support structure generation packages commercially available today, the supports' cellular structure design is implemented by combining a number of basic cell elements. For instance, the support generation software developed by a company named Materialise [6] locates and group close surfaces with same inclination and implements a list of rules to determine the appropriate type of supports, such as blocks for large surface areas, lines for narrow surfaces, points for very small features, gussets for overhanging parts and web support for circular areas [13]. Although this method presents the possibility for users to tailor the support topology by giving the possibility to choose among different cells type, few drawbacks need to be acknowledged. Very often, the operation of optimal support is initially approximated, and users need to refine it manually relying on their own experience. Also, unavoidably limits to the surface continuity at the junctions between struts and node fillets are introduced, when different cell types are in contact. This is a problem common to many solid modelling software applications, and it can lead to local concentration of stress that can degenerate into a structure collapse [3]. Furthermore, the eventual presence of sharp edges or cavities could facilitate the not uniform distribution of heat during the laser sintering process, therefore causing distortion. An additional drawback is also the impossibility to develop a regularly graded support structure, which could enhance to an optimal distribution of cellular structure density according to the object weight distribution. Clearly, an optimal distribution of support structures density that provides more robust support where the object weight concentrates, and reduced density elsewhere, would enhance the opportunity to achieve an optimal reduction of support volume.

1.2 Design of cellular support structures

There are several ways to design cellular structures; each method has its own advantages and disadvantages. Traditionally cellular structures were created using traditional commercial CAD packages. However, these packages have been proven to be unsuitable for potentially large complex micro-architectures due to vast number of Boolean operation needed [14]. Alternatively, voxel modelling presents a more straightforward way to perform Boolean operations. However, this method requires high resolution volumes to sufficient represent geometries using voxels.

A relatively simple image-based approach to the generation of cellular structures is presented in [12]. In this work, the bounding geometry, defined using a CAD model, is sliced into a number of binary images. Each slide is then treated with a Boolean operator to introduce a number of simple unit cells. This slice-based approach avoids the need of handling triangulated surfaces for the creation of a standard tessellation language (STL) file. However, this is likely limited to 3D printing where image-based slices may be used. As with any purely voxel-based method, it also results in a poorly defined geometry at the boundaries [5].

Another approach to the generation of micro-architectures is through the use of implicit functions. This approach has been employed in [3] and more recently in [7]. This approach uses a set of periodic implicit functions, such as the Schoen gyroid [10], to create microstructures. By introducing functional variations to the equations, it was possible to functionally grade the microstructure. However, there were no methods given to precisely control the grading, such as the minimum and maximum volume fractions. Furthermore, this method provides a compact representation of the complex structures, and through the use of an appropriate isosurfacing algorithm, a straightforward way to produce triangulated surfaces.

In this study, we adopt the implicit functions method to design cellular structure to act as support for AM platforms.

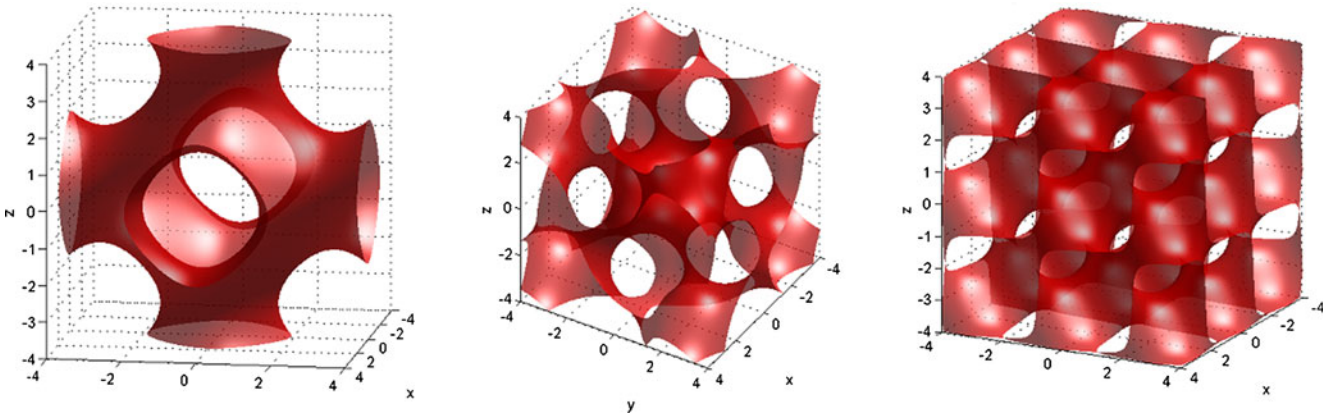

Fig. 1 From the left, representation of level surfaces expressed by Eqs. (1)–(3), respectively

The generation of 3D solid geometries is performed by implicit functions expressed in the form: $f(x, y, z)=0$, where $f = \Re^3\Re$.

Implicit functions provide flexible way to design complex cellular structures; also, they provide a compact representation for these structures.

The periodical surfaces that we present in this work are the "Schwartz" equations [11] and two others generated by the combination of trigonometric functions, known as "Gyroid", and "Diamond" equations.

Schwartz level surface equation:

$$\cos(x) + \cos(y) + \cos(z) = 0 \tag{1}$$

Gyroid level surface equation:

$$\cos(x)\sin(y) + \cos(y)\sin(z) + \cos(z)\sin(x) = 0 \tag{2}$$

Diamond level surface equation:

$$\begin{aligned}\sin(x)\sin(y)\sin(z) + \sin(x)\cos(y)\cos(z) \\ + \cos(x)\sin(y)\cos(z) \\ + \cos(x)\cos(y)\sin(z) = 0\end{aligned} \tag{3}$$

The surfaces generated through 3D pure mathematical expressions are triangulated to generate a 3D solid structure; the mesh is then transferred into STL file formal specifications, in order the support to be processed by the rapid prototyping machine (Fig. 1).

2 Design of optimal support structures for additive manufacturing

2.1 Optimisation of part builds orientation

For a given object, the amount of support structures is directly determined by the build orientation. In fact, depending on the artefact built orientation, the amount of bottom surface that need supports change sensitively.

The following is described: the procedure that is designed to locate the best orientation to minimise the volume of support, among all the possible orientations, was developed. The optimisation is performed by an algorithm implemented in Matlab code. Following, the structure of the algorithm that executes the orientation optimisation, i.e. the first step of the total support structure optimisation, is schematically proposed, as it is shown in Fig. 2. The geometry of the object is defined by the STL used as the input file for the

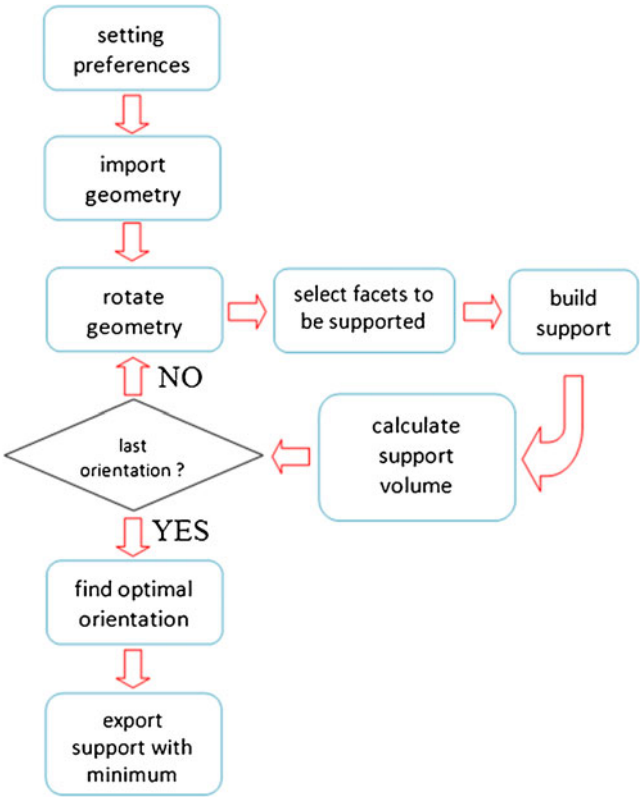

Fig. 2 Schematic of first step optimisation for optimal orientation to minimise support volume

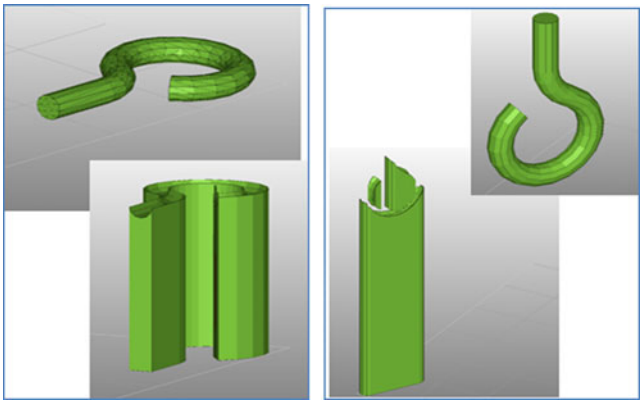

Fig. 3 Examples of solid supports generated for arbitrary orientations

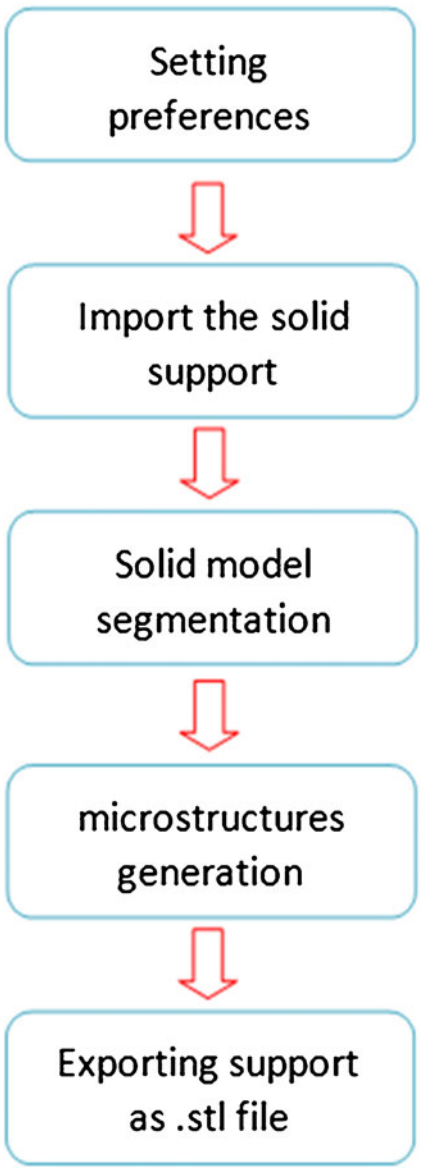

Fig. 4 Schematic of second step optimisation for generation of graded microstructure

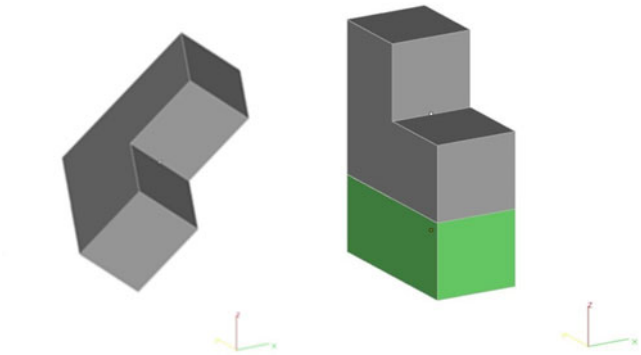

Fig. 5 "test.stl" Geometry in original (*left*) and optimal (*right*) orientations. In *green*, the associated solid support

optimisation system. The STL file, which provides a description of the surface geometry in $\Re^3$, is imported into the Matlab environment.

The initial step presents the possibility for users to choose (1) the distance "z_base" between the platform base and the lowest point on the bottom surface of the part and (2) the parameter "slop_deg", threshold angle of inclination with respect to the platform bed that is used to select the bottom surfaces that are to be supported. Surfaces that are sloped less than the threshold are considered to need support. On the next step, the input geometry is imported, either in the form of ASCII or binary STL file. For each possible generation, the geometry is then rotated around *x*- and *y*-axes, with default resolution of 5°. Higher resolutions can be easily specified by the user; however, this would increase the number of possible orientations (theoretically infinite resolution) and consequently the algorithm iterations and the total computational time required by the optimisation. Once the 3D object geometry is acquired in the STL format, as known, the solid rotation is performed by multiplying the transpose of the matrix V containing the vertices coordinates of the object mesh, by rotation matrices around the X- and Y-axes [4]. V_r matrix of vertices describing the rotated object is calculated as in Eq. (4):

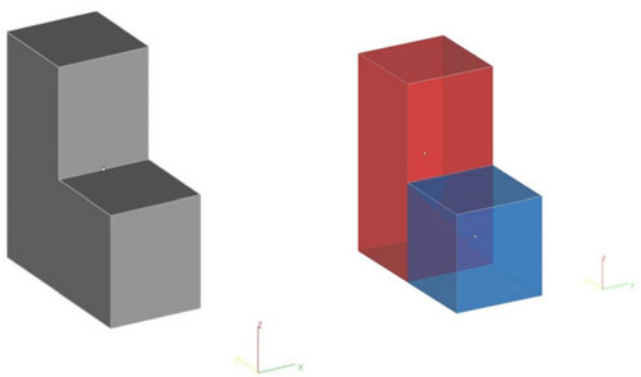

Fig. 6 Segmentation of entire volume of the object into sub-volumes

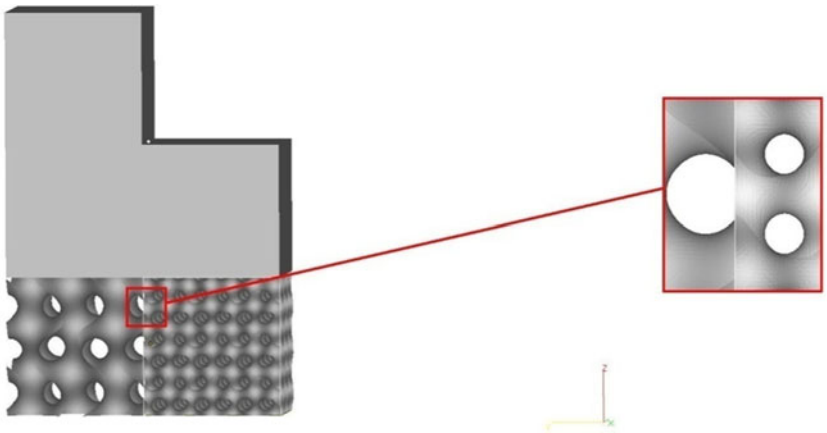

Fig. 7 Discontinuities might appear at the interface between block with different cell size

$$V_r = R_y \cdot R_x \cdot V^T = \begin{bmatrix} \cos(\vartheta_y) & 0 & \sin(\vartheta_y) \\ 0 & 1 & 0 \\ -\sin(\vartheta_x) & 0 & \cos(\vartheta_x) \end{bmatrix} \cdot \begin{bmatrix} 1 & 0 & 0 \\ 0 & \cos(\vartheta_x) & -\sin(\vartheta_x) \\ 0 & \sin(\vartheta_x) & \cos(\vartheta_x) \end{bmatrix} \cdot V^T \quad (4)$$

For each rotated geometry, the facets that need to be supported are selected, in accord with the inclination angle specified initially by a threshold value slop_deg in the preferences.

The support is built for the selected surfaces, and the relative support's volume is calculated and stored. Figure 3 shows some examples of the solid supports generated for "hook.stl" geometry file, at arbitrary chosen orientations, with the threshold value slop_deg set at *85*°. The threshold value of 85° has been chosen arbitrarily, in order the support structure (green colour in Fig. 3) to be emphasised.

The algorithm iteration loop is on until the supports for all the orientations are calculated. Once all the possible orientations are investigated, the orientation that requires minimum support volume is identified, and the relative support volume exported in the form of STL file for eventual visualisation/manipulation.

2.2 Design of supports structures through 3D mathematical functions

A second algorithm described in this paragraph is used for the design of optimal cellular structures, to act as support for AM platforms. The proposed method provides a function to tailor the volume fraction of the support structure to generate more robust support to where needed; thus, it enhances for efficient employment of support structures. Following in Fig. 4, the structure of the algorithm to design-graded support structures is schematically proposed.

The algorithm first starts by importing the STL geometry oriented optimally, as the result of the first stage optimisation. For the example purposes, we illustrate each algorithm step on a simple 3D geometry file, "test.stl".

Figure 5 shows the test.stl geometry in the original orientation (left), and the optimal orientation (right) that minimise the volume of support. For illustration purposes, a choice to fully support all the downward oriented surfaces has been done, by setting the threshold "slop_deg=90°". Also, in the preference settings, a distance from the platform

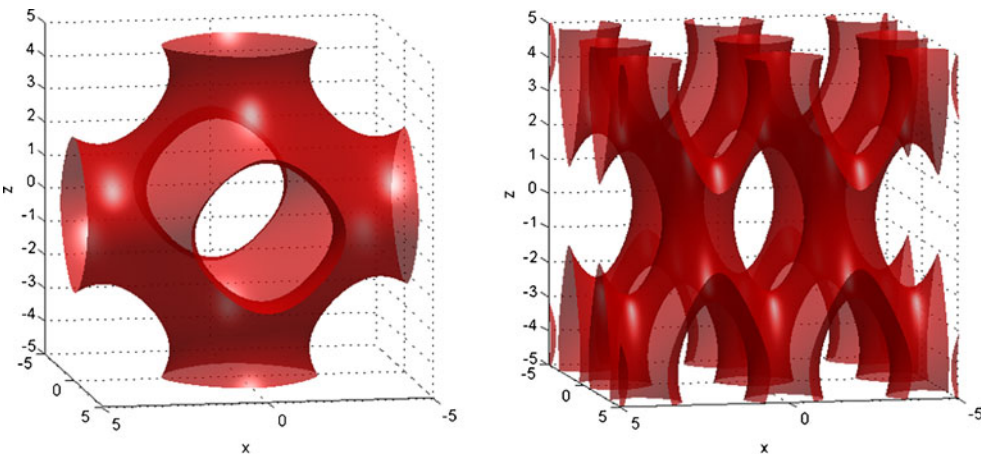

Fig. 8 Schwartz cells with same periodicity in z direction (k_{z1}=k_{z2})

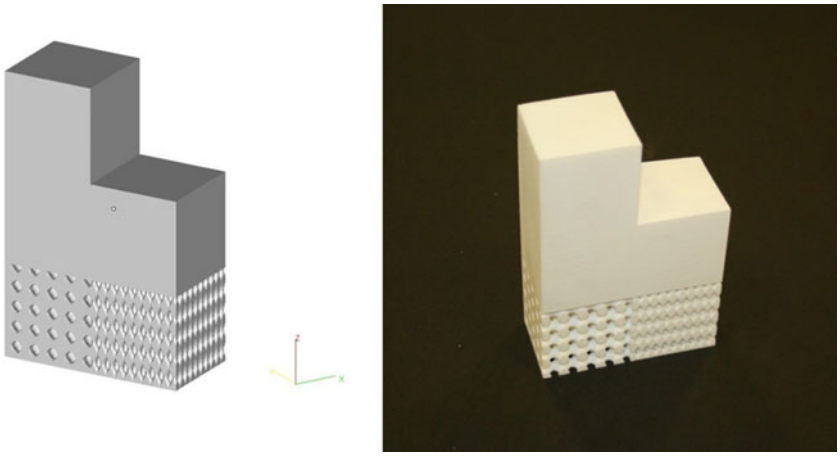

Fig. 9 Final support structure for test.stl geometry (*left*) and manufactured geometry (*right*)

base of the machine has been set to *2 cm*, in order to increase the height of support necessary. The choice of slop_deg and z_base has been done for the purpose of illustrative example. The optimally oriented test.stl geometry and the associated solid support are visible in Fig. 5.

Once the test.stl has been imported, the solid volume is segmented; in Fig. 6, two sub-volumes blocks have been identified, as represented in different colours. For each block, an associated microstructure support is generated through the use of implicit functions, and using cells with different volume fraction. The use of implicit functions in fact allows to specify the volume fraction by simply introducing a variation to the original equations. One possibility is changing the periodicity of the trigonometric terms of the equation, by adding a term *k*. Adding a term *k* is an effective way to change cell periodicity, and it can be employed as method to change the volume fraction of cellular structures. For illustration purposes, we modify the expression of the Schwartz equation as in Eq. (5); however, the cell periodicity of cellular structures defined by other implicit functions can be modified in the same way.

$$\cos(k_x \cdot \mathrm{x}) + \cos(k_y \cdot \mathrm{y}) + \cos(k_z \cdot \mathrm{z}) = 0 \tag{5}$$

It is important to acknowledge that, as changing the cell periodicity will generally affect the cell size, this typically causes that the continuity of the implicit trigonometric function is generally not conserved after having merged the support with different cells size, as clearly observable in Fig. 7. The detail of the support microstructure (in the figure, the red square at the right) highlights a typical discontinuity that can appear at the interface between block with different cell sizes.

However, from the structural point of view, the formation of discontinuities is not expected to represent a serious issue in the specific application of support structures. When a discontinuity appears, since each sub-volume of the object displaces a vertical load which is vertically sustained by the corresponding support block below, there are no transverse load conditions that could yield to stress concentrations such that to degenerate into a structure collapse. In fact, the use of minimal surfaces allows the stress to distribute into the structure homogeneously, due to the absence of cavities or peaks that would locally concentrate the stress otherwise [3]; thus, they present good potentialities to act as support.

In order to limit the number of discontinuities at interfaces between blocks of different cell types, the periodicity along one or more directions can be conserved. For instance, the two different Schwartz cells represented in Fig. 8 have been produced assuming the same periodicity along the *z* direction, fixed at $k_{z1}=k_{z2}=0.75$, and using the values $k_{x1}=0.75$, $k_{x2}=1.5$, and $k_{y1}=0.75$, $k_{y2}=1.5$ for the *x*-, and *y*-axis, respectively.

Figure 9 shows the final support cellular structure for the "Test.stl" part, in its optimal orientation. As noticeable, the support presents a graded volume fraction, given by the combination of the different periodic microstructures; in order to limit surface discontinuities, the periodicity on *z* direction has been conserved, by specifying $k_{z1}=k_{z2}$. The manufactured artefact and its support are shown in Fig. 9. In order to turn the surface model in Fig. 8 into final support structure in Fig. 9,

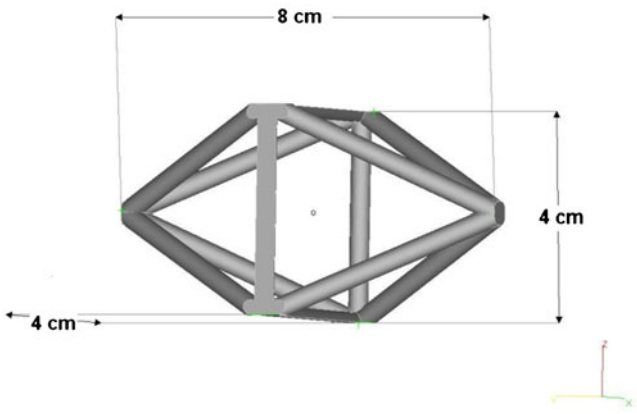

Fig. 10 Truss structure geometry "cell.stl"

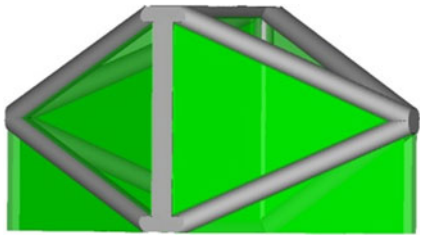

Fig. 11 Solid support for original orientation

the 3D surface is first tessellated, therefore mapped into 3D triangular mesh model; secondly the 3D mesh is exported as ASCII. STL file, so that it is can be processed by any additive manufacturing machine. Figure 9 shows the artefact manufactured, for prototyping purpose, by an EOSINT P 800 Selective Laser Sintering Machine (EOS GmbH 2011).

The STL file containing the support for the entire part is finally exported for eventual visualisation/manipulation. The diagram in Fig. 4 summarises the algorithm routines discussed.

3 Evaluation of a complex shape structure as a case study

A more complex shape geometry showed in Fig. 10 is used as a second case study to evaluate new support structure design and optimisation algorithm. The geometry "cell.stl" represents a cylindrical trusses cell core, typically employed for the production of lightweight aerospace applications. The limits of conventional manufacturing processes for the manufacturing of truss structures have been previously discussed; in this context, it is briefly stated that in manufacturing a complex geometry such as the cell.stl, one would be typically impossible without welding the single trusses, and the welding would produce weak junctions where cracks and corrosion could be facilitated.

In the parameters set for the optimisation, it has been set to support all the downward surfaces inclined less than *35*°, in accord with the actual standards on EOS M270 machine (EOS GmbH 2011). The height between the platform base and the part has been set to zero. The support microstructure has been generated using the Schwartz equation. The solid support for the original orientation generated by the algorithm is shown in green in Fig. 11; the support affects large portion of the object surface because in the original orientation almost all the trusses are horizontal or inclined less than 35°. In Fig. 12, the best orientation (with minimal amount of support needed) is shown at the left, and, for the purpose of comparison, the worst orientation (with maximum amount of support needed) is shown at the right, respectively.

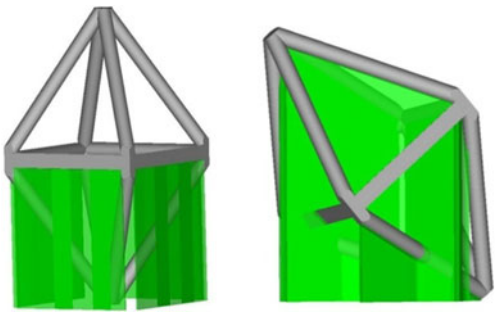

Fig. 12 Best (*left*) and worst (*right*) building orientation for cell.stl geometry

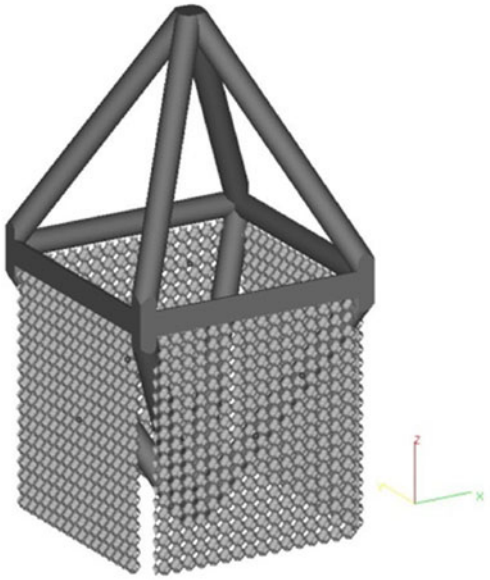

Fig. 13 Final support structure for cell.stl geometry

The final support structure generated for the cell.stl is shown in Fig. 13; unlike for the test.slt case study, the support does not have a graded microstructure. This is because of the part symmetry that makes the weight to distribute with equal intensity on each of the supported trusses.

Table 1 Comparison of material saving for different built orientations

Built orientation	Volume of support (mm^3)	Material saving[a]
Original (θ_x=0°; θ_y=0°)	142.795	–
Best (θ_x=0°; θ_y=90°)	81.059	+43 %
Worst (θ_x=50°; θ_y=10°)	172.723	−21 %

[a] In respect to the original orientation

4 Result and discussion on support structures for a complex structure

The solid support for the original orientation (Fig. 11) affects large portion of the object surface because in such orientation almost all the trusses are horizontal or inclined at less than 35° with respect to the platform bed; thus, they considered requiring support. As consequence of building the geometry with this orientation, large portion of the object surface will be deteriorated because of their contact with the support, and expensive and long-time operations of surface finishing will be required during post-manufacturing stage [2, 8]. Furthermore, the volume of support will require the sintering of large amount of material powder, which has extra costs in itself, and also will increase time and energy for manufacturing process. Furthermore, due to the complex shape of the geometry, the operations of support removal could be difficult, especially without running into a risk of damaging any trusses. Table 1 shows a comparison of material savings for different built orientations; the best orientation shown at the left of Fig. 12 allows to a 45 % saving of support with respect to the original orientation, and to a 55 % saving with respect to the worst orientation. In the optimal orientation, most of the part volume is displaced in a way to support itself; only four trusses need external support structure—this enhances to an easier support removal and also minimises the amount bottom surfaces deteriorated by the contact with the support.

The implicit functions approach for the design of periodical microstructure allowed to easily specify the support structure for the optimally oriented part (Fig. 13). The topology described by the Schwartz equation enhanced a further 50 % material saving with respect to the full dense support shown in Fig. 12 (left). Furthermore, the use of trigonometric functions for the definition of cellular structures might facilitate the stress to distribute into the structure homogeneously, due to the absence of cavities or peaks that would locally concentrate the stress otherwise, thus avoiding support structure collapse.

5 Conclusions

This study has presented a new approach to the design and optimisation of support structures in additive manufacturing platforms such as SLM. This optimisation provides functions to minimising support structures through both the definition of an optimal part built orientation and the definition of optimally graded cellular structures. A Matlab algorithm that performs a two-step optimisation has been developed; firstly, the part orientation that requires the minimum support has been located among all the possible orientations; secondly, the cellular support structures for the optimal orientation is generated, through pure mathematical 3D implicit functions. The implicit function approach for cellular support design is found to be very versatile because it allows geometries to be simply defined by mathematical expressions. Optimisation evaluation results on a truss part with complex shape geometry demonstrated that significant materials saving, for instance up to 45 % for this case, can be achieved by an optimal part positioning, and further reductions can be obtained by designing cellular structures defined by implicit mathematical functions. This newly developed design and optimisation approach of cellular support structures exhibit great potential to achieve higher efficiency of the SLM process and consequently deliver time, material and energy savings.

Acknowledgments The authors would like to thank Great Western Research and EADS Innovation Works UK for funding support.

References

1. Allen S, Dutta D (1995) Determination and evaluation of support structures in layered manufacturing. J Des Manuf 5:153–162
2. Frank D, Fadel G (1995) Expert system-based selection of the preferred direction of build for rapid prototyping processes. J Intell Manuf 6(5):339–345
3. Gabrielli, R. (2009). Foam geometry and structural design of porous material. Mechanical Engineering. Thesis (Doctor of Philosophy (PhD)). University of Bath
4. Goldstein H, Poole, CP, Safko, JL (2002) Classical mechanics, 3rd edition. Addison Wesley, ISBN 978-0-201-65702-9
5. Hao L, Raymond D et al (2011) Design and additive manufacturing of cellular lattice structures. The International Conference on Advanced Research in Virtual and Rapid Prototyping (VRAP). Taylor & Francis Group, Leiria, pp 249–254
6. Materialise, N. from www.materialise.com, Materialise develops 3D software for the medical, dental and additive manufacturing industries
7. Pasko A, Vilbrandt T et al (2010) Procedural function-based spatial microstructures. Shape Modeling International Conference (SMI), 2010
8. Pham DT, Demov SS (2001) Rapid manufacturing: the technologies and applications of rapid prototyping and rapid tooling. Springer, London
9. Putte BS, Bornem JP et al (1997) Method for supporting an object made by means of stereolithography or another rapid prototype production method. Materialise, Belgium
10. Schoen AH (1970) Infinite periodic minimal surfaces without self-intersection. National Aeronautics and Space Administration, Cambridge
11. Schwarz HA (1890) Gesammelte Mathematische Abhandlungen. Berlin, Springer (Reprinted by Chelsea Publishing Company, 1972, 1890)
12. Starly B (2006) Biomimetic design and fabrication of tissue engineered scaffolds using computer aided tissue engineering. Department of mechanical engineering and mechanics, Drexel University
13. Swaelens B et al (1995) Support generation for rapid prototyping. Sixth International Conference on Rapid Prototyping, University of Dayton
14. Wang H, Chen Y et al (2005) A hybrid geometric modeling method for large scale conformal cellular structures. ASME Conference Proceedings

Innovative Developments in Virtual and Physical Prototyping – Bártolo et al. (eds)
© 2012 Taylor & Francis Group, London, ISBN 978-0-415-68418-7

Surface roughness analysis in Selective Laser Melting

G. Strano, L. Hao, R.M. Everson & K.E. Evans
College of Engineering, Mathematics and Physical Sciences, University of Exeter, Devon, EX4 4QF, United Kingdom

ABSTRACT: Selective Laser Melting (SLM) is an increasingly employed additive manufacturing (AM) system in the production of medical, aerospace, and automotive parts. Despite progress in material flexibility and mechanical performance, relatively poor surface finish still presents a major limitation in SLM. This study analyses the effect of the stair step and particle bonding effect, to the surface roughness of SLM processed parts, at different orientations. Surface characterisation conducted for the surfaces at different inclination angles by surface profilometer and scanning electron microscope (SEM) revealed that the presence of partially-bonded particles on the top surfaces might affect the surface roughness significantly when the layer thickness is comparable to particle size. Classic models for roughness prediction, based on pure geometrical consideration of the stair step profile, fail to describe the trend of the experimental data observed. The paper presents key contribution factors influencing surface morphology and set the basis of a theoretical model for roughness prediction.

1 INTRODUCTION

1.1 *SLM and surface quality*

Selective Laser Melting (SLM) is an emerging additive manufacturing system for the production of end use parts with complex shape, for medical, aerospace, automotive applications. Its diffusion in recent years has been permitted by an increasing availability of processing materials and mechanical performance of the resulting SLM parts (Levy et al. 2003). The SLM process enables the direct melting of powders of a number of metals, such as Titanium, Steel, Chrome Cobalt, Aluminium alloys, and building of net-shape parts through a "layer by layer" approach; for each layer a scanning laser beam supplies the energy to locally melt a layer of deposited metal powder and fuse it onto previously melted layer.SLM still faces an apparent limitation in terms of surface quality if compared to some alternative metal manufacturing processes such as machining process. Surface quality is greatly influenced by the "stair step" effect, which is a stepped approximation of the edges of curve and inclined surfaces.

1.2 *Theoretical models based on geometrical considerations*

In the past a number of studies have been conducted to predict the surface roughness of parts processed through different AM platforms.a theoretical model was presented to predict the surface roughness for Stereolithography (SLA) parts by introducing two different expressions to predict the roughness of upward and downward-facing surfaces considering the layer thickness, surface angle and layer profile (Reeves & Cobb 1997). Campbell (Campbell et al., 2002) presented a comparison between theoretical roughness obtained from a trigonometrically derived equation, on the stair step profile, and empirical roughness measured on several different AM platforms. Luis Perez (Perez et al., 2001) proposed a geometrical roughness model to predict the average surface roughness of AM parts.

All the previous models based the prediction of surface roughness on the geometrical description of the stair-stepped profile of sloped surfaces. Such models could fail to accurately predict the surface roughness of AM parts, because surface roughness might be influenced also by other process parameters as shown in (Bacchewar et al., 2007). An alternative approach to roughness prediction has been used in (Ahn et al., 2009); the model interpolated data from empirical observations of test samples; theoretical and real distributions were compared through the fabrication of test parts manufactured by SLA. Strano (Strano et al., in press) developed a model for the prediction of roughness of parts manufactured by SLS, based on a phenomenological approach. Experimental roughness data were collected and interpolated for a range of deposition orientations, and a model for the evaluation of roughness objective part was formulated.

This study analyses the effect of the stair step and balling effect, to the surface roughness of SLM processed parts, at different orientations.A comparison between the measured roughness and the roughness predicted through classic models,based on pure geometrical consideration of the stair step profile, is investigated.

2 EXPERIMENTAL PROCEDURE

2.1 *Surface roughness*

The surface roughness, according to ISO 4287 standards (ISO 1997), is defined as the average deviations of the roughness profile from the mean line (Figure 1). Considering the surface profile of length L, the definition of surface roughness R_a is set in following Equation:

$$R_a = \frac{1}{L}\int_0^L |y(x)|dx \tag{1}$$

Supposed to have N values of measured surface roughness on the surface profile, $y_1, y_2, \ldots y_N$, the surface roughness is numerically calculated as:

$$R_a = \frac{1}{N}\sum_{i=1}^{N} |y_i| \tag{2}$$

The definition of surface roughness can be extended to a 2D surface profile of area A (Figure 1), is the average deviations of the roughness profile from the mean plane obtained through levelling of the mean square plane of the measured surface.

$$R_a = \frac{1}{A}\iint_A |z(x,y)|dxdy \tag{3}$$

Suppose to have NxM values of measured surface roughness on the surface profile, $y_1, y_2, \ldots y_{NxM}$, the surface roughness of a 2D surface profile is numerically calculated as:

$$R_a = \frac{1}{N \cdot M}\sum_{i=1}^{N}\sum_{j=1}^{M} |y_{i,j}| \tag{4}$$

Following is presented an analysis of the contributions, namely stair step and balling effect, to the surface roughness of SLM processed parts, at different orientations. For this purpose surface characterisation on manufactured samples was conducted at different inclination angles by surface profilometer and scanning electron microscope (SEM).

2.2 *Equipment and sample fabrication*

In order to characterise the actual surface roughness distribution of SLM processed part, a sample with the "truncheon" geometry (Figure 2) has been fabricated, using Steel 316L alloy. The sample was designed to measure roughness of all the angles in the range from 0° to 90° by a 5° step. The sample was fabricated through a EOS M270 machine; the process parameters were, layer thickness 20 micrometers, hatch spacing 100 micrometers, beam scan speed 900 mm/s, beam spot diameter 100 micrometers and laser power 195 W.

The analysis of sample surface was first carried out using a surface profilometer (Talyscan 150, Taylor Hobson Ltd). For each inclination, surface roughness was collected through stylus gauge on a surface of 10 mm × 1 mm, with a scanning spacing fixed at 5 μm and scanning speed at 2500 μm/s. Measurements on bottom surfaces were taken only for surface without support (range from 45° to 90° sloping angle). Secondly, to further investigate the surface morphology at microscopic scale, the sample was treated using isopropanol and surface analysis was carried out using a SEM (S-3200N, Hitachi).

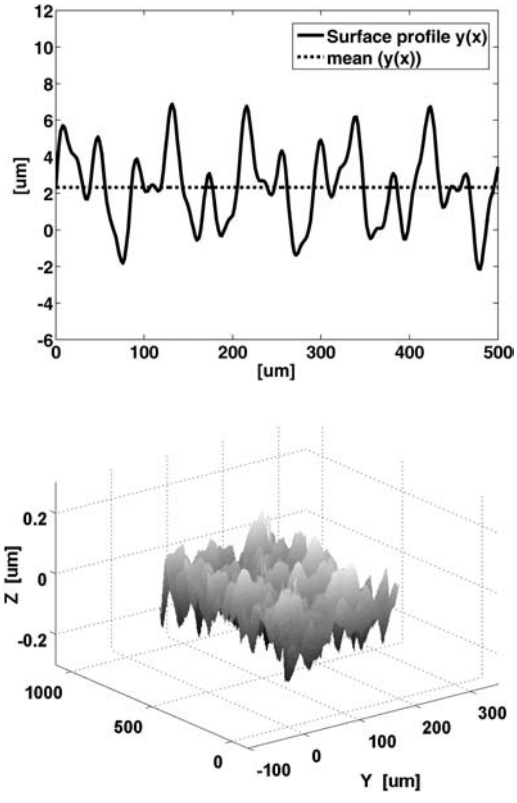

Figure 1. Representation of 1D (top) and 2D (bottom) surface profiles.

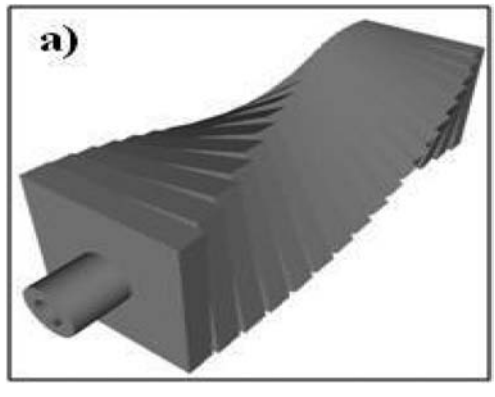

Figure 2. Sample geometry.

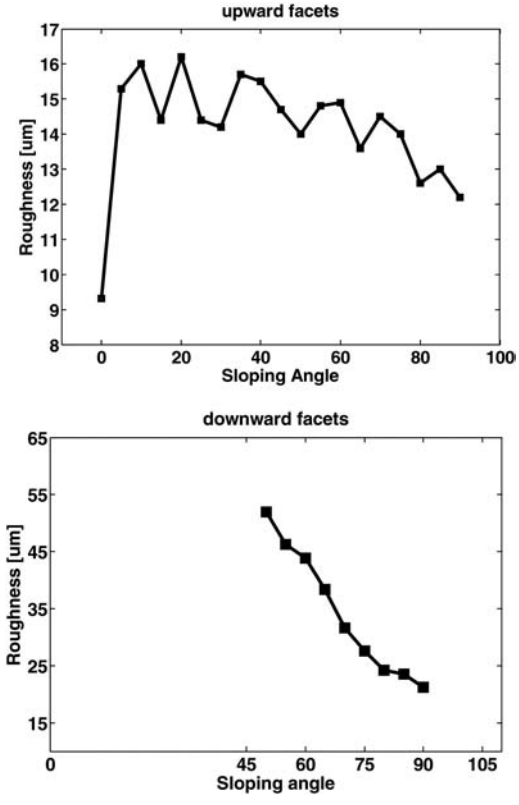

Figure 3. Experimental roughness in SLM process at different sloping angle; upward-facing (top), and downward-facing (bottom) oriented data.

3 ANALISYS OF SURFACE MORPHOLOGY

3.1 *Effects of sloping angle on surface roughness*

Roughness measured on downward oriented surfaces was (Figure 3, bottom) observed to have higher values of surface roughness if compared to top surfaces (Figure 3, top). A similar trend was observed in (Vandenbroucke & Kruth 2007) and it can be explained by the presence of stalactites formed during the solidification due to gravity.

As expected roughness of upward oriented surfaces presents a minimum value at 0° (flat surface); that is mainly caused by the rippling effect due to scan tracks, which occur on top surfaces. As the inclination angle increases from 0°, higher surface roughness has resulted from the introduced stair-step effect. In a prospective of surface roughness minimisation, it is important to notice that roughness of flat surfaces is possible to be eventually reduced through surface remelting process (Kruth et al., 2010). Nevertheless, as the surfaces are inclined, the laser remeltingon the top of the inclined surface is not possible, due to the SLM process limitation to sinter material only horizontally, hence the importance of a prediction of surface roughness of parts' surfaces inclined at certain angle.

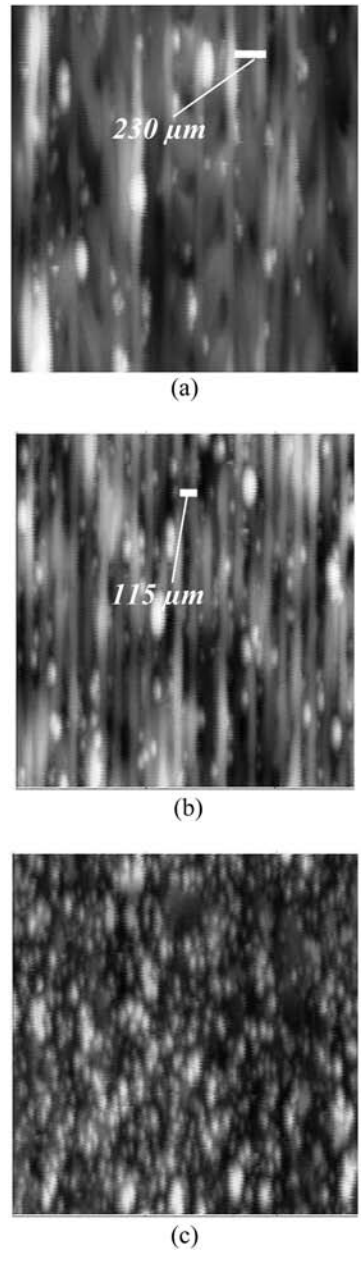

Figure 4. Surface profiles of a) 5° sloped surface, b) Profile of 10° sloped surface, c) 65° sloped surface

The trend of measured roughness is mainly constant in the range of 5°–45°, and presents a slight decrease in the range 50°–90°. A further investigation of the upward surfaces reveals the presence of patterns with vertically aligned reliefs for surfaces at low sloping angle. Figure 4a shows a number of surface profiles at different inclinations of 5°, 10° (white lines in Figure 4a, Figure 4b) and 65°. In each pattern, vertical lines occur regularly at distance equal to the distance between step edges, which is determined by the stair step between consecutive layers.

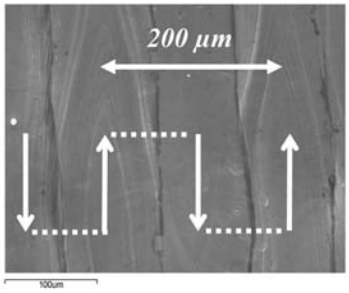

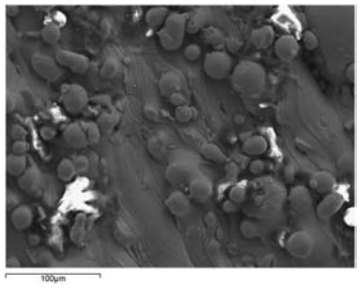

Figure 5. SEM picture of flat surface (Top); presence of particles on 90° sloped surface (Bottom).

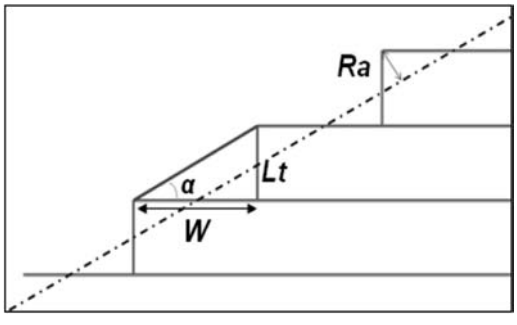

Figure 6. Schematic representation of sliced profile.

At higher sloping angles (65°), no vertical lines pattern war observed; surface was characterised by the presence of high peaks (Figure 4c). In order tocharacterize the surface morphology at higher sloping angles, and to investigate the contribution of other effects to surface roughness, a surface morphology analysis was carried out by SEM.

At the top of Figure 5 it is shown the profile of flat surface, normal to the build direction. When flat surfaces are sintered, there is not presence of spare unsintered particles on the top of the surface; this is because the low layer thickness (20 μm) and the high power (195 W) supplied by the laser beam, fully melt the powders and fused them into a relatively smooth and uniform layer. The effects of scan direction and strategy (highlighted by the spotted arrows) are visible in the figure; for each scan line it is noticeable cusp tracks oriented in the sense of the moving laser beam. The distance between cusps with same orientation is of about 200 μm, as results of the chosen hatch spacing (100 μm) and laser beam diameter (100 μm). At the bottom of Figure 5, it is shown the profile of 90° inclined surface. It confirms an high number of spare and grouped particles is present on the surface; particles can be considered the main cause of surface roughness at 90°, since no stair step effect occur, when layer consecutively overlapped(however a minor residual roughness might be expected, because of the limits on the repeatability of the process accuracy to a perfectly matching overlap between layers).

4 DISCUSSION

4.1 *Comparison between measured and theoretical roughness*

SLM processes start with a CAD model of the object that has to be built; slicing the geometry involves a level of approximation, described by the "stair step" effect (6). The surface roughness R_a for the inclined surface represented schematically in Figure 6, can be defined as:

$$R_a = \frac{1}{L}\int_0^L |y(x)|dx = \frac{1}{4}L_t\cos(\alpha) \quad (5)$$

with L_t layer thickness and α surface sloping angle. From Equation (5) is evident that, an improved surface finish it is expected through either the choice of low layer thickness or through increasing the surface inclination angle, according with the cosine term. The prediction of surface roughness expressed in Equation (5), has been formulated considering only the effect of the stair steps on inclined surfaces. Previous models in literature present similar expressions, deriving the expression of the surface roughness from trigonometrical considerations on the stair step profile; nevertheless, often these model were able to predict roughness for a partial range of surface inclinations with respect to the build directions (Campbell et al., 2002), (Luis Pérez et al., 2001). Following is proposed a comparison between our experimental data collected on SLM platform, and the theoretical roughness predicted considering only the stair-step effect.

The comparison shows a mismatching for almost the entire range of inclination angles; in particular, experimental roughness does not decrease as much as expected by the cosine function.When surfaces are low inclined (in the range of 5°–15°), the width of each step (228 μm–74 μm) is bigger than the average diameter of the particle (20 μm), therefore the surface conserves the characteristic of a "zig-zag" profile, due to the stair-step,and roughnesscan be well predicted by Equation (5). As the surface become more sloped, the width of each step get smaller, and it is comparable with the particle size; therefore the presence of spare particles influences the surface profile. As example, we can observe the roughness at very high sloping angles; at 90° the roughness due to the stair step effect is expected to be null, according to cosine term of Equation (5). It might expect that the predicted zero

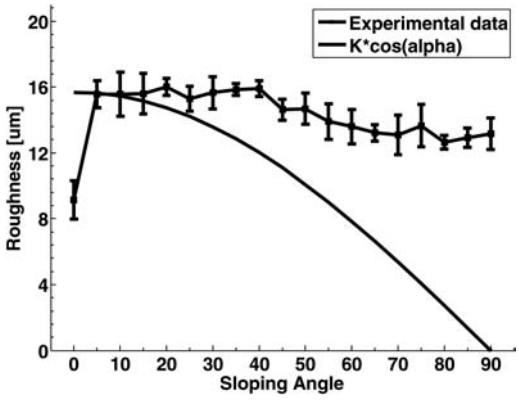

Figure 7. Comparison of experimental roughness, and roughness predicted considering only the stair-step effect.

roughness well interpreters the situation when layers are overlapped on the top of each other. In reality, the measured roughness presents is much higher (14 μm), caused by presence of particle on the surface.

5 CONCLUSIONS

An investigation of surface roughness and morphology has been conducted for Steel 316L alloy part made by Selective Laser Melting (SLM). In order to characterise the actual surfaces at different sloping angles, a truncheon sample has been produced and an analysis has been conducted at different scales, by surface profilometer and scanning electron microscope. Roughness measured by profilometer was different from the one predicted through the classic model based on pure geometrical consideration on the stair step profile due to the presence of spare particles on the surface. When layer thickness size is comparable to particle diameter, partially-bonded particles present at top surface, can fill the gaps between consecutive layers, thus affecting the actual surface roughness. This has been particularly evident at surface sloped at 90°; although minimum roughness would be predicted by classic models, experimental observations showed an high concentration of particles which justify the high roughness measured at that sloping angle.

REFERENCES

Ahn D., Kim H., & Lee S., 2009. Surface roughness prediction using measured data and interpolation in layered manufacturing. *Journal of Materials Processing Technology* 209(2): 664–671.

Bacchewar P. B., Singhal S. K., & Pandey P. M., 2007. Statistical modelling and optimization of surface roughness in the selective laser sintering process. *Proceedings of the Institution of Mechanical Engineers, Part B: Journal of Engineering Manufacture* 221(1): 35–52.

Campbell, R. I., Martorelli M., & Lee H. S., 2002. Surface roughness visualisation for rapid prototyping models. *Computer-Aided Design* 34(10): 717–725.

ISO 1997. 4287, Geometrical product specifications (GPS), Surface texture: profile method – terms, definitions and surface texture parameters.

Kruth, J. P., Badrossamay M., Yasa E., Deckers J., Thijs L. & Van Humbeeck J., 2010. Part and material properties in selective laser melting of metals. *16th International Symposium on Electromachining (ISEM XVI)*. Shanghai, China.

Levy G., Schindel R., & Kruth J. P., 2003. Rapid Manufacturing and Rapid Tooling with Layer Manufacturing (LM) Technologies, State of the Art and Future Perspectives. *CIRP Annals-Manufacturing Technology* 52(2): 589–609.

Luis Pérez C. J., Calvet J. V. & Pérez M. A. S., 2001. Geometric roughness analysis in solid free-form manufacturing processes. *Journal of Materials Processing Technology* 119(1–3): 52–57.

Reeves, P. E. & Cobb R. C. 1997. Reducing the surface deviation of Stereolithography using in-process techniques. *Rapid Prototyping Journal* 3 (1): 20–31.

Strano G., Hao L., Everson R.M. & Evans, K., 2011. Multi-Objective Optimisation of Selective Laser Sintering Processes for Surface Quality and Energy Saving, *Proceedings of the Institution of Mechanical Engineers, Part B: Journal of Engineering Manufacture*, in press.

Vandenbroucke, B. & J. P. Kruth 2007. Selective laser melting of biocompatible metals for rapid manufacturing of medical parts. *Rapid Prototyping Journal* 13(4): 196–302.

Multi-objective optimization of selective laser sintering processes for surface quality and energy saving

G Strano, L Hao, R M Everson and K E Evans

Proceedings of the Institution of Mechanical Engineers, Part B: Journal of Engineering Manufacture published online 8 August 2011
DOI: 10.1177/0954405411402925

Multi-objective optimization of selective laser sintering processes for surface quality and energy saving

G Strano*, **L Hao, R M Everson,** and **K E Evans**
College of Engineering, Mathematics and Physical Sciences, University of Exeter,
Devon, UK

The manuscript was received on 27 September 2010 and was accepted after revision for publication on 15 February 2011.

DOI: 10.1177/0954405411402925

Abstract: Selective laser sintering (SLS) is one of the most widely used additive manufacturing technologies and represents a valuable manufacturing process in the aerospace, automotive, and medical industries. Owing to the preheating requirement for the SLS of polymer materials, one of the main challenges is to reduce the energy required for the part-building process and at the same time maintain the surface quality of the parts, represented by surface roughness, as this has aesthetic and functional importance for industrial applications. These objectives are competing criteria and are significantly influenced by the build orientation of the parts in the SLS process. This study investigates a computational methodology for the simultaneous minimization of surface roughness and energy consumption in the SLS process, to locate the optimal trade-off set between these objectives, known as the Pareto set; thus, it provides a consistent decision support system for the identification of optimal build orientations for SLS.

Keywords: multi-objective optimization, additive manufacturing, part deposition orientation, surface roughness, manufacturing process efficiency

1 INTRODUCTION

Selective laser sintering (SLS) is nowadays one of the most mature additive manufacturing (AM) processes which can construct complex three-dimensional (3D) objects layer by layer with minimal material waste and tooling utilization. In recent years continuous technical and process control improvements [**1**, **2**] have allowed SLS to be utilized for the manufacture of end-use parts, in particular with robust plastics such as Nylon 12.

The surface finish of SLS parts is one of the major requirements for functional end-use components; surface finish considerably affects the amount of time spent on polishing and post-manufacturing operations of any SLS processed part, especially for parts subjected to fluid flows such as air ducts, which are used in the aerospace industry. Although thinner layer thicknesses can be used to reduce the 'stair stepping' effect and improve surface finish, this strategy drastically increases the number of layers and, consequently, the time for material layering and preheating, resulting in high manufacturing cost and energy consumption. Surface roughness is greatly influenced by the part build orientation [**3**], as the 'stair stepping' effect depends on the surface inclination. Part build orientation also affects the amount of energy needed for manufacturing; during the SLS process, as is well known, a number of preheating operations are required before the layer is sintered by laser, in order to minimize the amount of laser energy required for powder sintering, which thus minimizes warping of the sintered layers. The amount of energy used for powder preheating is proportional to the number of sintered layers, and hence is directly influenced by the build orientation of the part.

This study investigates a computational methodology, based on multi-objective optimization, for the simultaneous minimization of surface roughness and energy consumption in the SLS process, thus

**Corresponding author: College of Engineering, Mathematics and Physical Sciences, University of Exeter, Devon, EX4 4QF, UK.*
email: g.strano@exeter.ac.uk

providing a decision support system for the identification of optimal build orientations as a 'trade-off' between these two objectives. Multi-objective optimization problems can be found in various applications, financial problems, product and process design, automotive and aircraft design, and more generally in the presence of trade-offs between two or more conflicting objectives such as maximization of profit or performances and minimization of costs. In multi-objective problems the goal is to locate the optimal trade-off curve or surface between objectives, which is known as the Pareto set (see, for example, reference [**4**]). This set comprises the optimal 'non-dominated' solutions, which have the property that, in moving from one solution to another, it is not possible to improve one criterion without making at least one of the other criteria worse. There have been a number of applications of multi-objective optimization for additive manufacturing technologies.

Lan *et al.* [**5**] determined part deposition orientation for stereolithography (SL) parts based on surface quality, build time, or complexity of support structures. Surface quality was evaluated by maximizing the total area of perpendicular and horizontal faces, in order to minimize stair stepping. Aesthetically important faces were also considered by maximizing the sum of upward-facing surfaces and vertical faces, as they do not require the presence of any support structures that deteriorate their quality. In SL, like other additive layer platforms, there is a long non-productive time spent for the material deposition on each layer, considerably longer than the time for sintering. Lan *et al.* [**5**] considered uniform slicing of the part, and showed that the height of the part and the build time were affected by the deposition orientation. For each part inclination, support structures were then optimized by minimizing the number of supported points along the length of the hanging profile. Alexander *et al.* [**6**] proposed a study for optimal orientation to achieve better part accuracy and lower cost. Stair step effect was measured in terms of cusp height. The cusp height was calculated by geometrical consideration of the sliced profile of the part and was defined as the maximum normal distance between the triangular facet of the computer-aided design (CAD) model and the deposited part considering a uniform slice deposition.

The model for cost prediction has been generically developed for any layer manufacturing (LM) platforms and takes into account the prebuild, build, and post-processing costs. Cheng *et al.* [**7**] presented a multi-objective approach for determining an optimal part building orientation for SL. The two objectives, namely part accuracy and build time, were combined in a weighted sum for optimization. Part accuracy was calculated using different weight factors for different types of surface geometries and, based on their experience, they considered various contributions of fabrication errors, such as slicing effects, tessellation, distortion, stair stepping, etc. Minimization of build time was achieved by reducing the number of slices. More recently, Singhal *et al.* [**8**] have applied multi-objective optimization to optimize simultaneously average surface roughness, build time, and support structure of parts for SL and SLS processes. In their study the multicriteria optimization problem was solved by minimizing the weighted sum of the three different objectives, using a conventional optimization algorithm based on a trust region method [**9**] to find an optimum.

All of the cited works employ a weighted-sum of several objectives approach, without considering their minimization simultaneously. From the point of view of multi-objective optimization, although the conversion of a multi-objective functional into a scalar optimization by a combination of the different objectives has been very popular in the past, as Das and Dennis [**10**] show, this method only finds a single solution on the Pareto set for a particular weighting of the objectives. Varying the weighting obtains solutions across the entire Pareto set only when the set is convex, and even for convex sets, an evenly distributed set of weights fails to produce an even distribution of solutions from all parts of the Pareto set. To overcome these limitations, multi-objective optimization for problems with many objectives can be solved by one of the recently developed evolutionary algorithms; see reference [**4**] for a review. One evolutionary algorithm for multi-objective optimization called NSGA-II (non-dominated sorting algorithm) was used by Pandey *et al.* [**11**] for the optimization of fused deposition modelling (FDM) fabricated parts in order to find the Pareto trade-off between average surface roughness and build time. A tessellated CAD data file was used as input. An analytical expression based on geometrical observation of the stair stepping effect was used to formulate the surface roughness model; the build time and other non-productive times typical of FDM technology (such as lowering the platform after deposition of each layer) were based on a model previously developed by Alexander *et al.* [**6**].

A crucial point necessary to achieve high surface quality for the manufactured part is a mathematical model to predict accurately the surface roughness. Reeves and Cobb [**12**] presented a model to predict the surface roughness for SLA parts by introducing

two different expressions to predict the roughness of upward- and downward-facing surfaces considering the layer thickness, surface angle, and layer profile. All the models cited above predict surface roughness based upon geometrical considerations. However, such models have been shown able to predict roughness only for a partial range of surface inclinations with respect to the build directions [**13**]. Furthermore, as shown by Bacchewar *et al.* [**3**], for a given inclination, the average surface roughness on the downward-facing surface is lower than the average surface roughness on the upward-facing surfaces, mainly due to the filleting effect observed on downward-facing surfaces processed by SLS [**3**]. More recently, Ahn *et al.* [**14**] have presented an alternative phenomenological model which interpolates data from empirical observations of test samples; and the theoretical and real distributions were compared through the fabrication of test parts manufactured by SL.

One of the features of the current study is to extend the approach introduced by Ahn *et al.* [**14**] to the prediction of surface roughness to be manufactured by SLS; experimental surface roughness data were collected and interpolated for a range of deposition orientations in order to predict the overall part roughness. Furthermore, in section 2, a model for energy prediction of SLS processed parts is developed, which takes into consideration both the contribution of the energy required by the preheating operations and the energy required by the laser sintering. Section 3 discusses the implementation of the algorithm for multi-objective optimization and the computational advantages over an implementation using a genetic algorithm (GA). Results discussed in section 4 show the complete set of Pareto solutions which define the set of best compromises between the two objectives, thus permitting the operator to select the best trade-off between final surface roughness and energy consumption.

2 EXPERIMENTS AND METHODOLOGY

2.1 Surface roughness measurement for SLS process

The 'stair stepping' effect is responsible for the geometric layer-by-layer gaps between the CAD model and the fabricated part. This is particularly noticeable on inclined surfaces, as it gradually changes as the inclined surface angle increases, and therefore it is significantly influenced by the part build orientation. In a previous study carried by Bacchewar *et al.* [**3**], the part build orientation was found to play a more significant effect than the layer thickness in the average surface roughness of the part.

In order to characterize the actual surface roughness distribution of a SLS processed part, a 'truncheon' test part, shown in Fig. 1, has been fabricated. This geometry was used in previous work by Reeves and Cobb [**12**] because it allows the surface roughness for each inclination angle to be easily measured. The truncheon has been designed to measure roughness, defined as the mean absolute deviation from the average surface height, at all angles in the range from 0° to 90° by 5° steps, for both the upward- and downward-facing surfaces. The truncheon sample was made from Duraform polyamide material sintered by a SLS Sinterstation® 2000 platform (manufactured by DTM Corporation). The SLS process parameters were: layer thickness fixed at 0.1 mm; the hatch spacing at 0.15 mm; the beam scan speed at 12.50 mm/s; and the laser power at 4 W. Surface roughness measurements on the sample were carried out using a surface profilometer Talyscan 150 system (manufactured by Taylor Hobson Ltd). For each inclination, surface roughness of the sample was collected on a surface of 10 mm × 2 mm, with a scanning spacing fixed at 5 μm and scanning speed at 2500 μm/s.

The experimental data sample in Fig. 2 shows a trend similar to the data introduced by Bacchewar *et al.* on a similar geometry [**3**]; upward-facing

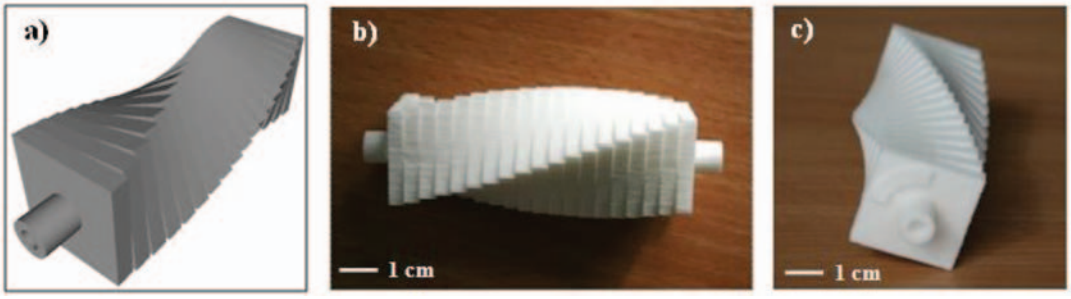

Fig. 1 Truncheon sample: (a) CAD model; (b) and (c) manufactured sample

surfaces present the highest values of surface roughness in the range of angle between 60° and 85°, where peak values are up to three times higher than those in the range 0° to 60°. Smaller peaks can be observed in the experimental measures of downward-facing surfaces; these can be the result of the 'filleting effect' that affects the downward-oriented surfaces during the laser sintering of polymer powder. The filleting effect is the result of gravity and surface tension forces on the molten pool during the sintering process; on downward-oriented surfaces the molten polymer tends to drop down owing to the action of gravity, thus filling the gaps between layers sintered consecutively and providing a 'compensation' to the stair stepping effect before solidifying. Figure 3(a) schematically shows this effect.

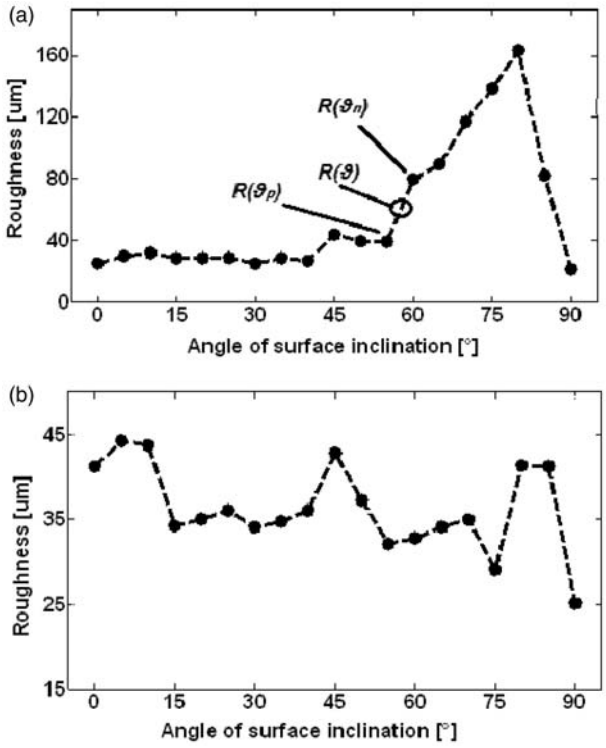

Fig. 2 Interpolation of (a) upward-facing and (b) downward-facing oriented data

Nevertheless, at higher layer thickness, the filleting effect was observed not to be significant in improving the surface finish [**3**]; this is because, for high layer thickness, gravity is not sufficient to produce complete filleting as a result of the counteracting effect of surface tension, which inhibits the spread of molten polymer, as represented in Fig. 3(b). On upward-oriented surfaces the filleting effect is observed not to be geometrically influent on surface profiles [**3**]. This is because of the absence of the action of gravity, although surface tension may slightly reduce the roughness by smoothing the sharp stair-step corners (see Fig. 3(c)).

2.2 Surface roughness prediction

Although different values could be expected depending upon the scan direction, the surface roughness has been observed to be independent of the measured direction [**15**]. This assumption has been experimentally confirmed by the present authors. Consequently, for each facet it can be assumed that the roughness function depends upon θ, the angle between the fabrication direction $\boldsymbol{z} = (0,0,1)$, and the vector normal to the surface facet $\boldsymbol{n}$ as shown in Fig. 4.

If the surface geometry is defined by K facets, the roughness value $R_i(\theta)$ ($i = 1, 2, \ldots, K$) for the ith facet, at any surface angle θ, can be calculated by interpolating the measured roughness function as follows

$$R_i(\theta) = R(\theta_\mathrm{p}) + \frac{R(\theta_\mathrm{n}) - R(\theta_\mathrm{p})}{\theta_\mathrm{n} - \theta_\mathrm{p}}(\theta - \theta_\mathrm{p}) \tag{1}$$

where $R(\theta_\mathrm{p})$ and $R(\theta_\mathrm{n})$ are the measured roughness values at the sample angles adjacent to θ; see Fig. 2.

The roughness objective is defined as the average roughness of the surface facets weighted by the facet area, A_i

$$R_\mathrm{a} = \frac{\sum_{i=1}^{K} R(\theta_i) A_i}{\sum_{i=1}^{K} A_i} \tag{2}$$

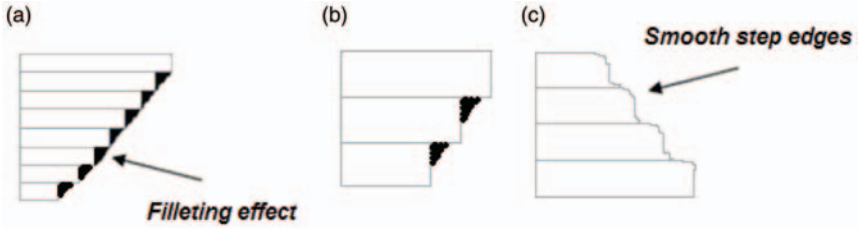

Fig. 3 Filleting effect caused by flow of molten polymer for (a) downwards-oriented facets, (b) the same but inhibited by surface tension to only partially smooth, thick layers. For (c) upward-facing facets, filleting is minimized although surface tension may smoothe sharp corners

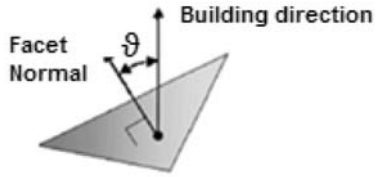

Fig. 4 Angle between the building direction and STL file facet normal vectors

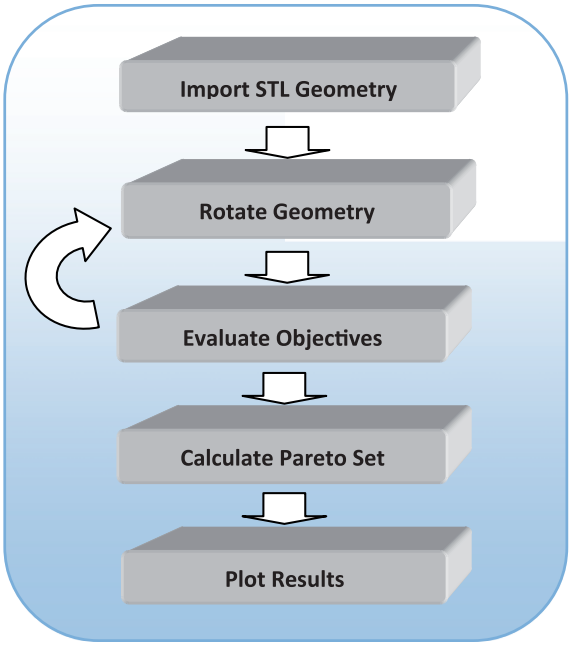

Fig. 5 Principal algorithm routines flowchart for surface roughness and energy prediction

2.3 Model for energy prediction

The energy employed in the manufacturing process influences the overall cost of SLS parts [**16**]. As is known, the SLS process involves a moving laser beam irradiating a polymer powder to sinter the individual powder particles. Before the sintering process, layer by layer, an amount of energy is employed to preheat the deposited powder, in order to reach a temperature just below the melt temperature (for Nylon 12, this is typically 178 °C). The laser power provides the energy to heat the powder locally, until the polymer reaches the liquid phase. After the laser scan is over the pool solidifies, thereby sintering powder particles to the previous layer of material. The proposed energy prediction model takes into consideration both the contributions of energy E_h required by the preheating operations and energy E_s required by the laser sintering of the part.

The volume of the powder spread out during the preheating operations V_p, is determined by the height of the object to be sintered; hence it is defined by the build orientation chosen. The term V_p can therefore be expressed as $V_p(\theta_x, \theta_y)$, a function of the orientation angles θ_x and θ_y around the X and Y axes respectively. Considering C_p the specific heat capacity (which for Nylon 12 = 1640 kJ/kg), l the latent heat of fusion (for Nylon 12 = 120 kJ/kg), ρ the green density of the powder (for Nylon 12 = 590 kg/m^3), and V_p the volume of the total preheated powders, the energy required for preheating operations can be calculated by the following expression

$$E_h(\theta_x, \theta_y) = (C_p\ \Delta T + l)\ \rho\ V_p(\theta_x, \theta_y) \tag{3}$$

where ΔT is the difference between the temperature of 178 °C (melting point of Nylon 12) and the environmental temperature; ΔT is modelled as being constant. The applied energy for part sintering E_s presented in equation (4) can be calculated from the model developed by Gibson and Shi [**16**] for the applied energy density. If P represents the power available from the laser beam at the powder bed surface; S_s the scan spacing, distance between two adjacent parallel scan vectors; B_S the scan beam speed; A_a the area of each slice; and N the total number of layers, then the energy E_s for the entire part is given by

$$E_s = \sum_{i=1}^{N} \frac{P}{B_s\ S_s}\ A_{ai} = \frac{P}{B_s\ S_s} \sum_{i=1}^{N} A_{ai} \tag{4}$$

The total amount of energy required for the manufacturing of the piece E_{tot}, is calculated as sum of the two terms in equations (3) and (4), $E_{tot}(\theta_x, \theta_y) = E_h(\theta_x, \theta_y) + E_s$.

3 PROBLEM DEFINITION AND ALGORITHM IMPLEMENTATION

Suppose there are k objectives $f_i(x)$ ($i = 1, 2, \ldots, k$), a general multi-objective minimization problem can be written as

$$\min F(x) = (f_1(x), f_2(x), \ldots, f_k(x)) \tag{5}$$

with

$$x \in \Omega \quad \text{and} \quad h(x) \le 0, \quad c(x) = 0 \tag{6}$$

where x is a solution (decision vector) defined in Ω, and the terms $c(x)$ and $h(x)$ are, respectively, equality and inequality constraints of the problem.

In this study the objectives considered are the weighted average roughness and the total energy required for SLS. The decision variables for the problem are θ_x and θ_y, the rotation angles around the X and Y axes respectively, in a range between 0° and 180°, by 5° steps. Thus, the complete problem of optimal part orientation can be summarized as follows

$$\min F(\theta_x, \theta_y) = (R_a(\theta_x, \theta_y), E_{tot}(\theta_x, \theta_y))$$
$$\text{subject to} \quad \begin{cases} 0^\circ < \theta_x \leq 180^\circ \\ 0^\circ < \theta_y \leq 180^\circ \end{cases} \tag{7}$$

Each component geometry is defined by the standard tessellation language (STL) used as the input file for the optimization system. The STL file, which provides a description of the surface geometry in 3D space, is imported into the Matlab environment where the multi-objective optimization is performed. At the beginning, an STL file containing the geometry surface information is imported; then the algorithm starts rotations around the two axis routines; for each rotation step each of the objectives is calculated and stored. Once the entire domain has been investigated, including all the possible orientations, the Pareto set of solutions is calculated and plotted. Finally, the geometry both with the original orientation and with any of the Pareto-optimized orientations is shown. Figure 5 is a schematic illustration of the main algorithm routines. The computational time required by the system to perform the optimization varies with the number of facets defining the STL geometry, and it is expected to be less than that required by a GA-based optimization; the first and second case studies have 21 054 and 11 438 facets respectively, the longer simulation took about 5 min on a Pentium® 4 2.00 GHz CPU, 512 Mb RAM computer.

Multi-objective optimization is often performed using a GA [**4**] in which a population of individuals (each representing a possible solution) is mutated and combined with other individuals to improve the overall fitness of the population. GAs and related methods are employed to search large solution spaces for global optima, and are seldom able to search the entire space due to computational limitations. In this problem, however, the solution space is two-dimensional (θ_x, θ_y,) and it is therefore possible to search the entire space without resorting to approximate methods. This has the combined benefit of exploring the entire space and thus locating the global Pareto front with certainty, and is computationally more efficient than GA approaches, which are stochastic searchers.

4 RESULTS AND DISCUSSION

The problem has been solved for two different industrial case studies shown at arbitrary orientations in Fig. 6; they are two real aerospace components, Fig. 6(a) shows a support for aluminium profiles manufactured by Polyamide Plastic (Boutet S.A.), while Fig. 6(b) shows a tension latch manufactured by Polyamide Plastic (POM) (Aerotecnica S.A.).

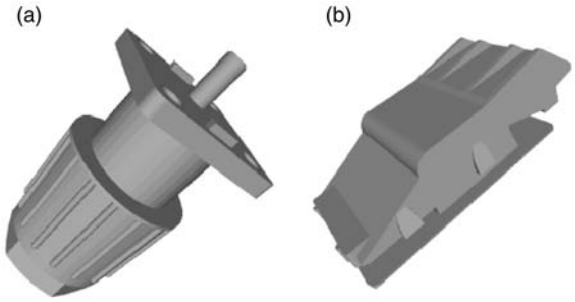

Fig. 6 Artefacts to be manufactured by SLS: (a) support for aluminium profile; (b) tension latch

The prediction of average surface roughness for the first case study, is shown in Fig. 7; it represents the value of predicted average roughness for each material deposition orientation. For a given inclination the roughness has been calculated by taking into account the contribution of each single mesh element and its surface area. The vertical orientation of the facet has also been taken into account, as, depending whether they are oriented upward or downward, facets present different roughness due to the filleting effect. The roughness function has a high degree of symmetry with respect to rotation angles of 90° around both axes. A similar characteristic has been observed for the energy objective function. The symmetry occurs when artefacts with significant geometric symmetry are processed; therefore it can be argued that, by reducing the search domain to 0–90°, a significant reduction in the algorithm computational time could be achieved.

The result from the optimization of the first case study is presented in Fig. 8, where the heavy dots highlight the complete set of Pareto solutions which define the set of best compromises between the surface roughness and energy-saving objectives. Also shown as light dots are non-Pareto-optimal solutions at other orientations; each of these is worse on at least one objective than a Pareto optimal solution, which are therefore to be preferred.

It is clear that orientations which yield low energy and low roughness in the Pareto curve are preferred, and the Pareto front shows that energy expenditure beyond ∼4.6 kJ yields to very small improvements in surface roughness. The non-dominated solutions have roughness values of about 50 per cent less than those of the worst orientation visible on the upper right of the figure. By choosing the solutions at the bottom left of the figure, it is also possible to save the total amount of energy used in the manufacturing process by a factor of two when compared to the worst orientations. Thus, a SLS operator can choose the optimal orientation for part building

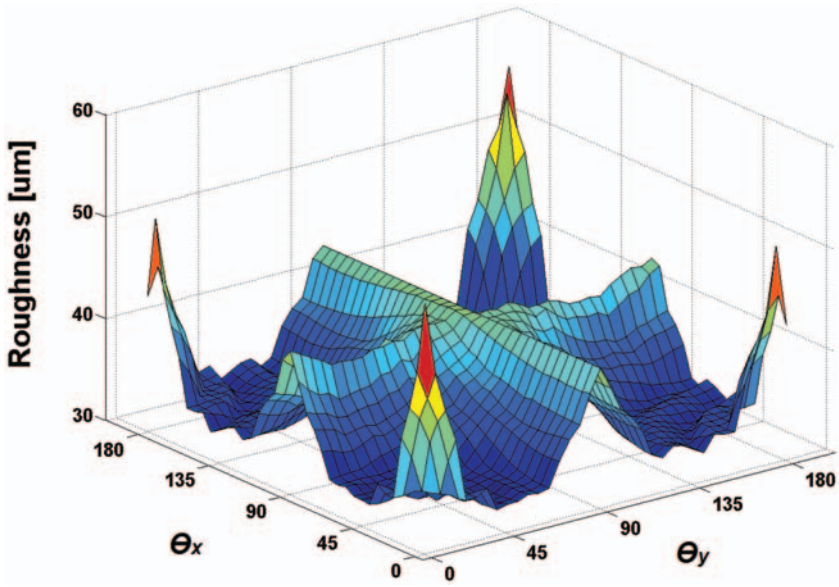

Fig. 7 Weighted average roughness function for the artefact shown in Fig. 6(a)

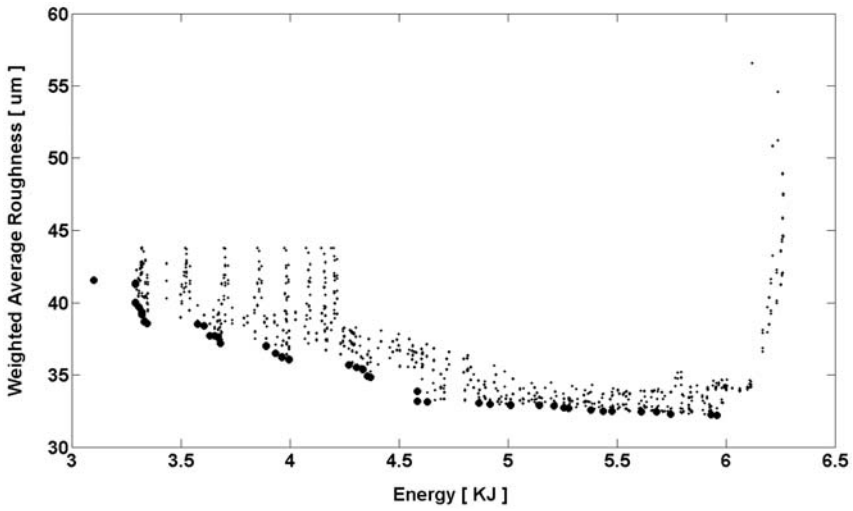

Fig. 8 Solutions and Pareto front for the first case study

based on the part requirements and the predicted results of the surface roughness and energy consumption, rather than relying on the pure experience and skill of the operator.

Figures 9(a) to 9(d) show a comparison between the original oriented geometries and three solutions chosen from the Pareto set of solutions in Fig. 8; Fig. 9(b) shows the orientations that minimize the surface roughness objective; Fig. 9(c) shows the orientations that minimize the total energy employed in the build process. Figure 9(d) represents a compromises between surface quality and energy saving chosen at arbitrary points on the Pareto set. It is noticeable that solutions that minimize the roughness objective, calculated as a weighted average (equation (2)), are the ones that orientate the artefact such that the mesh triangles with the biggest area are oriented at an angle characterized by lower roughness in Fig. 2. Furthermore, the solutions that minimize the energy are those that minimize the height of the artefact in the build position; this in fact allows the number of the layers of powder to be deposited to be minimized, and consequently the energy for preheating operations.

The multi-objective optimization in Fig. 10 shows the optimization of the second case study. If compared to non-optimal orientations such as the ones in the upper left of the figure, up to 50 per cent smaller

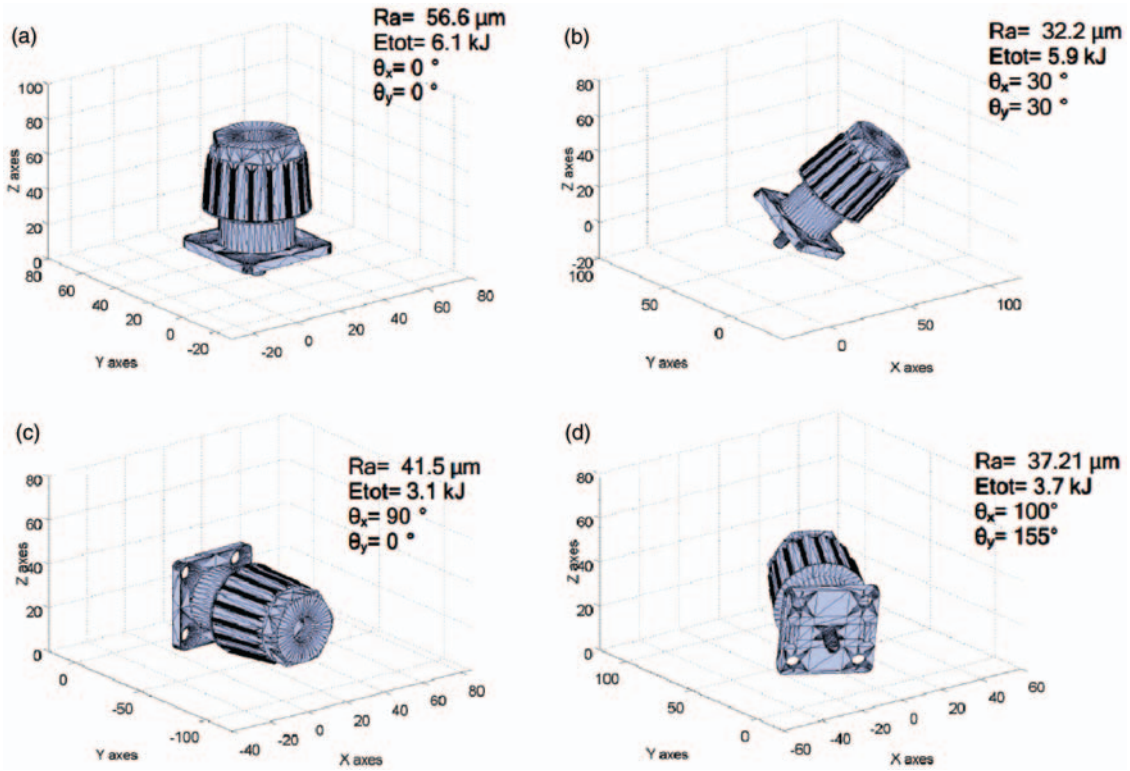

Fig. 9 First case study at different orientations: (a) original oriented geometry; (b) minimization of surface roughness; (c) minimization of build process energy; (d) compromise between the two objectives

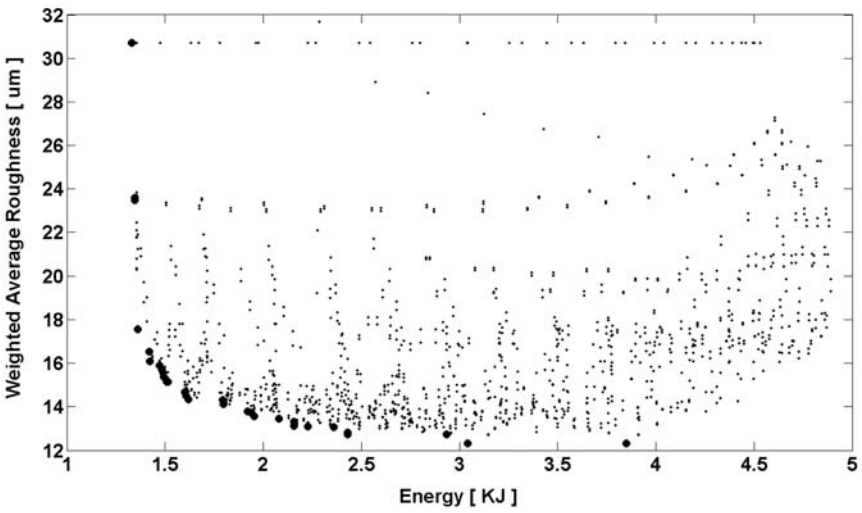

Fig. 10 Solutions and Pareto front for the artefact for the second case study

average roughness is achievable by choosing solutions lying on the Pareto curve. Figure 11 shows a comparison between the original oriented geometries and three solutions chosen from the Pareto set of solutions in Fig. 10; Fig. 11(b) shows the orientations that minimize the surface roughness objective; Fig. 11(c) shows the orientations that minimize the total energy employed in the build process. Figure 11(d) represents the compromises between surface quality and energy saving chosen at arbitrary points on the Pareto set. Similarly to the first case, it is confirmed that solutions that minimize the surface roughness objective are the ones that maximize the amount of mesh surface, at a sloping angle characterized by

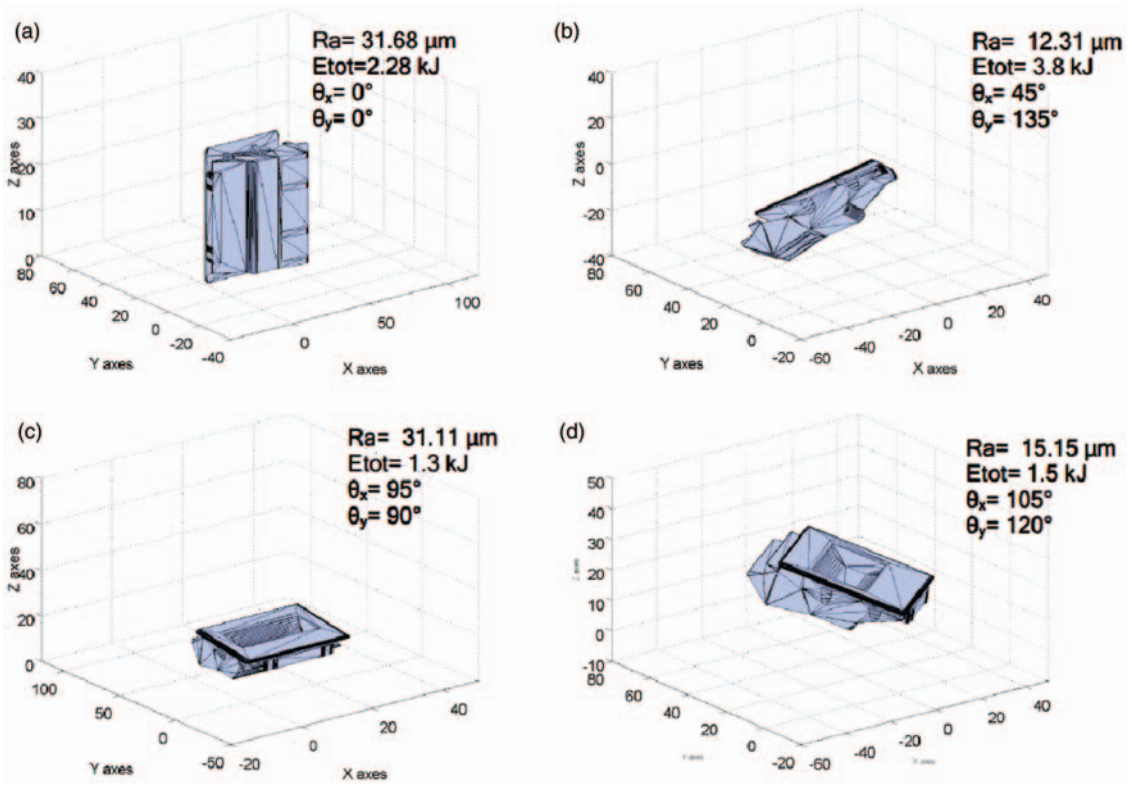

Fig. 11 Second case study at different orientations: (a) original oriented geometry; (b) minimization of surface roughness; (c) minimization of build process energy; (d) compromise between the two objectives

lower roughness values; also, solutions that minimize the energy are those that minimize the height of the artefact in the build position.

5 CONCLUSIONS

This study presents a computational model for the process optimization of parts manufactured through SLS. The multi-objective computational optimization provides the operator with the Pareto set of solutions which define the best compromises between the surface quality of the part and the manufacturing process efficiency, through the minimization of energy employed in the manufacturing process.

For this purpose, a model for the surface roughness prediction has been developed by using an interpolation of measured data on a SLS manufactured geometry sample. Such a model interpolates different sets of data from downward- and upward-oriented surfaces, in order to include the filleting effect that has been experimentally observed in the layer-by-layer sintering of polymer powder.

The modelling approach using experimental data extends the empirical observations of surface roughness to the SLS technology platform, and provides for a more complete and accurate description of the stair-step effect over the entire range of possible inclination angles. The model for manufacturing process efficiency takes into consideration both the contributions of the energy required for the preheating operations and the energy required for the laser sintering of the part. The optimization problem has been solved by an exhaustive search algorithm; the computational time required is expected to be less than that required by a GA-based optimization and the global optimum has been found within a reasonable time; also, further reductions of computational time for symmetrical parts are possible. Furthermore, the methodology and the mathematical approach presented are generally applicable to powder-bed-based additive layer manufacturing (ALM) platforms such as selective laser melting (SLM) and electron beam melting (EBM). The multi-objective approach, in addition to the studied objectives, can be employed for the optimization of more targets, for example by including the minimization of anisotropy in mechanical proprieties of a part produced by any ALM platform.

ACKNOWLEDGEMENTS

The authors would like to thank Great Western Research and EADS Innovation Works UK for funding support, and X-AT laboratory at the University of

Exeter for fabrication of the samples and access to surface roughness measurement equipment.

REFERENCES

1 **Levy, G. N., Schindel, R.,** and **Kruth, J. P.** Rapid manufacturing and rapid tooling with layer manufacturing (LM) technologies, state of the art and future perspectives. *Ann. CIRP*, 2003, **52**(2), 589–609.

2 **Kim, G. D.** and **Oh, Y. T.** A benchmark study on rapid prototyping processes and machines: quantitative comparisons of mechanical properties, accuracy, roughness, speed, and material cost. *Proc. IMechE, Part B: J. Engineering Manufacture*, 2008, **222**(2), 201–215. DOI: 10.1243/09544054JEM724.

3 **Bacchewar, P. B., Singhal, S. K.,** and **Pandey, P. M.** Statistical modelling and optimization of surface roughness in the selective laser sintering process. *Proc. IMechE, Part B: J. Engineering Manufacture*, 2007, **221**(1), 35–52. DOI: 10.1243/09544054JEM670.

4 **Deb, K.** *Multi-objective optimization using evolutionary algorithms*, 2001 (Wiley, Chichester).

5 **Lan, P. T., Chou, S. Y., Chen, L. L.,** and **Gemmill, D.** Determining fabrication orientation for rapid prototyping with stereolithography apparatus. *Comput. Aided Des.*, 1997, **29**(1), 53–62.

6 **Alexander, P., Allen, S.,** and **Dutta, D.** Part orientation and build cost determination in layered manufacturing. *Comput. Aided Des.*, 1998, **30**, 343–356.

7 **Cheng, W., Fuh, J. Y. H., Nee, A. Y. C., Wong, Y. S., Loth, H. T.,** and **Miyajawa, T.** Multi-objective optimisation of part-building orientation in stereolithography. *Rapid Prototyping J.*, 1995, **1**(4), 12–23.

8 **Singhal, S. K., Pandey, S. P., Pandey, P. M.,** and **Nagpal, A. K.** Optimum part deposition orientation for multiple objectives in SL and SLS prototyping. *Int. J. Prod. Res.*, 2009, **47**(22), 6375–6396.

9 **Moré, J. J.** and **Sorensen, D. C.** Computing a trust region step. *SIAM J. Sci. Statist. Comput.*, 1983, **3**, 553–572.

10 **Das, I.** and **Dennis, J. E.** A closer look at drawbacks of minimizing weighted sums of objectives for Pareto set generation in multicriteria optimization problems. *Struct. Optimization*, 1997, **14**(1), 63–69.

11 **Pandey, P. M., Thrimurtullu, K.,** and **Reddy, N. V.** Optimal part deposition orientation in FDM by using a multi-criteria genetic algorithm. *Int. J. Prod. Res.*, 2004, **42**(19), 4069–4089.

12 **Reeves, P. E.** and **Cobb, R. C.** Reducing the surface deviation of stereolithography using in-process techniques. *Rapid Prototyping J.*, 1997, **3**(1), 20–31.

13 **Campbell, R. I., Martorelli, M.,** and **Lee, H. S.** Surface roughness visualisation for rapid prototyping models. *Comput. Aided Des.*, 2002, **34**, 717–725.

14 **Ahn, D., Kim, H.,** and **Lee, S.** Surface roughness prediction using measured data and interpolation in layered manufacturing. *J. Mater. Processing Technol.*, 2009, **209**(2), 664–671.

15 **Kruth, J. P., Vandenbroucke, B., Vam Vaerenbergh, J., and Mercellis, P.** Benchmarking of different SLS/SLM processes as rapid manufacturing techniques. In Proceedings of the International Conference on Polymers and mould innovations (PMI), 20–23 April 2005, Gent, Belgium.

16 **Gibson, I.** and **Shi, D.** Material properties and fabrication parameters in selective laser sintering process. *Rapid Prototyping J.*, 1997, **3**, 129–136.

Optimisation of quality and energy consumption for additive layer manufacturing processes

*G. Strano, L. Hao, K. E. Evans, R. M. Everson[1]
[1]School of Engineering, Computing and Mathematics, University of Exeter, UK

ABSTRACT

Additive Layer Manufacturing (ALM) has great potential to be a viable automated direct manufacturing process for the aerospace, automotive and medical industries. By using layer-by-layer consolidation of raw materials to build three-dimensional near net or net shape objects, ALM enables the recycling of the non-consolidated powder materials and manufacturing of light weight parts, allowing energy and materials saving.
One of the main challenges in various ALM processes is to reduce the energy required for the part building process and at the same time maintain the surface quality of the parts, affected by the "stair stepping" effect, as this has aesthetic and functional importance for industrial applications. These objectives are competing criteria and significantly influenced by the build orientation of the ALM parts. This study investigates a computational technology for the identification of optimal part orientations for the minimization of surface roughness and simultaneously energy consumption in the manufacturing process. The computational model based on a multi-objective optimization technique has been developed to predict and optimise the energy consumption and surface quality objectives. The output of the computational optimisation includes the complete set of Pareto solutions, which define the set of best compromises between the chosen objectives.

Key words: Multi-object Optimization, Additive Layer Manufacturing, Part Deposition Orientation, Surface Roughness, Energy Consumption.

1 INTRODUCTION

Additive Layer Manufacturing (ALM) processes directly build up three-dimensional objects layer-by-layer. This technology has been utilised for the Manufacture of end-use parts, due to technical improvements, better process control and the possibility of processing a wide range of materials including plastics and metal alloys [1]. Without using moulding tools, ALM permits nearly free-from fabrication to produce complex

* Corresponding Author. Tel: +44 (0)1392 263740; *Email address: G.Strano@exeter.ac.uk.*

lightweight part and the minimal material waste as the non-consolidated material can be re-used. Hence, ALM is considered as a very sustainable production process. To be used for industrial scale production, the ALM process accuracy in terms of surface roughness, and the time and energy spent to build the part are often represented as two competing objectives [2].

For Selective Laser Sintering (SLS), one of the most widely used ALM process, the surface roughness and amount of energy is significantly affected by the building orientation [3, 4]; this important process parameter often relies on the experience and skill of the operator and there is therefore no consistent method available to provide an optimal solution. One of the main problems in predicting the surface roughness of the parts relies on the difficulty of describing the real roughness based on more or less sophisticated geometrical considerations, which only in few cases matches the measured data, and only for a relative range of surface inclinations [5], and on the distinction between upward and downward oriented facet roughness [3].

In this study, a multi-objective optimisation technique has been developed, to predict and minimize the surface roughness, and the energy required for part manufacturing by SLS technology. The technique directly imports the geometry of the part in the form of an STL file and performs computational optimisation in the Matlab environment. The developed roughness model interpolates data from empirical observations and allows differentiation of the orientation of each STL geometry facet for a more accurate prediction of part surface roughness.

2 EXPERIMENTAL PROCEDURES

2.1 MODEL FOR QUALITY PREDICTION

The surface roughness prediction model developed takes into consideration the difference between upward and downward oriented surface facets (Figure 1), interpolating for each case data from the specimens made using a 3D System SLS workstation. For both cases, the surface roughness data has been measured by changing the build orientation in the range of *0°* to *90°* [4].

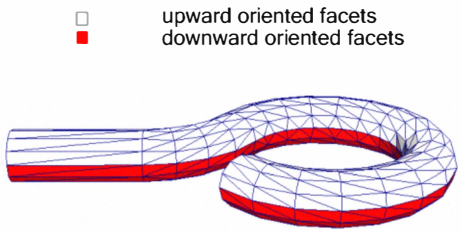

Figure 1: Distinction between upward and downward oriented facets for an arbitrary orientation.

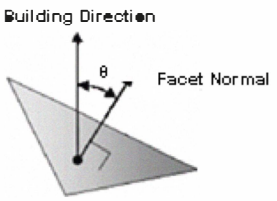

Figure 2: Angle between the building direction and STL file facet normal vectors.

Although different values could be expected depending upon the scan direction, the surface roughness is independent of the measured direction [3]; by following these assumptions, for each facet, it can be assumed that the roughness function depends upon θ, the angle between the fabrication direction $\vec{z}$ = (*0,0,1)* and the vector normal

to the surface facet $\vec{n}$ shown in Figure *2*. If the surface geometry is defined by *K* facets, the roughness value $R_i(\theta)$ *(i=1,2,…K)* for the *i*th facet, at any surface angle θ, can be calculated by interpolating the measured roughness function as follows:

$$R_i(\theta) = R(\theta_p) + \frac{R(\theta_n) - R(\theta_p)}{\theta_n - \theta_p}(\theta - \theta_p) \quad (1)$$

Where $R(\theta_p)$ and $R(\theta_n)$ are the measured roughness values at the samples angles adjacent to θ; see Figure 3.

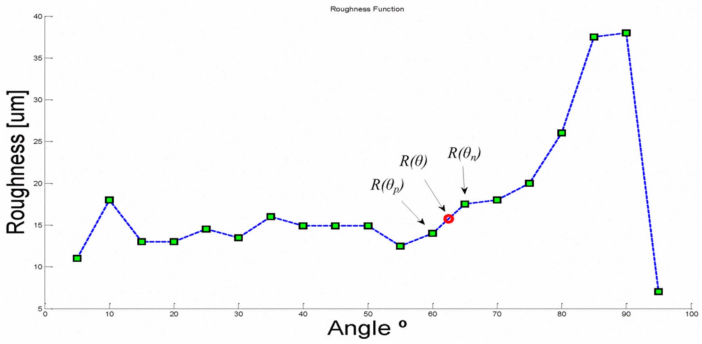

Figure 3: Surface roughness data interpolation.

The roughness objective is defined as the average roughness of the surface facets weighted by the facet area, A_i:

$$R_a = \sum_{i=1}^{K} R(\theta_i) A_i \quad (2)$$

2.2 MODEL FOR ENERGY PREDICTION

Energy employed in the manufacturing process influence the overall quality of ALM parts [6], and as with any manufacturing process, energy influences directly the cost of the part. As known, SLS process involves a moving laser beam irradiating a polymer powder, to sinter the individual powder particles. Before the sintering process, layer by layer, a consistent amount of energy is employed to preheat the deposited powder, in order to reach a temperature just below the melt temperature (for *nylon 12*, typically *178 C°*) which helps to minimise the distortion of sintered layer and the laser sintering energy.

The proposed energy prediction model, takes into consideration both the contributions of E_h energy required by preheating operations, and E_s energy required by the laser sintering of the part. Considering C_p the specific heat capacity (*nylon 12 = 1640 kJ/kg*), *I* the latent heat of fusion *(nylon 12 = 120 kJ/kg)*, ρ the green density of the powder *(nylon 12 = 590 kg/m^3)* and V_p the volume of the total preheated powders, the energy required for preheating operations, can be calculated by the following expression:

$$E_h = (C_p \cdot \Delta T + l) \cdot \rho \cdot V_p \quad (3)$$

The applied energy for the part sintering E_s presented (eq. 4), can be calculated from the model developed by Gibson et al. [6] for the applied energy density. *P* represents the power available from the laser beam at the powder bed surface; *SCSP* the scan

spacing, distance between two adjacent parallel scan vectors, *BS* the scan the beam speed and V_a the volume of the artefact.

$$E_s = \frac{P}{BS \cdot SCSP} \cdot V_a \tag{4}$$

The total amount of energy required for the manufacturing of the piece E_{tot}, is calculated as sum of the two terms in eq. 3 and 4, $E_{tot} = E_h + E_s$.

2.3 PROBLEM DEFINITION

The problem has been solved for a sample geometry, defined by the Standard Tessellation Language (STL) used as the input file for the optimisation system. The STL file, which provides a description of the surface geometry in $\Re^3$, is imported into the Matlab environment where the multi-objective optimisation is performed. Suppose there are *k* objectives $f_i(x)$ $(i= 1,2,\ldots,k)$, a general multi-objective minimisation problem can be written as:

$$min\, F(x) = (f_1(x), f_2(x), ..., f_k(x)) \quad with \quad x \in \Omega \text{ and } h(x) \le 0 \;\; c(x) = 0 \tag{5}$$

where x is a solution (decision vector) defined in Ω, and the terms $c(x)$ and $h(x)$ are, respectively, equality and inequality constraints of the problem.

The multi-objective optimisation problem is based on the research of the "non-dominated" solution with respect to all objectives; i.e. moving from one solution to another, it is not possible to improve one criterion without making at least one of the other criteria worse. A non-dominated solution is often called a Pareto solution and the set of all the Pareto solutions is called Pareto set. In this study, the objectives considered are the weighted average roughness and the total energy required for SLS. The decision variables for the problem are θ_x and θ_y, rotation angles around the *X* and *Y* axes respectively, in a range between *0*° to *180*° by 5° step. Thus, the complete problem of optimal part orientation can be summarized as follows:

$$min\, F(\theta_x, \theta_y) = (R_a(\theta_x, \theta_y), T_{tot}(\theta_x, \theta_y)) \qquad subjected \;\; to \;\; \begin{cases} 0° \le \theta_x \le 180° \\ 0° \le \theta_y \le 180° \end{cases} \tag{6}$$

3 RESULTS

Results in Figure 4 show the sample geometry to be manufactured and the related optimization. The best compromises between the surface roughness and energy saving objectives is represented by the Pareto set; Figure 4 shows that, moving along the Pareto front, although most solutions have similar values of energy required to manufacture the part, choosing certain angles allows part quality to be increased considerably.

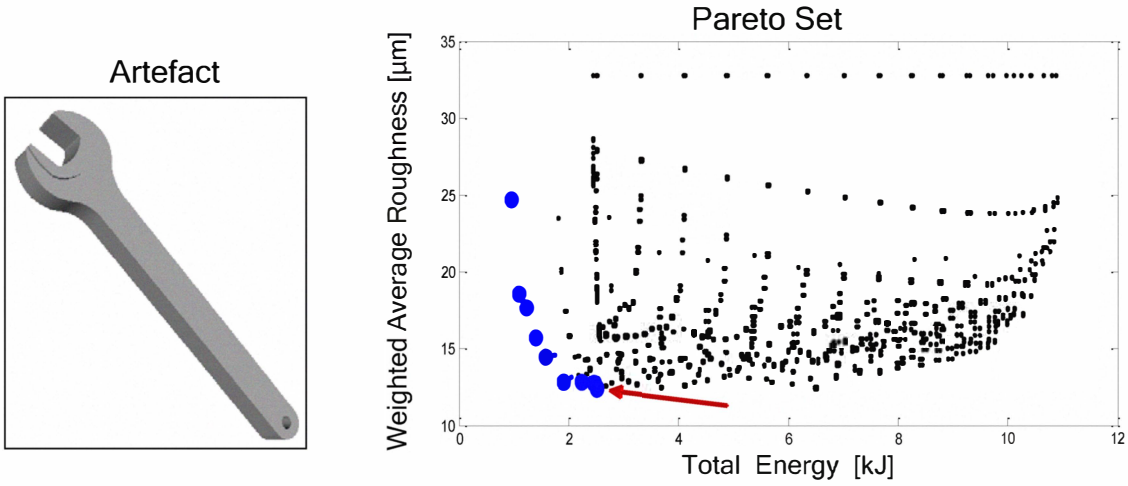

Figure 4: Artefact to be manufactured and related Pareto solutions.

Clearly orientations that yield energy and roughness close to the "knee" in the Pareto curve one to be preferred because moving away from the knee either produces a large increase in quality for small gain in energy saving or vice versa; for the studied geometry, the non-dominated solutions have roughness values of up to *60%* less than those of the worst orientation. The computational time required by the system to perform the optimization is expected to be less than that required by a GA based optimisation (the longer simulation took about *5 minutes* on *Pentium ® 4 2,00 GHz CPU, 512 Mb RAM,* computer). Figures 5 shows the original and the optimised geometry orientations in order to minimize the surface roughness objective, in accord with the solution highlighted by the arrow in Figure 4.

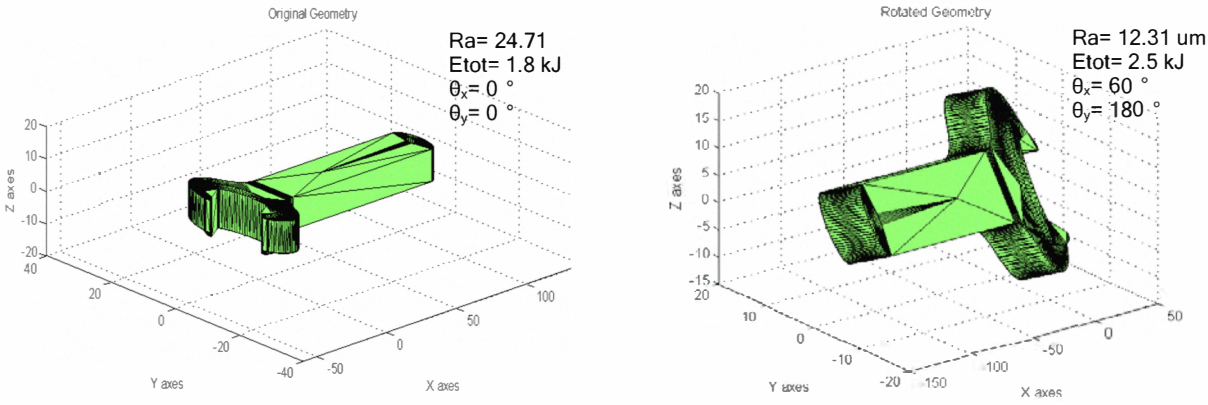

Figure 5: Case study original (left) and optimally oriented (right) geometries in order to minimize the surface roughness.

4 CONCLUSIONS

A model based on multi-objective optimisation technique has been developed, in order to find the Pareto set of solutions which define the best compromises between the weighted average surface roughness and energy saving for ALM processes such as SLS has been presented. The energy consumption and roughness prediction models have been developed; rather than using a geometric analytical model, an approach based on the interpolation of measured data on the SLS technology has been used for a more accurate roughness prediction. The optimisation problem has

been solved by an exhaustive searching algorithm, the computational time required is expected to be less than that required by a GA based optimisation; the global optimum has been found in a reasonable time.

REFERENCES

[1] **Levy G.N., Schindel R., Kruth J.P.,** (2003)**,** Rapid Manufacturing and Rapid Tooling with layer manufacturing (LM) technologies, state of the art and future perspectives**.** CIRP Annals, Vol.52/2.

[2] **Strano G., Hao L., Evans K.E., Everson R. M., Smith C. W., Meyer J., Johns D., Vanard G., Scarpa F.,** (2009), Multi-objective Optimization for Additive Layer Manufacturing. 11th National Conference on Rapid Design, Prototyping & Manufacturing, Bucks New University, UK, June 12.

[3] **Kruth J.P., Vandenbroucke B., Vam Vaerenbergh J., Mercellis P.,** (2005), Benchmarking of different SLS/SLM processes as Rapid Manufacturing techniques (2005). Int. Conf. Polymers & Mould Innovations (PMI), Gent, Belgium, April 20-23.

[4] **Bacchewar P.B., Singhal S.K., Pandley P.M.,** (2007), Statistical modelling and optimization of surface roughness in the selective laser sintering process. Proc ImechE vol. 221, pp. 35-52.

[5] **Campbell, R.I., Martorelli, M., and Lee, H.S.,** (2002), Surface roughness visualisation for rapid prototyping models. Computer-Aided Design, Vol. 34, pp.717-725.

[6] **Gibson I., Shi D.,** (1997), Material proprietiea and fabrication parameters in Selective Laser Sintering Process. Rapid Prototyping Journal, Vol. 3, pp. 129-136.

Enhancing the Sustainability of Additive Manufacturing

Liang Hao, David Raymond, Giovanni Strano, Sasan Dadbakhsh
[1]School of Engineering, Computing and Mathematics, University of Exeter, UK

ABSTRACT

Additive Manufacturing (AM) produces three dimensional objects directly from a digital model by the successive addition of material(s), without the use of a specialized tooling. AM allows the rapid development of sustainable products and has been increasingly used to produce lightweight components to save materials and costs. This particularly helps to save a considerable amount of material, energy and cost for the production of one-off or small volume products. In addition, the non-processed raw materials can be recycled and re-used by AM to reduce material waste drastically. AM is therefore considered as a sustainable manufacturing approach driving the rapid development of new products.
The paper will present and review the research activities performed in the University of Exeter to enhance the sustainability of AM. These research activities include: 1) sustainable product design by optimising internal lightweight structures; 2) improvement of process efficiency by optimising AM process parameters; 3) reduction of energy consumption by in situ thermite material reaction; 4) sustainable production of personalised chocolates.

Key words: Sustainability, Additive Manufacturing, Lightweight Structure, Process Optimisation.

1. INTRODUTION

Additive Manufacturing (AM) describes a family of technologies that, in an automatic process, produces three dimensional objects directly from a digital model by the successive addition of material(s), without the use of a specialized tooling. It is also known as Additive Fabrication, Solid Freeform Fabrication (SFF) and Layered Manufacturing and called by the names of specific applications such as Rapid Prototyping (RP), Rapid Tooling (RT), and Rapid Manufacturing (RM).
AM is considered as one of the most important emerging material processing technologies that will drive the future manufacturing industry. Many of the traditional

Design for Manufacture (DFM) principles are no longer applicable to AM as it can produce parts with complex internal and re-entrant features [1]. AM has been increasingly used to produce topologically optimized parts to save materials and costs. It also makes high value products withnout using tooling, jigs and fixtures. This particularly helps to save a considerable amount of additional material and process cost for the production of one-off or small volume parts or products. In addition, the non-processed raw materials can be recycled and re-used by AM to reduce material waste drastically. AM is therefore considered as a sustainable manufacturing approach driving the rapid development of new products, in particular lightweight and sustainable products which are now highly demanded by many industries due to the tighter environmental regulations. AM is potential to enable Manufacturing for Design (MfD) to produce complex, lightweight and high value products. The application of AM is therefore spreads widely from tradition industries (e.g. aerospace, automotive, defense, marine) to many new niche and emerging areas (medical devices, low-carbon vehicle, sport, art, creative industry).

2. SUSTAINABLE BENEFITS OF AM

AM brings many fundamental changes in material process, product design, manufacturing process and supply chain of products. It provides many opportunities to replace the traditional manufacturing approach as a more sustainable manufacturing method and minimise the carbon footprint in new product development, production and lift-cycle processes, in particular for complex, value added and custom-centric products. There are several major areas for AM to generate positive environmental impacts.

1. Materials utilisation: AM can efficiently utilise raw materials and their functionality. Non-consolidated raw materials in powder based process such as selective laser sintering/melting (SLS/SLM) and 3D printing can be reused so that the material waste can be minimised. AM can offer specific microstructure (e.g. finer microstructure in the part made by SLM) and advanced properties to the parts and flexibly manipulate process and materials mixture to fabricate advanced composites, multiple-materials and functional graded materials.

2. Product design optimisation: The free-form fabrication nature of AM remove the design constraints of traditional manufacturing processes and enables the redesign or the optimisation of the products. The optimal design will result in the reduction of the materials, energy, fuel or natural resources in the product manufacturing and operation process and the enhancement of the product performance, bringing significant sustainable and economic benefits.

3. Manufacturing process: The AM has the potential to replace processes where significant amounts of energy are wasted changing the phase of materials from solid to liquid, such as casting or moulding. It can also save many resources spent on the fabrication of specific tooling for the production.

4. Supply Chain: As a direct digital manufacturing approach, the AM machines can be distributed more close to customers and managed by web-based system to coordinate the demands and requirements of product stakeholders and maximise the

efficiency of the supply chains. This can reduce the need of long-distance transportation, warehousing, logistics and, for many cases, disposable packaging.
5. Life-cycle performance: AM can be used to repair and add advanced functions to existing products as such the life-time performance can be extended. Also, out-off-shelf or low volume components can be made by AM for part re-manufacturing and give a recycled life to the product. .

3. IMPROVEMENT OF THE SUSTAINIBILITY OF AM

As relatively new manufacturing process, AM itself need improvements to be more sustainable to encourage industrial uptake. There are great opportunities to develop new AM related technologies in the areas of material, design, manufacturing and application. The research group in Exeter has been focused on the following areas to improve the sustainability of AM.

3.1. Design sustainable products by optimising internal lightweight structures.

Lightweight material structures can save expensive functional materials and provide high performance to aerospace, medical and engineering products. Such structures are actually seen in the nature where the process of evolution has lead to the formation of highly efficient cellular material structures. For example, the human skull is a sandwiched cellular structure capable of sustaining large impacts in order to protect the brain. To fully explore the design spaces and lightweight material structure technologies for sustainable product development, computational approaches are developed to design, analyse and optimise the internal hollow or cellular structure for the sustainable product development. As see Fig.1, various cellular structures can be generated through mathematic approach and the size of the unit cells can be varied to manipulate the density and mechanical properties of the structure, providing an effective approach to optimise product functionality and minimise the material use and its environmental impact.

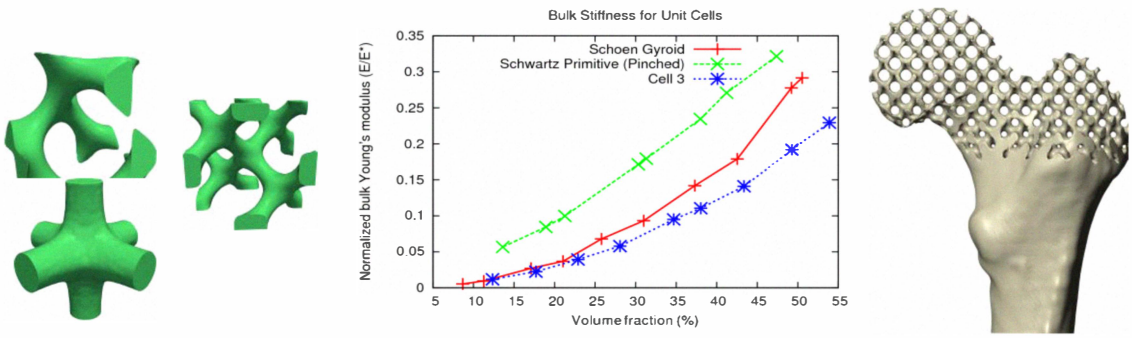

(a) (b) (c)

Figure 1. a) Various cellular units, b) the bulk stiffness for cellular structures, c) graded cellular lightweight implants.

3.2. Improvement of process efficiency by optimising AM process parameters

It is particularly important to select optimal AM processes parameters such as part orientation, layer thickness, laser parameters for SLS process. Computational model

can be developed to predict the energy and material input as well as the geometry accuracy and mechanical property of 3D objects.

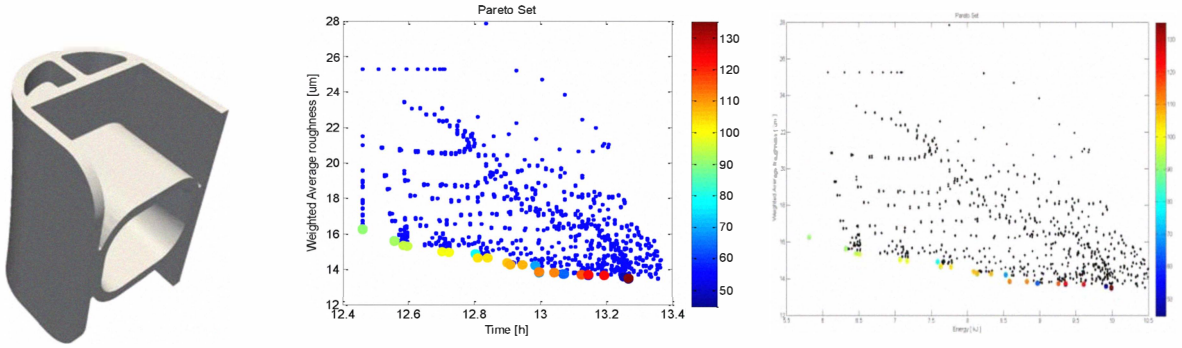

Figure 2. Aerospace part to be manufactured and related Pareto front

The objective of improving process efficiency such as time and energy input is often competitive to the quality objective of the products such as surface roughness of the part. Hence, a multi-objective optimization approach is applied to identify the optimal and efficient process parameters to build a part based on the complete set of Pareto solutions predicted by computational models. As shown in Figure 2, the Pareto set provides the results for the surface roughness and building time and enable the optimal part orientation to be selected for specific product requirements [2].

3.3. Reduction of energy consumption by in situ material reaction.

Metal matrix composites (MMCs) are highly demanded by various applications such as space industry. The existing MMCs manufacturing method requires complicate process procedures and tools and faces the challenges in product net-shape products. SLM process offers a new opportunity to consolidate and facilitate the in situ interaction of appropriate metal and metal oxide powders to form MMCs. A study has been performed on aluminium (Al) and iron oxide (Fe_2O_3) material system to produce in situ Al/Al_20_3 composite. As described in the Equation, thermite interaction between the mixture of Al and Fe_2O_3 can release additional heat to facilitate the melting and consolidation of Al MMCs.

$$Fe_2O_3 + 2Al \rightarrow 2Fe + Al_2O_3 + \sim 850\ kJ \quad (1)$$

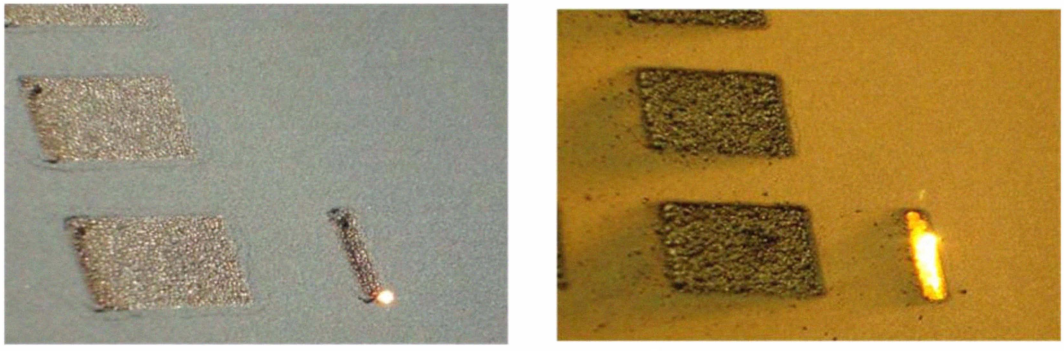

Figure 3. Selective laser melting of pure Al (left) and Al / Fe_2O_3 (right)

As shown in Figure 3, Al / Fe_2O_3 exhibits the higher temperature than the pure Al when same SLM parameter are used, indicating a lower energy density can be used to consolidate the Al/Fe_2O_3 for the fabrication of advanced Al MMCs.

3.4. Sustainable production of personalised chocolates.

An chocolate additive layer manufacturing (ChocALM) machine has been developed to produce innovative and personalised 3D chocolates through layer-by-layer approach [3]. As chocolates are one of most popular gift products, personalised chocolates are highly demanded by many customers. However, conventional chocolate mould method requires a specific mould to produce personalised product. This means a very expensive, but also not an efficient way to produce one-off or small volume personalised product. ChocALM process can efficiently deposit chocolate to form personalised products, removing the expense and material use of the moulding tool. In addition, low-cost and compact chocolate machines can be placed in high street or neighbour shops, offering distributed local production to minimise the transportation and logistics of the products. Hence, it offers a unique sustainable AM process for the production of personalised chocolates.

Figure 4. a) ChocALM machine, b) cellular chocolate heart, c) ChocALM logo made by Chocolate.

5. SUMMARY AND FUTURE PROSPECTIVE

Additive Manufacturing (AM) is able to produce complex, lightweight and advanced products without specific tools and large material waster. It brings fundamental changes in product development and supply and posts positive environmental impacts in terms of material utilisation, product design optimisation, manufacturing process, supply chain and life-cycle performance. There are still many opportunities to improve the sustainability of the AM. Research carried in the University of Exeter has offered lightweight structure and process optimisation techniques, thermite material system and novel ChocALM process that enable to AM to produce more sustainable product and reduce the material and energy consumption in the AM process. In order to fully understand and explore the environmental impact and sustainable potential of AM process, future research work are need to: 1) quantify the toxicity and waste of materials used in AM; 2) find the optimal sustainable design and operation solution for AM process; 3) measure sustainability of AM processes and products; 4) identify sustainable engineering materials for AM process.

REFERENCES

[1] **Neil H., Hague R.,** and **Dickens P.** Rapid Manufacturing: An industrial revolution for the digital age, Wiley, 2005

[2] **Strano G., Hao L., Evans K.E., Everson R. M., Smith C. W., Meyer J., Johns D., Vanard G.,** and **Scarpa F.,** (2009), Multi-objective Optimization for Additive Layer Manufacturing. 11th National Conference on Rapid Design, Prototyping & Manufacturing, Bucks New University, UK, June 12.

[3] **Hao L., Seaman O., Mellor S., Henderson J., Sewell N.,** and **Sloan M**. Extrusion Behaviour of Chocolate for Additive Layer Manufacturing. in The 4th Inter. Conf. on Advance Research in Virtual and Rapid Prototyping, Leiria, Portugal, 5th - 6th Oct. 2009

Multi-objective Optimization for Additive Layer Manufacturing

[1]G STRANO, L HAO, K E EVANS, R M EVERSON AND C W SMITH
School of Engineering, Computing and Mathematics, University of Exeter, UK
G.Strano@exeter.ac.uk, L.Hao@exeter.ac.uk, K.E.Evans@exeter.ac.uk, R.M.Everson@exeter.ac.uk, C.W.Smith@exeter.ac.uk

J MEYER, D JOHNS AND G VANARD
EADS – AIRBUS, UK
Jonathan.Meyer@airbus.com, Daniel.Johns@airbus.com, Gaelle.Vanard@airbus.com

F SCARPA
Department of Aerospace Engineering, University of Bristol, UK
f.scarpa@bristol.ac.uk

ABSTRACT

In recent years Additive Layer Manufacturing (ALM) has become accepted as a viable automated direct manufacturing process for end-use parts, with a large number of potential applications in the aerospace, automotive and medical industries. One of the main challenges in ALM is to reduce the time required for the building process and at the same time maintain the surface quality of the parts, as this has aesthetic and functional importance for industrial applications.
The Surface quality of ALM parts in terms of surface roughness is primarily the result of 'stair stepping' associated with the layer-by-layer building approach, and is significantly affected by the build orientation of the parts. This important process parameter often relies on the experience and skill of the operator and there is therefore no consistent method available to provide an optimal solution. This study investigates a computational technology for the definition of an optimal part orientation for the minimization of build time and stair-stepping effect (thus, refining time), ensuring surface quality and, simultaneously, total process time saving.
A computational model based on a multi-objective optimization technique has been developed to predict and optimise the build time and surface quality objectives, using process parameters such as build time for each layer and weighted average surface roughness of the part. A roughness prediction model has been developed based upon empirical observations. The output of the computational optimisation includes the complete set of Pareto solutions, which define the set of best compromises between the chosen objectives, thus permitting the operator to select the best trade-off between final surface quality and build time.

KEYWORDS

Multi-object optimization, Rapid Prototyping, part deposition orientation, surface roughness, build time.

[1] Corresponding Author. Tel: +44 (0)1392 263740; *Email address: G.Strano@exeter.ac.uk.*

1. INTRODUCTION

Additive Layer Manufacturing (ALM) processes build up three-dimensional objects layer-by-layer. This technology has been widely used for Rapid Prototyping and is increasingly utilised for the Manufacture of end-use parts; it is considered as a viable automated direct manufacturing process for the production of high value and innovative products, with a large number of potential applications in the aerospace, automotive and medical industries. Furthermore, ALM techniques, such as Selective Laser Sintering/Melting (SLS/SLM), have gained a wide acceptance, due to technical improvements, better process control and the possibility of processing a wide range of materials including plastics and metal alloys [1]. However, to enable these processes to be used in large-scale industrial production, the process accuracy, mainly in terms of surface roughness, and the time spent to build the part, including both fabrication and refining procedures time, represent two competing objectives. Reduced surface roughness can be achieved by using thinner layers material, perhaps saving time in post manufacturing procedures which themselves can be detrimental to the original geometry of the part, however, this increases the build time drastically.

The surface quality and build time of ALM parts made by powder bed SLS/SLM processes is significantly affected by the building orientation [2, 3]; this important process parameter often relies on the experience and skill of the operator and there is therefore no consistent method available to provide an optimal solution.

One of the main problems in predicting the surface roughness of the parts is the difficulty of describing the real roughness based on more or less sophisticated geometrical considerations, which only in few cases matches the measured data, and only for a relative range of surface inclinations [4]. Furthermore, in SLS/SLM processes consistent differences have been observed between upward and downward oriented facet roughness [2].

Recently, there have been a number of attempts to formulate build time and roughness models to deal with the optimal orientation problem for different technologies such as Fused Deposition Modelling (FDM) and Stereolithography (SLA).

Singhal et al. [5], studied the best orientation problem by performing a single objective optimisation of the average part surface roughness, using a trust region method based algorithm; the roughness model used is based upon geometrical considerations. Canellidis et al. [6], presented a multi-objective optimisation (roughness, build time) system, based on Genetic Algorithm (GA), to automate the deposition orientation in SLA.

Pandley et al [7] used Non-dominated Sorting GA II (NSGA-II) to find the Pareto trade-off between average part surface roughness and build time for FDM fabricated parts. A tessellated CAD data file is used as the input, the analytical expression of roughness is based on geometrical observations, and the build time and other non-productive times typical of FDM technology (such as lowering the platform after deposition of each layer) are based on a model developed by Alexander et al [8].

In this study, a multi-objective optimisation technique has been developed for SLS/SLM processes, to predict and minimize the building time and surface roughness objectives. The technique directly imports the geometry of the part in the form of an STL file and performs computational optimisation in the Matlab environment. The developed roughness model interpolates data from empirical observations and allows differentiation of the orientation of each STL geometry facet for a more accurate prediction of part surface roughness. The set of optimal solutions is provided by exhaustive research, so that the computational time required is expected to be less than the computational time required by a GA based optimisation.

2. EXPERIMENTAL PROCEDURES

2.1 Roughness prediction model

Surface roughness determines the quality and accuracy of the parts, as well as influencing the time to be spent in post-processing cleaning and refining procedures. It therefore has a direct effect on the total process time.
The prediction model developed takes into consideration the difference between upward and downward oriented surface facets, interpolating for each case data from the specimens made using a EOS P 380 SLS workstation. For both cases, the surface roughness data has been measured by changing the build orientation in the range of *0°* to *90°* [3].
Although different values could be expected depending upon the scan direction, the surface roughness is independent of the measured direction [2].
Following these assumptions, for each facet, it can be assumed that the roughness function depends upon θ, the angle between the fabrication direction $\vec{z}$ = (*0,0,1)* and the vector normal to the surface facet $\vec{n}$ shown in Figure 1.
If the surface geometry is defined by *K* facets, the roughness value $R_i(\theta)$ *(i=1,2,…K)* for the *i*th facet, at any surface angle θ, can be calculated by interpolating the measured roughness function as follows:

$$R_i(\theta) = R(\theta_p) + \frac{R(\theta_n) - R(\theta_p)}{\theta_n - \theta_p}(\theta - \theta_p) \qquad (1)$$

where $R(\theta_p)$ and $R(\theta_n)$ are the measured roughness values at the samples angles adjacent to θ; see Figure 2.

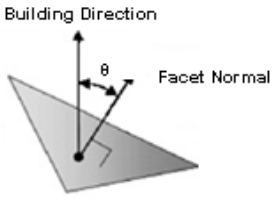

Figure 1: Angle between the building direction and STL file facet normal vectors.

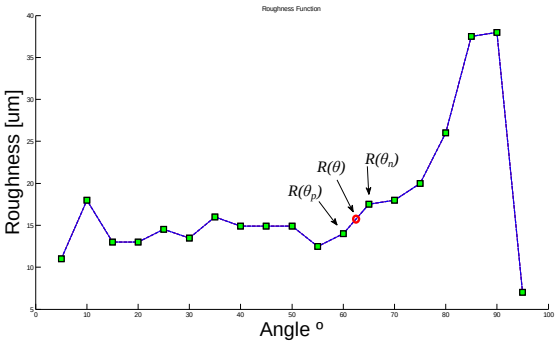

Figure 2: Surface roughness data interpolation.

The roughness objective is defined as the average roughness of the surface facets weighted by the facet area, A_i :

$$R_a = \sum_{i=1}^{K} R(\theta_i) A_i \qquad (2)$$

2.2 Build time prediction model

As with any manufacturing process, the cost of the part is directly related to the manufacturing time. Production time and costs influence the possibility of using SLS/SLM and other ALM technologies for industrial applications layer by layer deposition and consolidation takes considerable time which can be much longer than conventional manufacturing techniques.
In this study a fixed layer thickness has been considered; even though adaptive slicing is expected to further reduce build time and enhance surface quality.
In the proposed model, process deposition time has been characterized by three main factors: the time for moving the platform elevator down of one step T_z; time to melt each layer of powder T_s, and the total number of layers N. The build time T_{tot} for the entire piece is given by the following expression:

$$T_{tot} = N \cdot T_z + \sum_{i=1}^{N} T_{Si} \tag{3}$$

Note however that the time T_{si} to build each slice is proportional to the area of the slice. Consequently $\sum_{i=1}^{N} T_{Si}$ is α proportional to the volume V of the object and (3) may be simplified to:

$$T_{tot} = N \cdot T_z + \alpha V \tag{4}$$

We have empirically verified this linear relationship. As might be expected the build time is therefore a constant plus a factor proportional to the maximum height of the object when oriented for building.

2.3 Problem definition

The problem has been solved for two different geometries, both defined by the Standard Tessellation Language (STL) used as the input file for the optimisation system. The STL file, which provides a description of the surface geometry in $\Re^3$, is imported into the Matlab environment where the multi-objective optimisation is performed.
The two proposed geometries are shown in Figure 3, both their surfaces are described by adaptive triangle meshes.
Suppose there are k objectives $f_i(x)$ $(i= 1,2,\ldots,k)$, a general multi-objective minimisation problem can be written as follows:

$$min\, F(x) = (f_1(x), f_2(x), \ldots, f_k(x)) \qquad with \quad x \in \Omega \text{ and } h(x) \le 0 \;\; c(x) = 0$$

where x is a solution (decision vector) defined in Ω, and the terms $c(x)$ and $h(x)$ are, respectively, equality and inequality constraints of the problem.

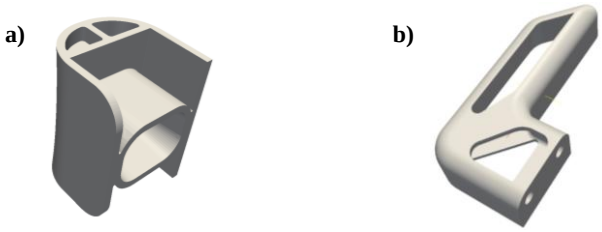

Figure 3: Artefacts to be manufactured.

The multi-objective optimisation problem is based on the research of the "non-dominated" solution with respect to all objectives; i.e. moving from one solution to another, it is not possible to improve one criterion without making at least one of the other criteria worse. A non-dominated solution is often called a Pareto solution and the set of all the Pareto solutions is called Pareto set.
In this case study, for each geometry, the objectives considered are the weighted average roughness and build time calculated by the expressions *(1), (4).*
The decision variables for the problem are θ_x and θ_y, rotation angles around the *X* and *Y* axes respectively. The rotation angles are kept in a range between *0°* to *180°* by *5°* step. Thus, the complete problem of optimal part orientation can be summarized as follows:

$$min\, F(\theta_x, \theta_y) = (R_a(\theta_x, \theta_y), T_{tot}(\theta_x, \theta_y))$$

$$subjected \quad to \quad \begin{cases} 0° \le \theta_x \le 180° \\ 0° \le \theta_y \le 180° \end{cases}$$

At the beginning, an STL file containing the geometry surface information is imported; then the algorithm starts the rotations around the two axis routines, for each rotation step each of the objectives is calculated and stored. Once the entire domain Ω has been investigated including all the possible orientations, the Pareto set of solutions is calculated and plotted. Finally the geometry both with the original orientation and with any of the Pareto-optimised orientations is shown. Following is a proposed schematic with the main algorithm routines.

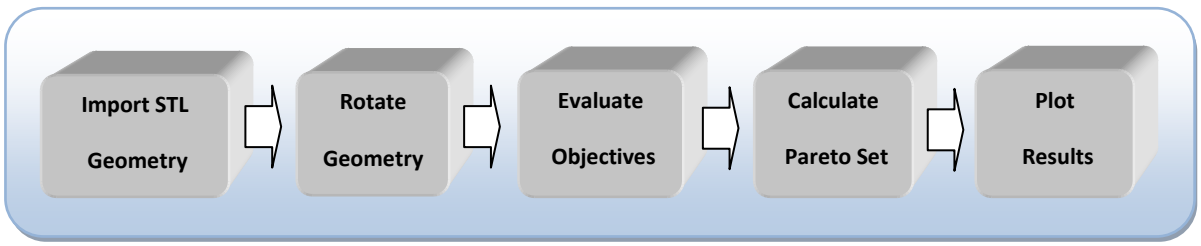

Figure 3: Principal algorithm routines flowchart.

3. RESULTS

In this section, the results from the optimisation of both the parts are presented; Figure 4 and 5 show the complete set of Pareto solutions which define the set of best compromises between the surface roughness and build time objectives, thus permitting the operator to select the best trade-off between final surface roughness and build time. The bar in the figures is

proportional to the angle between the fabrication direction and normal to the surface facet. However, the optimum part orientation is defined by the rotation angles around the *X* and *Y* axes. Results, for the first and the second geometry respectively, are summarized in Table 1 and in Table 2.

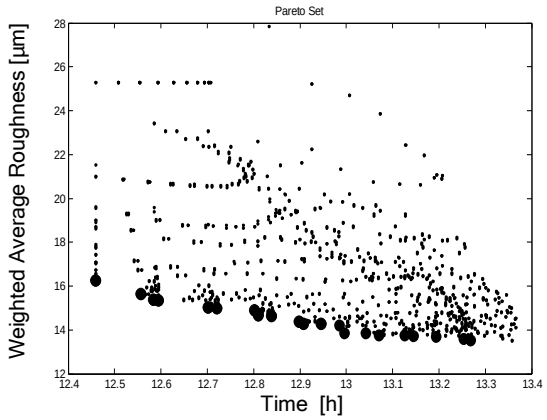

Figure 4: Solutions and Pareto front for the artefact shown in Figure 3a.

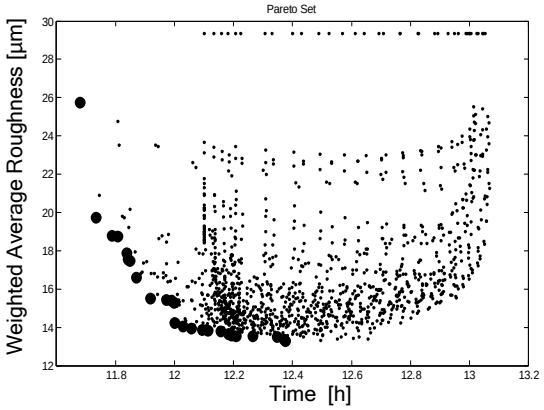

Figure 5: Solutions and Pareto front for the artefact shown in Figure 3b.

Roughness [µm]	***Build time [h]***	θ_x ***[°]***	θ_y ***[°]***
13.50	*13.27*	*35*	*30*
13.53	*13.27*	*35*	*150*
13.60	*13.25*	*40*	*30*
13.70	*13.14*	*55*	*20*
13.70	*13.19*	*125*	*20*
13.74	*13.14*	*55*	*160*
13.75	*13.13*	*120*	*30*
13.76	*13.07*	*60*	*30*
13.78	*13.07*	*60*	*5*
13.86	*12.99*	*65*	*30*
13.86	*13.04*	*115*	*30*
13.87	*12.99*	*65*	*150*
14.22	*12.98*	*65*	*35*
14.27	*12.91*	*70*	*30*
14.27	*12.95*	*110*	*30*
14.30	*12.91*	*70*	*150*
14.38	*12.90*	*70*	*35*
14.39	*12.90*	*70*	*145*
14.65	*12.84*	*105*	*30*
14.67	*12.81*	*75*	*30*
14.69	*12.81*	*75*	*150*
14.91	*12.80*	*75*	*35*
14.99	*12.72*	*100*	*30*
15.02	*12.70*	*80*	*150*
15.03	*12.70*	*80*	*30*
15.34	*12.59*	*95*	*30*
15.36	*12.58*	*85*	*150*
15.39	*12.58*	*85*	*30*
15.61	*12.56*	*85*	*120*
15.65	*12.56*	*85*	*60*
16.71	*12.55*	*85*	*115*

Table 1: Objective function values for the artefacts shown in *Figure 3a*.

Roughness [µm]	***Build time [h]***	θ_x ***[°]***	θ_y ***[°]***
13.28	*12.37*	*55*	*160*
13.38	*12.37*	*35*	*160*
13.52	*12.35*	*55*	*20*
13.54	*12.27*	*60*	*170*
13.56	*12.21*	*125*	*20*
13.57	*12.19*	*145*	*20*
13.66	*12.18*	*125*	*160*
13.80	*12.16*	*30*	*10*
13.82	*12.11*	*145*	*15*
13.89	*12.09*	*145*	*10*
13.96	*12.06*	*150*	*10*
14.06	*12.03*	*150*	*170*
14.23	*12.00*	*150*	*175*
15.30	*12.00*	*160*	*170*
15.41	*11.99*	*160*	*10*
15.44	*11.97*	*150*	*180*
15.52	*11.92*	*160*	*175*
16.61	*11.87*	*165*	*175*
17.50	*11.85*	*170*	*175*
17.57	*11.84*	*170*	*5*
17.89	*11.84*	*165*	*180*
18.75	*11.81*	*10*	*180*
18.81	*11.79*	*170*	*180*
19.75	*12.36*	*175*	*180*
25.75	*12.37*	*180*	*180*

Table 2: Objective function values for the artefacts shown in *Figure 3b*.

The Pareto sets in Figures 4 and 5 show that, moving along the Pareto front, although most solutions have similar values of roughness, choosing certain angles allows material deposition time to be saved considerably.
Clearly orientations that yield build times and roughness close to the "knee" in the Pareto curve one to be preferred because moving away from the knee either produces a large increase in roughness for small gain in build time or viceversa.
For both the studied geometries, the non-dominated solutions have roughness values of up to *50%* less than those of the worst orientation. The decrease in build time is relatively small: this is because in (4) the build time is dominated by the constant term $V = \sum_{i=1}^{N} T_{Si}$, compared with $N \cdot T_z$, time proportional to the number of slices.
The computational time required by the system to perform the optimization is expected to be less than that required by a GA based optimisation (the longer simulation took about *5 minutes* on *Pentium ® 4 2,00 GHz CPU, 512 Mb RAM,* computer).
Figure 6, represents the roughness function for the first geometry case study. It is possible to notice a high degree of symmetry of the function with respect to rotation angles of *90º* around both the axes; this may enable a significant reduction in algorithm computational time for objects with significant geometric symmetry.
Figures 8 show the original and the optimised geometry orientations in order to minimize the surface roughness objective, in accord with the solutions shown in Tables 1 and 2.

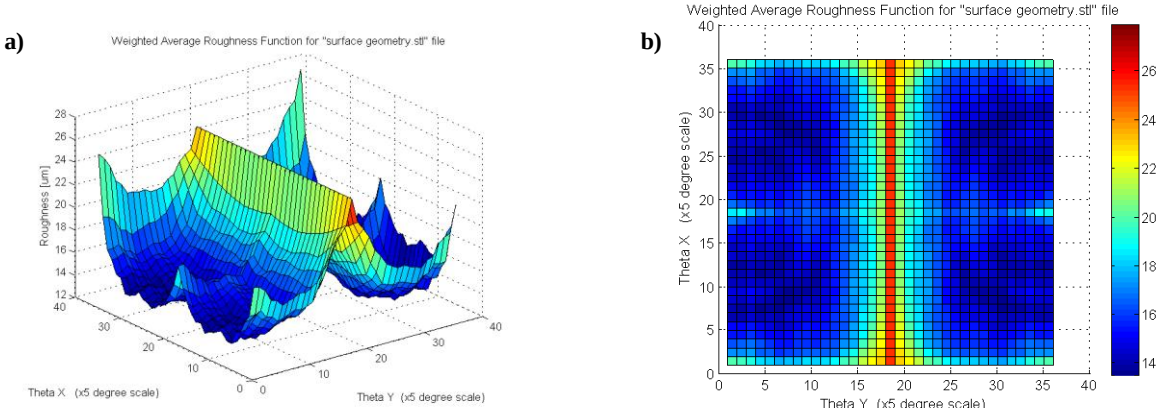

Figure 6: Weighted average roughness function for the artefact shown in Figure 3a.

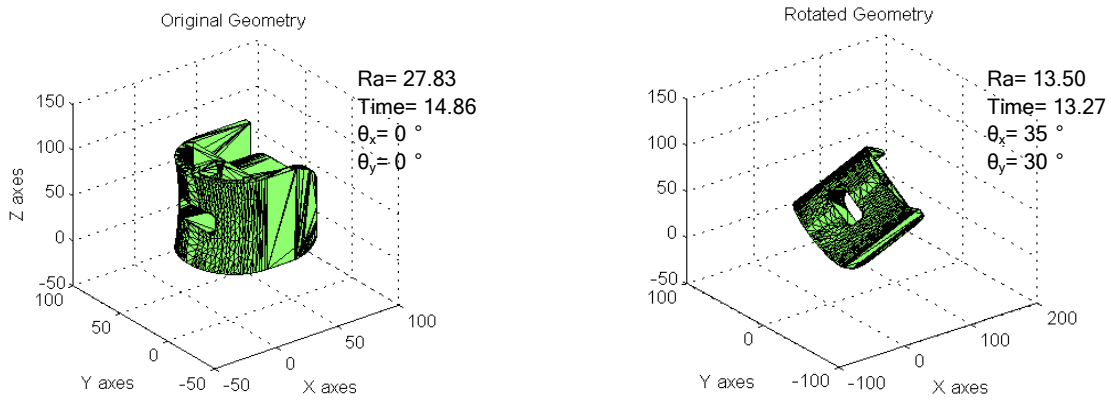

Figure 8a: First case study original and optimally oriented geometries in order to minimize the surface roughness.

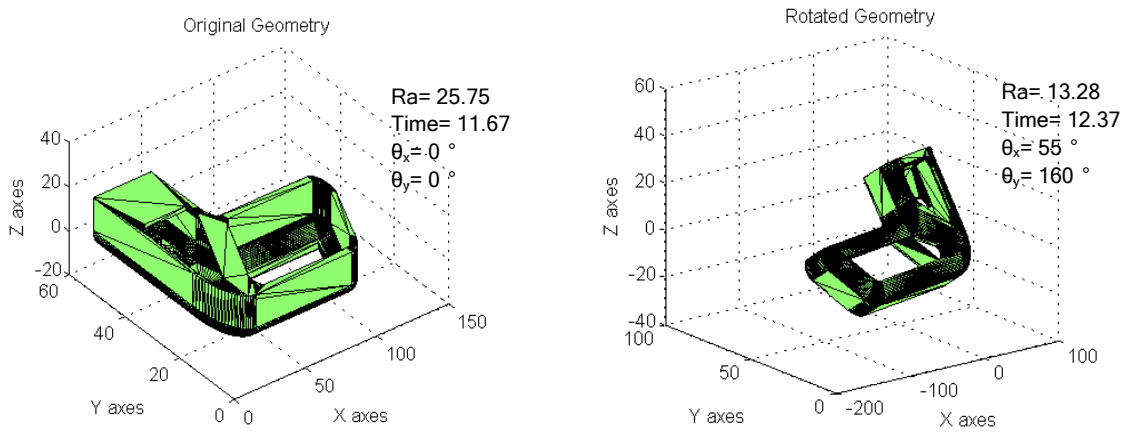

Figure 8b: First case study original and optimally oriented geometries in order to minimize the surface roughness.

4. CONCLUSIONS

In this study, a decision support system for optimal part orientation in ALM processes such as SLS/SLM has been presented. A model based on multi-objective optimisation technique has been developed, in order to find the Pareto set of solutions which define the best compromises between the weighted average surface roughness and build time. The optimisation has been performed for two different case studies.

A model for build time and roughness prediction has been developed for this purpose; rather than using a geometry based analytical model, an approach based on the interpolation of measured data on the SLS technology has been used. The weighted average surface roughness has been calculated by taking into consideration both the area and the orientation of each surface facet, and distinguishing between upward and downward oriented surface data. The optimisation problem has been solved by an exhaustive searching algorithm by rotation around the *X* and *Y* axes; the computational time required is expected to be less than that required by a GA based optimisation; the global optimum has been found in a reasonable time.

Furthermore, given a set of process data, the methodology and the mathematical model presented are generally applicable to powder bed based ALM platforms; in this sense further research will validate the developed optimisation technique for SLM and EBM platforms using experimental and computational data.

5. REFERENCES

1. G.N. Levy, R. Schindel, J.P. Kruth, CIRP Annals 2003, Vol.52/2.
2. J.P. Kruth, B. Vandenbroucke, J. Vam Vaerenbergh and P. Mercellis, Int. Conf. Polymers & Mould Innovations (PMI), Gent, Belgium, April 20-23, 2005.
3. P.B. Bacchewar, S.K. Singhal and P.M. Pandley, Proc ImechE vol. 221, 2007, 221
4. R.I. Campbell, M. Martorelli, H.S. Lee, Computer-Aided Design 2002, 34, pp.717-725.
5. S.K. Singhal, S.P. Pandey, P.M. Pandey and A.K. Nagpal, Computer-Aided Design 2005, 2, pp 319-328.
6. V. Canellidis, J. Giannatsis, V. Dedoussis, International Journal of Advanced Manufacturing Technology (In press, IJAMT3483).
7. P.M. Pandey, K, Thrimurthulu and N. Venkata Reddy, Int. Prod. Res, 2004, 42, 19, pp. 4069-4089.
8. P. Alexander, S. Allen and D. Dutta, Computer Aided Design, 1998, 30, pp. 343-356.

Glossary

5-axis machine - machine with simultaneous motion in the x, y and z axes and two rotational axes.

Build time - length of time for the physical construction of a rapid prototype, excluding preparation and post processing time.

Computer-aided design (CAD) – indicates the use of computer systems to assist in the creation, modification, analysis, or optimization of a design.

Green part - part that has been formed by a rapid prototyping process, but in a loosely-bonded state. It is then sintered by secondary operations.

Hatch spacing - in the laser sintering/melting process, distance between consecutive laser scans.

Layer thickness - Vertical dimension of a single slice of an STL file. Smaller dimensions may lead to smoother surfaces but may increase build time.

Near net shape - the name indicates items that are very close to the final (net) shape, thus that need reduced surface finishing operations.

Stair-step - approximation of curved and inclined edges of a part, consequence of additive fabricating a part in layers of necessarily finite thickness.

Standard Tessellation Language (STL) file - file Format widely used for rapid prototyping and computer-aided manufacturing. STL files describe the surface geometry of a three dimensional object without any representation of color, texture or other CAD model attributes.

Bibliography

3DSystems (2012). from http://www.3dsystems.com/ (accessed Sept 2011).

Ahn, D., H. Kim and S. Lee (2009). "Surface roughness prediction using measured data and interpolation in layered manufacturing." Journal of Materials Processing Technology 209(2): 664-671.

Alexander, P., S. Allen and D. Dutta (1998). "Part orientation and build cost determination in layered manufacturing." Computer-Aided Design 30(5): 343-356.

Allen, S. and D. Dutta (1995). "Determination and evaluation of support structures in layered manufacturing." Journal of Design and Manufacturing 5: 153-162.

Andersson, T., H. Strandberg and S. Sørbø (2009). Multi-objective optimization of an aluminium automotive part using modeFRONTIER. EnginSoft Newsletter

Arcam (2012). from http://www.arcam.com/ (accessed Sept 2011).

Bablani, M. and A. Bagchi (1995). "Quantification of Errors in Rapid Prototyping Processes, and Determination of Preferred Orientation of Parts." Transactions of the North American Manufacturing Research Institution of the SME XXIII(May 1995): 319-324.

Bacchewar, P. B., S. K. Singhal and P. M. Pandey (2007). "Statistical modelling and optimization of surface roughness in the selective laser sintering process." Proceedings of the Institution of Mechanical Engineers, Part B: Journal of Engineering Manufacture 221(1): 35-52.

Baeck T., Fogel D.B. and M. Z. (1997). Handbook on Evolutionary Computation, IOP Publishing Ltd and Oxford University Press.

Balla, V. K., S. Banerjee, S. Bose and A. Bandyopadhyay (2010). "Direct laser processing of a tantalum coating on titanium for bone replacement structures." Acta Biomaterialia 6(6): 2329-2334.

Bandyopadhyay, A., B. Krishna, W. Xue and S. Bose (2009). "Application of Laser Engineered Net Shaping (LENS) to manufacture porous and functionally graded structures for load bearing implants." Journal of Materials Science: Materials in Medicine 20(0): 29-34.

Bendsoe, M. P. and N. Kikuchi (1988). "Generating optimal topologies in structural design using a homogenization method." Comput. Methods Appl. Mech. Eng. 71(2): 197-224.

Bendsoe, M. P. and O. Sigmund (2003). Topology Optimization - Theory, Methods and Applications. New York, Springer.

Bitzer, T. (1997). Honeycomb technology. London, Chapman & Hall.
Black, J. T. and R. A. Kohser (2008). DeGarmo's Materials and Processes in Manufacturing, 10th Edition, Wiley.

Campbell, R. I., M. Martorelli and H. S. Lee (2002). "Surface roughness visualisation for rapid prototyping models." Computer-Aided Design 34(10): 717-725.

CanonInc. (2011, 2011). "Virtual Prototyping Technology." from http://www.canon.com/technology/canon_tech/explanation/pe_tech.html.

CastleIslandCo. (2011). "Worldwide Guide to Rapid Prototyping", from http://www.additive3d.com/ (accessed October 2011)

Coello, C. A. C. (1999). "A Comprehensive Survey of Evolutionary-Based Multiobjective Optimization Techniques." Knowledge and Information Systems 1: 269-308.

Coello, C. A. C., A. D. Christiansen, A. Hern\, \#225 and n. Aguirre (1998). "Using a new GA-based multiobjective optimization technique for the design of robot arms." Robotica 16(4): 401-414.

Coello, C. A., G. B. Lamont and D. A. v. Veldhuizen (2007). Evolutionary Algorithms for Solving Multi-Objective Problems, Springer.

Campbell, R. I., M. Martorelli and H. S. Lee (2002). "Surface roughness visualisation for rapid prototyping models." Computer-Aided Design 34(10): 717-725.

Chan, C. L. and J. Mazumder (1987). "Spectroscopic studies of plasma during laser material interaction." J. Appl. Phys. 2: 4579-4586

Cheng, W., J. Y. H. Fuh, A. Y. C. Nee, Y. S. Wong, H. T. Loh and T. Miyazawa (1995). "Multi-objective optimization of part- building orientation in stereolithography." Rapid Prototyping Journal 1(4): 12-23.

CRPGroup (2012). from www.crptechnology.com (accessed Jan 2012).

CustomPartNet (2008). from http://www.custompartnet.com/ (accessed Sept 2011).

Cutler, J. and J. Liber (2005). Understanding Aircraft Structures, Blackwell Publishing.

Daneshmand, S., R. Adelnia and S. Aghanajafi (2006). Proceedings of the 4th WSEAS International Conference on Fluid Mechanics and Aerodynamics, Elounda, Greece.

Das, I. and J. E. Dennis (1997). "A closer look at drawbacks of minimizing weighted sums of objectives for Pareto set generation in multicriteria optimization problems." Structural and Multidisciplinary Optimization 14(1): 63-69.

Das, S. and B. K. Panigrahi (2009). "Multi-Objective Evolutionary Algorithms." Encyclopedia of Artificial Intelligence: 1145-1151.

Deb, K. (2001). "Multi-objective optimization using evolutionary algorithms."

Deb, K., A. Pratap, S. Agarwal and T. Meyarivan (2002). "A fast and elitist multiobjective genetic algorithm: NSGA-II." Evolutionary Computation, IEEE Transactions on 6(2): 182-197.

DeGarmo, E. P., J. T. Black and R. A. Kohser (2011). Degarmo's Materials and Processes in Manufacturing, Wiley.

Ehrgott M. (2005). Multicriteria Optimization, Springer.

Fonseca, C. M. and P. J. Fleming (1993). Genetic Algorithms for Multiobjective Optimization: Formulation, Discussion and Generalization. Proceedings of the 5th International Conference on Genetic Algorithms, San Francisco, CA, USA, Morgan Kaufmann Publishers Inc.

Frank, D. and G. Fadel (1995). "Expert system-based selection of the preferred direction of build for rapid prototyping processes." Journal of Intelligent Manufacturing 6(5): 339-345.

Gabrielli, R. (2009). Foam geometry and structural design of porous material. Mechanical Engineering.

Gessenharter, A., O. Riemer and E. Brinksmeier (2003). Polishing Processes for Structured Surfaces. ASPE s 18th Annual Meeting, Portland, Oregon.

Gibson, I. and D. Shi (1997). "Material properties and fabrication parameters in selective laser sintering process." Rapid Prototyping Journal, 3(4): 129 - 136.

Goldberg D.E. (1989). Genetic Algorithms in Search, Optimization and Machine Learning, Addison Wesley.

Good, J. (2007). Fabrication in Space - *What Materials are Needed?*, NASA - Marshall Space Flight Center.

Hao, L., D. Raymond, C. Yan, A. Hussein and P. Young (2011). Design and additive manufacturing of cellular lattice structures. The International Conference on Advanced Research in Virtual and Rapid Prototyping (VRAP). Leiria, Portugal, Taylor & Francis Group: 249 - 254.

Hedges, M. (2004). Laser based additive manufacturing using LENSTM and M3DTM. Proceedings of the Fourth Laser Assisted Net Shape Engineering, Erlangen, Germany.

Hedges, M. and N. Calder (2006). Near net shape rapid manufacture & repair by LENS.

Hexweb (2000). Honeycomb sandwich design technology. Cambridge.

Hnaien, F., X. Delorme and A. Dolgui (2010). "Multi-objective optimization for inventory control in two-level assembly systems under uncertainty of lead times." Computers & Operations Research 37(11): 1835-1843.

Honess, C. (2006). Importance of Surface finish in the design of stainless steel. Engineering Utilities. Swinden Technology Centre.

Horn, J., N. Nafpliotis and D. E. Goldberg (1994). A niched Pareto genetic algorithm for multiobjective optimization. Evolutionary Computation, 1994. IEEE World Congress on Computational Intelligence., Proceedings of the First IEEE Conference on.

Hoyland, S. (2007). from http://en.wikipedia.org/wiki/File:Apis_florea_nest_closeup2.jpg (accessed Sept 2011).

Inst, B. S. (1972). British Standard BS 1134: Method for Assessment of Surface Texture. London.

Kadadevaramath, R. S. and K. M. Mohanasudaram (2007). "Multi-Objective Trade-off Analysis: State of art: Methods, Applications, and future Research Directions in Production and Operations Management." Manufacturing Engineering(2): 70-78.

Kim, G. D. and Y. T. Oh (2008). "A benchmark study on rapid prototyping processes and machines: quantitative comparisons of mechanical properties, accuracy, roughness, speed, and material cost." Proceedings of the Institution of Mechanical Engineers, Part B: Journal of Engineering Manufacture 222(2): 201-215.

Kruth, J. P., M. Badrossamay, E.Yasa, J. Deckers, L. Thijs and J. V. Humbeeck (2010). Part and material properties in selective laser melting of metals. 16th International Symposium on Electromachining (ISEM XVI). Shanghai, China.

Kruth, P. d. i. J. P., B. Vandenbroucke, I. J. Vaerenbergh van and P. Mercelis (2005). Benchmarking of different SLS/SLM processes as Rapid Manufacturing techniques. Proceedings of the PMI, paper 525.

Lan, P.-T., S.-Y. Chou, L.-L. Chen and D. Gemmill (1997). "Determining fabrication orientations for rapid prototyping with Stereolithography apparatus." Computer-Aided Design 29(1): 53-62.

Laumanns, M., E. Zitzler and L. Thiele (2001). On the Effects of Archiving, Elitism, and Density Based Selection in Evolutionary Multi-objective Optimization. Proceedings of the First International Conference on Evolutionary Multi-Criterion Optimization, Springer-Verlag: 181-196.

Levy, G. N., R. Schindel and J. P. Kruth (2003). "Rapid Manufacturing and Rapid Tooling with Layer Manufacturing (LM) Technologies, State of the Art and Future Perspectives." CIRP Annals - Manufacturing Technology 52(2): 589-609.

Li, Q., E. Y. Chen, D. R. Bice and D. C. Dunand (2008). "Mechanical Properties of Cast Ti-6Al-2Sn-4Zr-2Mo Lattice Block Structures." Advanced Engineering Materials 10(10): 939-942.

LLC, A. M. (2012). from http://www.lasersintering.com (accessed Jan 2012).

Luis Pérez, C. J., J. Vivancos Calvet and M. A. Sebastián Pérez (2001). "Geometric roughness analysis in solid free-form manufacturing processes." Journal of Materials Processing Technology 119(1-3): 52-57.

Maniscalco, M. (2003). Choosing resins in the 21st century. IMM Magazine

More, J. J. and D. C. Sorensen (1983). "Computing a Trust Region Step." SIAM Journal on Scientific and Statistical Computing 4(3): 553-572.

Mumtaz, K. and N. Hopkinson (2009). "Top surface and side roughness of Inconel 625 parts processed using selective laser melting." Rapid Prototyping Journal 15(2): 96-103.

Noorani, R. L. (2006). Rapid Prototyping: Principles and Applications, Jon Wiley and Sons Inc.

Optomec (2012). from http://www.optomec.com/ (accessed Jan 2012)

Ott, E. (2002). Superalloy Lattice Block, GEAE-NASA RASER.

Pandey, P. M., K. Thrimurthulu and N. V. Reddy (2004). "Optimal part deposition orientation in FDM by using a multicriteria genetic algorithm." International Journal of Production Research 42(19): 4069 - 4089.

Pasko, A., T. Vilbrandt, O. Fryazinov and V. Adzhiev (2010). Procedural Function-Based Spatial Microstructures. Shape Modeling International Conference (SMI), 2010

Pera, L. and G. Marinsek (1992). "The role of the laser in rapid prototyping." Proceeding of the NATO Advanced Study Institute (ASI) laser applications for mechanical industry, Erice, Sicily: 293-303.

Pham, D. T. and S. S. Demov (2001). Rapid Manufacturing: The Technologies and Applications of Rapid Prototyping and Rapid Tooling.

Putte, B. S., J. P. Bornem and W. V. Huldenberg (1997). Method for supporting an object made by means of stereolithography or another rapid prototype production method. Belgium, Materialise.

Quiza Sardiñas, R., M. Rivas Santana and E. Alfonso Brindis (2006). "Genetic algorithm-based multi-objective optimization of cutting parameters in turning processes." Engineering Applications of Artificial Intelligence 19(2): 127-133.

Reckhouse W. (2010). Optimisation of Short Term Conflict Alert Safety Related Systems, University of Exeter.

Reeves, P. E. and R. C. Cobb (1997). "Reducing the surface deviation of Stereolithography using in-process techniques." Rapid Prototyping Journal 3 (1): 20 - 31

Rotheroe, K. C. (2005). Unitary metal structural member with internal reinforcement. US

Roy, R. and J. Mehnen (2008). "Dynamic multi-objective optimisation for machining gradient materials." CIRP Annals - Manufacturing Technology 57(1): 429-432.

Sachs, E. (2001). Manufacturing by solid freeform fabrication. Solid Freeform Fabrication Proceedings (2001).

Santos, E. C., M. Shiomi, K. Osakada and T. Laoui " Rapid manufacturing of metal 01components by laser forming." International Journal of Machine Tools and Manufacture 46(12–13): 1459-1468.

Schoen, A. H. (1970). Infinite periodic minimal surfaces without selfintersection. Cambridge, Mass., National Aeronautics and Space Administration.

Schwarz, H. A. (1890). Gesammelte Mathematische Abhandlungen. Berlin Springer-Verlag (Reprinted by Chelsea Publishing Company, 1972, 1890).

Singhal, S. K., P. K. Jain, P. M. Pandey and A. K. Nagpal (2009). "Optimum part deposition orientation for multiple objectives in SL and SLS prototyping." International Journal of Production Research 47(22): 6375 - 6396.

Sreeram, P. N. and D. Dutta (1994). Determination of optimal orientation based on variable slicing thickness in layered manufacturing. Department of Mechanical Engineering, University of Michigan.

Srinivas, N. and K. Deb (1994). "Multiobjective optimization using nondominated sorting in genetic algorithms." Evolutionary Computation 2: 221-248.

Starly, B. (2006). Biomimetic design and fabrication of tissue engineered scaffolds using computer aided tissue engineering. Department of mechanical engineering and mechanics, Drexel University.

Steen, W. M. and J. Mazumder (2010). Laser Material Processing, Springer.

Strano, G., L. Hao, R. M. Everson and K. E. Evans (2011). "Multi-objective optimization of selective laser sintering processes for surface quality and energy saving." Proceedings of the Institution of Mechanical Engineers, Part B: Journal of Engineering Manufacture.

Strano G. , Bucolo M., Di Grazia F. and Tomarchio G. (2008). Optimization Problem and Capacity Allocation Process in a Semiconductor Company. International Symposium on Mathematical Theory of Networks and Systems, Virginia Tech, Blacksburg, Virginia, USA

Sypeck, D. J. (2005). "Cellular Truss Core Sandwich Structures." Applied Composite Materials 12(3): 229-246.

Swaelens, Bart, Pauwels, Johan and Vancraen (1995). Support Generation for Rapid Prototyping. Sixth International Conference on Rapid Prototyping, University of Dayton.

Szulczynski, H. and E. Uhlmann (2002). Material Removal Mechanisms in Abrasive Flow Machining. Proc. of the 17th Annual Meeting of the ASPE, St. Louis, Missouri, USA.

Tomlin, M. and J. Meyer (2011). Topology Optimization of an Additive Layer Manufactured (ALM) Aerospace Part. The 7th Altair CAE Technology Conference 2011. Altair.

Townsin, R. L., D. Byrne, T. E. Svensen and A. Milne (November 1981). "Estimating the technical and economic penalties of hull and propeller roughness." Soc. Nav. Archit. Mar. Eng., Trans. .

Trego, L. (2010). "Honeycomb structure material.", from http://www.sae.org/mags/SVE/8061 (accessed Jan 2012).

Villar, R. (1999). "Laser Cladding." Journa of Laser Applications 11(2): 64-75.

Vorburger, V. and J. Raja (1990). Surface Finish Metrology Tutorial. NISTIR 89-4088,. Gaithersburg, MD National Institute of Standards and Technology.

Wadley, H. N. G. (2006). "Multifunctional periodic cellular metals." Philosophical Transactions of the Royal Society A: Mathematical, Physical and Engineering Sciences 364(1838): 31-68.

Wallach, J. C. and L. J. Gibson (2001). "Mechanical behavior of a three-dimensional truss material." International Journal of Solids and Structures 38(40-41): 7181-7196.

Wang, H., Y. Chen and D. W. Rosen (2005). A hybrid geometric modeling method for large scale conformal cellular structures. ASME Conference Proceedings.

Wang, L., A. H. C. Ng and K. Deb (2011). Multi-objective Evolutionary Optimisation for Product Design and Manufacturing.

Weigert, G., S. Werner and D. Hamp Multi-objective decision making - Solutions for the optimisation of manufacturing processes. Dresden University of Technology, Electronics Technology Laboratory.

Wiesner, C. and I. Norris (2007). Joining and Near-Net Shape Manufacturing Processes, World Centre for Materials Joining Technology.

Xie, Y. M., X. Huang, J. W. Tang and P. Felicetti (2005). Recent Advances in Evolutionary Structural Optimization. Keynote Lecture for Frontiers of Computational Science Symposium. Nagoya University, Japan.

Xie, Y. M. and G. P. Steven (1993). "A simple evolutionary procedure for structural optimization." Computers & Structures 49(5): 885-896.

Zitzler, E., K. Deb and L. Thiele (2000). "Comparison of Multiobjective Evolutionary Algorithms: Empirical Results." Evolutionary Computation 8(2): 173-195.

Zitzler, E., M. Laumanns and S. Bleuler A Tutorial on Evolutionary Multiobjective Optimization. Swiss Federal Institute of Technology (ETH) Zurich, Computer Engineering and Networks Laboratory (TIK), Gloriastrasse 35, CH-8092 Zurich, Switzerland